

CHAPTER 4

Global Ozone: Past and Future

Lead Authors:

M.P. Chipperfield
W.J. Randel

Coauthors:

G.E. Bodeker
M. Dameris
V.E. Fioletov
R.R. Friedl
N.R.P. Harris
J.A. Logan
R.D. McPeters
N.J. Muthama
T. Peter
T.G. Shepherd
K.P. Shine
S. Solomon
L.W. Thomason
J.M. Zawodny

Contributors:

J. Austin
M. Bourqui
P. Braesicke
C. Brühl
N. Butchart
D.B. Considine
D. Cunnold
D.W. Fahey
E.L. Fleming
P.M. de F. Forster
M.A. Geller
S. Godin-Beekmann
V. Grewe
J.D. Haigh
C.H. Jackman
P. Johnston
U. Langematz
K.S. Law
J.B. Liley
I.A. Megretskaya
A.J. Miller
T. Nagashima
G. Pitari
R.W. Portmann
V. Ramaswamy
B. Rognerud
J.E. Rosenfield
M.N. Ross
C. Schnadt
M.D. Schwarzkopf
D.T. Shindell
C.A. Smith
S. Smyshlyaev
R.S. Stolarski
G.J.M. Velders
R. Wang
D.K. Weisenstein
F. Wu
R.J. Zander

CHAPTER 4

GLOBAL OZONE: PAST AND FUTURE

Contents

SCIENTIFIC SUMMARY	4.1
4.1 INTRODUCTION	4.5
4.2 DESCRIPTION OF PAST CHANGES IN OZONE	4.6
4.2.1 Introduction	4.6
4.2.2 Changes in Total Ozone	4.7
4.2.2.1 Global Ozone: NH and SH Midlatitudes and Tropics	4.7
4.2.2.2 Seasonal Changes in Total Ozone	4.10
4.2.3 Changes in the Vertical Profile of Ozone	4.16
4.2.3.1 Upper Stratosphere	4.16
4.2.3.2 Lower Stratosphere	4.18
4.2.4 Vertical Integral of the Profile Trends vs. Column Trends	4.19
4.2.5 Tropospheric Ozone	4.22
4.2.6 Solar Cycle Effects on Ozone	4.22
4.2.6.1 Column Ozone	4.22
4.2.6.2 Vertical Profile of the Solar Signal	4.24
4.2.6.3 Summary	4.25
4.3 CURRENT UNDERSTANDING OF PAST CHANGES IN STRATOSPHERIC AEROSOL, WATER VAPOR, AND NO ₂	4.25
4.3.1 Stratospheric Aerosol Variability	4.25
4.3.2 Stratospheric Water Vapor Trends	4.27
4.3.3 Trends in Stratospheric NO ₂	4.28
4.4 CURRENT UNDERSTANDING OF PAST CHANGES IN STRATOSPHERIC TEMPERATURE	4.29
4.4.1 Updated Observations of Stratospheric Temperature	4.29
4.4.2 Causes of Past Temperature Changes	4.30
4.4.2.1 Simulated Temperature Trends Due to Observed Ozone Trends	4.31
4.4.2.2 Simulated Temperature Trends Due to Increased WMGG Concentrations	4.33
4.4.2.3 The Role of Trends in Stratospheric Water Vapor	4.34
4.4.2.4 Synopsis of Simulated Temperature Trends	4.35
4.5 CHEMICAL INFLUENCE ON PAST CHANGES IN OZONE	4.37
4.5.1 Chemical Processes that May Contribute to Ozone Changes	4.37
4.5.1.1 Gas-Phase Chemical Processes	4.37
4.5.1.2 Midlatitude Lower Stratospheric Heterogeneous Processes	4.38
4.5.2 Quantifying the Chemical Influence on Ozone: Modeling Tools	4.41
4.5.2.1 2-D Models	4.41
4.5.2.2 3-D Models	4.42
4.5.3 Quantifying the Chemical Influence on Ozone: Model Results	4.43
4.5.3.1 Effects of NO _x - and ClO _x -Related Processes	4.43
4.5.3.2 Effect of Polar Vortex on Midlatitudes	4.45
4.5.3.3 Effect of Water Vapor Trends	4.45
4.5.3.4 Assessment Model Simulations of Past Ozone Changes	4.46

4.6	DYNAMICAL INFLUENCE ON PAST CHANGES IN OZONE	4.52
4.6.1	Introduction	4.52
4.6.2	Dynamical Processes that May Contribute to Ozone Changes	4.54
4.6.2.1	Changes in Planetary-Wave Drag	4.54
4.6.2.2	Effects of Tropospheric Circulation and Tropopause Changes	4.55
4.6.2.3	Hemispheric Variations and Annular Modes	4.56
4.6.3	Statistical Analysis of Observations	4.56
4.6.3.1	Changes in Planetary-Wave Driving	4.56
4.6.3.2	Changes in Tropospheric Circulation and Tropopause Height	4.57
4.6.3.3	Coupling Issues	4.58
4.6.4	Modeling Studies	4.58
4.6.5	Cause of the Dynamical Changes	4.60
4.6.6	Effects of Mt. Pinatubo Eruption	4.61
4.6.7	Conclusions	4.62
4.7	IMPLICATIONS FOR CLIMATE OF UPDATED STRATOSPHERIC OZONE CHANGES	4.62
4.8	FUTURE CHANGES IN OZONE	4.63
4.8.1	Effect of Decreasing Halogens	4.64
4.8.2	Influence of Changing Climate Gases	4.65
4.8.3	Other Stratospheric Influences	4.66
4.8.3.1	Dynamical Effects	4.66
4.8.3.2	Future Effects of Aircraft	4.67
4.8.3.3	Rocket Emissions	4.67
4.8.4	Future Tropospheric Ozone	4.68
4.9	SYNTHESIS OF CURRENT UNDERSTANDING OF PAST AND FUTURE CHANGES IN OZONE	4.70
4.9.1	Discussion of Past Changes	4.70
4.9.2	Discussion of Future Changes	4.72
	REFERENCES	4.72
	APPENDIX 4A: DESCRIPTION OF OZONE DATASETS	4.85
4A.1	Ground-Based Total Ozone Measurements	4.85
4A.2	Satellite Total Ozone Measurements and Merged Datasets	4.85
4A.3	Ozone Profile Measurements	4.88
	APPENDIX 4B: 2-D MODEL SCENARIOS	4.90

SCIENTIFIC SUMMARY

Total Column Ozone

- Global mean total column ozone for the period 1997-2001 was approximately 3% below the pre-1980 average values. Since systematic global observations began in the mid-1960s, the lowest annually averaged global total column ozone occurred in 1992-1993 (5% below the pre-1980 average). These changes are evident in each available global dataset.
- No significant trends in total column ozone have been observed in the tropics (25°N-25°S) for 1980-2000. A decadal variation of total column ozone (with peak-to-trough variations of ~3%) is observed in this region, approximately in phase with the 11-year solar cycle. Total column ozone trends become statistically significant in the latitude bands 25°-35° in each hemisphere.
- There are a number of differences in total column ozone behavior between the two hemispheres:
 - Averaged for the period 1997-2001, total column ozone in the Northern Hemisphere (NH) and Southern Hemisphere (SH) midlatitudes (35°-60°) are about 3% and 6%, respectively, below their pre-1980 average values.
 - The seasonality of total column ozone changes (1997-2001 relative to pre-1980) is different in the NH and SH midlatitudes. Over NH midlatitudes, larger ozone decreases are observed during winter-spring (~4%); summer-autumn decreases are approximately half as large. Over SH midlatitudes, long-term ozone decreases exhibit similar magnitude (~6%) during all seasons.
 - Pronounced negative anomalies are observed in the NH midlatitude time series during 1992-1995 in the winter-spring seasons. Similar anomalies are not seen in the SH midlatitudes.
 - There is a sharp drop in ozone at SH midlatitudes during 1985-1986. A similar drop is not observed in the NH.

Vertical Ozone Distribution

- Ozone profile trends derived from Stratospheric Aerosol and Gas Experiment (SAGE I and SAGE II, version v6.1) data show significant negative trends over latitudes 60°N to 60°S for altitudes ~35-50 km (with extremes near 40 km). Trend maxima of 7-8%/decade over the period 1979-2000 are observed in latitude bands 35°-60° of both hemispheres, with no significant interhemispheric difference. These satellite results are in good agreement with independent Umkehr ozone measurements available over the NH midlatitudes. Ozone decreases in the upper stratosphere (above 25 km) contribute 15-30% to changes in the total column at midlatitudes.
- The updated SAGE data reveal significant negative trends in the small amount of ozone above 30 km extending throughout the tropics, a feature not observed in previous Assessments based on shorter time records.
- Ozonesonde measurements over the NH midlatitudes show that ozone between 20 and 27 km decreased continuously during 1980-2000, while ozone between 10 and 20 km decreased through the early 1990s and was relatively constant thereafter. This behavior is consistent with observed changes in NH midlatitude column ozone.
- The ozonesonde measurements show no trend in tropospheric ozone for 1980 to 2000 for most stations, and the mean trend averaged over all midlatitude stations is also zero.

Ozone-Related Constituents

- Stratospheric aerosol variability over the past 25 years has been dominated by the effects of episodic volcanic eruptions, with subsequent recovery. Following the large eruption of Mt. Pinatubo in 1991, relaxation to a nonvolcanic level continued to at least 1999. There is currently no evidence of a trend in the nonvolcanic aerosol loading over the past 25 years.

GLOBAL OZONE

- Stratospheric water vapor measurements at Boulder, Colorado, U.S. (40°N), for the period 1981-2000 show a statistically significant increase of approximately 1%/year over altitudes 15-28 km. For the shorter period 1991-2001, global satellite measurements covering latitudes 60°S to 60°N show a similar trend of 0.6-0.8%/year for altitudes ~25-50 km, but no significant trend at lower altitudes. This increase in water vapor is substantially larger than can be explained by tropospheric methane (CH₄) trends. Characterization of stratospheric water vapor trends is limited by the lack of global long-term measurements.
- Stratospheric column nitrogen dioxide (NO₂) measurements from Lauder, New Zealand (45°S), for the period 1981-2001, and Jungfraujoch, Switzerland (46°N), for 1985-2001, show statistically significant positive trends of approximately 6%/decade. Transient decreases are also observed following the El Chichón and Mt. Pinatubo volcanic eruptions, which are broadly simulated by models that include heterogeneous chemistry on sulfate aerosols.

Stratospheric Temperature Trends

- Satellite observations indicate that, on an annual and global mean, the stratosphere has cooled over the last two decades. In the lower stratosphere, global and annual mean temperatures for the late 1990s are approximately 1 K lower than values in the late 1970s. Significant annual-mean cooling of the lower stratosphere for the past two decades is found over midlatitudes of both hemispheres (approximately 0.6 K/decade), but no significant trends are observed near the equator. The annual mean temperature trends in the upper stratosphere are larger, with an approximately globally uniform cooling for 1979-1998 of about 2 K/decade near the stratopause (~50 km).
- Modeling studies indicate that changes in ozone, well-mixed greenhouse gases, and stratospheric water vapor can explain the major features of the observed global and annual-mean stratospheric cooling over the past two decades. Cooling due to ozone depletion dominates over the impact of well-mixed greenhouse gases in the lower stratosphere. Upper stratospheric temperature trends are due, roughly equally, to ozone and well-mixed greenhouse gas changes. At 20 km, the observed annual-mean cooling in northern midlatitudes is much larger than that simulated using observed ozone and greenhouse gas changes. In this region increases in water vapor may have been as important as ozone loss in determining the cooling. The inclusion of water vapor generally improves agreement with observations, but uncertainties in the spatial and temporal distribution of its change are large.

Attribution of Past Changes in Ozone

- The vertical, latitudinal, and seasonal characteristics of changes in midlatitude ozone are broadly consistent with the understanding that halogens are the primary cause of these changes, in line with similar conclusions from the 1998 Assessment.
- Assessment models forced by observed changes in halocarbons, source gases, and aerosols broadly reproduce the long-term changes observed in midlatitude total column ozone (35°N-60°N and 35°S-60°S) for 1980-2000, within the uncertainties of the observations and model range. However, the range of model results is large over SH midlatitudes, which is at least partly due to their treatment of the Antarctic ozone hole. In addition, models suggest that the chemical signal of ozone loss following the major eruption of the Mt. Pinatubo volcano in the early 1990s should have been symmetric between hemispheres, but observations show a large degree of interhemispheric asymmetry in midlatitudes.
- There is increased evidence that changes in atmospheric dynamics have had a significant influence on NH midlatitude column ozone on decadal time scales. Natural variability, changes in greenhouse gases, and changes in column ozone itself are all likely to contribute to these dynamical changes. Furthermore, because chemical and dynamical processes are coupled, their contributions to ozone changes cannot be assessed in isolation.
- The observed ozone depletion in the upper stratosphere is consistent with observed changes in anthropogenic chlorine. The vertical and latitudinal profiles of trends in the upper stratosphere are reproduced by photochemical models, but the magnitudes of changes are sensitive to concurrent trends in temperature and other constituents such as CH₄.

- Stratospheric planetary-wave drag drives the wintertime ozone buildup in the extratropics, so the observed decrease in NH planetary-wave drag likely has contributed to the observed decrease in NH total column ozone over the last 20 years. The relationship between planetary-wave drag and ozone is understood, but its quantification in observations is relatively crude.
- There is an observed relationship between total column ozone and tropopause height, and several tropospheric circulation indices. These indices have changed over the last 20 years in the NH in such a way as to imply a decrease in total column ozone. However, the causality of these relationships is not well understood, which makes their extrapolation to long time periods problematic.

Future Changes in Ozone

- The expected decrease in stratospheric chlorine loading over the next 50 years is predicted to lead to an increase in the global total column ozone, although there are differences in the rate of increase between different two-dimensional assessment models. Future ozone levels will also be influenced by other changes in atmospheric composition and by climate change. Because of year-to-year variability it could take as long as a decade to demonstrate a leveling of total column ozone.
- Stratospheric cooling (due mainly to projected carbon dioxide (CO₂) increases) is predicted to enhance future ozone increases in the upper stratosphere. This effect in isolation would substantially hasten the predicted rate of total ozone increase in coming decades. However, a reliable assessment of effects on total column ozone is limited by uncertainties in the lower stratospheric response to these changes.
- Projected increases in methane (CH₄) and nitrous oxide (N₂O) are predicted to have small effects on the rate of increase of global column ozone in the next 50 years, when chlorine changes are the dominant effect. After that time, changes in CH₄ and N₂O become relatively more important.
- Future large volcanic eruptions would be expected to cause transient enhancements of chemical ozone depletion (lasting 3-4 years) but should not alter the overall predicted evolution of ozone.
- Future changes in tropospheric ozone are highly dependent upon the scenario adopted for future emissions of ozone precursors, but all scenarios adopted by the Intergovernmental Panel on Climate Change (IPCC) lead to increases in tropospheric ozone up to 2050. Allowing for climate change leads to smaller increases in tropospheric ozone compared with simulations using present-day climate.

4.1 INTRODUCTION

Concentrations of ozone in the atmosphere can change as a result of both natural processes and human activities, and accurate knowledge of past changes is important both for attribution of causes and for prediction of future changes. Past ozone assessments have documented long-term decreases in stratospheric ozone and have devoted separate chapters to ozone observations, interpretation of past changes, and predictions of future change. In contrast, this chapter takes a comprehensive view of past and future changes in global ozone, combining observational and modeling results. In brief, we seek to address the following questions:

- What have been the changes to stratospheric ozone in the past, and how well do we understand those changes?
- What is our best estimate for stratospheric ozone in the future, and what are the main uncertainties in this estimate?

The bulk of atmospheric ozone is found in the stratosphere, with approximately 90% of the vertically integrated column amount occurring above the tropopause (the “ozone layer”). Long-term changes of stratospheric ozone are related to changes in tropospheric source gases (transported into the stratosphere), to variations in solar radiation and volcanic effects, and to changes in large-scale transport. Changes in tropospheric ozone (which is an environmental pollutant near the surface) are mainly associated with increased urban pollution and biomass burning. Stratospheric ozone has decreased over the last several decades, while tropospheric ozone has increased (at least over Northern Hemisphere (NH) midlatitudes, where long-term observations are available; Logan et al., 1999). In the extratropics the stratospheric decreases greatly outweigh the tropospheric increases in terms of column amount, and therefore observed column ozone changes primarily reflect the stratospheric decreases. Long-term changes in stratospheric ozone are the primary focus of this chapter, and tropospheric ozone is discussed only briefly (in regard to its contribution to past and future column ozone changes). Detailed discussions of tropospheric ozone are included in IPCC (2001); some of those results are highlighted here where relevant.

The distribution of ozone in the atmosphere is maintained by a balance between photochemical production and loss, and by transport between regions of net production and net loss. Understanding long-term changes in ozone, both past and future, requires knowledge of these processes and a quantification of their relative importance and coupling. The basic structure and zonal mean circulation of the stratosphere are summarized in Figure 4-1.

There is an important distinction between the different vertical regions in the stratosphere, which can be characterized by their radiative, dynamical, and transport behavior. The photochemical lifetime of odd-oxygen ($O_x = O + O_3$, where O is atomic oxygen and O_3 is ozone) varies strongly with altitude between these regions (and also with latitude and season; e.g., Garcia and Solomon (1983)). (In the stratosphere, O and O_3 are in a rapidly established equilibrium, and so any analysis of processes that control O_3 should be based on the family O_x .) The lowermost stratosphere (LMS) covers the region between the tropopause and the isentropic surface of about 380 K (about 15 km), and this region is distinct because air can be transported between the troposphere and stratosphere by isentropic transport alone. Above the LMS, between the 380-K surface and about 25 km is the lower stratosphere (LS). In both the LMS and LS, the lifetime of odd-oxygen is long (~months-years), and odd-oxygen will react to chemical changes slowly and be strongly influenced by atmospheric transport. The region between 30 and 50 km is typically referred to as the upper stratosphere (US) based on radiative/dynamical behavior. However, the odd-oxygen photochemical lifetime is relatively short (less than transport time scales) above 25 km, hence dominated by photochemical control, and for simplicity we refer to the region from 25 to 50 km as the US throughout this chapter.

By considering the factors that control the abundance of ozone in the stratosphere, we can classify the three different regions in Figure 4-1 by the complexity of the processes that need to be understood. The US can be

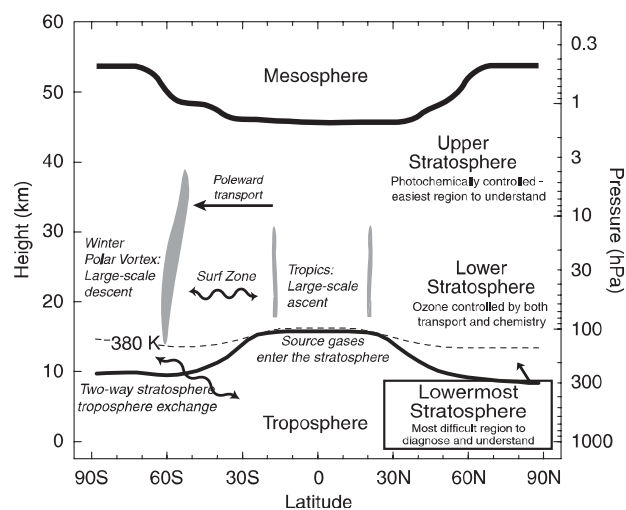


Figure 4-1. Schematic diagram showing the structure of, and transport within, the stratosphere. The three stratospheric regions (LMS, LS, US) discussed in the text are indicated.

GLOBAL OZONE

regarded as the easiest region to analyze, because ozone there is under direct photochemical control and direct transport effects can be neglected (although transport affects the abundance of ozone-destroying species). The LS and LMS are more difficult to analyze, because both transport and chemistry directly affect ozone. Within these lower altitude regions, the LMS region can be considered more difficult than the LS because it is directly coupled by isentropic transport to the troposphere.

As discussed in the previous Assessment (WMO, 1999), there is strong evidence that the main driver for the upper stratospheric ozone loss near 40 km and the polar lower stratospheric springtime loss is halogen chemistry. In the upper stratosphere, ozone loss occurs through purely gas-phase chlorine chemistry. In the polar lower stratosphere, heterogeneous chemistry in or on polar stratospheric clouds (PSCs) causes the conversion of stable chlorine reservoirs to more active forms. Ozone loss then occurs through reactions involving chlorine and bromine species (see Chapter 3). It is also well established that some of the chemical depletion that occurs during spring in the high latitudes must eventually lead to a decrease (or “dilution”) of ozone at midlatitudes when the polar vortices break down. However, this process is poorly quantified at present. A number of other processes, both chemical and dynamical, have been proposed as contributing to ozone decreases in the midlatitude lower stratosphere. The chemical processes include wintertime transport of chlorine-activated air from the vortex followed by chemical loss, and in situ loss initiated by heterogeneous chemistry on liquid sulfate aerosols. The dynamical processes include changes in planetary-wave driving (and associated stratospheric transport circulation), and changes in tropospheric circulation and in tropopause height. While there is good mechanistic evidence that these processes occur and affect ozone, quantifying their contribution to the long-term change is difficult. Furthermore, the chemical and dynamical contributions are coupled and not truly separable, but rather act synergistically.

Past ozone assessments have focused on estimates of linear trends in ozone, usually determined via a multiple regression analysis (including terms to account for other known sources of periodic variability, such as the solar cycle or quasi-biennial oscillation). The choice of fitting a linear trend was based on the expected response to the approximate linear increases in ozone-depleting substances (ODSs) such as chlorofluorocarbons (CFCs) and halons (prior to the middle 1990s). However, this linear increase in ODS has not continued beyond the middle 1990s (see Chapter 1), and the continued representation of ozone variations as simple linear trends is not

appropriate. The philosophy adopted here is to focus primarily on the observed time series of ozone variations updated through 2001, including their detailed latitude and altitude structure, and use these time variations as fingerprints of the mechanisms that influence change. Linear trends are calculated for some variables, namely, for ozone profile variations (where data availability limits the information in time series), and in comparison of the model results to ozone observations in Section 4.5 (where trends are a useful summary diagnostic). For clarity, we reserve the use of the term “trend” to refer to linear trends calculated over a specific time period (typically determined by regression fit).

The overall layout of this chapter is as follows. Section 4.2 provides an update of observed changes in ozone through 2001, including the latitudinal and temporal changes in column and profile ozone. We focus on global or near-global variability (90°N-90°S or 60°N-60°S), together with specific analyses of the tropics (25°N-25°S) and Northern Hemisphere/Southern Hemisphere midlatitudes (which are defined, somewhat arbitrarily, as latitudes 35°N-60°N and 35°S-60°S). The latitude bands 25°-35°N and S are transition zones, where observations show that decadal ozone trends start to become significant. Tropospheric ozone is briefly discussed, and its role in column ozone is estimated. We also specifically discuss the 11-year solar cycle in ozone evaluated from observations and models; this topic is important for quantifying decadal variability in the relatively short observational record. Sections 4.3 and 4.4 describe the complementary observations of past changes in stratospheric aerosol, water vapor, nitrogen dioxide (NO₂), and temperature, and summarize our understanding of their causes. Section 4.5 describes our current understanding of the chemical influence on ozone changes at midlatitudes, and Section 4.6 discusses the dynamical influences on midlatitude ozone changes. Section 4.7 discusses what effect the observed changes in ozone may have had on climate, and Section 4.8 provides updated estimates of how global ozone may evolve in the future. An overall synthesis of current understanding of past and future global ozone changes is presented in Section 4.9.

4.2 DESCRIPTION OF PAST CHANGES IN OZONE

4.2.1 Introduction

Global and hemispheric-scale variations in stratospheric ozone can be quantified from extensive observational records covering the past 20-30 years. The goal

here is to provide an updated description of interannual variability in ozone over the most recent decades (approximately 1970-2000), with a focus on changes outside of the polar regions (over latitudes approximately 60°N-60°S). There are numerous ways to measure ozone in the atmosphere, but they fall broadly into two categories: measurements of total or column ozone (the vertically integrated amount of ozone above the surface) and measurements of the vertical profile of ozone. There are more independent datasets, longer time series, and better global coverage for total ozone. Regular measurements of total ozone are available from a network of surface stations, mostly in the midlatitude Northern Hemisphere, with reasonable coverage extending back to the 1960s (although geographical coverage is limited before the 1970s). Near-global, continuous total ozone data are available from satellite measurements beginning in 1979. However, changes in availability and calibration of ground-based measurements and satellite datasets, and interruptions in observational records, produce datasets in which the systematic errors are complicated functions of time. Systematic errors of 1% are typical even for the most reliable instruments, whereas interannual changes in global or hemispherically averaged ozone are typically a few percent. The methodology adopted in the past (and used here) is to compare estimates of ozone change from several different and independent techniques (i.e., ground-based and satellite datasets), and use their differences to provide a measure of overall uncertainty. The results indicate an overall good agreement among the different data sources for changes in total ozone, and thus we have reasonable confidence in describing the spatial and temporal characteristics of past changes.

There are fewer independent datasets describing long-term changes in the vertical profile of ozone. Satellite observations are the only dataset with global profile coverage, but they are limited in vertical extent and temporal coverage. Reasonably long time records are available from balloonborne ozonesonde and ground-based Umkehr data, but these are primarily concentrated in NH midlatitudes. Thus, in the case of ozone profile measurements, direct comparison of long records from independent datasets is possible only over NH midlatitudes. Over that region there is reasonably good agreement for long-term changes between the satellite and Umkehr data (in the upper stratosphere), and satellite and ozonesondes (in the lower stratosphere), and this suggests that the satellite data are reliable for global analyses. There is approximate but not exact agreement between trends in NH midlatitude total ozone and the vertically integrated profile changes (from ozonesondes in the lower stratosphere, and satellite/Umkehr in the upper strato-

sphere); the lack of more detailed agreement is probably related to the sparse ozonesonde sampling.

4.2.2 Changes in Total Ozone

4.2.2.1 GLOBAL OZONE: NH AND SH MIDLATITUDES AND TROPICS

Five datasets of zonal and monthly mean total ozone values developed by different scientific teams are examined in this Assessment. These consist of various combinations of ground-based and merged satellite datasets, as described in Fioletov et al. (2002) and summarized in Appendix 4A (p. 4.86). The global and latitudinal structure of total ozone variability is analyzed based on seasonal (3-month average) and zonally averaged time series (on a 5° latitude grid). The ground-based dataset extends in time over ~1965-2001 (depending on latitude, with longer and more reliable records available in the midlatitude NH), and the satellite datasets span 1979-2001. Details of the data analyses are discussed in Fioletov et al. (2002). Briefly, the seasonal cycle of total ozone for each dataset is removed by taking monthly averages for each month of the year for the period 1979-1987, and subtracting these from the original data. Area-weighted ozone deviations are then calculated and expressed as anomalies with respect to the period 1964-1980. For regions with missing data, ozone deviations are assumed identical to the surrounding latitude belt where data are available, prior to area averaging. Systematic differences between the separate datasets of up to 3% are found (for global average ozone), although the deseasonalized total ozone deviations agree to within 0.9% (95% confidence). Overall, each of the total ozone datasets gives similar estimates of large-scale changes; each of the datasets is included in the figures below, and the spread between them gives an estimate of the uncertainty due to measurement technique and sampling.

The total ozone deviations for the 60°S-60°N latitude belt are shown in Figure 4-2 (top), and corresponding results for the global mean (90°S-90°N) are shown in Figure 4-2 (bottom). All five datasets indicate very similar ozone variations, with differences typically less than 0.5%. The global ozone (60°S-60°N or 90°S-90°N) amount shows overall decreasing values between the late 1970s to early 1990s, a relative minimum during 1992-1994, and a slight increase during the late 1990s. A relatively large decadal variation of global total ozone is seen in Figure 4-2, which is likely associated with the 11-year solar cycle (e.g., Chandra and McPeters, 1994; Bojkov and Fioletov, 1995; see further discussion in Section 4.2.6). Figure 4-3 shows the deseasonalized global anom-

GLOBAL OZONE

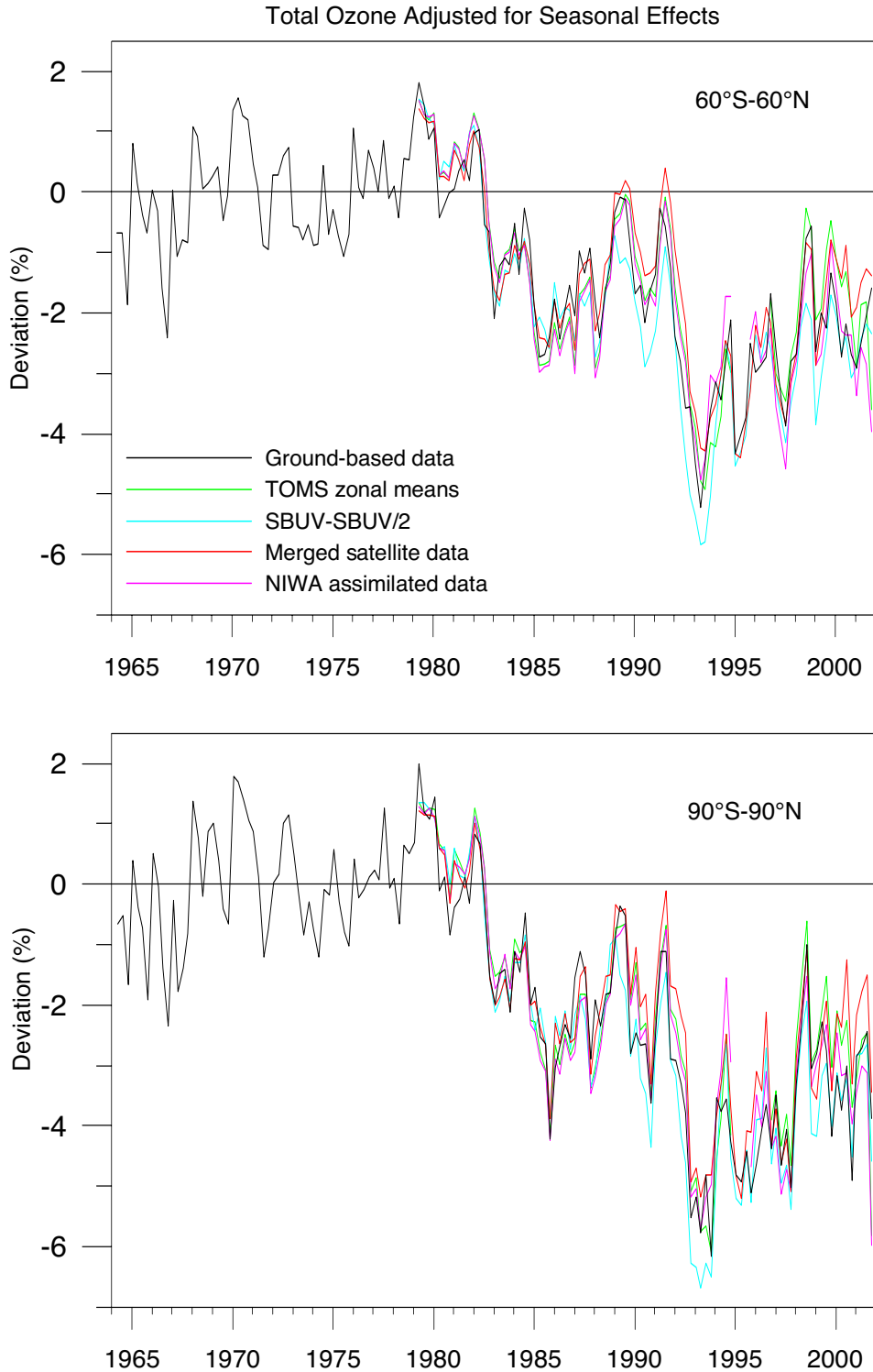


Figure 4-2. Deseasonalized, area-weighted seasonal (3-month average) total ozone deviations, estimated from five different global datasets. Each dataset was deseasonalized with respect to the period 1979-1987, and deviations are expressed as percentages of the ground-based time average for the period 1964-1980. Results are shown for the region 60°S-60°N (top) and the entire globe (90°S-90°N) (bottom). The different satellite datasets cover 1979-2001, and the ground-based data extend back to 1964. TOMS, Total Ozone Mapping Spectrometer; SBUV, Solar Backscatter Ultraviolet; NIWA, National Institute of Water and Atmospheric Research (New Zealand). Adapted from Fioletov et al. (2002).

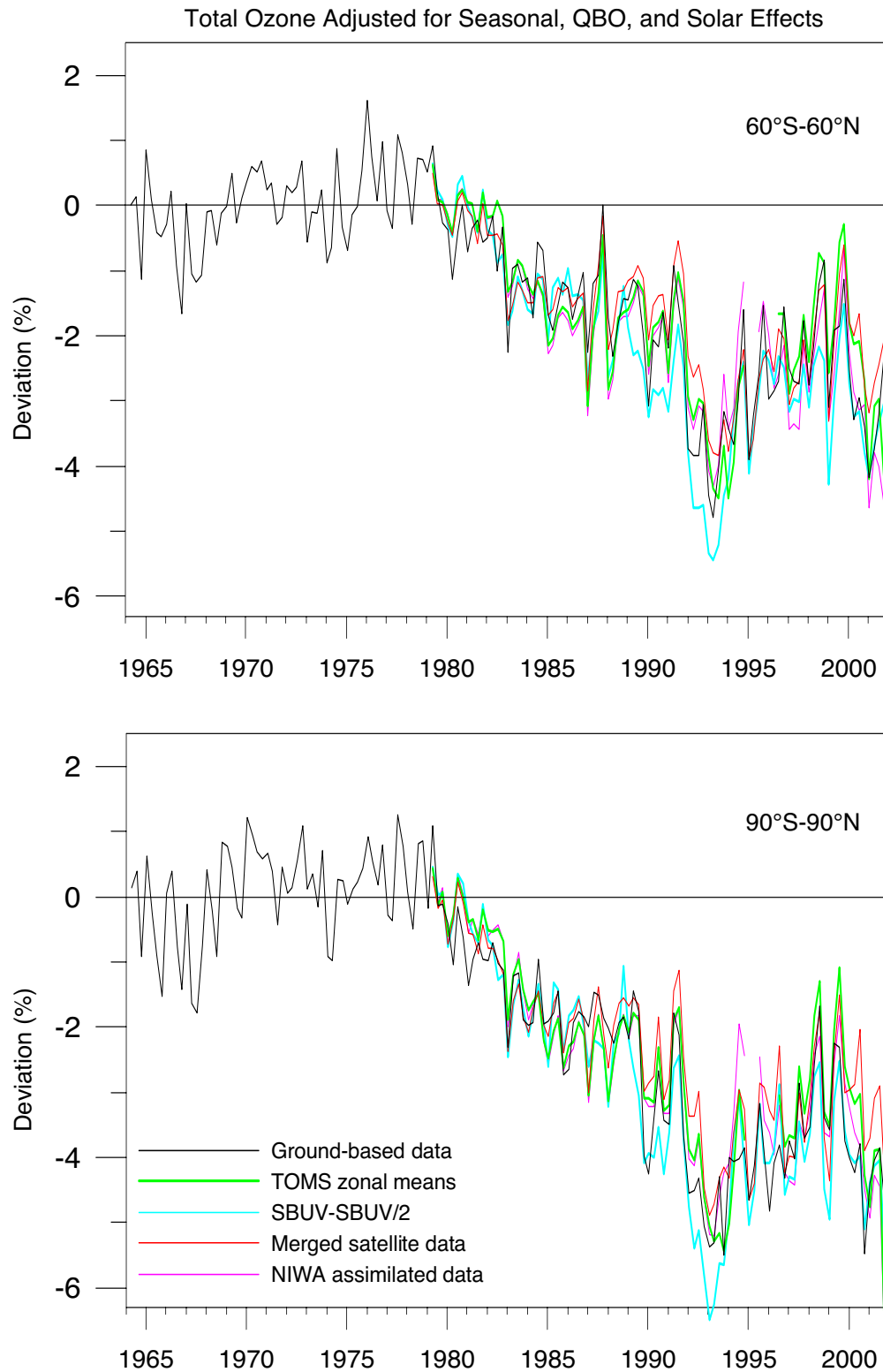


Figure 4-3. Deseasonalized, area-weighted total ozone deviations from five datasets (as in Figure 4-2), adjusted for solar and QBO effects, for the region 60°S-60°N (top) and the entire globe (90°S-90°N) (bottom). The solar and QBO effects were estimated using the ground-based data only and subtracted from all five datasets. Adapted from Fioletov et al. (2002).

GLOBAL OZONE

alies, after statistical removal of the solar cycle and quasi-biennial oscillation (QBO)-related variations (based on standard regression analyses, as discussed in detail in SPARC (1998)). The details of the solar cycle statistical fit, and possible aliasing of solar and volcanic signals in ozone, are discussed in detail in Section 4.2.6. The time series in Figure 4-3 show that the residual global ozone variability can be described by an approximately linear decline from the late 1970s to the early 1990s, a minimum during 1992-1994, increases during the late 1990s, and relatively low values in 2000-2001. The global ozone levels for the years 1998-1999 are similar to those of the early 1980s, but about 2% lower than the late 1970s values. However, the relatively low global ozone values in 2000-2001 suggest caution in interpreting the higher values for 1998-1999. A smoothed version of the global ozone anomalies is shown in Figure 4-4, based on applying four passes of a 13-month running mean to the global anomalies in Figure 4-3. These smoothed time series highlight the low-frequency interannual changes, and provide concise estimates of global ozone changes for comparison with the assessment model results in Section 4.5.

About 40% of global ozone is located in the tropics between 25°N-25°S, and variability in this region over the period 1979-2001 is shown in the middle curves of Figure 4-5. There is a strong decadal variation of total ozone in the tropics, with peak-to-trough variations of approximately 3%, and maxima approximately in phase with the 11-year solar cycle (top panel in Figure 4-5). After statistical removal of the solar signal (bottom curves in Figure 4-5), the residual tropical ozone shows a 1-2% decline in ozone during ~1992-1993, followed by an increase back to pre-1990 values. Significant long-term trends in tropical total ozone have not been observed for the period 1979-2001. H.J. Wang et al. (2002) find weak negative trends ($-1.2 \pm 0.8\%/decade$) in the tropics (20°N-20°S) using vertically integrated Stratospheric Aerosol and Gas Experiment (SAGE) II ozone (15-50 km) for 1985-2000. Although these trends are different from the near-zero trends derived for column ozone, uncertainty levels do overlap.

Figure 4-6 shows deseasonalized ozone values integrated over the 35°-60°S and 35°-60°N latitude belts. These time series show that ozone levels in the late 1990s are several percent lower than in the late 1970s in the mid-latitudes of both hemispheres, although there is a large degree of year-to-year variability in both cases. Smoothed versions of these time series are shown in Figure 4-7. Time series over NH midlatitudes show an overall decrease in ozone beginning in the early 1980s, pro-

nounced negative ozone anomalies during ~1992-1996, and a partial rebound thereafter. The minimum from ~1992-1996 in the smoothed time series (Figure 4-7) is associated with several individual winters of low ozone over midlatitudes during that time, namely 1991/1992, 1992/1993, and 1994/1995. The large anomalies in 1991/1992 and 1992/1993 have been associated with the Mt. Pinatubo volcanic eruption in June 1991 (e.g., Brasseur and Granier, 1992; Gleason et al., 1993; Hofmann et al., 1994).

Total ozone changes in the midlatitude SH also show a general decline after ~1980 (Figure 4-7), but the time series show a more consistent and gradual decline than in the NH. Net ozone levels in the SH midlatitudes are currently ~6% lower than pre-1980 values. It is especially interesting that the large negative anomalies observed in the NH extratropics during 1992-1996 are not particularly evident in the SH. Furthermore, there are relatively large negative anomalies in the SH during ~1985-1986, which lead to anomalies in the smoothed time series extending over several years (Figure 4-7), with the result that the low-frequency midlatitude variability is quite different between the hemispheres.

4.2.2.2 SEASONAL CHANGES IN TOTAL OZONE

The seasonal changes of total ozone changes over 35°-60°N and 35°-60°S are shown in Figure 4-8, for the time period 1979-2001. A high degree of year-to-year variability is observed during the dynamically active winter and spring periods in each hemisphere: December-January-February (DJF) and March-April-May (MAM) in the NH; June-July-August (JJA) and September-October-November (SON) in the SH. In the NH the largest absolute changes are observed during winter (DJF) and spring (MAM), with maximum deviations during the early to middle 1990s of -6 to -12%. During NH summer (JJA) and fall (SON) the interannual changes show similar time variation (with maximum anomalies during ~1992-1997), but the magnitudes of ozone changes are less (about -3 to -5%). Total ozone changes in the SH midlatitudes in Figure 4-8 show a systematic decline during all seasons, and relatively less seasonal dependence compared with the NH. Although natural variability is highest during SH winter (JJA) and spring (SON), there is relatively little difference for long-term changes between these active seasons and SH summer-fall. Thus the characteristic seasonal signatures of long-term ozone loss are distinct between the NH and SH. Seasonally varying trend calculations are consistent with these time series results, and results for NH and SH midlatitudes are shown in Section 4.5.3.

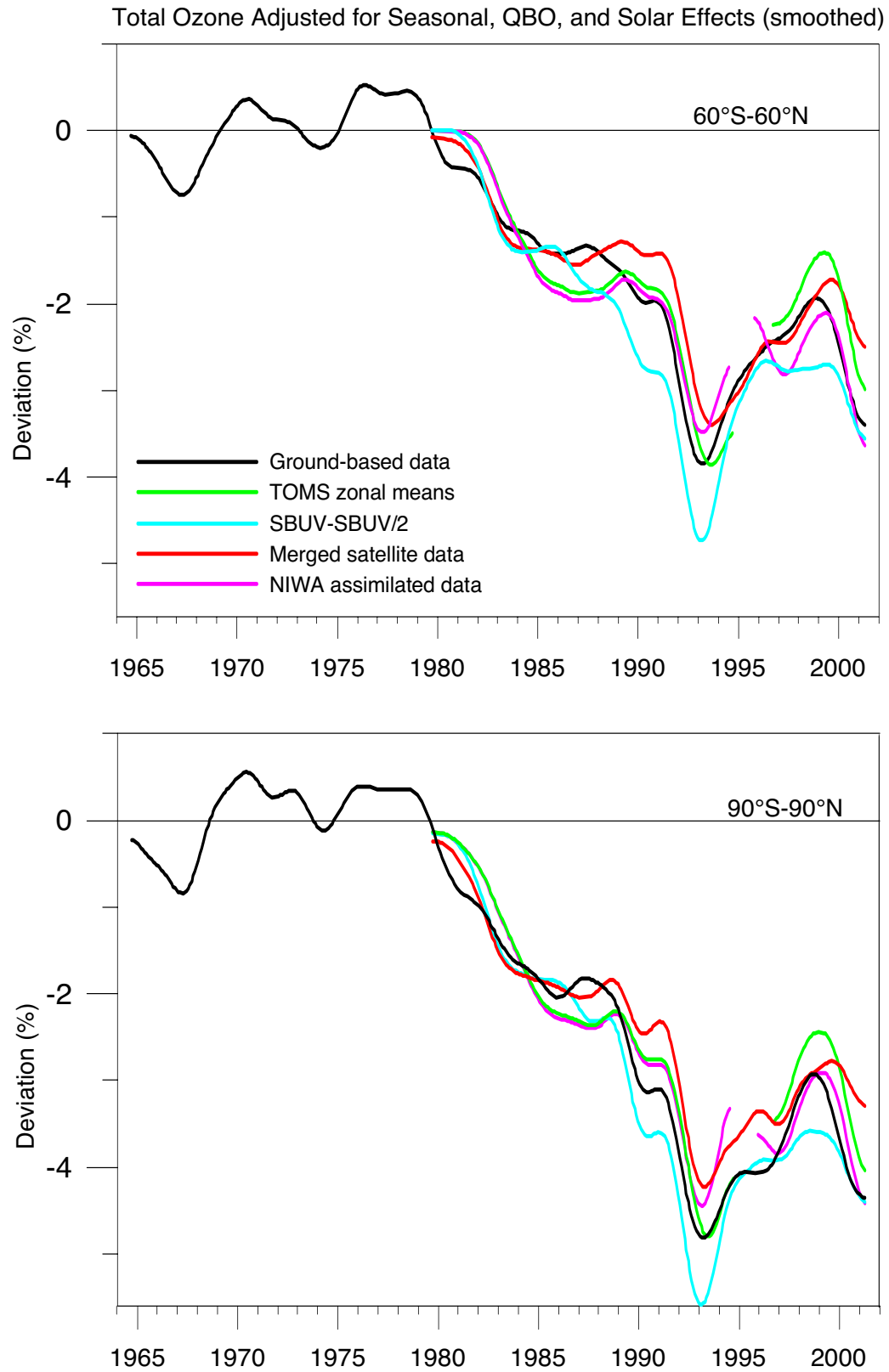


Figure 4-4. Deseasonalized, area-weighted total ozone deviations, adjusted for solar and QBO effects (as in Figure 4-3), smoothed in time using four passes of a 13-month running mean to highlight the lowest frequency interannual variations. Adapted from Fioletov et al. (2002).

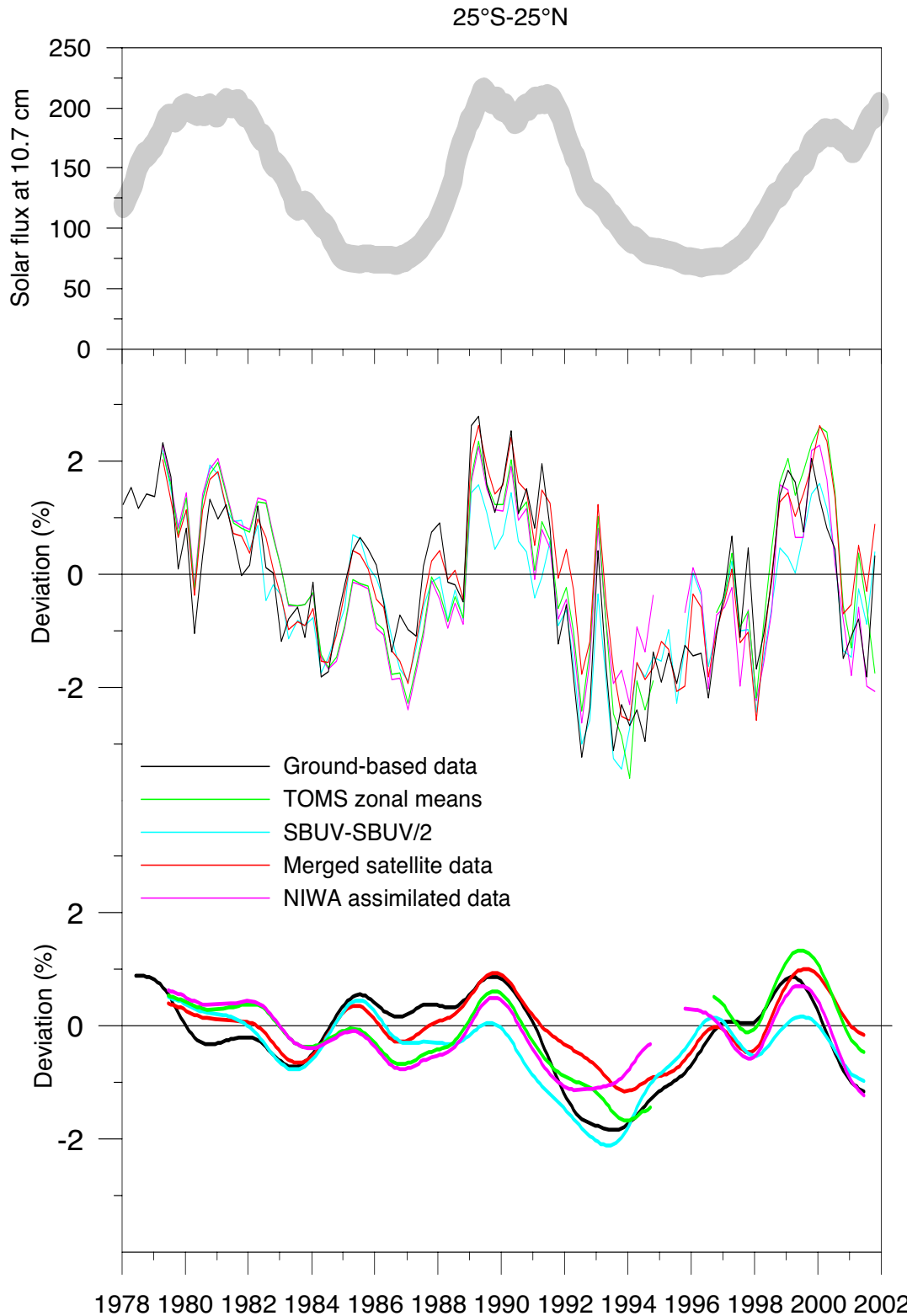


Figure 4-5. Upper curve: The smoothed solar flux at 10.7 cm, shown as a proxy for solar cycle variability. Middle curves: Deseasonalized, area-weighted total ozone deviations from the five datasets for the latitude range 25°S-25°N. Anomalies were calculated with respect to the ground-based data during 1964-1980. Lower curves: Deseasonalized data with the effect of the solar cycle removed by statistical regression, and then smoothed by four passes of a 13-month running mean. Adapted from Fioletov et al. (2002).

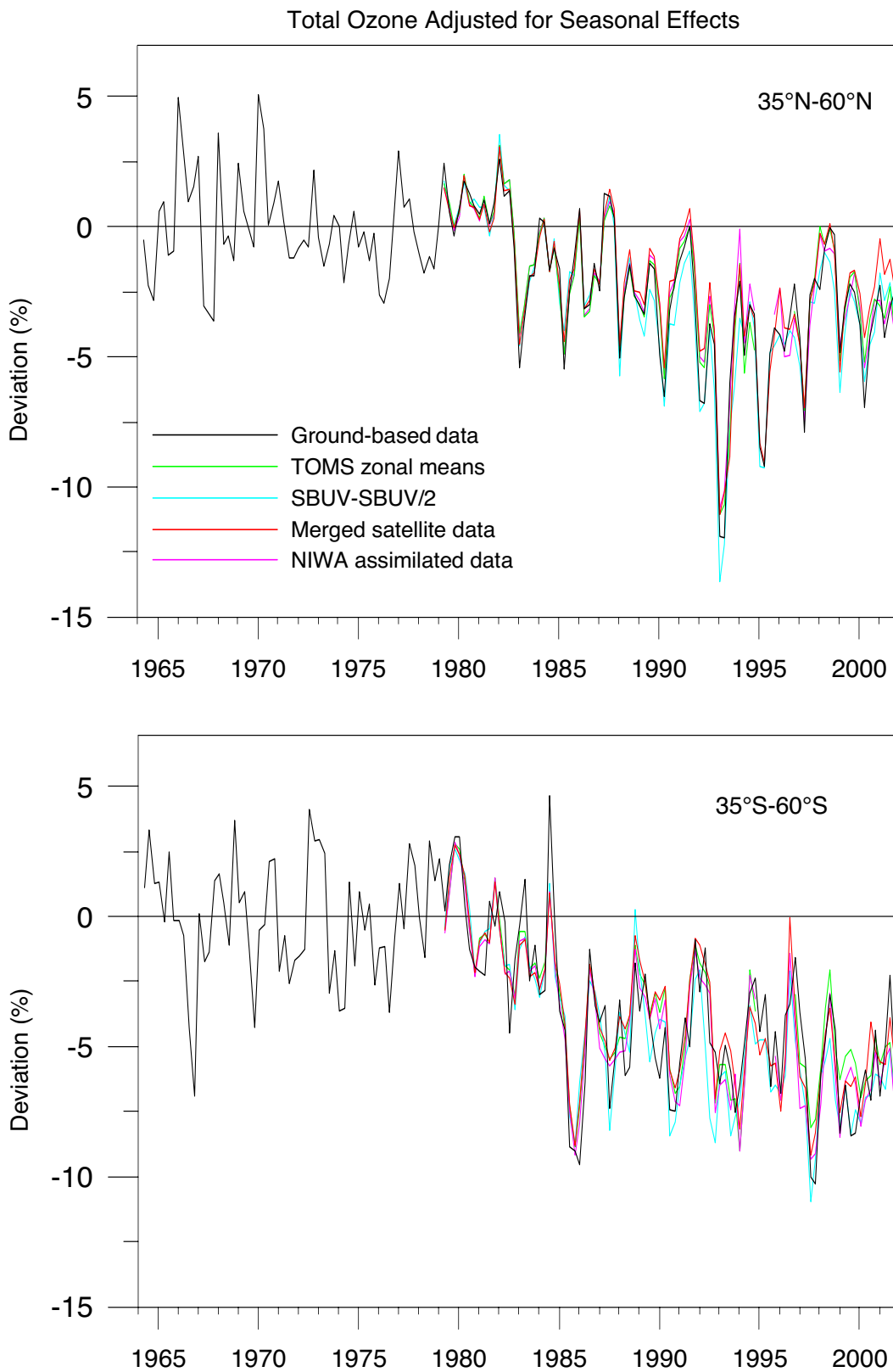


Figure 4-6. Deseasonalized, area-weighted total ozone deviations from five datasets for the latitude bands 35°N-60°N (top) and 35°S-60°S (bottom). Anomalies were calculated with respect to the time average during 1964-1980. Adapted from Fioletov et al. (2002).

GLOBAL OZONE

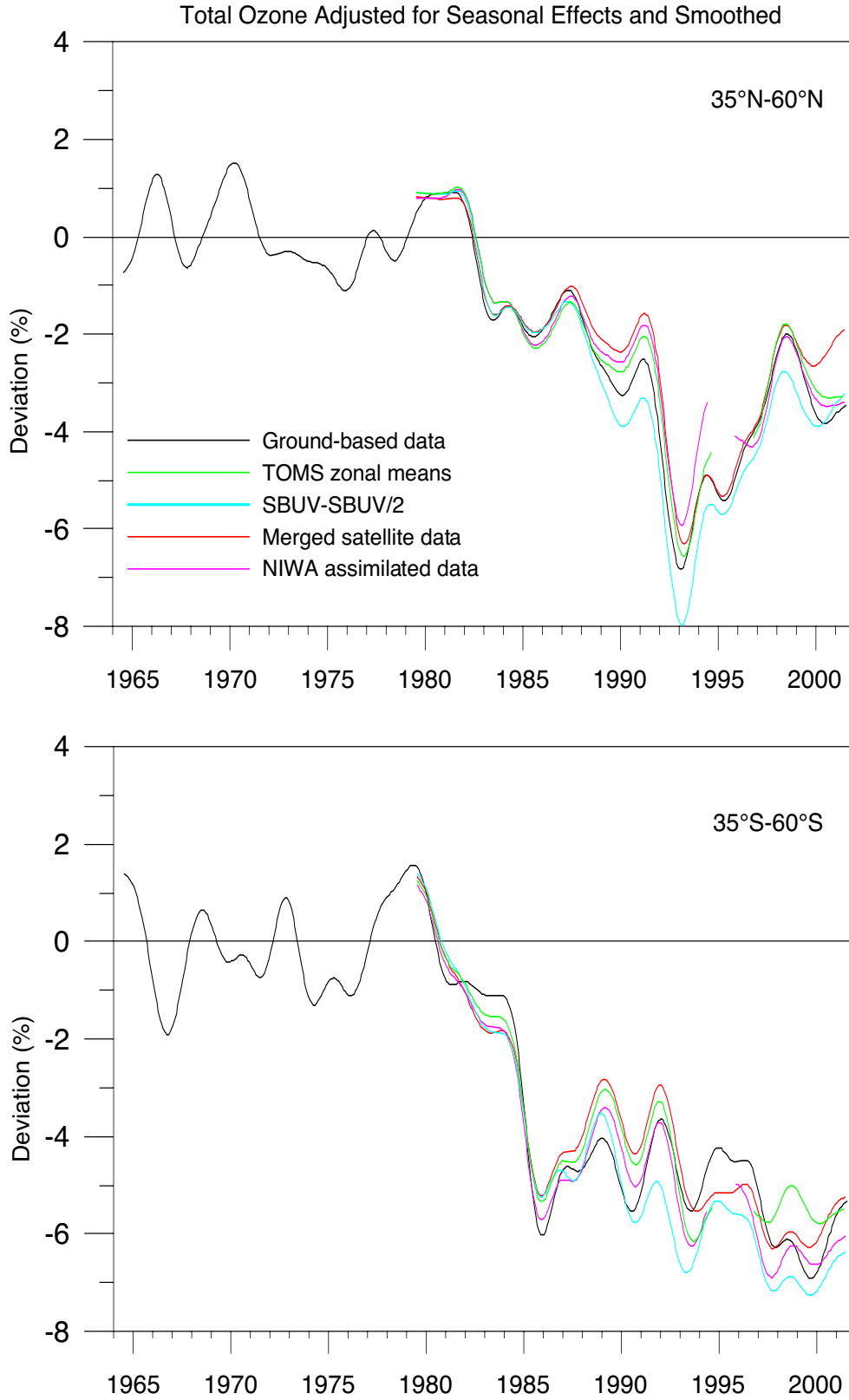


Figure 4-7. Deseasonalized, area-weighted total ozone deviations for the midlatitude regions of 35°N-60°N (top) and 35°S-60°S (bottom) (as in Figure 4-6), but smoothed by four passes of a 13-point running mean. Adapted from Fioletov et al. (2002).

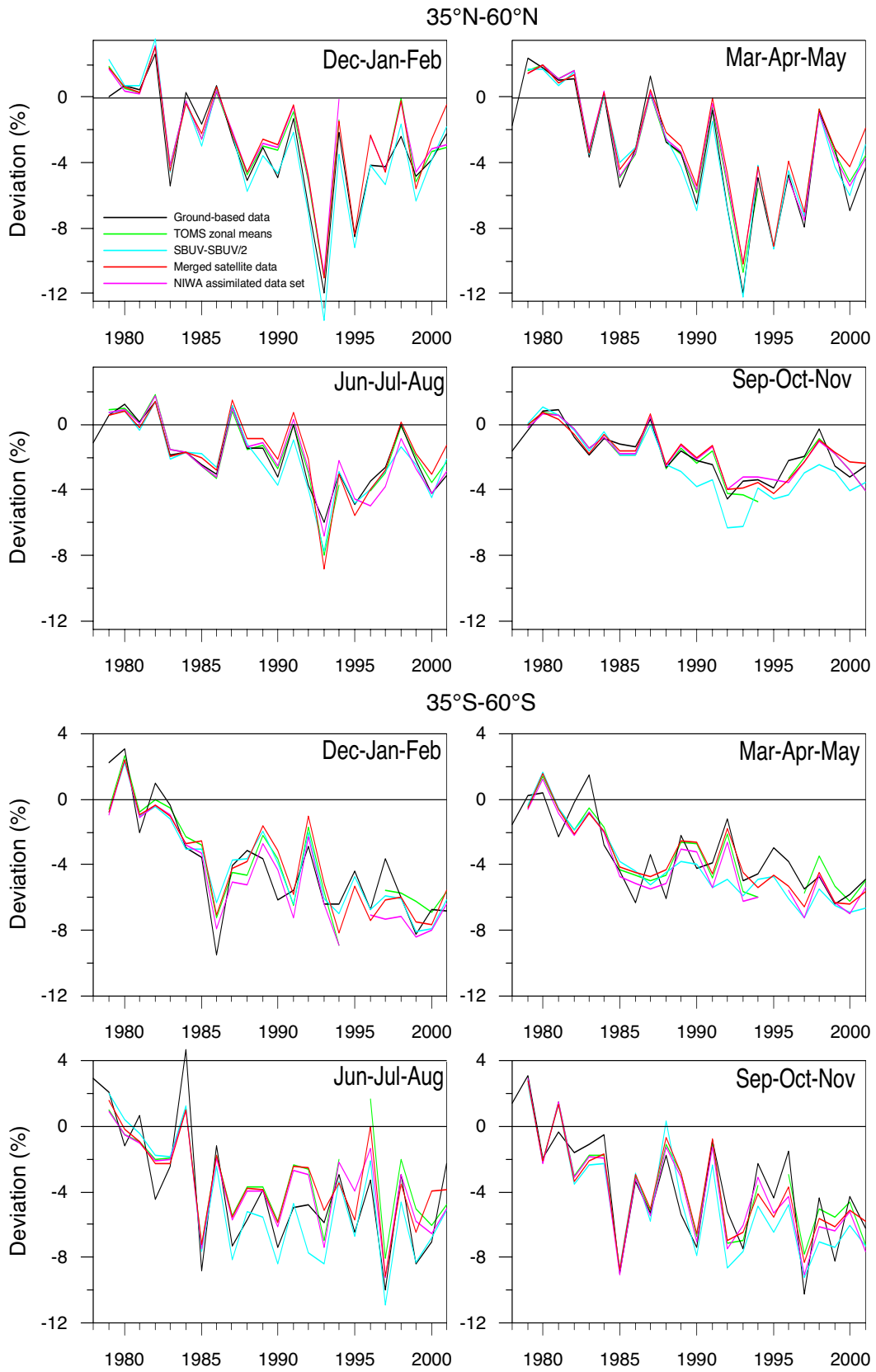


Figure 4-8. Area-weighted total ozone deviations from the 1964-1980 means, calculated for four seasonal averages, for the latitude bands 35°N-60°N (top) and 35°S-60°S (bottom). Adapted from Fioletov et al. (2002).

GLOBAL OZONE

4.2.3 Changes in the Vertical Profile of Ozone

Changes in the vertical profile of ozone are a key part of the overall fingerprint that helps constrain the understanding of long-term ozone changes. The SPARC (1998) and WMO (1999) Assessments demonstrated that long-term changes in the ozone profile (for the period 1979-1996) have local maxima in the upper stratosphere (centered near 40 km) and lower stratosphere (15-20 km), with a relative minimum around 30 km. A similar result has been discussed by Smyshlyaev and Geller (2001) based on SAGE II measurements incorporated into a data assimilation model. The analyses here focus on updated ozone changes in the upper and lower stratosphere, using both time series and updated trend analyses (the latter are useful to highlight spatial patterns of change in sparse datasets, although the observed time variations are not linear). SAGE I+II data provide near-global measurements covering both regions, whereas the Umkehr and ozonesonde data provide independent information primarily over NH mid-latitudes. Trend calculations reported here use standard statistical analyses (SPARC, 1998).

4.2.3.1 UPPER STRATOSPHERE

SAGE I+II

A meridional cross section of the trends derived from the combined SAGE I (1979-1981) and SAGE II version 6.1 (v6.1) (1984-2000) data is shown in Figure 4-9. The overall pattern is very similar to previous SAGE I+II results that are based on shorter time records (e.g., the 1979-1996 results in WMO (1999)). The largest percentage changes are observed in the upper stratosphere (~35-45 km); maxima are in middle-high latitudes of both hemispheres, with a magnitude of about -5 to -7% /decade for the period 1979-2000. The 2σ uncertainty levels for these trends are of order $\pm 1-3\%$ /decade, depending on location. These trend maxima are slightly less than the WMO (1999) estimates, which are based on SAGE I+II data for 1979-1996. The region of significant negative trends in the upper stratosphere extends throughout the tropics, which is a change from previous results based on shorter time records (SPARC, 1998; WMO, 1999). There are no statistically significant differences between the upper stratospheric trends in the two hemispheres.

Trends derived from the SAGE II v6.1 data record alone (for the shorter period 1984-2000) are shown in

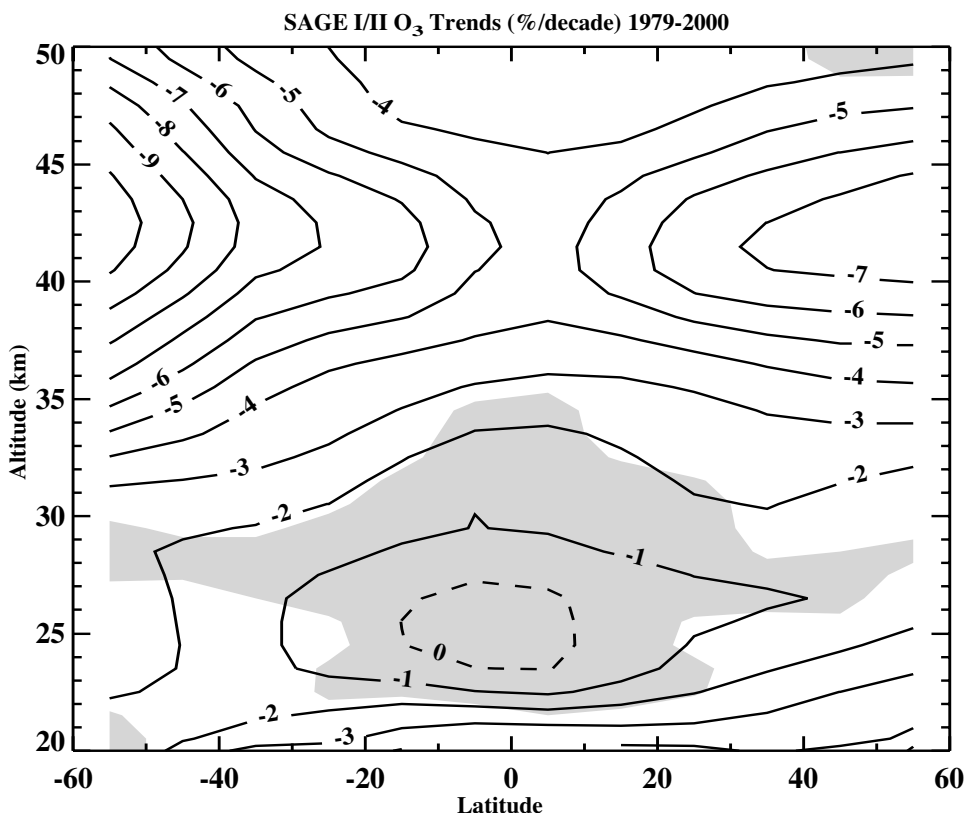


Figure 4-9. Meridional cross section of ozone profile trends derived from the combined SAGE I (1979-1981) and SAGE II (1984-2000) datasets. Trends were calculated in percent per decade, relative to the overall time average. Shading indicates that the trends are statistically insignificant at the 2σ (95%) level. Updated from H.J. Wang et al. (2002).

Figure 4-10. The spatial patterns of the trends are similar to the SAGE I+II record (Figure 4-9), but with smaller negative trends. Significant upper stratospheric trends for the 1984-2000 period extend into the tropics over 35-40 km. Upper stratospheric trends in the SH extratropics are somewhat more negative than those in the NH, but the differences are not statistically significant. At 40 km, the 30°-50°S trends are $-6.9 \pm 2.2\%$ /decade, while those over 30°-50°N are $-6.2 \pm 2.2\%$ /decade (2σ uncertainty). Time series of the SAGE I+II record in the upper stratosphere over 40°-50°N are shown in Figure 4-11 (integrated over 38-43 km, corresponding to Umkehr layer 8). The SAGE II data alone show a step-like change between ~1991 and 1993, with relatively constant ozone over ~1984-1991 and over ~1993-2000. Similar behavior is observed from SAGE data in SH midlatitudes (not shown). Inclusion of the SAGE I data (for 1979-1981) suggests an overall trend of approximately -5 to -7% per decade. Note that while the percentage changes in ozone are relatively high in the upper stratosphere (Figures 4-9 and 4-10), the associated contribution to the total ozone column change is relatively small (the changes over 1979-2000 in Figure 4-11 are less than 2 Dobson units (DU), compared with NH midlatitude column ozone changes of ~10-15 DU for the same period).

Umkehr

Umkehr ozone profile data have recently been reanalyzed using a new retrieval algorithm (Petropavlovskikh et al., 2001), and these data have been discussed in detail by Bojkov et al. (2002). Although historic Umkehr data are available from 13 sites, only a few have continuous long-term records free from significant discontinuities. Time series and trend analyses of Umkehr data here are estimated using the combination of measurements from Arosa, Switzerland (47°N), Boulder, Colorado, U.S. (40°N), Haute-Provence, France (44°N), and Belsk, Poland (52°N). The vertical structure of trends for the time period 1979-1999 in Figure 4-12 shows a maximum in the upper stratosphere (layer 8 trends of -5 to -7% /decade), a minimum near layer 5, and a separate maximum in the lower stratosphere. The vertical structure and magnitude of the trends are consistent with the SAGE I+II results in Figure 4-9. Umkehr trends for the shorter period corresponding to SAGE II (1984-1999) are smaller than those for 1979-1999 (layer 8 trends of -4 to -5% /decade), similar to the differences between the SAGE I+II and SAGE II-only results.

A time series of the deseasonalized Umkehr anomalies in Layer 8 (38-43 km) is included in Figure 4-11 for

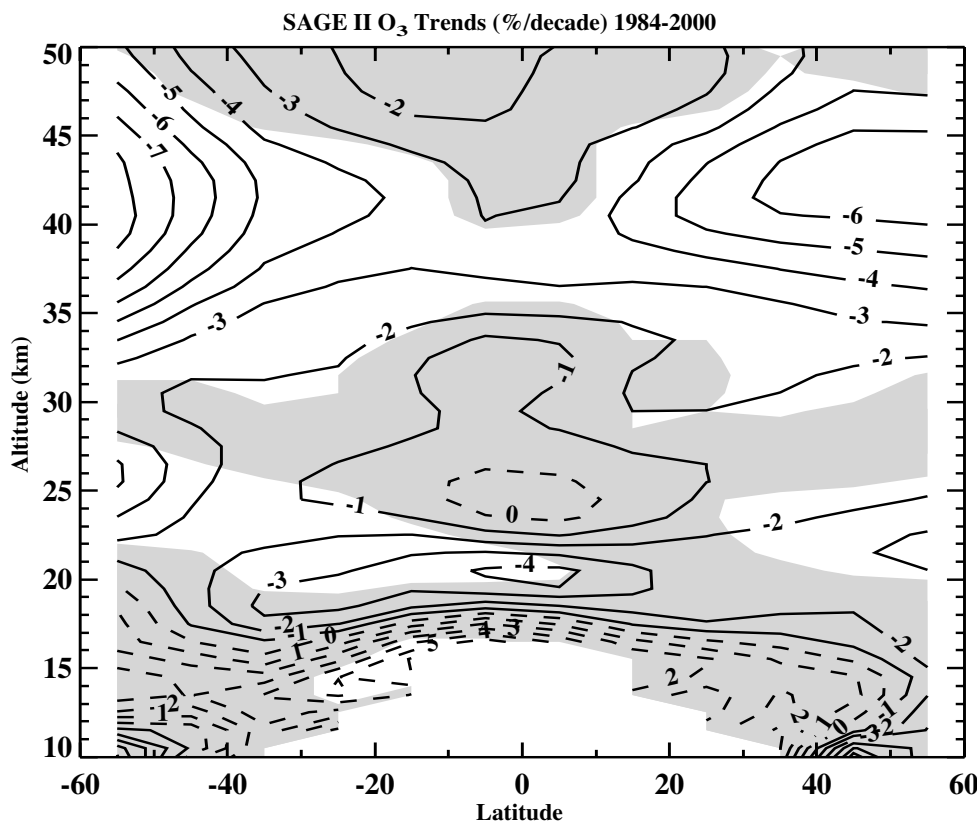


Figure 4-10. Meridional cross section of ozone profile trends derived from SAGE II v6.1 data for the period 1984-2000. Trends were calculated in percent per decade, relative to the overall time average. Shading indicates that the trends are statistically insignificant at the 2σ (95%) level. Updated from H.J. Wang et al. (2002).

GLOBAL OZONE

direct comparison with the SAGE I+II time series. There is a drop in the Umkehr ozone anomalies between 1982 and 1984 (of order $\sim -10\%$ background values), and a similar decrease is found in Nimbus-7 Solar Backscatter Ultraviolet (SBUV) spectrometer data covering 1979-1990 (Figure 3.12 of SPARC, 1998). There is a period of relatively constant Umkehr values over ~ 1984 -1994, and slight decreases after ~ 1995 . These latter decreases are not obvious in the SAGE II data, but direct comparisons of details between these time series are difficult due to the vastly different space-time sampling.

4.2.3.2 LOWER STRATOSPHERE

SAGE I+II

The SPARC (1998) analyses suggested that the SAGE I data are only of sufficient quality for trend studies above 20 km, so trend estimates with the combined SAGE I+II data cover 20-50 km. Trend estimates for 1979-2000 (Figure 4-9) show significant negative trends over the 20- to 25-km altitude region in the extratropics of both hemispheres, with magnitudes of -1 to -3% /decade. These trends are somewhat larger in the NH. The SAGE II data allow analyses to extend downward in altitude to the region of the tropopause (~ 10 km in the extratropics and ~ 16 km in the tropics). For the SAGE II period of 1984-2000, significant negative trends of order -2% /decade are observed in the lower stratosphere over approximately 20-25 km (Figure 4-10). However, significant extratropical trends are not found below ~ 20 km in either hemisphere for the 1984-2000 record.

Ozonesondes

Long records of ozonesonde observations (time series that extend back to at least the early 1970s) are available for 14 stations covering the latitude region 32° - 75° N (SPARC, 1998). Detailed trend analyses of these data for the periods 1970-1996 and 1980-1996 are discussed in SPARC (1998), Logan et al. (1999), and WMO (1999). For both time periods these results reveal significant negative trends that maximize in the lower stratosphere (over pressure levels ~ 200 -50 hPa, or altitudes ~ 12 -20 km). Trends for the period 1980-2000 have been compared with those for 1980-1996 (based on stations in the latitude range 36° - 59° N), and there are notable differences in the trends with the inclusion of 4 additional years of data (Figure 4-13). The difference in trends is largest in the lower stratosphere over ~ 200 -80 hPa (where the 1980-1996 trends are most negative): the mean decrease in stratospheric ozone for 1980-2000 is 5% /decade at 80

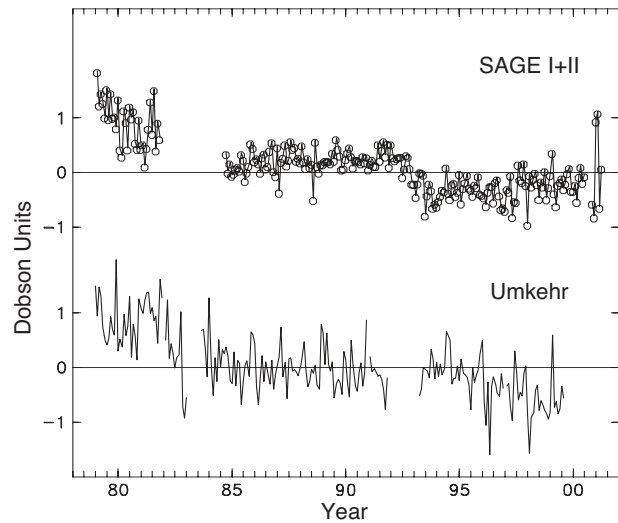


Figure 4-11. Top: Time series showing deseasonalized ozone anomalies over latitudes 40° N- 50° N, derived from SAGE I+II data integrated over altitudes 38-43 km. Bottom: Time series derived from an average of Umkehr measurements at Arosa, Boulder, Belsk, and Haute-Provence, for data in Umkehr layer 8 (approximately 38-43 km).

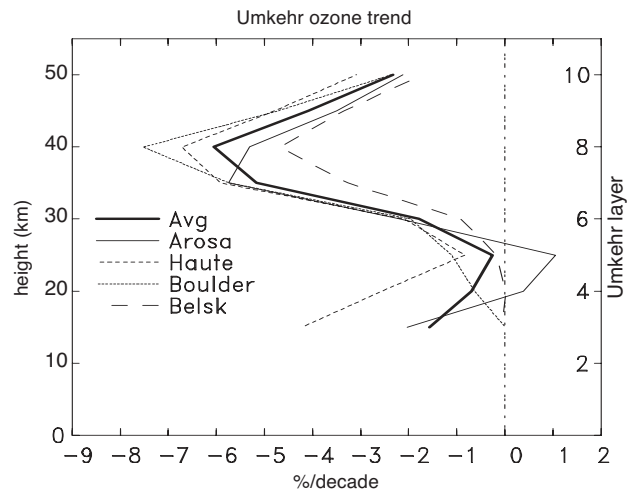


Figure 4-12. Vertical profile of ozone trends derived from Umkehr measurements at Arosa (1979-1999), Haute-Provence (1984-1999), Boulder (1979-1999), and Belsk (1979-1999). The dark line indicates the average trend. The 2σ (95%) uncertainty levels are near $\pm 3\%$ /decade throughout the profile.

hPa, 2.5% /decade smaller than that for 1980-1996. In contrast, there is little change in the trend results for pressure levels near and above 50 hPa (altitudes above ~ 21 km). Comparison of trends for the two periods 1970-1996

and 1970-2000 gives results with similar vertical structure (not shown), but the magnitude of the differences is much less for the longer record.

The reason for the change in the magnitude of the trends as a function of altitude can best be understood by inspection of time series for monthly ozone anomalies. Figure 4-14 shows deseasonalized ozone anomalies for four ~3-km layers spanning the lower to middle stratosphere, derived from the average measurements at three European stations: Hohenpeissenberg, Germany (48°N); Uccle, Belgium (51°N); and Payerne, Switzerland (47°N). Time series at the upper levels (63-40 hPa and 40-25 hPa) show a relatively continuous ozone decline throughout the record. In contrast, ozone in the lower stratosphere (the 158-100 hPa and 100-63 hPa levels) shows a decrease through the early 1990s, with relatively constant levels thereafter. Similar time series results are found for other locations. This flattening of the time series after ~1995 results in the reduced trends in the lower stratosphere for the 1980-2000 period compared with 1980-1996.

The longest continuous ozonesonde record in SH midlatitudes is from Lauder, New Zealand (45°S), covering the period 1986-2000. Figure 4-15 shows a time series of these data in 3-km layers, with similar format to the NH time series in Figure 4-14. While there is substantial interannual variability in these time series (much of it apparently related to the QBO), there are no significant stratospheric trends observed in the Lauder data for 1986-2000. This is somewhat different from the SAGE II trends in Figure 4-10 (showing negative trends over ~22-27 km near the latitude of Lauder), but direct comparisons are difficult in light of the very different space-time sampling. Note also that the lack of trends at Lauder for 1986-2000 is not inconsistent with the column ozone decreases seen

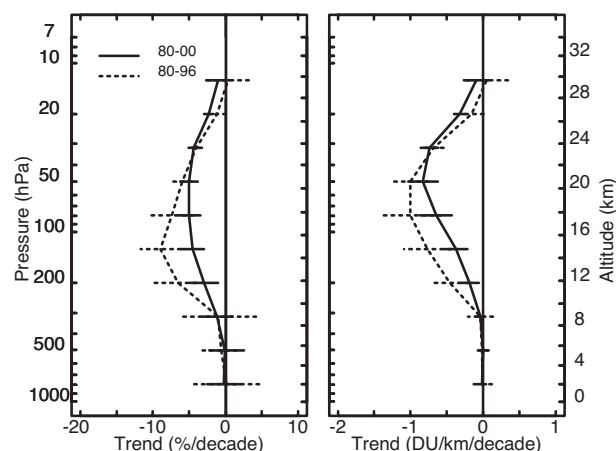


Figure 4-13. Annual mean profile of ozone trends for eight sonde stations located between 36°N and 59°N, for the time periods 1980-1996 and 1980-2000. Trend results are shown in percent per decade (left) and (DU/km/decade) (right). The 2σ error bars are shown.

in Figure 4-6, because much of the column decrease occurs between the pre- and post-1984 periods.

4.2.4 Vertical Integral of the Profile Trends vs. Column Trends

The ozonesonde results show that the largest contribution to interannual column ozone changes (over NH midlatitudes) occurs in the lower stratosphere, over approximately 160-40 hPa (13-23 km). To quantify that result, and directly compare the profile-versus-column ozone changes over NH midlatitudes, Table 4-1 shows the

Table 4-1. Comparison of vertically integrated ozone profile trends (DU/decade) over NH midlatitudes derived from ozonesondes (an average of eight stations over 36°-59°N), zonal mean SAGE I+II (35°-60°N), and zonal mean column ozone (35°-60°N), for the period 1980-2000. Results are calculated for seasonal and annual means. Column ozone trends are calculated from the merged satellite data. The 1σ uncertainty estimates are included in parentheses.

Altitude	Ozone Profile Trends (DU/decade)				
	DJF	MAM	JJA	SON	Annual
25-50 km (SAGE I+II)	-3.8 (0.9)	-2.0 (0.9)	-0.9 (0.9)	-2.1 (0.9)	-1.7 (0.5)
10-25 km (ozonesondes)	-8.5 (3.3)	-13.2 (2.8)	-6.8 (1.8)	-4.1 (1.6)	-8.2 (1.3)
0-10 km (ozonesondes)	+0.9 (0.6)	-0.2 (0.9)	-1.2 (0.9)	-0.2 (0.5)	-0.2 (0.4)
Column (merged satellite)	-9.0 (3.0)	-10.9 (2.8)	-5.9 (2.0)	-4.0 (1.7)	-7.4 (1.2)

GLOBAL OZONE

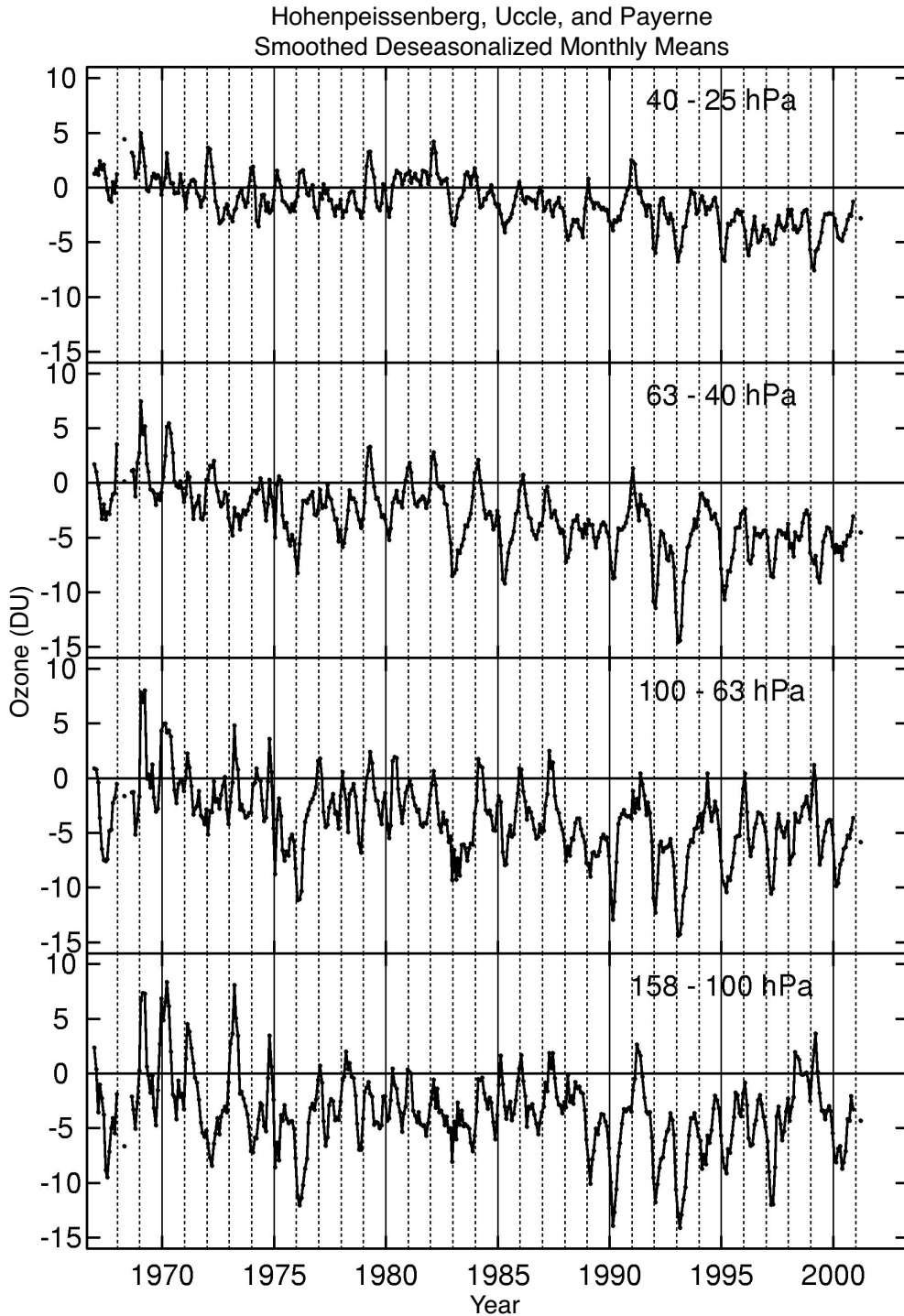


Figure 4-14. Time series of deseasonalized ozone anomalies for four altitude (pressure) layers, each approximately 3 km thick, based on ozonesonde measurements at three European stations (Hohenpeissenberg, Uccle, and Payerne). Anomalies were calculated with respect to 1970-1971.

vertical integral of the profile trends derived from ozonesondes (integrated over 10-25 km), compared with the zonal mean trends derived from the merged satellite data (these results are very similar to trends derived from the other column ozone datasets, as shown in Fioletov et al. (2002)). Also included are the integrated trends from SAGE I+II (over 25-50 km), to quantify the contribution of US ozone losses to the column trends, and tropospheric

ozone trends calculated from ozonesondes integrated over 0-10 km. Trends are calculated from all data for the period 1980-2000 (to directly compare with the ozonesonde results), and both seasonal and annual mean results are shown.

The integrated profile and column ozone trends in Table 4-1 show a number of important features. Ozone trends in the upper stratosphere (>25 km) derived from

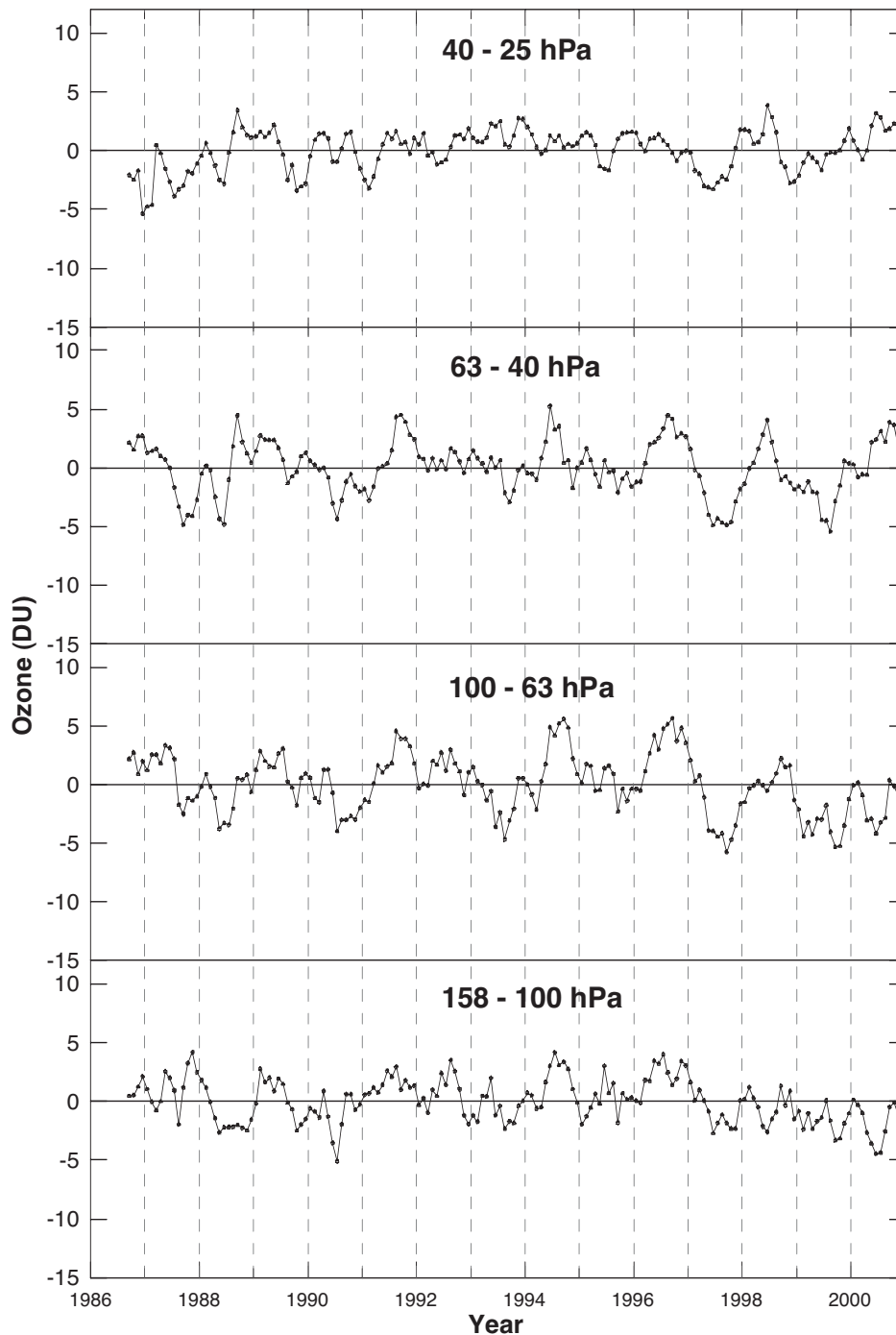


Figure 4-15. Time series of deseasonalized ozone anomalies for four altitude (pressure) layers, each approximately 3 km thick, based on ozonesonde measurements at Lauder, New Zealand.

SAGE I+II data are relatively small (of order ~ -2 -3 DU/decade), and account for a small fraction (15-30%) of the observed column losses. Tropospheric ozone trends do not contribute substantially to the column. There is reasonable agreement between the integrated ozonesonde trends (over 10-25 km) and column trends in terms of seasonality (largest losses in NH winter-spring), but less agreement in terms of magnitude. Partial column trends for 10-25 km calculated from the ozonesonde data are

consistently larger than the total column trends, for most seasons and for the annual mean. The agreement with the total column trends is even worse if the ozone losses above 25 km are included. The reason for the disagreement is not understood, but is likely related to the sparse sampling of the ozonesondes (only eight stations are included in these calculations). Note that the individual ozonesonde profile integrals are constrained to match co-located Dobson measurements, and hence the integrated profile

GLOBAL OZONE

trends will necessarily match the Dobson trends for these eight stations. The fact that the aggregated ground-based data from ~50 stations agree well with the zonal mean satellite data (e.g., Figure 4-6) suggests spatial sampling is at the root of the quantitative imbalances in Table 4-1. In any case, these results show that the major part of NH midlatitude column ozone trends is due to loss in the lower stratosphere (below 25 km), as stated in all previous Assessments.

4.2.5 Tropospheric Ozone

Trends in tropospheric ozone were discussed in detail in the previous Assessment (WMO, 1999), and here we summarize the key points from that report and provide a brief update. Trends in tropospheric ozone are highly variable and depend on region and on the time period considered (e.g., Logan et al., 1999; Oltmans et al., 1998; Tarasick et al., 1995). There were decreases or zero trends at the Canadian stations for 1970-1996, and decreases of -2 to -8%/decade for the mid-troposphere for 1980-1996. The three European stations showed increases for 1970-1996, but trends were close to zero for two stations for 1980-1996, and positive for one. There were increases in ozone for the three Japanese stations for 1970-1996, but trends were either zero or positive for 1980-1996. Time series of ozone given in Logan et al. (1999) and Oltmans et al. (1998) show that much of the increase in ozone in the middle troposphere over Europe occurred before the mid-1980s.

Trends have been calculated for 1970-2000 and for 1980-2000 and compared with those given by Logan et al. (1999) for the periods ending in 1996. The addition of 4 years of data makes the tropospheric trends for 1970-2000 less negative for the Canadian stations, and makes the trends statistically insignificant at Edmonton and Churchill (these stations have data starting in 1973). The extra 4 years of data make the trends for the European and Japanese stations slightly less positive. For the period 1980 to 2000, there is no significant trend in mid-tropospheric ozone for the Canadian stations, the U.S. stations, two Japanese stations, and one European station, Uccle; Hohenpeissenberg, Germany, gives a small decrease in tropospheric ozone, about 4%/decade, and Payerne, Switzerland, an increase of about 8%/decade. The lack of trend shown at most stations for 1980-2000 is responsible for the zero mean tropospheric trend shown in Figure 4-13 for the stations located between 36°N and 59°N.

Updated time series for tropospheric ozone (integrated over 1-10 km) are shown for three stations, in Europe, Canada, and Japan, in Figure 4-16. At Hohenpeissenberg, ozone has been lower in the past few years than the values reached in the mid-1980s and in

1996. All three European stations show continuing ups and downs in the 1990s, but these are not correlated among the stations (unlike for the stratosphere, where the behavior among the three stations is highly correlated). The Canadian stations show interannual variability in the 1990s, but little long-term changes (e.g., Goose Bay in Figure 4-16); at most stations, values are lowest in 1992 and 1993, as they are in the stratosphere. Tarasick et al. (2000) find an increase in tropospheric ozone at all six Canadian stations, but the increase has occurred only since 1993. The Japanese stations (e.g., Tateno in Figure 4-16) show relatively little interannual variability in the 1990s. These results show that tropospheric ozone trends vary considerably depending on location and the time period under consideration.

4.2.6 Solar Cycle Effects on Ozone

Global ozone observations display both a long-term decline and considerable interannual variability on a decadal time scale, which is approximately in phase with the 11-year solar cycle (Figures 4-2 and 4-5). In order to accurately characterize decadal variations in global ozone, and most directly compare them with model results that do not include solar forcing, it is important to quantify the solar cycle effect in the observational record. However, this is difficult for two reasons. First, the global observational record is relatively short, containing only two or three solar cycles (somewhat more for ground-based measurements at a few isolated locations; e.g., Angell (1989)). Second, a complicating factor for the recent record is that the large volcanic eruptions of El Chichón (1982) and Mt. Pinatubo (1991) occurred near the declining phases of the solar cycle in 1982-1984 and 1992-1994, and therefore there is the possibility of aliasing the volcanic and solar effects on ozone (Solomon et al., 1996). In this section the structure of the solar cycle in the updated data record is analyzed, including the most recent solar maximum period during 1999-2001. The availability of data from 1995-2001 provides a new opportunity to distinguish solar from volcanic signals better than was previously possible, as this is a period of no new volcanic activity together with an additional solar maximum. Hence, we present an updated analysis that uses the added years to examine the structure and statistical significance of the estimated solar signal in ozone, and we discuss comparisons with idealized model simulations.

4.2.6.1 COLUMN OZONE

Changes in solar ultraviolet (UV) spectral irradiance directly modify the production rate of ozone in the upper stratosphere (e.g., Huang and Brasseur, 1993), and

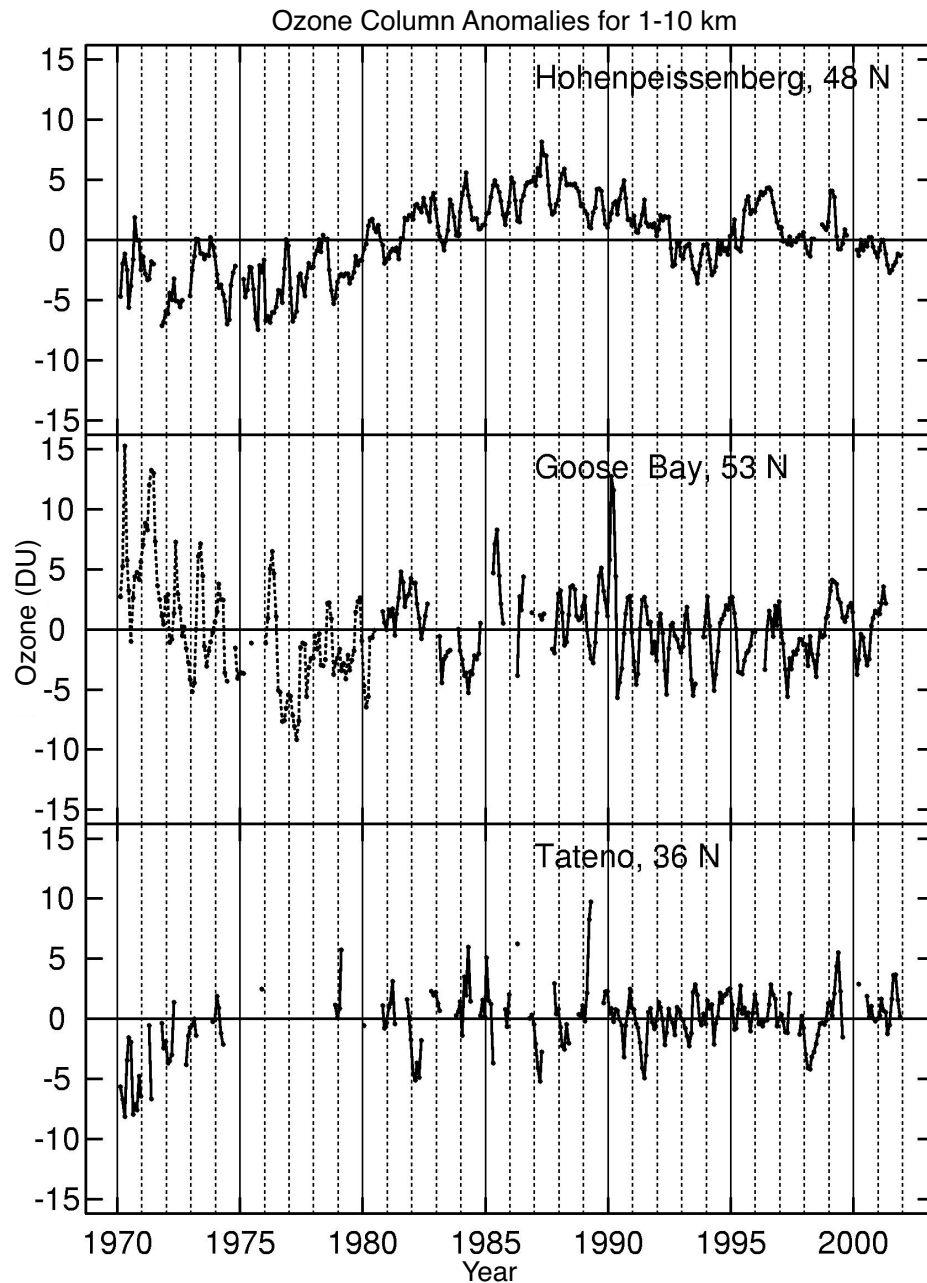


Figure 4-16. Time series of deseasonalized ozone anomalies for tropospheric column ozone, integrated between 1 and 10 km, for Hohenpeissenberg, Germany; Goose Bay, Canada; and Tateno, Japan. The dashed lines in the Goose Bay time series denote measurements by Brewer Mast ozonesondes, which were replaced by electrochemical concentration cell (ECC) measurements (solid lines).

hence it is reasonable to expect a solar cycle variation in total ozone amount. Analyses of ground-based records extending over three to six decades indicate the existence of a decadal time scale variation in column ozone, which is approximately in phase with the solar cycle (e.g., Angell, 1989; Miller et al., 1996; Zerefos et al., 1997). The global satellite records since 1979 show evidence for a decadal oscillation of column ozone with large amplitude at low latitudes (Chandra and McPeters, 1994; Hood et al., 1997; see also Figure 4-5). During at least the last three solar cycles, the decadal oscillation has been approximately in phase with proxies for solar ultraviolet flux,

and statistical representation is typically based on correlation with the 10.7-cm solar radio flux (F10.7).

The latitudinal structure of the solar cycle variation in column ozone derived from several updated datasets is shown in Figure 4-17. Here the solar cycle amplitude is derived from standard regression analyses (e.g., WMO, 1990), using F10.7 as a proxy for solar variability. These results are derived for several updated data including (1) the merged satellite data for 1979-2001, (2) the combined SBUV-SBUV/2 data, (3) the ground-based data for 1979-2001, and (4) the ground-based data for 1964-2001. Results based on the other satellite datasets

GLOBAL OZONE

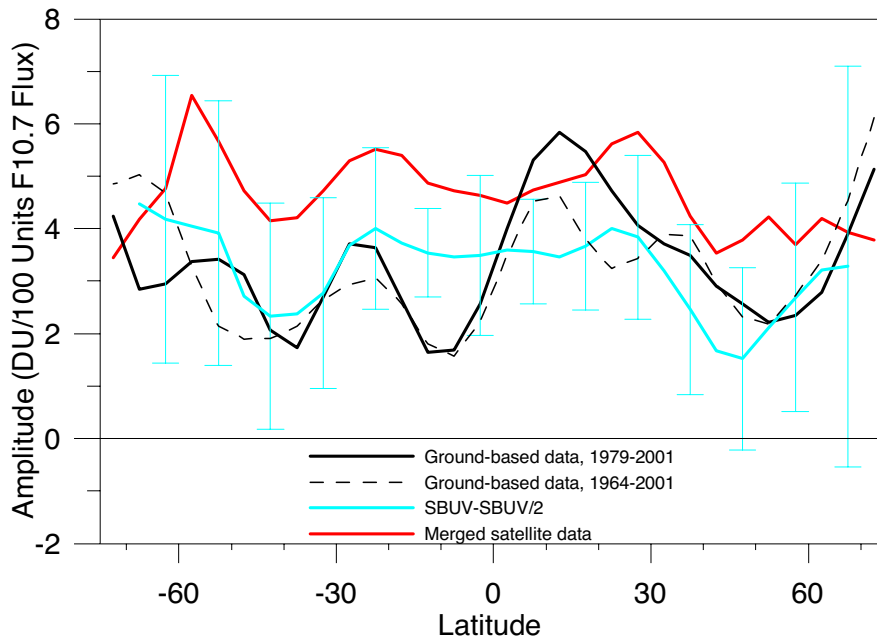


Figure 4-17. Latitudinal structure of the solar cycle regression coefficient calculated from the merged satellite data, SBUV+SBUV/2 data, and ground-based data for the period 1979-2001, and also from the longer record of ground-based data over 1964-2001. Error bars show 2σ regression uncertainty estimates for the SBUV+SBUV/2 results, and uncertainties for the other data are similar (not shown).

for 1979-2000 (which rely heavily on Total Ozone Mapping Spectrometer (TOMS) data) are similar to those from the merged satellite data and are not shown here. The derived solar cycle amplitude in Figure 4-17 from the satellite datasets shows a relatively flat latitudinal structure, with amplitudes in the tropics of approximately 5 DU/(100 units of F10.7) for the merged satellite data and 3.5 DU/(100 units of F10.7) for the SBUV-SBUV/2 data; the larger amplitude in the merged satellite data may be an artifact of the Nimbus-7 TOMS data, as discussed in Appendix 4A. Note that F10.7 varies from ~ 75 to ~ 200 units over a solar cycle (Figure 4-5), and therefore these derived amplitudes should be multiplied by ~ 1.25 to obtain the corresponding column ozone change over a solar cycle (tropical column ozone variations work out to approximately 2-3% between solar maximum and solar minimum). The statistical uncertainty of these fits is relatively large, with 2σ uncertainty levels of order $\pm 1-2$ DU/(100 units of F10.7) or larger, and the regression fits are most statistically significant in the tropics ($\sim 30^\circ\text{N}-30^\circ\text{S}$).

The solar cycle amplitudes derived from the ground-based data for both the 1964-2001 and 1979-2001 time periods are similar to each other, and have significantly more latitudinal structure than seen in the satellite data results. Results over the NH (where the ground-based data are most dense) show values roughly consistent with the range of satellite-derived values. However, in the less well sampled SH, the ground-based solar signal is smaller than that derived from the satellite data, ranging from 2 to 3 DU/(100 units F10.7). The similarity of results from the two time periods (1964-2001 and 1979-2001) shows

that an increase of sampling from two solar cycles to three does not strongly influence these empirical estimates.

Solar cycle variations in ozone have been studied in a number of idealized modeling studies (e.g., Huang and Brasseur, 1993; Fleming et al., 1995; Lee and Smith, 2002). While this is (conceptually) a straightforward calculation, given knowledge of the variations in solar spectral irradiance over a solar cycle (e.g., Lean et al., 1997), there are possible dynamical feedbacks in the stratospheric climate system that can complicate the full solar influence. In addition, because there is likely some confusion between direct solar forced and volcanic effects on ozone for recent decades (as demonstrated in the idealized model results in SPARC (1998)), it is useful to perform model simulations with and without realistic aerosol variations to study this influence.

The simulated solar cycle in column ozone shows similarity between different model results, with details depending on the specific model. Fleming et al. (1995) and Lee and Smith (2002) derive a solar signal in column ozone with broad latitudinal structure, and a solar maximum-to-solar minimum amplitude of 1.5-2% (corresponding to 3-5 DU / (100 units of F10.7)), which is in reasonable agreement with observations in Figure 4-17. Lee and Smith (2002) include realistic aerosol effects for 1979-2000, which slightly increases the apparent solar signal in their model, but primarily outside of the tropics.

4.2.6.2 VERTICAL PROFILE OF THE SOLAR SIGNAL

The dependence on altitude of the ozone solar cycle has been investigated using SAGE I+II data by H.J. Wang

et al. (1996) and SPARC (1998). The results show coherent, in-phase ozone variations in the upper stratosphere (~35-45 km), with local variations of ~2-4%/(100 units F10.7), and these values are not substantially changed by the update of the SAGE II data through 2000 (not shown). Similar overall results are obtained from the shorter record of SBUV+SBUV/2 data for 1979-1994 (Chandra and McPeters, 1994; SPARC, 1998), and from analyses of Umkehr data over NH midlatitudes (Miller et al., 1996). The results from both SAGE I+II and SBUV+SBUV/2 measurements show an upper stratospheric solar signal with a minimum in the tropics and maxima in midlatitudes of both hemispheres, which is different from the broad latitudinal structure derived in idealized model simulations (e.g., Huang and Brasseur, 1993). Lee and Smith (2002) have suggested that this pattern arises in the short satellite observational record because of aliasing with volcanic and possibly QBO effects. The SAGE I+II and SBUV+SBUV/2 analyses also suggest a solar signal in the tropical lower stratosphere, which is not simulated in idealized models; SPARC (1998, Section 3.4.2) suggests that signal may arise from volcanic aliasing effects.

4.2.6.3 SUMMARY

Both global observations and idealized model simulations show column ozone variations that are approximately in phase with the 11-year solar cycle. The calculations of Lee and Smith (2002) suggest that volcanic aerosol effects alias onto the solar cycle in column ozone for the 1979-2000 period, but the effect is not excessive in the tropics (<30%), where solar effects are most significant in observations. The amplitude of the modeled response in the tropics is broadly within the range of observations in Figure 4-17, i.e., ~3-5 DU/(100 units F10.7), although there is considerable uncertainty in details of the observed "signal." In spite of these uncertainties, the decadal variability in column ozone observed in the tropics (and in the global mean) is reasonably consistent with modeled solar variability, and model results suggest that the effect can be approximately isolated during 1979-2000 based on regression analyses. In contrast, there may be large uncertainties in isolation of the solar signal in the extratropics.

4.3 CURRENT UNDERSTANDING OF PAST CHANGES IN STRATOSPHERIC AEROSOL, WATER VAPOR, AND NO₂

Important components of the stratospheric climate system that directly influence ozone (and that are not dis-

cussed explicitly in Chapter 1) include stratospheric aerosol, water vapor, and nitrogen dioxide (NO₂). This section discusses the updated observations and current understanding of long-term changes in these constituents.

4.3.1 Stratospheric Aerosol Variability

Since the late 1970s, stratospheric aerosols have been observed by a variety of ground-based, in situ, and space-based instruments. In this two-decade time period, volcanic eruptions have strongly influenced stratospheric aerosol loading. The eruptions include those of El Chichón (Mexico, 1982) and Mt. Pinatubo (Philippines, 1991), the latter probably having the largest stratospheric impact of any volcano since Krakatau in 1883. On the other hand, stratospheric aerosol loading reached very low levels in the late 1970s, the late 1980s, and from the late 1990s to the present. On this time scale, stratospheric aerosol is perhaps the most variable component of the stratospheric composition. This variability is important because of the role aerosol plays in stratospheric ozone change through heterogeneous chemical processes as well as through aerosol-induced changes in stratospheric circulation.

Figure 4-18 shows a 25-year record of stratospheric aerosol variability based on integrated backscatter from the Fraunhofer Institute for Atmospheric Environmental Research (IFU) lidar (Jäger et al., 1995), together with 17 years of 1020-nm aerosol optical depth measurements by SAGE II. The dominant features are the 1982 eruption of El Chichón and the 1991 eruption of Mt. Pinatubo, which raised the integrated backscatter and aerosol optical depth values to more than 100 times their minimum values observed during this period. The effects of several smaller volcanic eruptions (indicated in the figure) can also be seen. The volcanic aerosols from the large tropical eruptions of El Chichón and Mt. Pinatubo were mixed relatively rapidly throughout the stratosphere, and time series over most of the globe are similar to those in Figure 4-18. With no significant eruptions after 1991, it is clear from Figure 4-18 that the relaxation to a nonvolcanic aerosol level lasted at least until 1999, i.e., more than 8 years. Therefore, with the possible exception of the late 1970s and the last few years, the entire record can be characterized as continual recovery from episodic volcanic injections of aerosol and their gaseous precursors (Bluth et al., 1992). This has made it extremely difficult to infer any long-term trends in aerosols associated directly with human activities or associated with other climate change phenomena. Longer-term measurements from individual stations (such as for the IFU lidar in Figure 4-18) show that current stratospheric integrated backscatter levels are

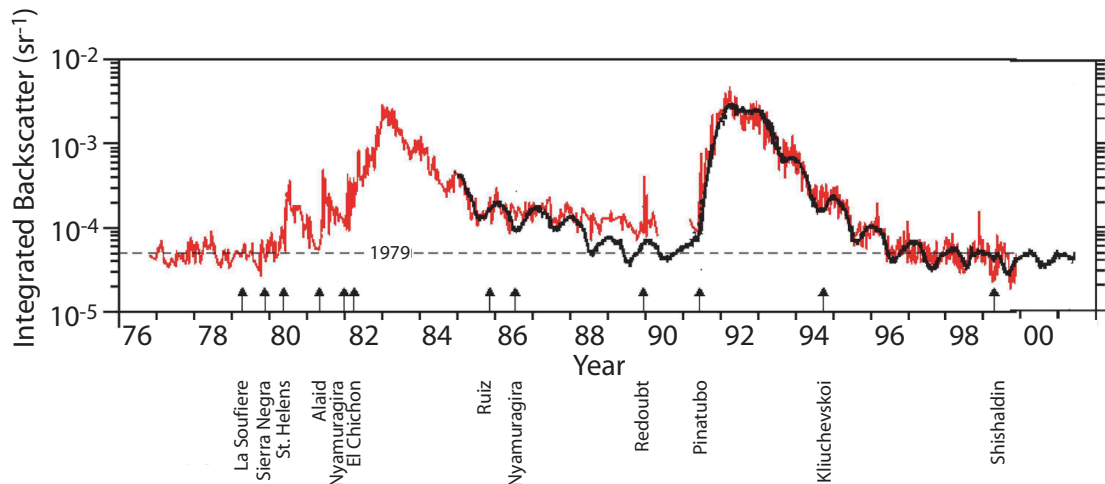


Figure 4-18. Multiyear time series of stratospheric aerosols measured by lidar (694.3 nm) at Garmisch (47.5°N, 11.1°E) in Southern Germany (red curve) and zonally averaged SAGE II stratospheric aerosol optical depth (1020 nm) in the latitude band 40°N-50°N (black curve). Vertical arrows show major volcanic eruptions. Lidar data are given as particle backscatter integrated from 1 km above the tropopause to the top of the aerosol layer. The curve referring to SAGE II data was calculated as optical depth divided by 40. For reference, the 1979 level is shown as a dashed line. Data from Garmisch provided courtesy of H. Jäger (IFU, Germany).

about the same or even less than those observed in the late 1970s, the period commonly considered the nominal stratospheric background period. Although various mechanisms have been suggested (e.g., Hofmann, 1990, 1991), there is currently no compelling evidence of a trend in the nonvolcanic aerosol loading, at least as it is measured by bulk parameters such as extinction or backscatter (Thomason et al., 1997).

The midlatitude records shown in Figures 4-18 reveal a clear annual cycle in addition to the long-term recovery from volcanic eruptions. In the tropics, the record mainly reflects monotonic decreases between volcanic events. However, during the recent clean period, an annual cycle in the column optical depth can be observed. The Climate Monitoring and Diagnostics Laboratory (CMDL) lidar record at Mauna Loa, Hawaii, shows an annual cycle during the current clean period that has been attributed to a transport of new material introduced into the tropics (Barnes and Hofmann, 2001).

Unlike instruments that measure ozone and most other stratospheric species, the instruments that quantify stratospheric aerosol often measure fundamentally different aerosol properties. Rather than measuring number density of a molecule, satellite-based instruments and aerosol lidar measure optical properties that arise from an underlying size distribution and composition that can only be indirectly inferred. As a result, assessing the quality of remotely sensed data and consistency between instruments can be challenging. This problem is illustrated in comparing the SAGE II 1020-nm stratospheric aerosol

optical depth with the IFU integrated backscatter in Figure 4-18 (with the optical depth divided by 40 for comparison). In most time periods the agreement between the two records is very good, because both capture the long-term recovery and the annual cycle. However, in the late 1980s the lidar value is nearly 50% larger than the adjusted SAGE II values. This could reflect the conversion between optical depth and backscatter (an extinction-to-backscatter ratio of 40), though it does not occur in a similar period in the 1990s, or it could reflect limitations in one or both instruments. However, the nature of the measurements makes an objective assessment difficult.

This problem has a direct impact on the assessment of the effect of aerosol on heterogeneous chemical processes and radiative/dynamical processes, and ultimately on ozone. The rates of most heterogeneous reactions are directly related to the aerosol surface area density, whereas extinction (i.e., total scattering plus absorption) is roughly proportional to aerosol volume density. Many models use a climatology of aerosol surface area and volume densities based on satellite observations as either direct input (e.g., Section 4.5.3) or as a verification of an internal simulation. Two long-term, global climatologies are derived from SAGE II and the Halogen Occultation Experiment (HALOE), which both use solar occultation measurements. SAGE II measures aerosol extinction in the visible and near-infrared, where extinction is dominated by scattering, whereas HALOE measures extinction in the infrared where extinction is dominated by aerosol absorption. Surface area and volume

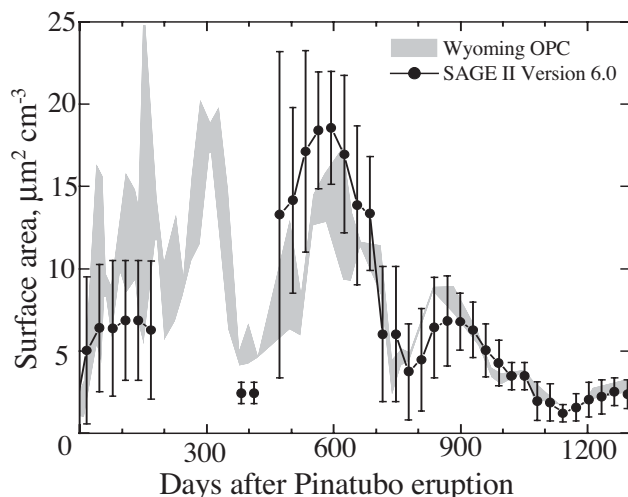


Figure 4-19. Comparison of surface area density inferred from the University of Wyoming optical particle counter (OPC) in Laramie, Wyoming, and that from SAGE II (zonally averaged between 35°N and 45°N). Figure updated from Thomason et al. (1997).

density data from these instruments agree reasonably well with data derived from the in situ optical particle counter (OPC) (Thomason et al., 1997; Hervig et al., 1997; Hervig and Deshler, 1998; Hervig and Deshler, 2002), with differences generally within 30 to 50%. An example of this reasonable agreement is shown in Figure 4-19. On the other hand, comparisons with measurements of aerosol surface area density by the in situ Focused Cavity Aerosol Spectrometer of Denver University are systematically larger than SAGE II estimates by as much as 100%. These differences may reflect the surface area of particles with radii smaller than 100 nm, which are effectively invisible to SAGE II because of their poor scattering efficiency in the visible and near-infrared (J.C. Wilson, University of Denver, personal communication). These differences between inferred surface area densities are large enough to introduce significant uncertainties into modeling of heterogeneous chemistry.

4.3.2 Stratospheric Water Vapor Trends

The recent Stratospheric Processes and their Role in Climate (SPARC) assessment of upper tropospheric and stratospheric water vapor (SPARC, 2000) has provided an extensive review of data sources and quality for stratospheric water vapor, together with detailed analyses of observed seasonal and interannual variability. The longest continuous reliable dataset is at a single location (Boulder, Colorado, U.S.), based on balloonborne frost-point hygrometer measurements, and dates back to 1981.

Over the period 1981-2000, a statistically significant positive trend of approximately 1%/year is observed at all levels between about 15 and 28 km (SPARC, 2000; Oltmans et al., 2000) (Figure 4-20). Increasing water vapor trends of ~2%/year are also found for 19-28 km in balloon measurements made from Washington, D.C., U.S., during 1964-1976 (Oltmans et al., 2000). However, although a linear trend can be fitted to these data, there is a high degree of variability in the infrequent sampling at individual locations, and the increases in either record are neither continuous nor steady. Long-term increases in stratospheric water vapor are also inferred from a number of other ground-based, balloon, aircraft, and satellite datasets spanning ~1980-2000 (Rosenlof et al., 2001), although the sampling uncertainty is high in many cases. Hurst et al. (1999) did not find a significant trend in the quantity $[H_2O+2CH_4]$ in the lower stratosphere from Earth Resources (ER)-2 aircraft measurements between 1993 and 1997, but this result is based on only eight infrequent time samples.

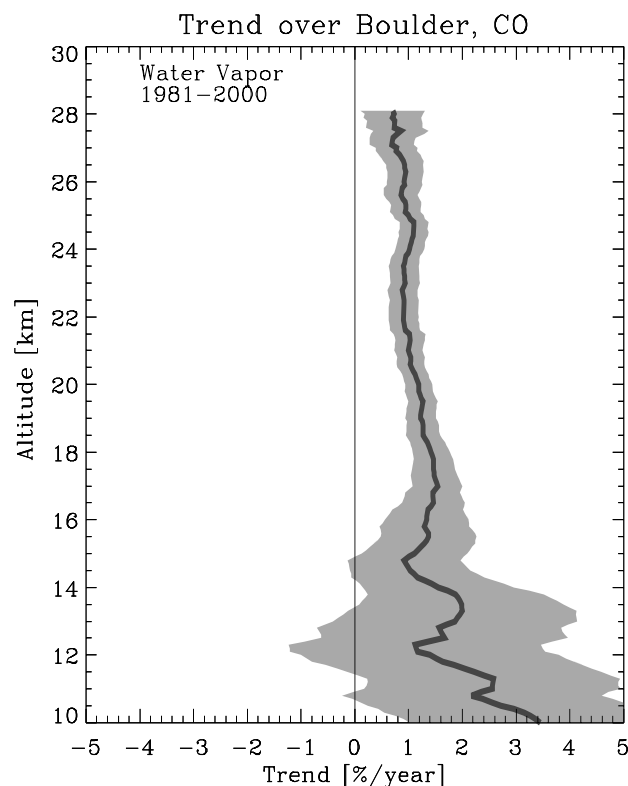


Figure 4-20. Vertical profile of trends in water vapor over Boulder, Colorado, U.S., for the period 1981-2000, expressed in percentage of the long-term means. The solid line is the trend computed at 250-m intervals, and the shaded region is the 95% confidence region. From Oltmans et al. (2000).

GLOBAL OZONE

Global stratospheric water vapor measurements have been made by the HALOE satellite instrument for more than a decade (Russell et al., 1993). These data show long-term increases over almost the entire stratosphere above 25 km (Nedoluha et al., 1998a; Evans et al., 1998; Randel et al., 1999; C.A. Smith et al., 2000). For the period 1991-2001 the HALOE-derived water vapor trends have a magnitude of ~25 to 45 parts per billion by volume (ppbv) per year, which corresponds to local increases of ~0.6 to 0.8%/year, slightly smaller than the 1981-2000 Boulder balloon measurements. However, the HALOE data do not show significant trends in the lower stratosphere (between 20 and 25 km), which is a curious result given the strong coupling of stratospheric water vapor to the tropical tropopause region. Time series of the HALOE data furthermore show relatively large increases during the period 1991-1996, and a flattening after 1996 (Randel et al., 1999).

Causes of decadal-scale increases in stratospheric water vapor are not well understood at present. A substantial fraction of the stratospheric water vapor budget originates from the oxidation of methane, which accounts for the increase of climatological water vapor with altitude for 20-50 km. However, the observed ~1%/year water vapor increase observed in balloon and satellite observations is more than twice the magnitude that would be expected from observed trends in tropospheric methane alone. A simple explanation for the stratospheric water vapor increase would be an increase in average saturation mixing ratio at the tropical tropopause. However, observations of tropical tropopause temperature do not show a corresponding increase, but rather suggest a small decrease during the period 1979-1998 (Simmons et al., 1999; Randel et al., 2000; Seidel et al., 2001; Zhou et al., 2001a). The inability to explain past changes diminishes our confidence in the projection of future increases in stratospheric water vapor.

4.3.3 Trends in Stratospheric NO₂

Nitrogen dioxide (NO₂) plays a key role in stratospheric ozone chemistry, not only through the NO_x (NO + NO₂) catalytic destruction cycle, but also by interacting with the ClO_x (chlorine radicals) and HO_x (odd hydrogen) families, leading to the formation of important stratospheric reservoirs such as chlorine nitrate (ClONO₂) and nitric acid (HNO₃). Long-term monitoring of all these nitrogen compounds is among the priority tasks of the Network for the Detection of Stratospheric Change (NDSC; see <http://www.ndsc.ws>).

The longest record of column-integrated stratospheric NO₂ is available from measurements made since

1981 at the primary NDSC station of Lauder, New Zealand (45°S, 170°E, 370 m above sea level (asl)). The data (Liley et al., 2000) have been derived from UV-Visible scanning spectrometers that measure sunlight scattered from the zenith sky during sunrise and sunset. The time series at 90° solar zenith angle is continuous from 1981 to the present except for a break of 6 months in 1986. Measurement intercomparisons (Hofmann et al., 1995; Roscoe et al., 1999) have shown that the instruments and analysis procedure meet the standards of the NDSC. Time series of deseasonalized NO₂ anomalies in the sunrise and sunset Lauder measurements are shown in the lower panel of Figure 4-21 for the period 1981-2001. Large episodic decreases of NO₂ are observed following the volcanic eruptions of El Chichón (1982) and Mt. Pinatubo (1991), persisting for 2-3 years in each case. Linear-trend statistical fits to these data (Liley et al., 2000) show an upward trend of $5 \pm 1\%$ /decade over the period 1981-1999; trends extended through 2001 are somewhat larger, i.e., $6 \pm 1\%$ /decade.

Midday NO₂ column abundances have also been derived from the analysis of infrared solar spectra recorded since 1985 at the primary NDSC site of Jungfraujoch, Switzerland (46.5°N, 8.0°E, 3580 m asl). These measurements were made with Fourier transform instruments on clear-sky days during observation campaigns that became more regular and frequent after the NDSC was formalized in 1989. The deseasonalized anomalies from the Jungfraujoch measurements (Figure 4-21) show an overall increase with time, together with a transient NO₂ decrease associated with the Mt. Pinatubo volcanic eruption and its subsequent recovery (De Mazière et al., 1998), similar to that seen at Lauder. Trends calculated from the Jungfraujoch data give a linear rate of increase of $6 \pm 2\%$ per decade for the period 1985-2001 (an update of Mahieu et al., 2000). This trend is in good agreement with the Lauder results, indicating that the stratospheric burden of NO₂ has been evolving similarly in midlatitudes of both hemispheres since the mid-1980s.

The observed trends in stratospheric NO₂ above Lauder and the Jungfraujoch are about twice that of the total reactive nitrogen (NO_y) source gas, nitrous oxide (N₂O), for which surface emissions are known to be increasing the tropospheric concentration by about 3% per decade (WMO, 1999; also Chapter 1 of this Assessment). Model studies (Fish et al., 2000; McLinden et al., 2001) show that much of this difference is largely a result of ozone depletion. The model predictions of McLinden et al. (2001) of a +4.3%/decade trend in NO₂ consist of +2.4%/decade due to the N₂O increase, +2.5%/decade due to ozone depletion, and -0.6%/decade from the halogen

trend's impact on odd-nitrogen partitioning. Changes in the vertical distribution also contributed +0.4%/decade to the trend in slant-column density. However, this study ignored the effect of H₂O increases, which would decrease the modeled trend by 0.6%/decade (Fish et al., 2000). Overall the observed N₂O increases and decreases in ozone appear sufficient to explain (within uncertainties) an NO₂ trend of $5 \pm 1\%$ / decade.

4.4 CURRENT UNDERSTANDING OF PAST CHANGES IN STRATOSPHERIC TEMPERATURE

An evaluation of stratospheric temperature trends is an integral part of understanding ozone trends. Ozone is a key radiatively active gas throughout the stratosphere, and it is important to assess the degree of consistency between observed ozone trends and temperature trends. Furthermore, in the lower (upper) stratosphere halogen-related ozone depletion is generally accelerated (decelerated) by lower temperatures, and therefore quantification of temperature changes is crucial for understanding past and predicting future ozone changes.

4.4.1 Updated Observations of Stratospheric Temperature

An extensive evaluation of stratospheric temperature trends was conducted by the SPARC Stratospheric Temperature Trends Assessment, with results included in WMO (1999), along with some updates in Ramaswamy et al. (2001). We briefly report updated satellite-derived time series, based on Microwave Sounding Unit (MSU) and Stratospheric Sounding Unit (SSU) measurements; the latter are described in detail in WMO (1999). MSU channel 4 provides a measure of the weighted mean temperature for altitudes of 13-22 km, while several different channels of SSU provide temperatures for layers spanning the lower to upper stratosphere, with vertical resolution of about 10-15 km. We also include brief comparisons with temperatures from the National Centers for Environmental Prediction/National Center for Atmospheric Research (NCEP/NCAR) reanalyses (Kalnay et al., 1996), which incorporate both satellite and radiosonde measurements in global analyses. The earlier assessments have discussed other sources of temperature trend data and the reasonable agreement between these and the satellite data.

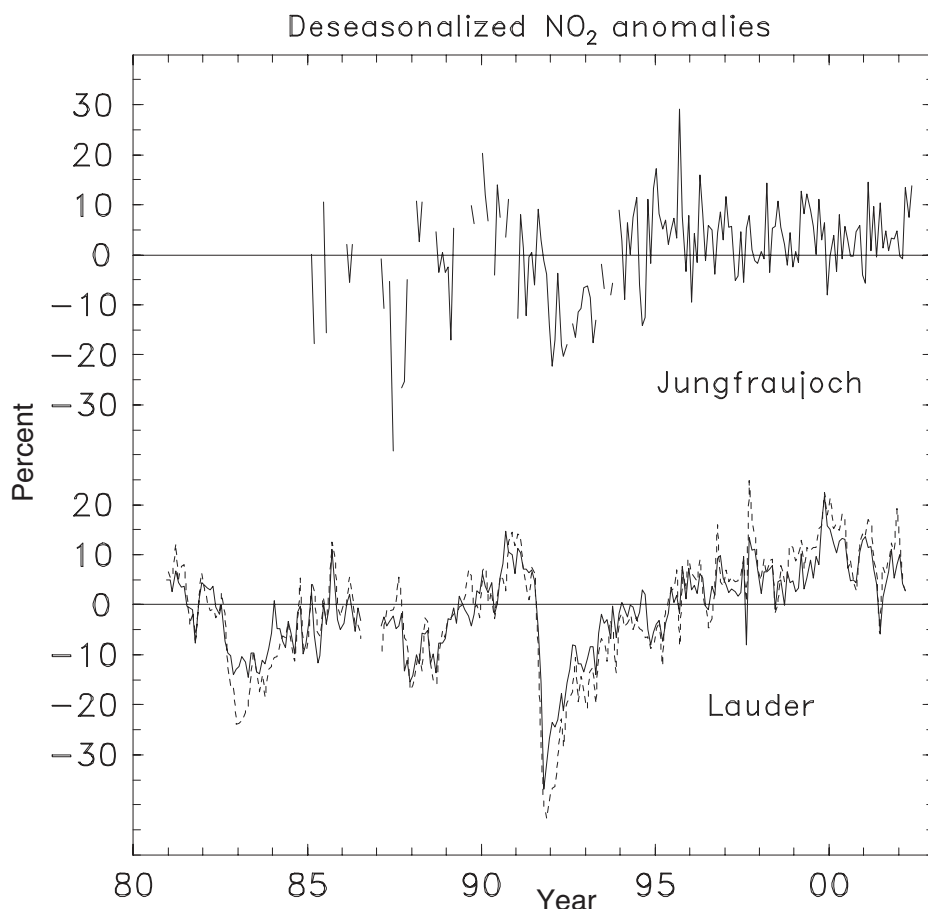


Figure 4-21. Time series of deseasonalized anomalies in slant column measurements of nitrogen dioxide (NO₂) measured at Jungfraujoch, Switzerland (46°N), during 1985-2001, and at Lauder, New Zealand (45°S), for 1981-2001. Lauder results are shown for measurements made at sunrise (dashed lines) and sunset (solid lines).

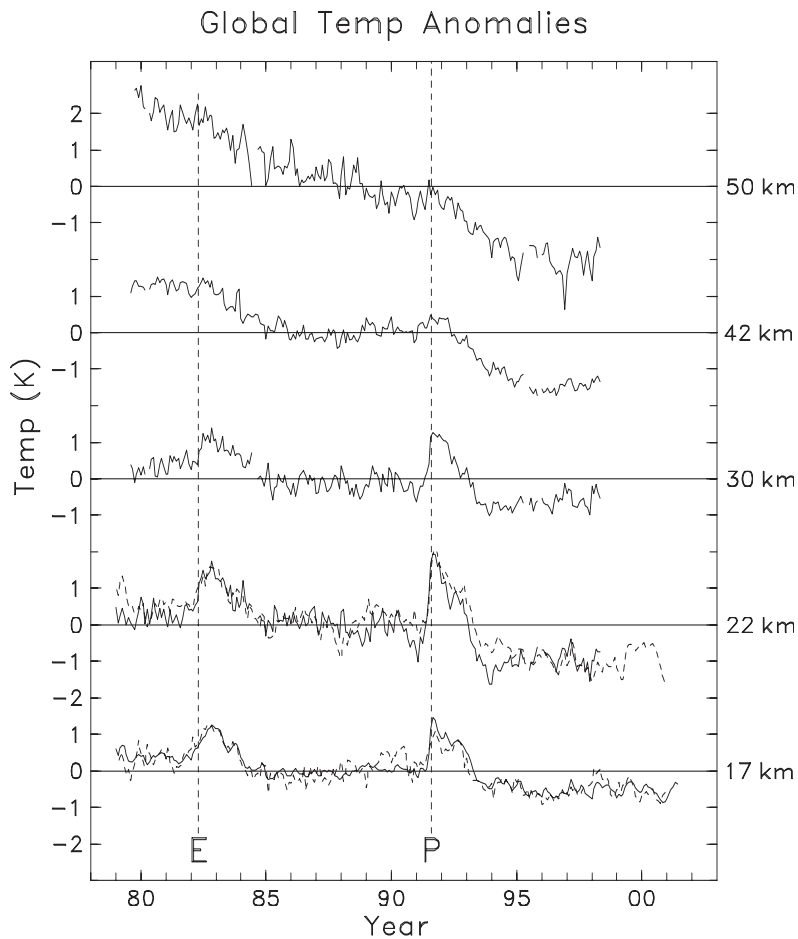


Figure 4-22. Time series of global mean temperature anomalies derived from satellite radiance measurements. The upper four curves (solid lines) are from the Stratospheric Sounding Unit (SSU) channels 47X, 27, 26X, and 15X (top to bottom) and represent mean temperatures for 10- to 15-km layers centered near 50, 42, 30, and 22 km, respectively. The bottom time series (solid line) is a global mean from the Microwave Sounding Unit (MSU) channel 4, which has a peak contribution near 17 km. The dashed lines for the two lower levels show global temperature anomalies derived from the NCEP/NCAR reanalyses, for pressure levels 50 hPa (22 km) and 100 hPa (17 km). The vertical dashed lines indicate the volcanic eruptions of El Chichón (1982) and Mt. Pinatubo (1991).

Time series of global mean temperature anomalies at levels spanning the lower to upper stratosphere are shown in Figure 4-22, based on deseasonalized monthly mean MSU (1979-2001) and SSU (1979-1998) datasets. Globally averaged temperatures in the lower and middle stratosphere (up to about 30 km) show a strong imprint of volcanic eruptions, with warming for 1-2 years following El Chichón (1982) and Mt. Pinatubo (1991) eruptions. Globally averaged temperatures near 17 km show an overall cooling from 1979 to 2001, but the anomalies are relatively constant for the period between the large eruptions; the time series suggest a “step-like” global-scale cooling of approximately 0.5 K following the eruptions. Also included for the lowest two levels in Figure 4-22 are globally averaged anomaly time series derived from the NCEP/NCAR reanalyses for 1979-2000 (100-hPa data plotted at 17 km, and 50-hPa data at 22 km). There is good overall agreement between the thick-layer satellite measurements and the reanalyses time series in the lower stratosphere.

The spatial structure of the annual mean stratospheric temperature trends for 1979-1998 is shown in Figure 4-23. Trends were calculated using a standard regression analysis, including proxies for the QBO and

solar cycle variations, and the two years following the El Chichón and Mt. Pinatubo volcanic eruptions were omitted from the time series to remove any volcanic influences (this has a small effect on the calculated trends, as shown in WMO (1999)). The annual mean trends show a high degree of interhemispheric symmetry. In the lower stratosphere there is statistically significant cooling in the extratropics (20°-60°N and S) of about 0.4 to 0.8 K/decade, which is relatively constant throughout the year (not shown). On the basis of satellite data, the equatorial lower stratosphere exhibits weak cooling (less than 0.4 K/decade), which is not statistically significant. There is a relative minimum in cooling in the middle stratosphere (around 30-35 km). The cooling increases monotonically with height from 35 to 50 km, with maximum values of about 2.5 K/decade near the stratopause (50 km).

4.4.2 Causes of Past Temperature Changes

The previous Assessment (WMO, 1999) concluded that ozone depletion was the dominant cause of global-mean temperature trends in the lower stratosphere. Ozone

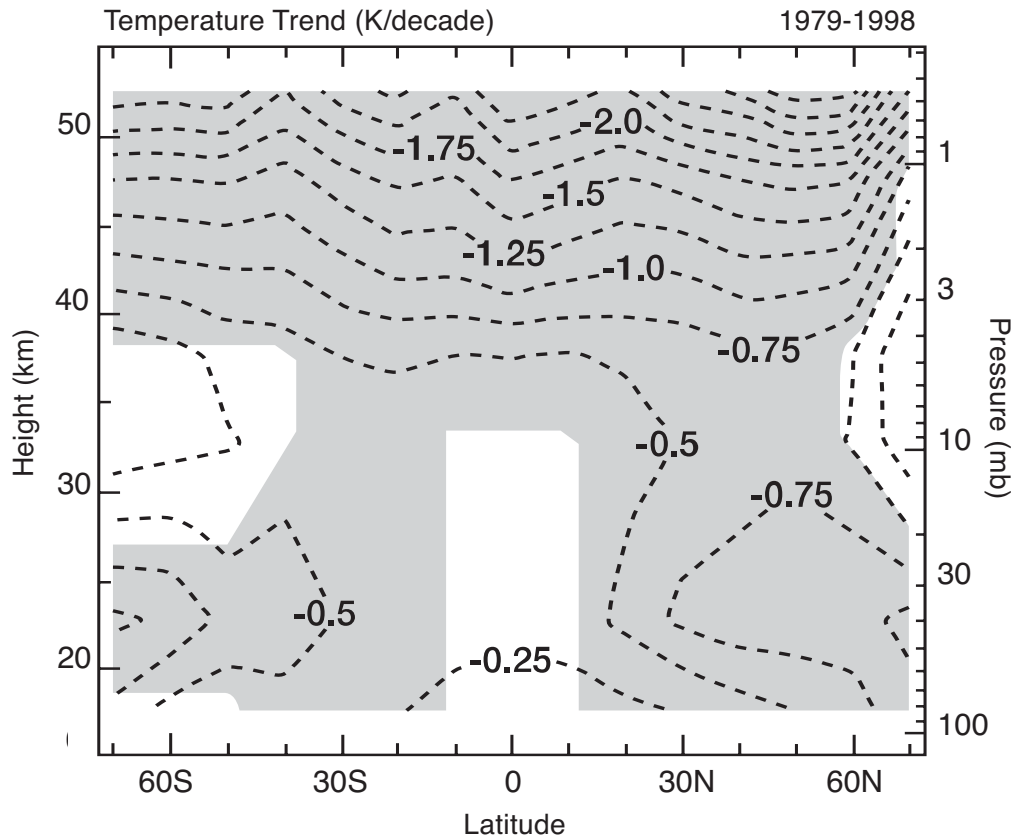


Figure 4-23. Meridional cross sections of trends (K/decade) in stratospheric temperature during January 1979-May 1998, derived from combined SSU and MSU satellite datasets. Shading indicates that the trends are significant at the 2σ level.

depletion and increases in the more well-mixed greenhouse gases (WMGGs) both contributed significantly in the middle and upper stratosphere. It also noted that there was little evidence that changes in tropospheric climate and sea surface temperatures have played a significant role in global-mean stratospheric temperature trends.

There have been significant developments in this area since WMO (1999). First, at the time of WMO (1999), most model studies used rather idealized vertical distributions of ozone change; more refined datasets on the vertical trends in ozone are now in widespread use. Second, several groups have reported simulated temperature trends using coupled chemistry-climate models. Third, much attention has been paid to the potential role of stratospheric water vapor changes on temperature trends.

The analysis here is centered on an intercomparison of available model results that have appeared in the literature or that have used established models. The models range from simple fixed dynamical heating (FDH) models, to two-dimensional (2-D; latitude-height) models, to general circulation models (GCMs) that use imposed ozone trends. The 2-D models and GCMs that incorporate coupled chemistry are discussed in Shine et al. (2002). Table 4-2 lists the contributors to this intercomparison,

together with some model details. More details of these intercomparisons were reported by Shine et al. (2002).

The emphasis of this section is on global-scale temperature changes. Chapter 3 considers polar temperature trends. All plots here include trends from the MSU and SSU data discussed above (Section 4.4.1). They are included on all plots for individual temperature trend mechanisms for reference, but the summary discussion will bring together the information from these individual mechanisms into a coherent picture. The abbreviation WMGG will be used to indicate the longer-lived and more well-mixed greenhouse gases: carbon dioxide (CO_2), methane (CH_4), nitrous oxide (N_2O), and the halocarbons. For the GCM simulations, the 2σ unforced variability of the global-mean temperature is less than 0.25 K.

4.4.2.1 SIMULATED TEMPERATURE TRENDS DUE TO OBSERVED OZONE TRENDS

Improved analyses of vertical profiles of ozone change over the period from about 1979 to 1997 (e.g., Randel and Wu, 1999; Langematz, 2000) have now been used in models to re-examine the effect of ozone loss on temperature trends (Langematz, 2000; Ramaswamy and

GLOBAL OZONE

Table 4-2. Contributors to the temperature trend intercomparison. “Timeslice” refers to the calculation of temperature trends by doing steady-state integrations of the model for conditions representative of 2 or more years and calculating the trend from the difference between these simulations. Transient models perform continuous integrations through the given period. The column labeled C refers to whether CO₂ changes are included, O refers to whether other well-mixed greenhouse gases are included, and H refers to whether water vapor trends are imposed. Note that in the absence of imposed water vapor trends, most models will have some water vapor change in response to other perturbations.

Institute	Contributor	Model	Ozone Trend	C	O	H	Experiment	Reference
Univ. of Cambridge, U.K.	P. Braesicke	GCM	Coupled but no changes in trace gases	N	N	N	Transient, obs. SSTs	Braesicke et al. (2002)
Freie Universität, Berlin, Germany	U. Langematz	GCM	Observed trend	Y	N	N	Timeslice	Langematz (2002)
DLR, Germany	V. Grewe, C. Schnadt	GCM	Coupled	Y	N	N	Timeslice	Schnadt et al. (2002)
Imperial College, U.K.	C.A. Smith, J.D. Haigh	2-D	Observed trend	N	N	Y	Timeslice	C.A. Smith et al. (2001)
Imperial College U.K.	C.A. Smith, J.D. Haigh	GCM	–	N	N	Y	Timeslice	Model is Rosier and Shine (2000)
NOAA Aeronomy Laboratory, U.S.	R.W. Portmann, S. Solomon	2-D	Coupled	Y	N	Y	Timeslice	Dvortsov and Solomon (2001)
NOAA GFDL, U.S.	V. Ramaswamy, M.D. Schwarzkopf	GCM	Observed trend	Y	Y	Y	Timeslice	Ramaswamy and Schwarzkopf (2002)
NASA GISS, U.S.	D. Shindell	GCM	Coupled	Y	Y	Y	Transient	Shindell (2001)
Met Office (UKMO), U.K.	J. Austin, N. Butchart	GCM	Coupled	Y	Y	N	Transient	Austin (2002)
Met Office (UKMO), U.K.	N. Butchart	GCM	–	Y	Y	N	Transient	Butchart et al. (2000)
Natl. Inst. of Env. Studies, Japan	T. Nagashima	GCM	Coupled	Y	Y	N	Transient	Nagashima et al. (2002)
Univ. of Reading, U.K.	M. Bourqui, K. Shine	GCM	Observed trend	Y	Y	N	Timeslice	Rosier and Shine (2000)
Univ. of Reading, U.K.	P. Forster	FDH	Observed trend	N	N	Y	Timeslice	Forster et al. (2001)

DLR, Deutsches Zentrum für Luft- und Raumfahrt; NOAA, National Oceanic and Atmospheric Administration; GFDL, Geophysical Fluid Dynamics Laboratory; NASA, National Aeronautics and Space Administration; GISS, Goddard Institute for Space Studies.

Schwarzkopf, 2002; Rosier and Shine, 2000; Smith, 2001; and Forster et al., 2001, who used three different radiation schemes). Figure 4-24 shows the vertical profile of the global and annual mean temperature trends as a function of pressure when only ozone changes are imposed. All models have the same qualitative behavior, with a peak cooling near the stratopause (~1 hPa) exceeding 1 K/decade, a minimum near 10 hPa, and a secondary cooling peak near 80 hPa of about 0.4 K/decade. However, there is a significant amount of disagreement in both the exact size of the cooling and the altitude of the main features, most particularly near 1 hPa. The dominant

reason for these differences seems likely to be the particular radiation codes being used (Forster et al., 2001) and the assumed background climatology of ozone (Ramaswamy and Schwarzkopf, 2002).

The latitudinal structure of annual and zonal mean temperature trends at 50 hPa from observations and models with observed ozone trends is shown in Figure 4-25. It is important to appreciate that whereas dynamical processes exert little direct influence on global-mean temperature at any given level (in the stratosphere), this is decidedly not true of temperatures over particular latitude bands. The general pattern in the GCMs is of a cooling of

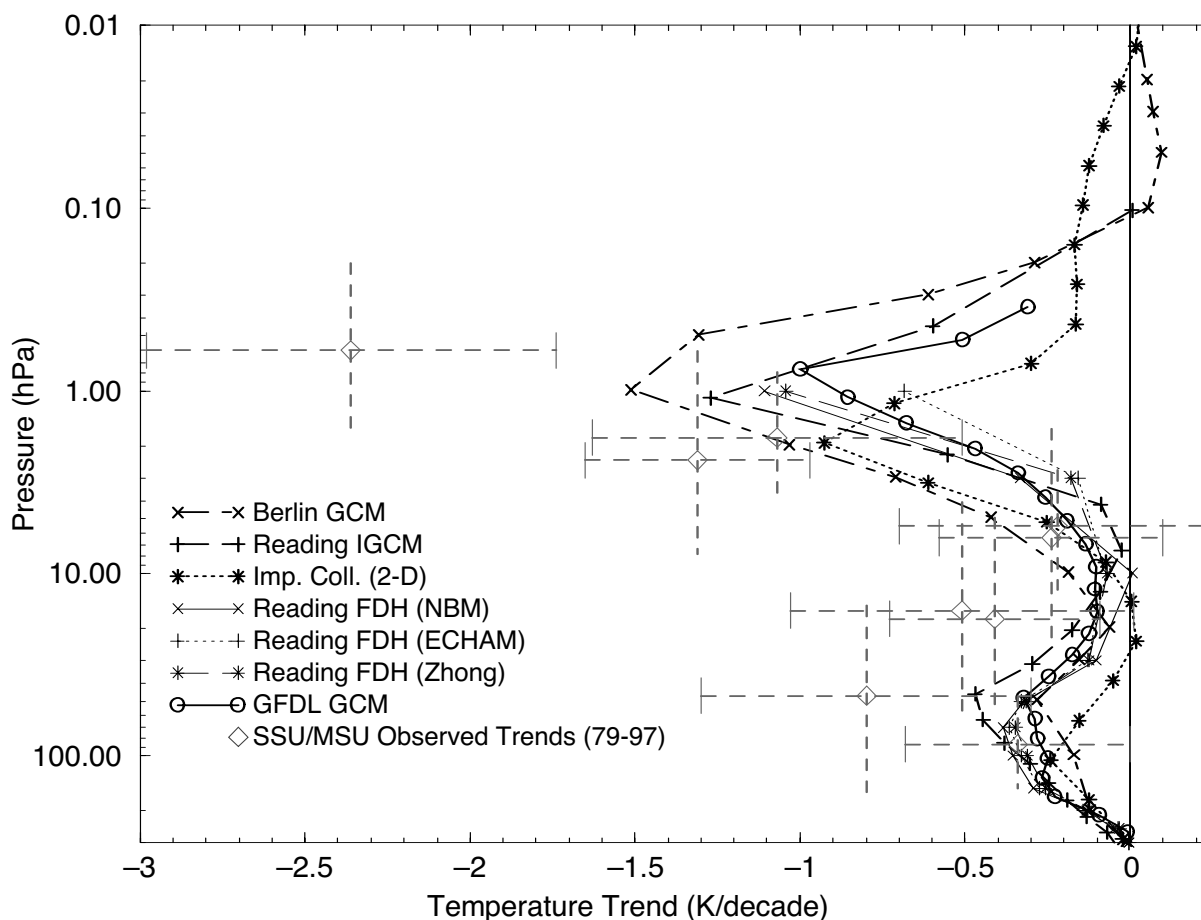


Figure 4-24. Global and annual mean temperature trends for models using imposed height-resolved ozone trends. The observations from MSU and SSU are also shown. The 2σ error bars in the observations are included; the vertical bars are intended to give the approximate altitude range sensed by the particular satellite channel. NBM, ECHAM, and Zhong refer to different radiative transfer codes used in the Forster et al. (2001) fixed dynamical heating model. NBM is a moderately high-resolution narrow band code; ECHAM and Zhong are general circulation model codes.

a few tenths of a Kelvin per decade, which is substantially less than the observed cooling in midlatitudes. At 100 hPa (not shown) the GCMs are in better agreement with observations: the models exhibit midlatitude cooling trends of around 0.3 K/decade, which overlaps the uncertainty levels of the (somewhat larger) observed trends. As a note, there are considerably larger latitudinal gradients in the temperature trends near Antarctica in the FDH models compared with the GCMs in Figure 4-25 (with the exception of the GFDL GCM); as discussed in Rosier and Shine (2000), changes in the GCM model circulation tend to ameliorate the radiatively driven high-latitude cooling.

A further contributor to temperature trends in the lower stratosphere comes from changes in tropospheric ozone concentrations (WMO, 1999); these change the amount of upwelling radiation that can be absorbed by

stratospheric ozone. Sexton et al. (2002), using tropospheric ozone increases derived from a chemical transport model (CTM), found a global mean cooling of about 0.05 K/decade at 50 hPa in recent decades. Although this cooling is smaller than that due to stratospheric ozone loss, it has likely been sustained over many decades; Sexton et al. (2002) estimated a 50-hPa cooling of about 0.5 K from tropospheric ozone changes over the 20th century.

4.4.2.2 SIMULATED TEMPERATURE TRENDS DUE TO INCREASED WMGG CONCENTRATIONS

There is qualitative agreement between the modeled cooling resulting from increases in WMGG concentrations. It generally increases monotonically with height from near zero at 100 hPa to about 0.8 K/decade at the

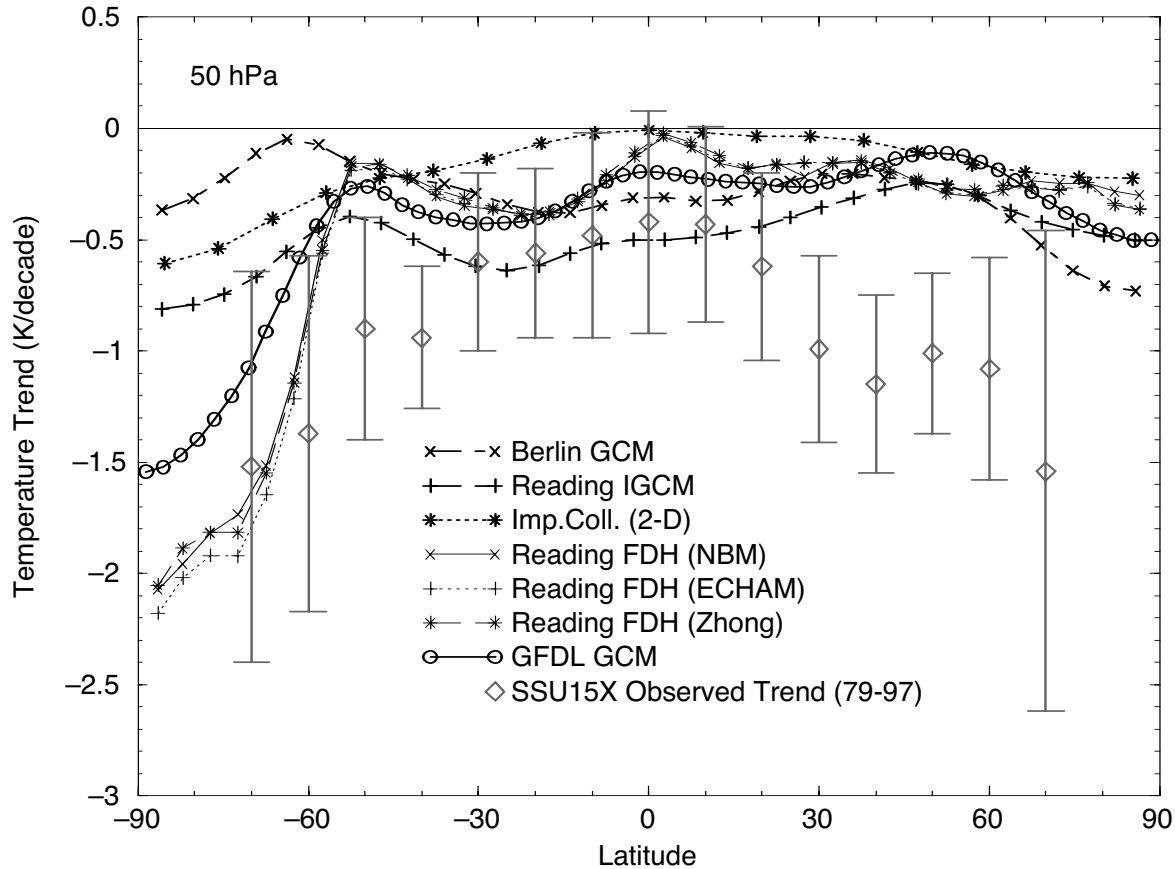


Figure 4-25. Global and zonal mean temperature trends at about 50 hPa for models using imposed height-resolved ozone trends. The observations from SSU channel 15X are also shown. The 2σ error bars in the observations are included. The peak of the SSU channel 15X weighting function is at about 46 hPa. Acronyms as defined in text and in Figure 4-24.

stratopause (not shown, but see Figure 5-24 of WMO (1999)). Between 100 and 10 hPa, there is general agreement between most models, but there is considerable divergence at about 1 hPa, with almost a factor of 4 difference between the model with the most cooling (UKMO, the United Kingdom Meteorological Office model) and that with the least (GISS, the Goddard Institute for Space Studies model). Given that the greenhouse gas changes are fairly linear and well constrained over this period, this divergence is surprising and may be related to the ability of individual radiation codes to simulate heating rates at lower pressures.

The zonal mean cooling at 100 hPa and 50 hPa (not shown) indicates near-zero cooling at all latitudes at 100 hPa and about 0.1 K/decade cooling at 50 hPa in most models. The GISS model gives considerably higher cooling at higher latitudes than other models; it reaches 0.5 K/decade at 60°N and S at 100 hPa and about 1 K/decade at the same locations at 50 hPa.

4.4.2.3 THE ROLE OF TRENDS IN STRATOSPHERIC WATER VAPOR

Observations of increases in stratospheric water vapor (Section 4.3.2) have led to renewed interest in its climatic implications (Forster and Shine, 1999, 2002; Dvortsov and Solomon, 2001; Oinas et al., 2001; Shindell, 2001; C.A. Smith et al., 2001). A major difficulty in comparing estimates of the impact on temperature of stratospheric water vapor changes is in estimating their temporal and geographical variation. Calculations with idealized water vapor changes (i.e., 700 ppbv from a background of 6000 ppbv) adopted by Forster and Shine (1999) and Oinas et al. (2001) are not included here. As noted by Forster and Shine (2002), it is not so much the idealized nature of the change that biases these estimates, but more the idealized background water vapor that is adopted. Both Oinas et al. (2001) and Forster and Shine (2002) demonstrate a strong dependence of the effect of a given perturbation on the assumed background concentrations.

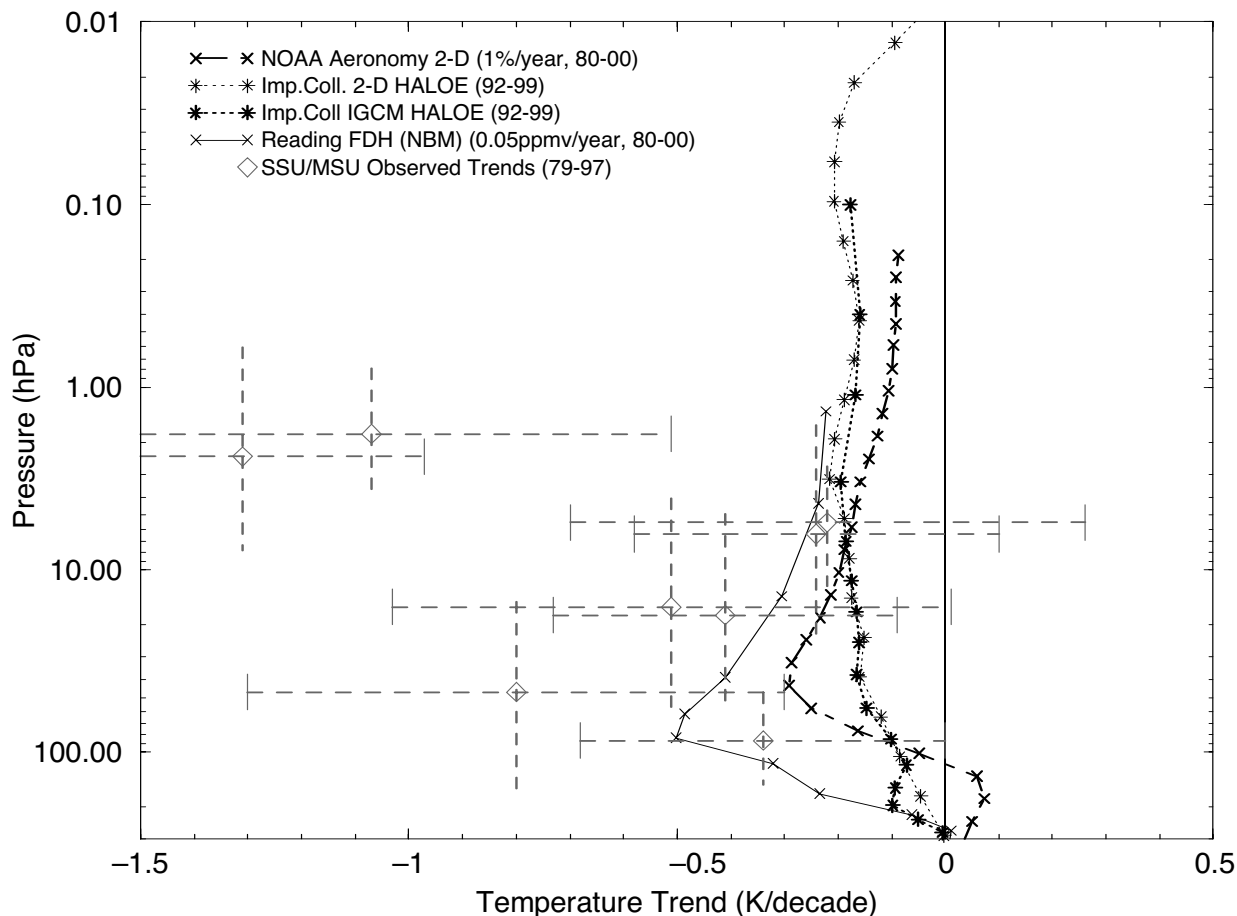


Figure 4-26. Global and annual mean temperature trends for models using imposed water vapor trends. The observations from MSU and SSU are also shown. The 2σ error bars in the observations are included; the vertical bars are intended to give the approximate altitude range sensed by the particular satellite channel. Acronyms as defined in text and in Figure 4-24.

Figure 4-26 shows the vertical profile of the modeled global and annual mean temperature trend, derived for water vapor changes specified ideally (e.g., constant percentage global increases) or derived from HALOE observations. Much of the divergence between the models is likely due to differences in the adopted water vapor trend; this uncertainty is severe. In the mid-to-upper stratosphere the models all produce a cooling of about 0.2 K/decade, but at lower levels there is significant divergence. The latitudinal structure of zonal mean trends at 100 and 50 hPa (not shown) reflects this divergence; furthermore, at mid-to-high latitudes water vapor increases could be causing cooling of order 0.5 K/decade.

4.4.2.4 SYNOPSIS OF SIMULATED TEMPERATURE TRENDS

Figure 4-27 consolidates the above results. An average profile of cooling has been generated from the

imposed observed ozone change calculations and WMGG change experiments. For water vapor, the Imperial College HALOE IGCM trends are used, because these are based on more global observations, albeit for quite short periods. Summing these three components generates the “total” trend.

At 1 hPa, ozone change is the dominant contributor to cooling (1.0 K/decade), with WMGGs at 0.7 K/decade and water vapor much smaller at 0.2 K/decade. Throughout the upper stratosphere, the total model cooling is within the 2σ error bars of the observed cooling. Ozone depletion and increases in WMGGs contribute roughly equally to the temperature trends in this region, although the ozone contribution is more peaked at the stratopause.

At 10 hPa, WMGGs are the dominant cooling mechanism (0.4 K/decade), followed by water vapor (0.2 K/decade) and ozone (less than 0.1 K/decade). There is a significant disagreement with observations. The total

GLOBAL OZONE

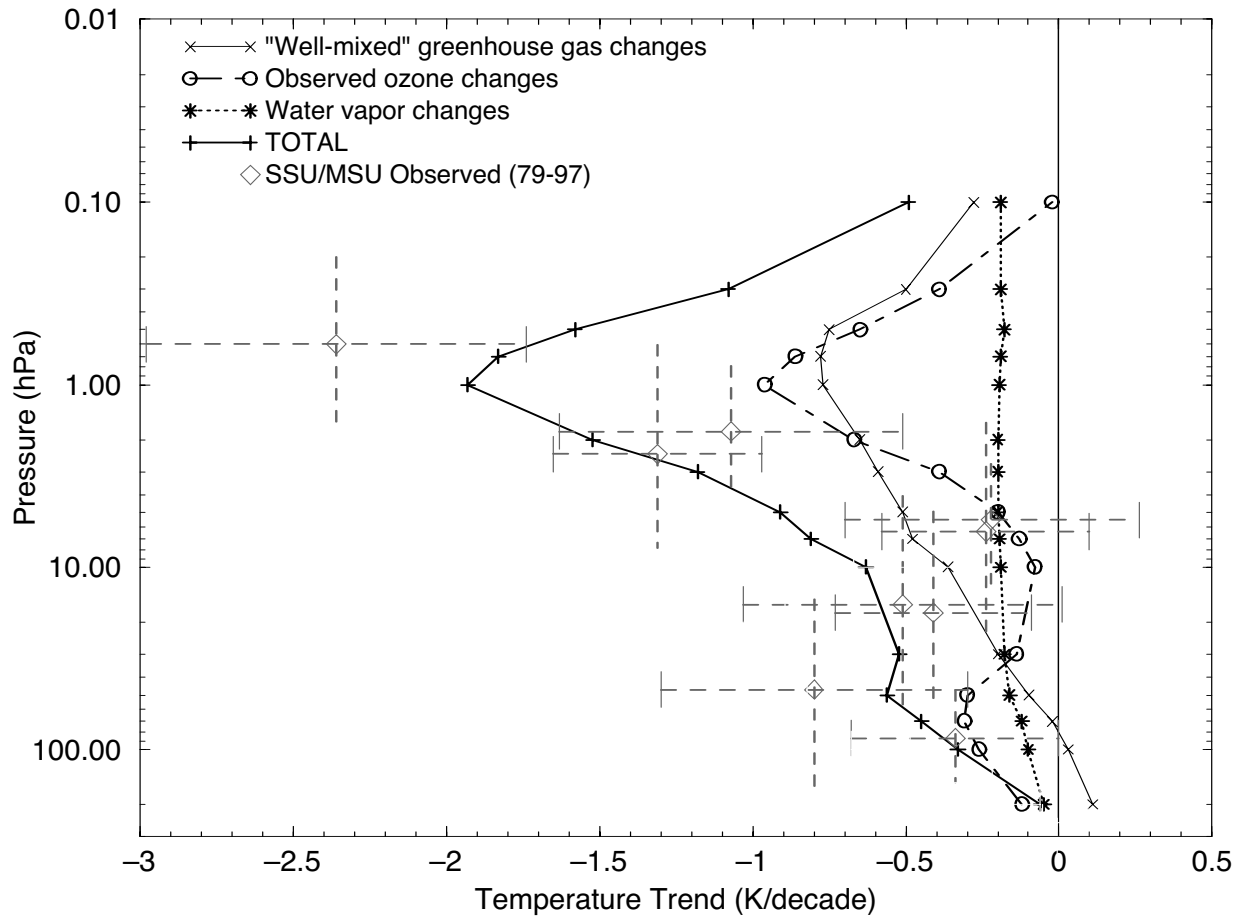


Figure 4-27. Global and annual mean temperature trends from an approximate average of the model results for the imposed height-resolved ozone trends (Figure 4-24) and greenhouse gases; the water vapor results are the trends derived from the HALOE results in Figure 4-26. The observations from MSU and SSU are also shown. The 2σ error bars in the observations are included; the vertical bars are intended to give the approximate altitude range sensed by the particular satellite channel.

model cooling at 5 and 6 hPa is outside the 2σ errors bars of the two SSU channels observing at those altitudes, and indeed, WMGGs alone are toward the edges of these error bars. A similar disagreement was found in the coupled model runs (not shown).

The source of this discrepancy is not clear. If the minimum cooling from any of the contributing models is used (ozone change (zero cooling); WMGGs (0.45 K/decade); and water vapor (less than 0.1 K/decade)), then there would at least be agreement within the error bars at 6 hPa. This would require the water vapor trend for the HALOE period to be unrepresentative of the long-term trend, but it is also possible that there are inaccuracies in the observed ozone trend or the observed temperature trends at these levels.

At 100 hPa, ozone loss is again the dominant cooling mechanism (about 0.3 K/decade) followed by

water vapor (0.1 K/decade) and WMGGs (near zero cooling). The net cooling is within the 2σ error bars of the observations. At 50 hPa, the cooling due to ozone alone is not able to explain the observed trend, and a significant contribution from stratospheric water vapor appears to be needed to achieve agreement.

Considering next the zonal average trends at 50 hPa, in the tropics at least one of the GCMs with imposed ozone trends (Figure 4-25) is within the 2σ error bars of the observations; however, in midlatitudes of both hemispheres, there is a substantial difference between the ozone-induced trend and observations. At 40°N , the gap between the modeled cooling and the observed error bar is about 0.5 K/decade. This difference is more than can be explained by WMGGs alone (most models report a cooling of about 0.2 K/decade, although one model reports 0.4 K/decade) and would need a cooling of about 0.3

K/decade from some other mechanism. Water vapor trends could cause such a cooling, but it requires trends in excess of those deduced from HALOE and more consistent with the trends used in the Reading FDH model (50 ppbv/year). Such a trend would also improve agreement at 50 hPa in the global and annual mean plot (Figure 4-27). In addition, none of the coupled chemistry models (not shown) lie within the 2σ bars of the observations between 30° and 50°N . Another possibility at these latitudes is that part of the cooling trend during 1979-1998 is driven by dynamical causes (this is qualitatively consistent with the observed decreases in NH planetary-wave drag discussed in Section 4.6.3).

For the zonal average trends at 100 hPa, ozone depletion alone can explain the observed trend at all latitudes within the uncertainty of the observations. The WMGG trend is small, and a cooling due to water vapor of several tenths of a Kelvin per decade could be present and would improve the midlatitude agreement with the observations, particularly for those models generating a small ozone-induced cooling.

In summary, there is encouraging agreement between the observed and model temperature trends, particularly in the upper stratosphere. But the degree of agreement is not always good, and the explanations required to improve agreement are not always consistent. In the global annual mean, one way to achieve agreement near 10 hPa would be for the water vapor contribution to be small, and yet at 50 hPa at midlatitudes in the annual zonal means, a significant water vapor contribution is one explanation that would improve agreement with observations.

4.5 CHEMICAL INFLUENCE ON PAST CHANGES IN OZONE

This section discusses the role of chemistry in causing the observed long-term changes in global ozone. Section 4.5.1 discusses updates to our understanding of the important gas-phase and heterogeneous chemical processes. Section 4.5.2 describes the modeling tools that are used to quantify the role of these chemical processes on ozone changes and their key uncertainties. Section 4.5.3 then assesses the role of chemistry in driving extrapolar global ozone changes, based on 2-D and 3-D assessment model simulations compared with the observed ozone changes from Section 4.2.

4.5.1 Chemical Processes that May Contribute to Ozone Changes

In the photochemically controlled US region above about 25 km, ozone trends may be driven by trends in the

gases that provide the sources for reactive radicals (such as N_2O , which produces NO_x , and H_2O , which produces HO_x). Models summarized in WMO (1999) showed that the dominant driver for ozone trends in this region has been the observed trends in reactive chlorine (which are due in turn to the known trends in chlorofluorocarbons). Observed changes in CH_4 , H_2O , and N_2O also have the potential to contribute to chemical ozone changes, but their contributions were estimated to have been relatively small in the past two decades (less than 1% per decade at 40 km). Furthermore, the chemistry of the US is strongly dependent upon temperature, and therefore it is important to consider the feedbacks between ozone depletion and temperature changes in model estimates, and to consider changes in radiatively important gases (especially CO_2 and H_2O ; see, e.g., Evans et al., 1998).

In the LS and LMS, where the chemical lifetime of ozone is comparable to or longer than the transport time scale, both dynamical and chemical processes have the potential to affect ozone and its trends. In particular, changes in chemical loss processes may deplete ozone, but only if they can remove ozone rapidly enough to compete with the seasonally varying transport that moves ozone through this region of the atmosphere. Trends in reactive chlorine may chemically deplete ozone at these altitudes, and can be particularly effective in combination with reactive bromine. Iodine may influence the background concentrations of ozone near the tropopause, but is unlikely to be present in large enough abundances to contribute significantly to the observed trends in the midlatitude ozone column based on the most recent observations.

Ozone in the midlatitude LS and LMS can be affected both by chemical processes occurring locally and by chemical changes occurring in other regions, notably the winter/spring polar vortices, which are then transported to midlatitudes. In this way trends in stratospheric halogens may drive midlatitude ozone trends either by in situ midlatitude chemistry, involving heterogeneous chemistry on liquid sulfate aerosols, or by chlorine activation and/or ozone loss in the polar regions (see Chapter 3) that is then exported to lower latitudes.

4.5.1.1 GAS-PHASE CHEMICAL PROCESSES

Since WMO (1999) there have been many refinements to our understanding of gas-phase reactions including changes in rate coefficients, identification of new and potentially important reaction channels, and reduced uncertainty limits on a host of evaluated rate constants for halogen, HO_x , and NO_x reactions. The discussion in WMO (1999) was based on data summarized in the Jet Propulsion Laboratory (JPL) 1997 recommenda-

GLOBAL OZONE

tion (DeMore et al., 1997). Since then a further recommendation has been published, JPL 2000 (Sander et al., 2000). Here we summarize the main updates (see Table 4-3) and separate the discussion into those updates that were contained in JPL 2000 and those that are more recent. Whereas the implications for ozone trends of the data in JPL 2000 have been assessed (e.g., Section 4.5.3), the full implications for the more recent data have not been determined.

Updates Included in JPL 2000

The discovery of a small hydrogen chloride (HCl) product channel in the hydroxyl radical + chlorine monoxide (OH + ClO) reaction reported in WMO (1999) has been confirmed by further laboratory studies (Lipson et al., 1999; Wang and Keyser, 2001; Tyndall et al., 2002). The HCl channel substantially impacts model-observation comparisons of atmospheric HOCl/HCl, ClO/HCl, and ClONO₂/HCl ratios (Chance et al., 1996; Dubey et al., 1998). However, because of the relatively large dispersion in laboratory results (factor of 2 range in derived rate constant), the magnitude of the HCl channel remains highly uncertain.

Reactions involving NO_x have received substantial attention, motivated in large part by observations of reactive nitrogen partitioning in the summer Arctic (see discussion in Chapter 3). Recent laboratory measurements have led to significant revisions in rate coefficients for O + NO₂, OH + NO₂ + M (where M is any atmospheric molecule that collides and dissipates the reaction's released energy), and OH + HNO₃, especially at the low end of the temperature range (Sander et al., 2000; Brown et al., 1999, 2001). The changes in rate coefficients are found to substantially increase NO_x abundance and NO_x-catalyzed O₃ destruction in the lower stratosphere (Portmann et al., 1999).

Updates Since JPL 2000

There is continued uncertainty regarding the OH + NO₂ + M reaction, particularly the reconciliation of low- and high-pressure measurements. The reaction has now been shown to occur via two channels, one producing HNO₃, the other giving rise to pernitrous acid (HOONO). The laboratory data indicate that HOONO is a relatively weakly bound molecule (Donahue et al., 2001; Golden and Smith, 2000) that decomposes back to OH + NO₂. This finding is supported by theoretical quantum chemical calculations (Li and Francisco, 2000). Because of its weak bond, HOONO will have a much shorter atmospheric lifetime than HNO₃, and the fraction of the OH +

NO₂ reaction forming HOONO will not effectively sequester NO_x. Inclusion of the HOONO channel in atmospheric models could potentially affect NO_x levels under high-pressure and/or low-temperature conditions where the HOONO channel takes on its greatest significance.

Another NO_x reservoir, peroxyoxynitric acid (HO₂NO₂), has been found to have a photolytic decomposition pathway in the near infrared through excitation to the first vibrational overtone (Roehl et al., 2002). This path serves to substantially increase the rate of HO_x production under high solar zenith angles and may explain observed OH behavior at sunrise in the lower stratosphere (see Chapter 3).

New data on HO_x reactions (Herndon et al., 2001; Nizkorodov et al., 2000) have reduced the uncertainty associated with the rate coefficients of hydroperoxy radicals plus ozone (HO₂ + O₃) and OH + O₃. Extensive observations of HO₂/OH ratios in the lower stratosphere have provided stringent tests of the measured rate coefficients and support the results of the newer laboratory studies (Lanzendorf et al., 2001).

For halogen chemistry, several studies have shed new light on the kinetics and mechanism of the ClO + HO₂ reaction (Nickolaisen et al., 2000; Knight et al., 2000). In contrast to previous work, the recent studies find a different temperature dependence, which implies a slower atmospheric cycling through the catalytic mechanism involving HO₂ + ClO and increased importance of longer-lived reservoir species ClONO₂ and HO₂NO₂ formed via reactions of HO₂ and ClO with NO₂.

Further progress has been made in defining the chemistry of iodine in the stratosphere. Kinetics data have been reported for iodine monoxide (IO) reactions with HO₂, bromine monoxide (BrO), and IO (Cronkhite et al., 1999; Knight and Crowley, 2001; Rowley et al., 2001; Bloss et al., 2001). The rate coefficient measured for IO + HO₂ is ~30% higher than that used in the calculations of Solomon et al. (1994). This will slightly increase the (small) calculated impact of iodine species on stratospheric ozone.

4.5.1.2 MIDLATITUDE LOWER STRATOSPHERIC HETEROGENEOUS PROCESSES

In the midlatitude LS, heterogeneous reactions occur mainly on liquid sulfuric acid aerosols. This heterogeneous processing causes the chemical loss of ozone to be dominated by HO_x reactions, with an important contribution from halogen species. Given an accurate knowledge of atmospheric temperature, there are three main limitations on our ability to quantify the importance of

Table 4-3. Changes in the data on gas-phase reactions relevant to stratospheric ozone photochemistry. Minor changes in some of the other reactions are not listed. Reactions for which the most recent revisions were included in JPL 2000 (Sander et al., 2000), and hence in the Assessment model runs in Section 4.5.2, are indicated by “[JPL 2000]” in the final column.

Reaction	Information for 1998 Assessment (WMO, 1999)	Update	Impact	Reference
$\text{OH} + \text{NO}_2 \rightarrow \text{products}$	Few data at lower stratospheric T	Refit of p -dependence at T ; decrease k by ~30%; small yield of short-lived HOONO suggested	Increased NO_x/NO_y and O_3 loss rate in 20-30 km region	Sander et al. (2000), Golden and Smith (2000) [some updates in JPL 2000]
$\text{O} + \text{NO}_2 \rightarrow \text{NO} + \text{O}_2$	Few, and scattered, data at low T	Measured over larger T range; increase k by ~20% at low T	Decreased NO_x catalytic cycle between 24 and 36 km	Sander et al. (2000) [JPL 2000]
$\text{OH} + \text{HNO}_3 \rightarrow \text{H}_2\text{O} + \text{NO}_3$	Few data at lower T	Improved characterization of p - and T -dependences; increase k by ~50% in lower stratosphere	Increased NO_x/NO_y and O_3 loss rate in 20-30 km region	Sander et al. (2000), Brown et al. (1999), Brown et al. (2001) [JPL 2000]
$\text{OH} + \text{O}_3 \rightarrow \text{HO}_2 + \text{O}_2$	~30% offset between various T -dependent datasets	Better definition of T -dependence; reduced uncertainty	Improved model fit to measured HO_2/OH	Nizkorodov et al. (2000)
$\text{HO}_2 + \text{O}_3 \rightarrow \text{OH} + 2\text{O}_2$	Low T -dependence uncertain, possibly nonlinear	Additional low T data; uncertainty reduced	Improved model fit to measured HO_2/OH	Herndon et al. (2001)
$\text{Cl} + \text{O}_3 \rightarrow \text{ClO} + \text{O}_2$	Scatter in data increases at lower T	No new data; reanalysis increases k at low T by ~7%	Compensates for change in $\text{Cl} + \text{CH}_4$; no impact on ozone	Sander et al. (2000) [JPL 2000]
$\text{Cl} + \text{CH}_4 \rightarrow \text{HCl} + \text{CH}_3$	Data variance due to nonlinear T -dependence	No new data; reanalysis increases k at low T by ~7% and reduces uncertainty	Compensates for change in $\text{Cl} + \text{O}_3$; no impact on ozone	Sander et al. (2000) [JPL 2000]
$\text{ClO} + \text{HO}_2 \rightarrow \text{HOCl} + \text{O}_2$	Poorly defined T -dependence, possibly nonlinear	T -dependence better defined and linear; k ~50% smaller at low T	Decreased chlorine catalytic cycle efficiency at low T	Nickolaisen et al. (2000), Knight et al. (2000)
$\text{ClO} + \text{ClO} + \text{M} \rightarrow \text{ClOOC} + \text{M}$	Large uncertainty at low T	Low T behavior better defined	Increased catalytic efficiency at low T	Sander et al. (2000), Bloss et al. (2001)
$\text{HOCl} + \text{h}\nu \rightarrow \text{OH} + \text{Cl}$	Large uncertainty above 380 nm	Third absorption band identified; extend database to 420 nm	Increased production rate of active chlorine	Sander et al. (2000), Barnes et al. (1998) [JPL 2000]
$\text{IO} + \text{HO}_2 \rightarrow \text{products}$	No data below 298K	Fast reaction; hypoiodous acid (HOI) product observed	Iodine catalytic cycle defined	Knight and Crowley (2001)

T , temperature; p , pressure; k , rate constant.

GLOBAL OZONE

heterogeneous chemistry on midlatitude LS and LMS ozone: variations of the surface area densities of sulfuric acid (H_2SO_4)/ H_2O aerosols of about a factor of 2 in volcanically unperturbed periods (cf. Figure 4-19); estimated uncertainties in the reaction probabilities of 15-30% on cold H_2SO_4 / H_2O aerosols and of factors of 2-3 on ice (Sander et al., 2000); and large uncertainties in how much air is processed through humid, cold conditions close to the local tropopause, i.e., how pervasive cold, dilute H_2SO_4 / H_2O aerosols or subvisible cirrus are in the LMS.

Hydrolysis Reactions on Acidic Droplets

The important hydrolysis reactions of dinitrogen pentoxide (N_2O_5) and bromine nitrate (BrONO_2) on H_2SO_4 / H_2O aerosols have large reaction probabilities that are essentially independent of the temperature and concentration of the droplet solutions. Recently, progress has been achieved in the quantitative understanding of BrONO_2 hydrolysis. Heterogeneous bromine chemistry can potentially enhance OH, suppress the $\text{NO}_x:\text{NO}_y$ ratio, and activate HCl (Hanson and Ravishankara, 1995; Hendricks et al., 1999, 2000). The heterogeneous/homogeneous sequence $\text{BrONO}_2 + \text{H}_2\text{O} \rightarrow \text{HOBr} + \text{HNO}_3$, $\text{HOBr} + \text{h} \rightarrow \text{Br} + \text{OH}$, and $\text{OH} + \text{HCl} \rightarrow \text{H}_2\text{O} + \text{Cl}$ was quantified in calculations by Lary et al. (1996), who found that heterogeneous bromine chemistry in the midlatitude lower stratosphere increased bromine radicals (BrO_x), ClO_x , and HO_x each by about 20%. Erle et al. (1998) provided observational evidence for the presence of BrONO_2 hydrolysis by showing that measurements of BrO and chlorine dioxide (OCIO) during winter outside the polar vortex (at temperatures above 200 K) agreed better with photochemical box model calculations when the heterogeneous chemistry of both chlorine and bromine was taken into account.

Chlorine Activation on Cold Aerosol Droplets

At very low temperatures, H_2SO_4 / H_2O droplets in the stratospheric aerosol layer grow into liquid polar stratospheric clouds (PSCs) caused by uptake of HNO_3 (see Chapter 3). At about 200 K, i.e., several degrees above the formation temperature of liquid PSCs, heterogeneous chlorine activation starts (Hanson and Ravishankara, 1995) due to increasing HCl and ClONO_2 solubilities (Carslaw et al., 1997) before the onset of major HNO_3 uptake. It remains an open issue as to what extent such low-temperature processes may also affect LS chemistry at midlatitudes (Michelsen et al., 1999). The requirement of low temperatures concomitant with high inorganic chlorine (Cl_y) is best fulfilled at the midlatitude tropopause, or at high latitudes in winter. Keim et al. (1996)

found enhanced ClO mixing ratios of up to 80 parts per trillion by volume (pptv) peaking about 600 m above the local tropopause at 38°N, and interpreted this as a consequence of the heterogeneous reactions $\text{ClONO}_2 + \text{HCl}$ and $\text{ClONO}_2 + \text{H}_2\text{O}$. These processes would be supported by (1) locally increased water and low temperatures in the vicinity of the tropopause (i.e., high HCl solubility), and (2) enhancements in aerosol surface areas due to high aerosol loading (resulting from the Mt. Pinatubo eruption). The observations of Keim et al. (1996) were corroborated by Borrmann et al. (1997), who also showed a correlation between ClO and aerosol surface area. Because a cooling of 3 K enhances the rate of $\text{ClONO}_2 + \text{HCl}$ by an order of magnitude, the presence of the volcanic aerosols appears to provide an additional enhancement of the rate but is not a necessary requirement.

Currently it is unclear how often situations suitable for chlorine activation directly above the midlatitude tropopause occur. The few available observations seem to provide contradictory results. Regular humidity measurements onboard a commercial airliner within the Measurement of Ozone and water vapor by Airbus In-service Aircraft (MOZAIC) project provide evidence that about 2% of all data above the tropopause show supersaturation with respect to ice (Gierens et al., 1999, 2000). This would turn aqueous sulfuric acid aerosols into dilute solutions (<40 wt% H_2SO_4) highly suited for chlorine activation and should occasionally trigger ice clouds (see below). A recent analysis by J.B. Smith et al. (2001) of ER-2-borne H_2O and ClO observations in the midlatitudes suggests relative humidities decrease strongly within 500 m above the local tropopause (with negligible supersaturation with respect to ice). Therefore, these authors classify cases like the one described by Keim et al. (1996) as exceedingly rare. However, they found 0.8% of measurements in the first kilometer above the local tropopause indicated the presence of enhanced ClO (5 out approximately 660 data points). This value is not so different from the 2% of supersaturation specified by Gierens et al. (1999), and therefore there need not be a contradiction.

Potential Chlorine Activation on Ice Particles

In addition to cold liquid aerosols, ice particles are also a potential host of heterogeneous reactions in the midlatitude LS. Although ice clouds have been observed above the high-latitude tropopause, the different temperature profile at midlatitudes must make the particles less frequent. Borrmann et al. (1997) identified a cirrus event near the local tropopause near Bangor, Maine (45°N), accompanied by ClO mixing ratios ranging between a few and several tens of pptv in the vicinity of the clouds. On

the basis of this measurement, Solomon et al. (1997) included additional very thin (subvisible) ice clouds derived from satellite observations (P.-H. Wang et al., 1996) in their model and suggested that chlorine activation might occur through heterogeneous chemical reactions on aerosol and cloud particles. Bregman et al. (2002) incorporated tropopause ice cloud fields in a 3-D model and found local perturbations in ClO and NO_x to be comparable to the observations of Keim et al. (1996). However, quantitative differences between these studies are substantial, and Bregman et al. (2002) concluded that it would seem unlikely that heterogeneous chemistry on subvisible clouds could explain the observed negative ozone trends in the midlatitude lowermost stratosphere.

A three-year record of continuous lidar observations at the Observatoire de Haute-Provence (OHP, 44°N, 6°E) suggests ice cloud occurrence frequencies in the lowermost stratosphere of 10-20%, with 5% of the cloud top heights observed at least 1 km above the tropopause (Goldfarb et al., 2001). However, this study relies on temperature sonde measurements made 120 km east of OHP, and possible changes in tropopause height over this distance lead to uncertainty in these numbers. Given the contradictory results from the ER-2 and MOZAIC data with respect to extent of ice saturation above the tropopause (see above), the existence and occurrence frequency of ice particles (subvisible cirrus) *above* the midlatitude tropopause remain highly uncertain.

Other Reactions and Surfaces

In the search for other heterogeneous reactions, alternative reaction pathways and reaction partners have been suggested. For example, Drdla et al. (1999) suggested that heterogeneous reactions of formaldehyde (CH₂O) + HNO₃ and nitrous acid (HONO) + HNO₃ (Iraci and Tolbert, 1997; Longfellow et al., 1998) could cause an increase in NO_x of up to 25% in the LMS. Another proposed heterogeneous reaction on sulfuric acid aerosol is carbon monoxide (CO) + HNO₃ (Fairbrother et al., 1997). This reaction could also enhance the NO_x:NO_y ratio, particularly in the LS (Lary and Shallcross, 2000). An assessment of these reactions in long-term modeling studies requires a reduction of the remaining uncertainties in the reaction probabilities.

Soot is another surface that could potentially be important for ozone chemistry in the midlatitude LS. Modeling studies have suggested that ozone could be destroyed on the soot surface, forming O₂, and that NO₂ and HNO₃ could react to form HONO, which photolyzes to yield HO_x (Bekki, 1997; Lary et al., 1999). However, recent laboratory studies and measurements indicate that

soot is likely to have only a negligible impact on ozone chemistry in the lower stratosphere (Choi and Leu, 1998; Gerecke et al., 1998; Kalberer et al., 1999; Strawa et al., 1999; Disselkamp et al., 2000).

4.5.2 Quantifying the Chemical Influence on Ozone: Modeling Tools

Studies of global O₃ changes have used two-dimensional (2-D) latitude-height models or, recently, three-dimensional (3-D) models. These models contain representations of atmospheric transport, radiation, and both gas-phase and heterogeneous chemistry. Some of these processes may be coupled (e.g., chemically integrated ozone being used in the radiation calculation). Alternatively, some models may use fixed fields for certain processes (e.g., transport specified from meteorological analyses). Different models make different approximations, for example, 2-D models approximate the atmosphere as a zonal mean, whereas 3-D models may use a simplified chemistry scheme because of computational costs. Box 4-1 summarizes how well components of these global models are known to reproduce key processes in the stratosphere.

Recent studies have provided more information on the ability of 2-D and 3-D chemical models to quantitatively explain the midlatitude ozone changes. Considine et al. (1999) performed a Monte Carlo study to assess the effects of uncertainties in photochemical data on calculated ozone trends, and found a 46% model uncertainty at the 1σ level. Similar conclusions were obtained by Fish and Burton (1997), who inferred a 50% uncertainty in midlatitude ozone loss rates based upon a quantitative analysis of uncertainties in photochemical data. Both studies argued that, given these large model uncertainties, the discrepancy between the chemically modeled and observed trend could not be used as a critical test of theory. This conclusion remains valid based upon current photochemical uncertainties. Hence, comparisons of observations and numerical models in this Assessment continue to rely upon a broad range of factors in assessing their merits, such as seasonal, latitudinal, and vertical variations in calculated ozone depletion, as well as model-data comparisons for other trace gases such as ClO.

4.5.2.1 2-D MODELS

Two-dimensional radiative-dynamical-chemical models are still a widely used tool for assessing the effects of long-term (many decade) changes in chemical species (e.g., CFCs) on stratospheric ozone. They are computationally inexpensive and can be used for many sensitivity studies. However, these models cannot account for all of

Box 4-1. Components of 2-D and 3-D Chemical Models**Gas-Phase Chemistry**

Most (if not all) stratospheric models use photochemical modules that are based on standard compilations of laboratory data (e.g., JPL 2000; see Section 4.5.1.1). This procedure ensures that results from different models and different runs can be readily compared. All “full chemistry” models contain a complete description of what are believed to be the main species and reactions that control stratospheric ozone. Model-model intercomparisons have shown that, when constrained by the same photodissociation rates, the gas-phase chemical packages from the assessment-type models agree very well (Park et al., 1999; Kawa et al., 1999).

Heterogeneous Chemistry

Modeling the processes that can contribute to changes in ozone in the LS and LMS depends critically on including a realistic treatment of heterogeneous chemistry in the model. For nonpolar studies, the key parameter is the sulfate aerosol surface area density (SAD) and composition. Particularly in the LMS below the maximum in aerosol abundance, the SAD is subject to large uncertainties (of the order of 30%; see Section 4.3.1). For the period perturbed by volcanic eruptions, the inversion of satellite observations to infer aerosol densities below the peak of the aerosol distribution is a source of uncertainty. For diagnostic studies of observed trends, global 2-D and 3-D models can use observations based on satellite data (e.g., SAGE II back to 1984). Outside of this period, global distributions need to be derived from other data.

Temperature

Even with a realistic SAD, model studies have demonstrated that temperatures must be known to better than 2 K to simulate accurately the highly temperature-sensitive Cl-activating heterogeneous chemistry that is critical to ozone loss (see, e.g., Solomon et al., 1998; Tie et al., 1997). Models that use meteorological analyses will almost certainly have more realistic temperatures than 2-D models or GCMs in which they are calculated. However, in the past, meteorological analyses have been far less accurate than this stringent 2-K criterion in the polar vortices of both hemispheres (see, e.g., Manney et al., 1996), although recent analyses show much better agreement (Pommereau et al., 2002). In any case, uncertainties in polar temperatures add to our uncertainties in the ozone depletion in polar regions (see Chapter 3) and thus in the transport of ozone-depleted air to lower latitudes (van den Broek et al., 2000).

Transport

Accurate assessment of the cause of global ozone changes requires models with a realistic treatment of the slow, meridional Brewer-Dobson circulation and eddy transport. Since WMO (1999), a great deal of work has been carried out on comparing models with tracer observations using age-of-air diagnostics (Hall et al., 1999; Park et al., 1999). These studies showed that many 2-D and 3-D models had vertical transport that was too rapid, and hence they underestimated the mean age in the stratosphere derived from observations (see Figure 4-28, p. 4.44). This implies that the models would transport CFCs too rapidly, giving insufficient time for the release of Cl_y , for example, from halogen-containing source gases. This may adversely affect trend calculations, not only through the incorrect Cl_y values in the lower stratosphere, but also because of possible errors in the rate of ozone replenishment through transport. However, the effect of this uncertainty on trend calculations has not been quantified.

the factors that influence interannual variability or trends in atmospheric circulation, though they may capture some of the feedbacks. Also, they are not well suited to the treatment of polar processes, because, for example, they cannot account fully for the dynamics of the polar vortex and its coupling with midlatitudes. For similar reasons they are not well suited to the treatment of transport processes close to the midlatitude tropopause in the LMS. They are probably most reliable in the US and LS, outside of the polar regions (WMO, 1999). Even though the models represent atmospheric zonal means, allowance

can be made for departures from the zonal mean in, for example, the temperature field, which is important for capturing the in situ Cl activation on cold sulfate aerosols (e.g., Solomon et al., 1998; Jackman et al., 1996).

4.5.2.2 3-D MODELS

Three-dimensional models aim to represent the full altitude-latitude-longitude variations in the atmosphere. These models are computationally more expensive than 2-D models, especially when using “full” chemistry. Full-chemistry 3-D models are now used routinely, but gener-

ally for short periods of a few months, e.g., to study seasonal polar ozone loss. However, recently full-chemistry 3-D models have become more widely used for multiannual (or decadal) time scale integrations (e.g., Chipperfield, 1999; Rummukainen et al., 1999; Austin et al., 2000).

Three-dimensional models can be classified into general circulation models (GCMs) and off-line chemical transport models (CTMs) that use winds specified from an external source. When these winds (and temperatures) are taken from meteorological analyses, the model will have a reasonably realistic representation of the atmosphere on a given day, which is useful for interpreting specific observations. However, CTMs are still dependent upon the accuracy of the analyzed temperature fields, and errors of a few degrees may cause substantial errors in calculated ozone losses. The use of analyzed winds may lead to horizontal and vertical winds and temperatures that are not self-consistent. 3-D models (like 2-D models) are also subject to errors in the treatment of the slow, meridional circulation (see Figure 4-28). GCMs calculate their own (self-consistent) winds and temperatures, but they tend to suffer from large uncertainties in the key parameter of calculated polar temperatures (see Chapter 3). Although GCMs should be able to more accurately simulate interactions between the stratosphere and the troposphere than 2-D models, they are still subject to uncertainties, raising questions about the accuracy of some calculated feedbacks to the dynamical fields (see Section 4.6). Furthermore, because 3-D models are relatively new and expensive to use, the exact nature of these models' circulations over long time scales has not been extensively characterized.

4.5.3 Quantifying the Chemical Influence on Ozone: Model Results

Numerical models of the stratosphere have achieved substantial success in simulating many of the observed features of the ozone layer and its depletion. Previous Assessments (e.g., WMO, 1995, 1999) and model intercomparison reports (e.g., Park et al., 1999) showed that both two-dimensional and three-dimensional numerical models could reproduce the general behavior of a wide variety of stratospheric constituents, including reactive species such as nitrogen oxides, source gases such as CFCs, and ozone itself. More than three decades of such comparisons between models and observations, and between differing models of varying complexity, have been a cornerstone of current confidence in the ability of models to represent many key stratospheric processes, albeit with remaining quantitative uncertainties. Here we briefly discuss new information on modeled trends and

distributions of gases other than ozone, to gain insight into the factors that are likely to have affected ozone trends over the past decade. We then discuss current model simulations of past ozone changes.

4.5.3.1 EFFECTS OF NO_x - AND ClO_x -RELATED PROCESSES

Koike et al. (1994), Van Roozendaal et al. (1997), and Liley et al. (2000) presented observations from New Zealand and Europe indicating decreases in NO_2 abundances following the Mt. Pinatubo eruption (see Figure 4-21). These were in general accord with model calculations and support the view that this volcano introduced major perturbations to the photochemistry of the global stratosphere during the period from about 1992 to 1995 (see Section 4.6.6).

A recent study by Froidevaux et al. (2000) examined trends in satellite observations of ClO during the 1990s. Near the 2-hPa level, they showed a positive trend in ClO, which is likely to be caused in part by the trend in Cl_y over this period. However, they also demonstrated that variations in methane (which play a controlling role in the partitioning between ClO and HCl) dominated the changes in observed ClO during this period, as illustrated in Figure 4-29. The observed US methane changes in the mid-1990s (Nedoluha et al., 1998b; Randel et al., 1999) are poorly understood and not included in standard models, raising important questions for the modeled ClO and hence for model-calculated ozone trends in the upper stratosphere.

In the lower stratosphere, the ClO time series presented by Froidevaux et al. (2000) showed enhancements at 22 and 46 hPa following eruption of Mt. Pinatubo, and that perturbation was fairly well reproduced by a 2-D model to which the data were compared. Observations of the ratio of HCl/Cl_y (Webster et al., 2000) provide a separate and important test of the long-term responses of chlorine compounds to variations in sulfate aerosols in the lower stratosphere, since increased ClO is expected to be associated with decreased HCl at those levels. Webster et al. (2000) examined balloonborne and spaceborne data from 1985 to 1994 and argued for an impact on HCl/Cl_y under cold high-aerosol conditions that exceeds current model calculations. However, Dessler et al. (1997) also studied in situ observations of HCl/Cl_y near 50 hPa from aircraft data obtained from 1992/1993 (immediately after Pinatubo) to 1995/1996, showing evidence for chlorine activation close to that predicted by chemical model calculations.

Thus these recent studies have at least qualitatively supported earlier work showing that the observed changes

GLOBAL OZONE

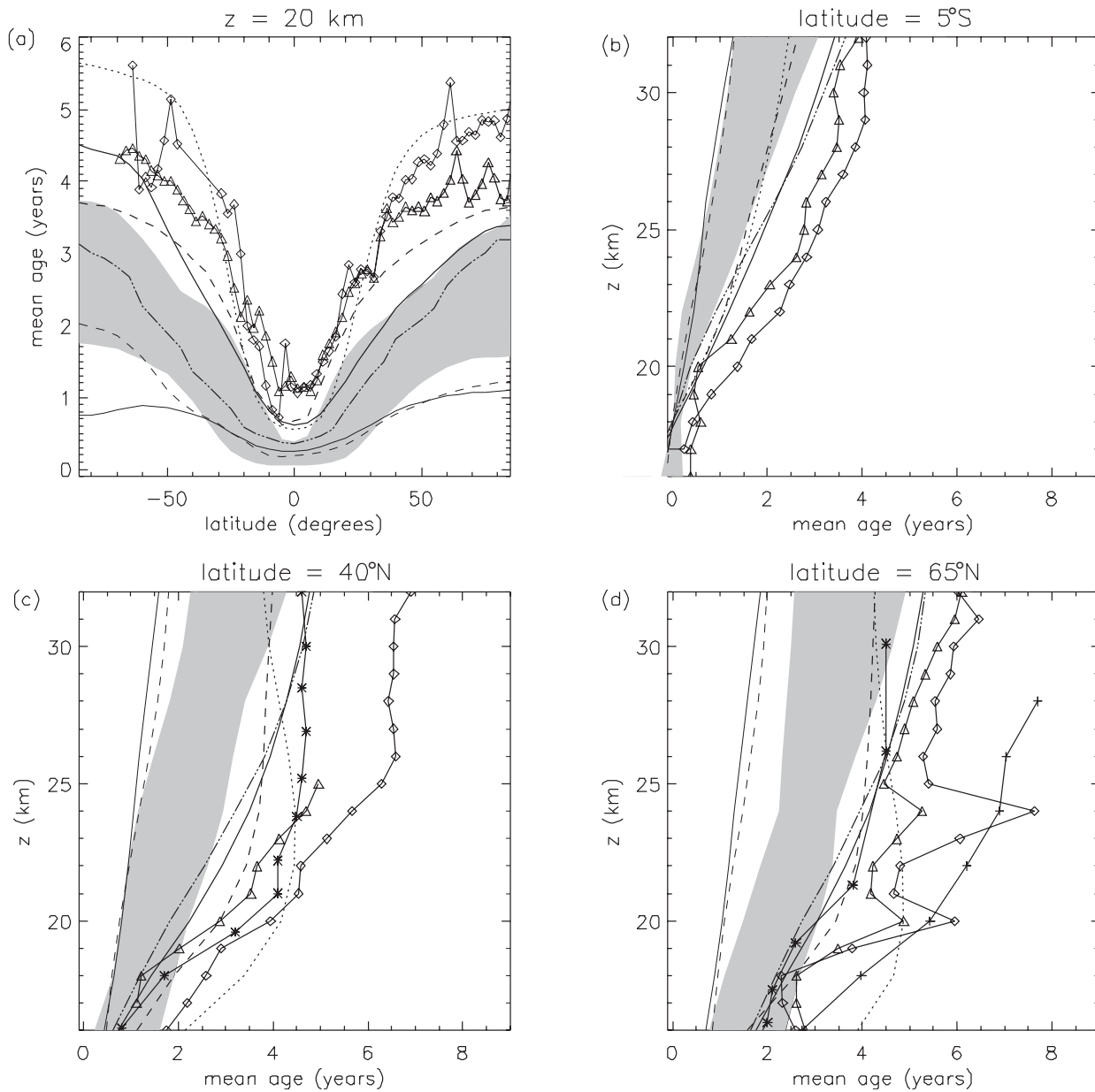


Figure 4-28. Mean age of air estimated from a range of 2-D and 3-D models. In all panels the shaded region indicates the range of mean ages of 17 2-D and 3-D models, not including Harvard-3D (dotted line), MONASH1-3D (heavy solid line), GSFC-2D (heavy dashed line), GSFC-3D (light dashed line), UC123 (dot-dashed line), and UIUC-3D (light solid line), which are shown separately. The symbols represent observations: mean age from in situ CO_2 (triangles) and in situ SF_6 (diamonds). (a) Latitude profile versus in situ aircraft data. (b) Vertical balloon profiles at 7°N . (c) Balloon flight of September 1996, at 35°N (diamonds and triangles) and SF_6 whole-air samples from 44°N (asterisks). (d) Balloon flight of June 1997, 65°N (diamonds and triangles) and whole-air SF_6 samples at 68°N inside (asterisks) and outside (crosses) the winter polar vortex. From Hall et al. (1999).

in the ClO and NO_x abundances of the lower stratosphere were generally matched by models that included the effects of the Mt. Pinatubo eruption (e.g., Fahey et al., 1993; Solomon et al., 1996). Taken together, the meas-

urements and models continue to provide support for the view that heterogeneous reactions on sulfuric acid aerosols suppress the abundances of NO_x species (mainly through N_2O_5 and BrONO_2 hydrolysis), while enhancing

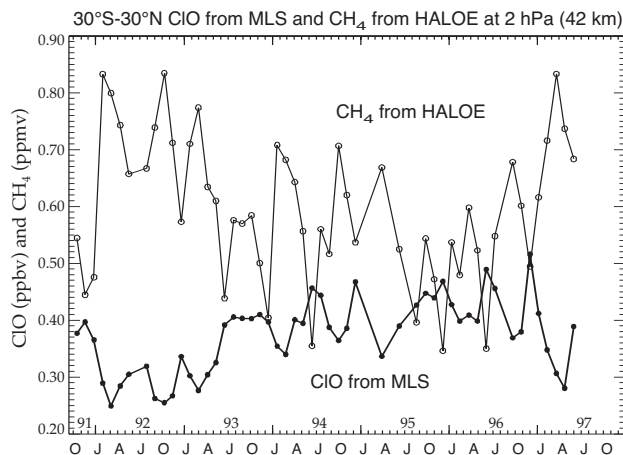


Figure 4-29. Time series of zonal mean abundances of ClO from Microwave Limb Sounder (MLS) data (filled circles) and CH₄ from Halogen Occultation Experiment (HALOE) observations (open circles) for 2 hPa (42 km) and averaged over 30°S-30°N. From Froidevaux et al. (2000).

concentrations of ClO. The net effect of increased sulfuric acid aerosols is an ozone increase above about 25 km, where NO_x dominates ozone losses (Hofmann et al., 1994; Mickley et al., 1997; Solomon et al., 1996), and decrease in the lower stratosphere, where ClO abundances control the impact of halogen chemistry on ozone loss. The changes in stratospheric aerosol content during the 1990s following the massive perturbation of Mt. Pinatubo should therefore be expected to exert a substantial influence on ozone changes during the past decade. Standard models generally include the observed changes in aerosol based upon SAGE observations, as noted (Box 4-1), and hence incorporate a representation of these chemical effects.

4.5.3.2 EFFECT OF POLAR VORTEX ON MIDLATITUDES

Recent model-based studies have attempted to quantify the effect of Arctic polar processing on midlatitude ozone amounts. Knudsen and Grooß (2000) used a seasonal reverse domain filling (RDF) trajectory calculation to study the dilution of ozone-depleted air into northern midlatitudes. They estimated that approximately 40% of the 6.8% decline in midlatitude ozone observed by TOMS between 1979 and 1997 could be accounted for by transport of polar ozone-depleted air into midlatitudes. Other studies have used tracers mapped in equivalent latitude, or discriminated between polar and nonpolar air in 3-D CTMs, to evaluate the connection between polar and midlatitude ozone loss. From the analysis of several

Arctic winters in the late 1990s, Millard et al. (2002) showed that the contribution to the seasonal midlatitude ozone loss from high latitudes was strongly dependent on the meteorological conditions and the stability of the polar vortex. They found the largest contribution to midlatitude ozone loss for winter 1999/2000, with half the midlatitude loss originating north of 60°N. A much smaller contribution was found in the winter 1996/1997, characterized by a strong and pole-centered vortex prior to the final breakup. Using a different model and set of tracers, Marchand et al. (2002) found similar results for the winter 1999/2000. Godin et al. (2002) used a high-resolution model together with ground-based ozone measurements to study the influence of vortex excursions and polar air filaments on midlatitude ozone amounts during several winters, finding the largest impact during 1999/2000 due to the large Arctic ozone loss that occurred that winter coupled with several vortex excursions at the end of the winter.

The accumulated effect of polar vortex loss on midlatitudes has been studied by Chipperfield (1999) using multiannual simulations of the 1990s in a 3-D CTM with full chemistry and horizontal resolution of 7.5° × 7.5°. That study estimated that overall PSC-related depletion processes in or at the edge of the vortex results in 2-3% less ozone at 50°N throughout the year. The effect was larger in the Southern Hemisphere (5% less O₃ at 50°S), reflecting the large losses occurring in the Antarctic.

The fate of ozone-depleted air subsequent to NH polar vortex breakup was studied by Piani et al. (2002). They showed that by the end of June, much of the ozone-depleted air above 420 K has been transported from the polar region to the subtropics. In contrast below 420 K, most of ozone-depleted air remains poleward of 55°N, due to the influence of the upper extension of the tropospheric subtropical jet that provides a transport barrier at lower levels.

4.5.3.3 EFFECT OF WATER VAPOR TRENDS

Observations suggest a positive trend in stratospheric water vapor during the past several decades, which can in turn increase HO_x concentrations and feed back into other chemical cycles involving NO_x and ClO_x. Solomon (1999) and Kirk-Davidoff et al. (1999) also noted the strong dependence of heterogeneous chemistry on water vapor content; the former work emphasized the lowermost stratosphere and temperature variability whereas the latter focused on polar regions. The observed water vapor increases to date substantially exceed the contribution expected from methane oxidation in the lower stratosphere, raising important questions about the source

GLOBAL OZONE

of the increases (see Section 4.3.2). While standard photochemical models do not include this additional water vapor, several modeling groups have carried out specific tests of its likely effects, guided by observations of the magnitude of the water vapor change. Evans et al. (1998) showed that the water vapor trend was unlikely to make a significant contribution to ozone trends in the upper stratosphere (see also WMO, 1999). Dvortsov and Solomon (2001) showed that the observed trend in water vapor could have contributed about 1% to the total column and peak ozone depletions at northern midlatitudes. They argued that this depletion was due to enhancements in HO_x chemistry and to the coupling between HO_x and ClO_x chemistry in the lower stratosphere (which contributed about 0.2%/decade).

Aircraft emissions can potentially affect the composition of the atmosphere. The Intergovernmental Panel on Climate Change (IPCC) Special Report on *Aviation and the Global Atmosphere* (IPCC, 1999) summarized the present understanding and concluded that the 1992 subsonic fleet was responsible for total ozone column changes (at 45°N latitude) of approximately +0.4%, with approximately a quarter of that change occurring in the stratosphere. This impact is likely to increase with future growth in fleet emissions (see Section 4.8.3).

4.5.3.4 ASSESSMENT MODEL SIMULATIONS OF PAST OZONE CHANGES

Within the framework of this Assessment, nine models have performed simulations of past ozone trends in order to test current understanding. The participating 2-D models, which have all been widely used in scientific studies of stratospheric ozone, are listed in Table 4-4. For this Assessment the models were run with the observed surface halocarbon abundances described in Chapter 1 (see Appendix 4B). The surface values of N₂O, CH₄, and CO₂ were taken from IPCC (2001). (Note that these model runs ignore other drivers of chemical change, such as additional H₂O trend or aircraft emissions.) The models used photochemical data from JPL 2000 (Sander et al., 2000), which is the most recent recommendation available. The aerosol distribution in all models was specified from a monthly climatology based on satellite data, similar to that used in Jackman et al. (1996) and updated by D.B. Considine (NASA Langley Research Center).

The previous Assessment (WMO, 1999) demonstrated that these models simulate many features of the state of the ozone layer prior to the onset of major depletion reasonably well. They are able to reproduce the observed ozone column minimum in the tropics, the inter-hemispheric differences in the ozone maxima in the extra-

tropics, and the general features of the seasonal cycles of both hemispheres. One important difference in the model simulations is that two models (NOCAR and GSFC-INT) incorporate interactive temperature changes due to changes in greenhouse gases (GHGs) (particularly CO₂) and in ozone itself, which result in US cooling of ~1 K/decade. This feedback has a significant effect on simulations of past and future ozone changes in the US, as seen below.

Figure 4-30 shows the annually averaged ozone profile trends for 1980-2000 at northern and southern midlatitudes as calculated by eight of the 2-D assessment models. In the photochemically controlled region above 25 km, there is a large variation in the (maximum) model-calculated trends, which range from around -4 to -5%/decade (NOCAR, GSFC-INT and OSLO) to -8 to -10%/decade for the other models, with observations in the middle (-6 to -7%/decade). The most important difference between the models is the temperature feedbacks included in the NOCAR and GSFC-INT simulations. While the non-interactive models overestimate the observed ozone trends for 40-50 km (probably due in part to the neglect of stratospheric cooling), the interactive model trends are significantly smaller than observations over this region. However, the observed shape of the profile is well reproduced by all the models, and this is controlled by ClO/Cl_y partitioning. Although there is confidence that halogen chemistry is the main driver for the observed trend in the upper stratosphere (WMO, 1999), the model-model differences indicate the important feedback that other changes (especially temperature) have on modulating the ozone depletion.

At lower altitudes the models underestimate the observed NH ozone trends over this period. The model values cluster in the range of -1 to -3%/decade, while the SAGE and ozonesonde trends near 20 km are approximately -3 and -5%/decade, respectively. One caveat is that the ozonesonde trends (derived from an eight-station average) are larger than can be reconciled with the zonal mean column ozone trends, and are likely an overestimate due to limited sampling (see Section 4.2.4). However, the model trends are probably still smaller than observed changes in this region, and because 70-85% of the column trends originate below 25 km (Section 4.2.4), these profile underestimates are the main reason why modeled column ozone changes in NH midlatitude are less than observations (shown below). There may be several reasons for these differences. Part of the model trend underestimate (of order 1%/decade) is likely to be due to the neglect of the observed water vapor trend, and uncertainties in kinetics may also contribute. Further, some recent observations suggest that the bromine content of the low-

Table 4-4. 2-D models participating in simulations of past ozone trends.

Model Name	Institution(s)	Investigators	Temperatures	PSC Scheme	Reference
AER	AER, Inc., U.S.	D.K. Weisenstein, C.J. Scott, M.K.W. Ko	Specified from NCEP analyses	Based on model T	Weisenstein et al. (1998)
MPIC-2D	MPIC, Germany	C. Brühl, J.U. Groo , P.J. Crutzen	Specified from CIRA/MAP data	Based on prescribed T and probability function	Groo et al. (1998)
GSFC	NASA Goddard, U.S.	C.H. Jackman, E.L. Fleming, D.B. Considine	Specified from UKMO analyses	Distribution based on NCEP temperatures	Fleming et al. (1999)
GSFC-INT	NASA Goddard, U.S.	J.E. Rosenfield, D.B. Considine	Calculated by model; interactive with CO ₂ , O ₃ , and H ₂ O	PSC from [ob- served T minus 2 K]	Rosenfield et al. (1997)
NOCAR	NOAA/NCAR, U.S.	R. Portmann, R.R. Garcia, S. Solomon	Calculated above 10 hPa (interactive with CO ₂ , O ₃ , H ₂ O, and CH ₄); NCEP analyses below 10 hPa	NCEP T for PSC	Portmann et al. (1999)
OSLO	University of Oslo, Norway	B. Rognerud	Specified	Based on climatology	Stordal et al. (1985)
RIVM	RIVM, The Netherlands	G. Velders	Climatology (noninteractive)	No solid PSCs	Velders (1995)
SUNY-SPB	SUNY, U.S.; St. Petersburg, Russia	S. Smyshlyaev, M. Geller	Specified from NCEP	Based on NCEP temperatures	Smyshlyaev et al. (1998)
ULAQ	University of L'Aquila, Italy	G. Pitari, E. Mancini	Specified from NCAR dataset	Based on model T	Pitari and Rizi (1993)

AER, Atmospheric and Environmental Research, Inc.; MPIC, Max-Planck-Institut für Chemie; RIVM, Rijkinstituut voor Volksgezandheiden en Milieu; SUNY, State University of New York; CIRA, Committee on Space Research (COSPAR) International Reference Atmosphere; MAP, Middle Atmosphere Project.

ermost stratosphere may be larger than estimated in these models that are based on long-lived bromine sources only (Harder et al., 2000). The bromine content of the LMS may be affected by transport of short-lived substances such as bromoform and BrO to the upper troposphere and stratosphere (Ko et al., 1997; Dvortsov et al., 1999; Schauffler et al., 1999; Sturges et al., 2000; Fitzenberger et al., 2000; Pfeilsticker et al., 2000; and Chapter 2). Even if there are no trends in these largely natural sources of Br_y, they could enhance anthropogenic ozone depletion through chemical coupling with Cl_y trends, especially via the ozone-destroying reaction of ClO + BrO. A further reason for the discrepancy in northern midlatitudes may be related to the formulation of the 2-D models, in that they do not accurately simulate polar ozone loss and its transport to midlatitudes. Finally, dynamical contribu-

tions could also contribute to past ozone changes over NH midlatitudes, as discussed in Section 4.6.

Figure 4-31 shows the observed and calculated annual mean column ozone trends as a function of latitude for the period 1980-2000. The largest trends occur at high southern latitudes, associated with the Antarctic ozone hole. The models show a wide variation in their ability to reproduce this feature, with most underestimating the observed trend, though the GSFC and GSFC-INT models produce very large depletions (which extend into SH midlatitudes). In the Arctic, the inter-model differences are smaller and match the observations fairly well near 60°N. The models tend to underestimate the northern midlatitude column ozone loss, consistent with the profile comparisons (Figure 4-30) discussed above. In the tropics, all of the models overestimate the observed

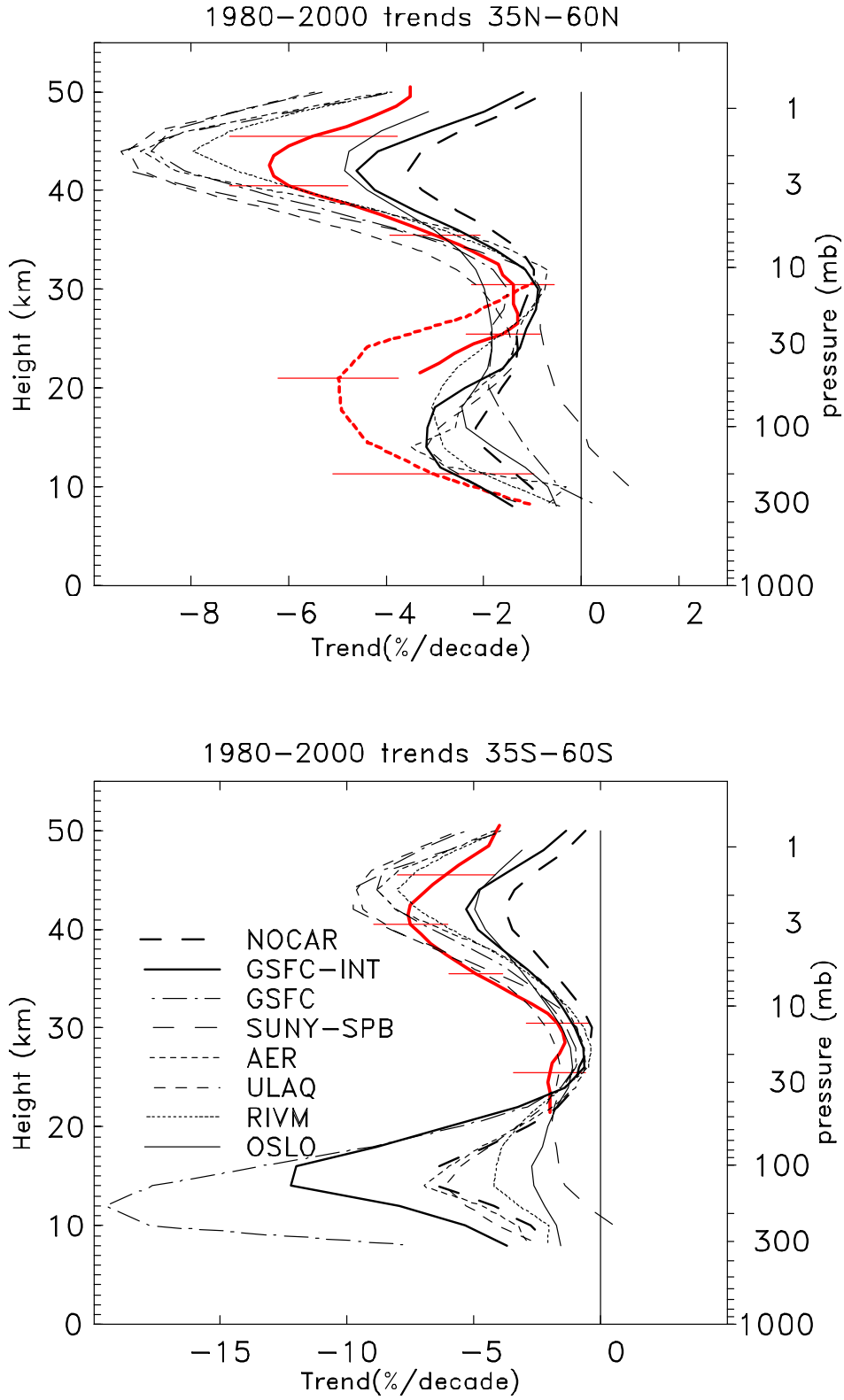


Figure 4-30. Vertical profiles of ozone trends over the period 1980-2000 from observations compared with eight 2-D model calculations for statistics for 35°N-60°N (top) and 35°S-60°S (bottom). The observations are from SAGE I+II (solid red line with 2σ error bars) and averaged ozonesondes (dashed red line; data only available in the NH). The trend units are %/decade calculated with respect to the climatology of each model.

(near-zero) trend, which may be associated with model overestimates of the mixing between the tropical and mid-latitude LS.

Figure 4-32 shows the seasonal variation of the modeled column ozone trends compared with the observations, with results separated for NH and SH midlatitude (35° - 60°) and polar (60° - 90°) regions. In the Antarctic region, most models underestimate the amplitude of the seasonality, because of an underestimation of the spring-time depletion. The two models that produce the largest ozone hole depletions (GSFC and GSFC-INT) substantially overestimate the trend in southern midlatitudes at that time of year. The other models generally reproduce the observed SH midlatitude trends (within the error bars) and its weak seasonality. In the Arctic region, although the models do not capture the same amplitude of seasonal variation as the observations, they do fall within the 2σ uncertainty. At northern midlatitudes the models do a reasonable job of reproducing the magnitude and seasonality of the trend, although the winter-spring maximum is underestimated in most models.

Figure 4-33 compares the smoothed time series of the observed ozone depletion with the 2-D model results, for the near-global average (60° N- 60° S) and for NH and SH midlatitudes. Note that for the 60° N- 60° S average (Figure 4-33, top panel) the observations use the data with the solar cycle statistically removed (Figure 4-4), because these 2-D models do not include a parameterization of the solar cycle. The models all overestimate the decadal ozone changes over 60° N- 60° S (Figure 4-33), because of the overestimate of tropical trends (Figure 4-31). For the

latitude band of 35° - 60° N (Figure 4-33, middle panel), the 2-D models are in broad agreement with many aspects of the observations, but slightly underestimate the decreases. Both the observations and the models display decreases in northern midlatitude ozone following the El Chichón eruption in the early 1980s and the Mt. Pinatubo eruption in the 1990s. However, the magnitudes of the observed changes are larger than most calculations, and there is also an observed dip in the late 1980s that is not simulated by the 2-D models. Chipperfield (1999) noted the important role of polar processing in driving spring-time midlatitude ozone decreases following eruption of Mt. Pinatubo, which may be linked to the underestimate seen in some of the 2-D models in that time period. Also, some of this post-Pinatubo dip may be dynamically induced (see Section 4.6). Current model results are also sensitive to changes in photochemical rates when compared with earlier studies (such as Solomon et al., 1996; Jackman et al., 1996; WMO, 1999). In particular, new data for NO_x reactions (used in the runs presented here) caused reductions in both the calculated trends and in the amplitude of the estimated Mt. Pinatubo perturbation, compared with studies carried out for the previous Assessment (as shown by Portmann et al., 1999). One preliminary run of the NOCAR model using the updated kinetics discussed in Section 4.5.1, but not included in JPL 2000, yielded extremely small changes in calculated midlatitude depletion.

Figure 4-33 (bottom panel) shows the observed and calculated trends for the region of 35° - 60° S. The observations suggest an overall change for the 20 years of about

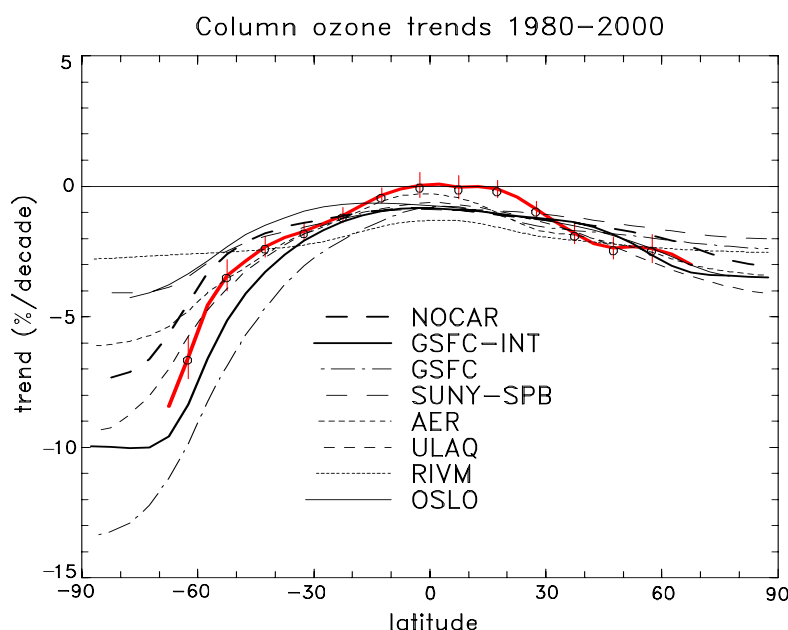


Figure 4-31. Latitudinal profile of annual mean column ozone trends from the merged TOMS+SBUV2 satellite dataset (solid red line) (see Section 4.2) compared with results from eight 2-D models, for 1980-2000. The trend calculations use a standard regression analysis, including a QBO term for the observations but not for the models. The error bars for the observations indicate 2σ uncertainties.

GLOBAL OZONE

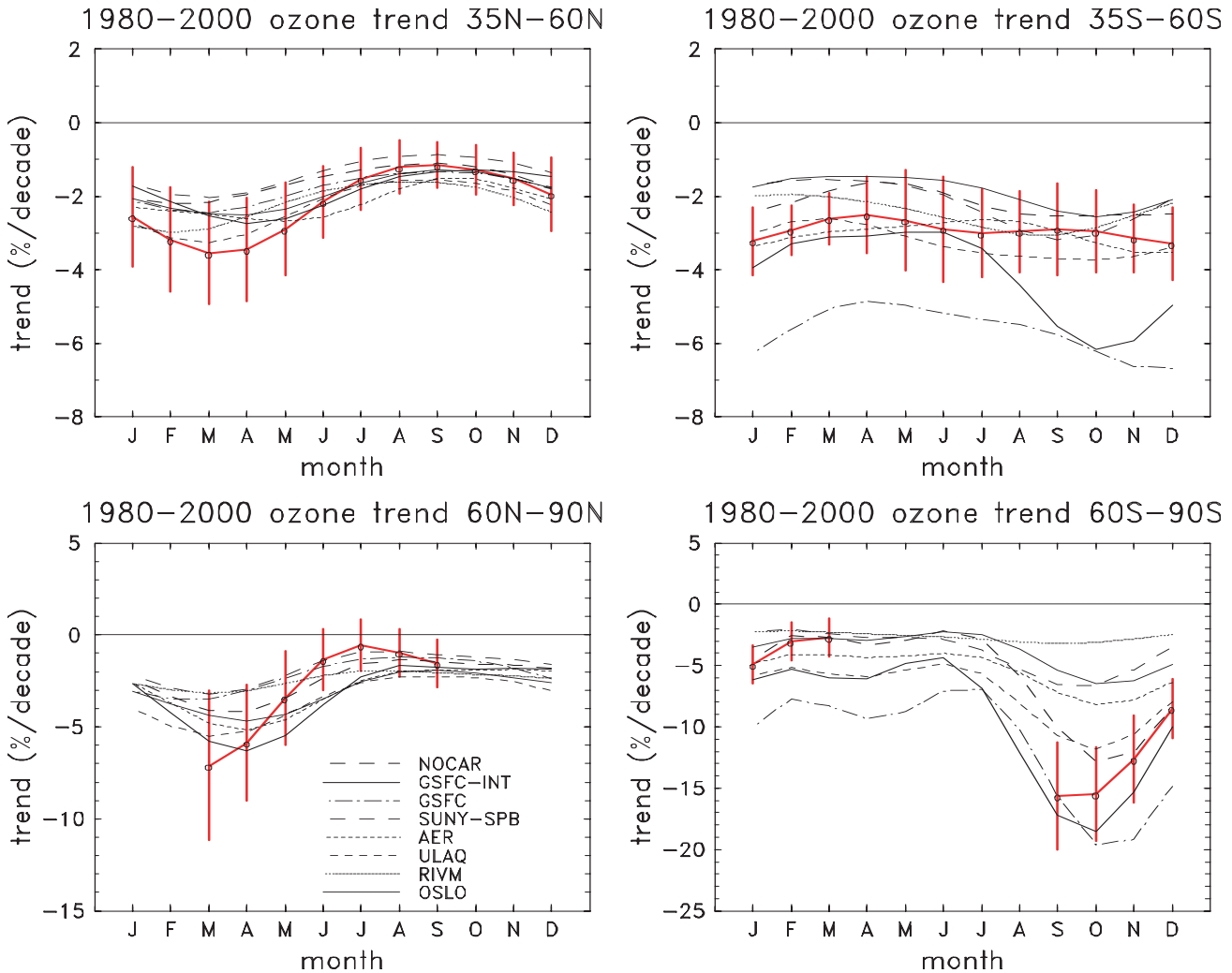
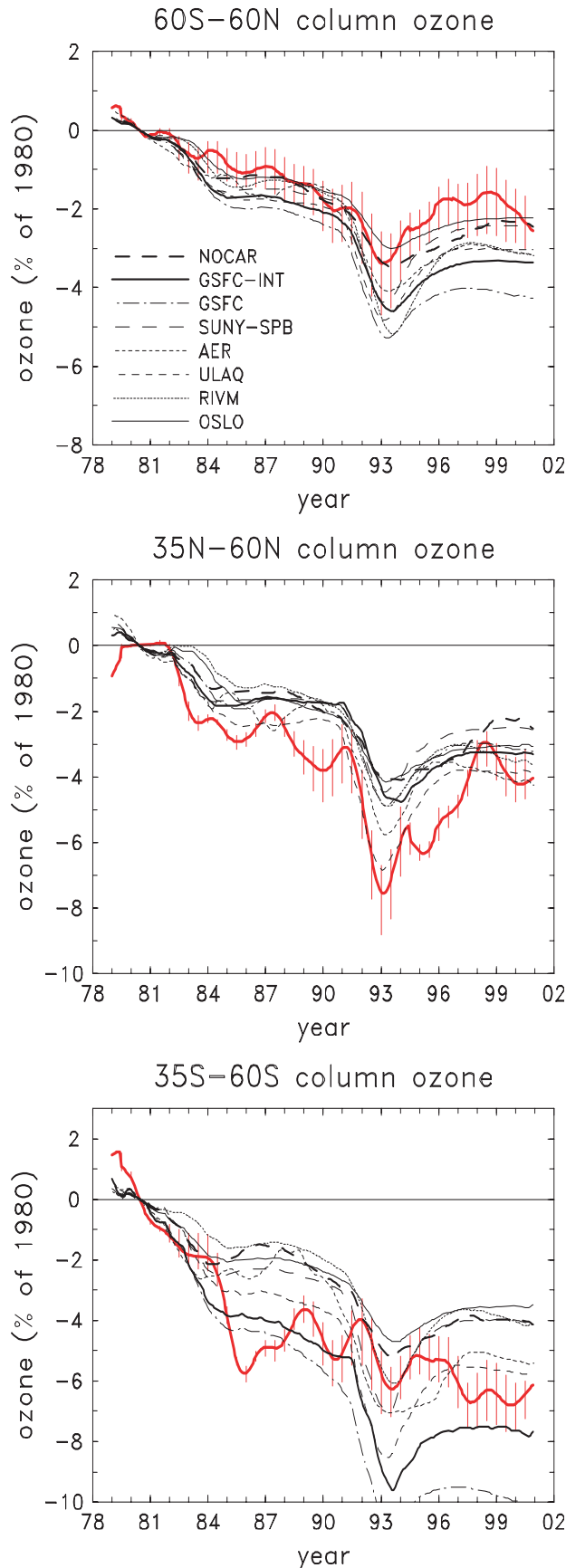


Figure 4-32. Seasonal variation of observed and modeled column ozone trends at 35°N–60°N (top left), 35°S–60°S (top right), 60°N–90°N (bottom left), and 60°S–90°S (bottom right). Observed trends (red lines) were derived from the merged satellite data using a seasonally varying regression model, with error bars denoting 2σ uncertainty estimates.

6%, while the model values range from 4% to 10%. Each of the models displays an ozone decrease in the SH following the eruption of Mt. Pinatubo, approximately similar to the model calculations in the NH, but observations show a much smaller signal. There are relatively large differences of about 2% between the various satellite datasets during that time, implying caution regarding exact details. The largest short-term ozone perturbations for SH midlatitudes are the low values in the mid-1980s, which are not simulated in any model and have not been explained. Closer inspection of the data reveals that the unusual values occurred during a short period (1985–1986), when ozone was low over midlatitudes throughout the SH (see Figure 4-6). The short duration of the pertur-

bation for 1–2 years argues against a solar irradiance-driven mechanism, or attribution to a recurring process such as the El Niño–Southern Oscillation (ENSO) or the QBO. Thus these comparisons show that although SH decadal-scale trends are reasonably well reproduced by some present models (with a wide spread related to different treatments of the Antarctic ozone hole), there are mechanisms for shorter-term interannual variability that are not well simulated by any 2-D model.

As discussed above, it is only very recently that three-dimensional models have been used to study multi-decadal past changes in ozone. Figure 4-34 shows results from a 20-year run of the SLIMCAT 3-D chemical transport model (CTM) (Chipperfield, 1999) over the period



1979-1998. The model was forced by European Centre for Medium-Range Weather Forecasts (ECMWF) meteorological analyses in two separate simulations, one with time-dependent halogen loading and one with constant (1979) halogen loading. Although the atmospheric halogen loading in 1979 itself was well above natural levels, the difference between the two model experiments shows the modeled chemical loss relative to 1980. The 3-D CTM results produce more interannual variability (on the time scale of a few years) than the 2-D models, because of the use of analyzed winds. In the early 1980s and the early 1990s, and again in the late 1990s, the 3-D model with the imposed halogen trend matches much of the observed decreases in column ozone. However, there are periods, during the mid-1980s and mid-1990s, when the model variations differ significantly from the observations. There are still large interannual changes, e.g., related to the low SH ozone in the mid-1980s, that have not been explained.

In summary, the 2-D assessment models generally perform better in simulating the NH changes than the SH changes, both in the polar regions and in midlatitudes. It is likely that the models' ability to simulate the middle latitudes realistically is related to correctly reproducing the polar region. The larger losses in the SH polar region (where the models show large differences) compared with the NH make this connection more critical. In spite of these detailed differences, the overall agreement between the modeled and observed trends in their vertical and latitudinal profiles and seasonal variation support the view of WMO (1999) that increases in halogens are a main driver of the observed changes.

Figure 4-33. Time series of column ozone variations from observations (red lines) and from eight 2-D models for latitude bands of 60°S-60°N (top), 35°N-60°N (middle), and 35°S-60°S (bottom). Changes are calculated in percent with respect to 1980 values for each time series. The observations for 60°S-60°N use results from Figure 4-4, with the solar cycle component removed by statistical regression, whereas the midlatitude observations are from Figure 4-7, with no explicit solar cycle adjustments. The error bars on the observations represent the spread of the different datasets, which provides a minimum estimate of their uncertainty.

GLOBAL OZONE

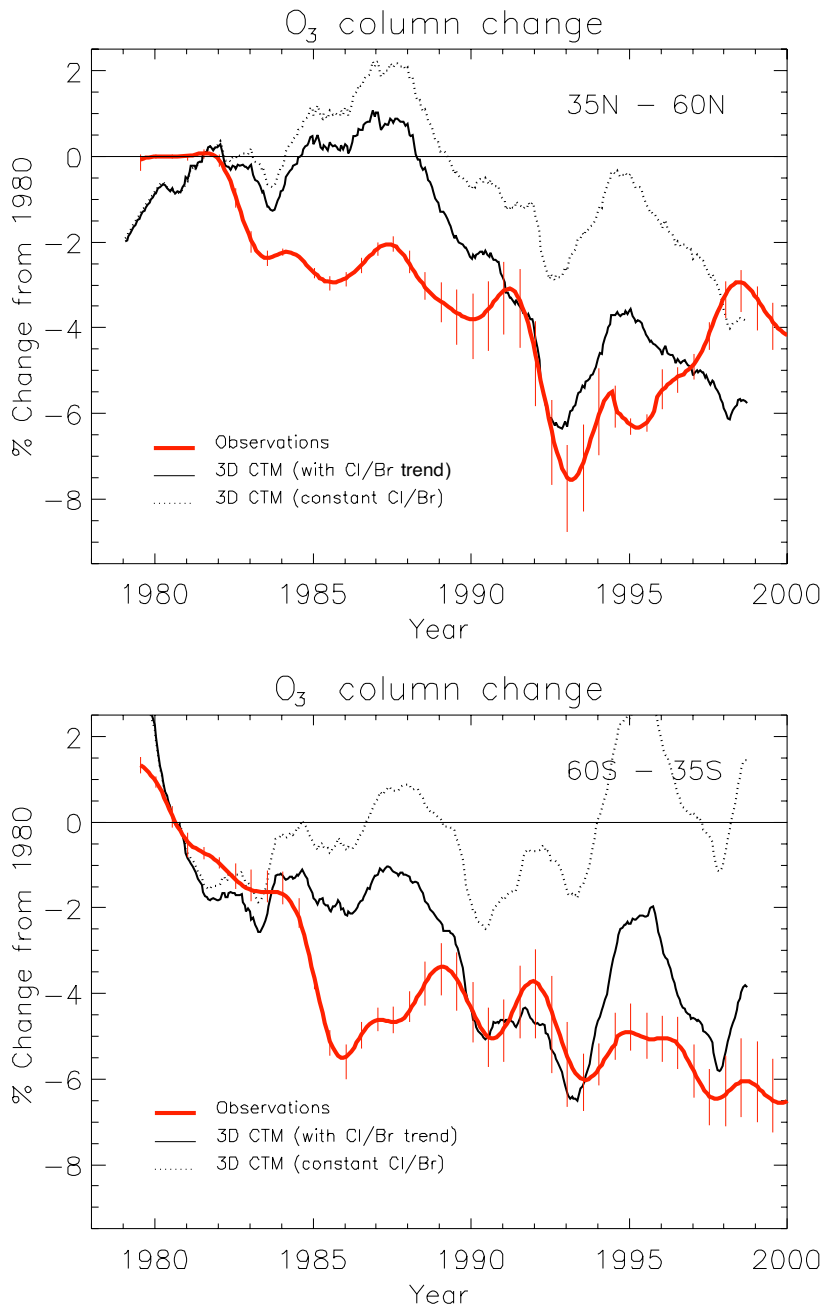


Figure 4-34. Time-series of column ozone change (% change from 1980) from the SLIMCAT 3-D CTM compared with observations (as in Figure 4-33) for 35°N-60°N (top) and 35°S-60°S (bottom). Results from two model simulations are shown: with a halogen trend and with constant (1979) halogen loading.

4.6 DYNAMICAL INFLUENCE ON PAST CHANGES IN OZONE

4.6.1 Introduction

Transport of stratospheric ozone is a key factor influencing its seasonal and interannual variability. The large seasonal cycle in column ozone over the extratropics (in both hemispheres), as seen in Figure 4-35, is due primarily to enhanced transport from the tropical source region during the winter-spring seasons, and the hemispheric differences in ozone amount are mainly a result of

differential transport (larger in the NH). Figure 4-35 also shows that the interannual variability in the winter-spring ozone buildup is greater in the NH than the SH, reflecting the greater dynamical variability of the NH stratosphere. Given the observed large interannual and decadal-scale variability in stratospheric dynamical quantities, it is reasonable to consider a dynamical influence on decadal ozone trends on both regional and hemispheric scales (e.g., Hood and Zaff, 1995).

In WMO (1999), as well as in previous Assessments, the possible influence of long-term changes in

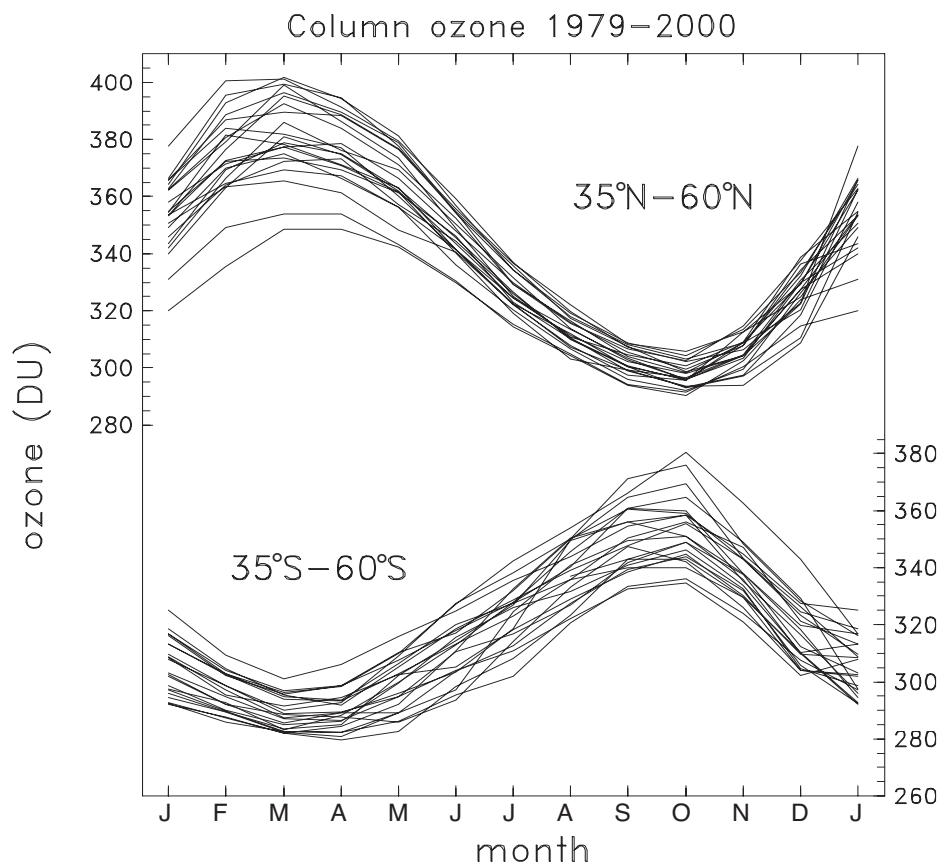


Figure 4-35. Seasonal cycle of total ozone (from the merged satellite dataset) averaged over 35°N-60°N (upper set of curves) and over 35°S-60°S (lower set of curves), with each curve corresponding to a different year in the period 1979-2000.

dynamical processes on ozone changes was discussed. However, the statistical trend analyses presented there did not include explicit dynamical variables (except for the QBO and solar cycle) because of difficulties of interpretation. One particular concern is that establishing the existence of correlations using observations is far from proving cause and effect; sound mechanistic information is also needed. In particular, it is necessary to assess the extent to which the dynamical changes might be a consequence of the ozone changes, rather than a cause. A further problem is that using correlations to attribute causality assumes that linear relationships can represent what are, in reality, complex nonlinear interactions. Although this is a relatively minor issue for periodic signals such as the QBO and solar cycle, it becomes problematic when trying to apply daily or monthly mean correlations to longer time scales.

Recently there has been interest in trying to understand and diagnose the effects of dynamical changes on stratospheric ozone over decadal time scales, and there is now substantially more information available than at the time of the previous Assessment. The relevance of dynamical changes is underlined by related issues such as the unexplained long-term trend in stratospheric water vapor (see Section 4.3.2), and the apparent trend in the

North Atlantic Oscillation (NAO) and other hemispheric-scale meteorological phenomena (Graf et al., 1995; Thompson et al., 2000). Furthermore, the opportunity for long-term dynamical studies on a global scale has been facilitated by the recent availability of meteorological reanalysis products.

The relevant studies may be largely grouped into two categories; neither addresses the cause of the observed dynamical changes. The first consists of modeling studies using observed circulation statistics derived from meteorological analyses to drive the transport in the model. These have been performed in the presence of constant chemical forcing to determine the ozone response to the dynamical forcings alone, and in the presence of a changing chemical forcing so that the two effects can be assessed together. The second category consists of statistical studies that combine mechanistic understanding of the atmosphere with the statistical demonstration of correlations in time series. For such studies the previous caveat about interpreting correlations still holds, both in assessing the results of individual studies and especially in comparing the results from different studies. A simple example makes this point clearly. Increases in both tropopause height and mini-hole frequency have been suggested as being responsible for decreases in ozone over

GLOBAL OZONE

northern midlatitudes. However, since they are intimately linked (mini-holes occur when the tropopause is exceptionally high), the two influences on ozone cannot be simply added.

This section on dynamical influences is organized as follows. An overview of key dynamical processes associated with midlatitude ozone trends is provided in Section 4.6.2. The statistical analysis of observations is discussed in Section 4.6.3, and the impact of dynamical changes estimated using 3-D chemical transport modeling is detailed in Section 4.6.4. The possibility that the dynamical changes might be the result of the ozone changes is assessed, and the dynamical impact of GHG changes considered, in Section 4.6.5. We note that most of the discussion focuses on the NH because uncertainties in the SH circulation statistics do not permit reliable calculation of trends in dynamical forcing (e.g., Randel et al., 2002).

4.6.2 Dynamical Processes that May Contribute to Ozone Changes

Recent studies of dynamical influence on midlatitude ozone trends have discussed variations and trends in dynamical quantities related to ozone transport. These studies have broadly fallen into topics focused on two processes that although ultimately coupled, are in principle independent:

- Stratospheric planetary-wave drag (PWD), which drives the stratospheric Brewer-Dobson circulation and is a principal dynamical influence on ozone above 20 km although also affecting ozone below 20 km.
- Tropospheric circulation, which affects the ozone distribution in the lowermost stratosphere (up to about 20 km) through both planetary-scale and synoptic-scale disturbances and the location of the tropopause.

Decadal ozone changes induced by these processes can be produced from natural variability, from changes in climate resulting from greenhouse gases, or from ozone depletion itself. The importance of knowing the cause depends on the issue being addressed. To quantify the ozone depletion that can be attributed to ozone-depleting substances such as CFCs and halons, the causes of the dynamical influences on ozone changes are unimportant, as long as they are not a result of the chemical ozone depletion itself. However, to make valid predictions of future ozone levels, it is important to understand the fundamental causes of the dynamical influence on ozone changes. Thus it is useful to distinguish between the identification of dynamical contributions to ozone changes, and their explanation.

The effects discussed above concern the direct impact of transport on ozone. In addition to these purely

dynamical effects, there are chemical and radiative feedbacks between temperature and ozone that are both positive in the lower stratosphere. These chemical and radiative feedbacks may amplify or skew the effect of natural dynamical variability on ozone. It is thus not possible to cleanly separate “dynamical” and “chemical” contributions to ozone changes, attributing a certain fraction to each, because they are nonlinearly coupled. Whether the coupling is a first-order or a second-order effect, and what the causality of the relationship is between dynamics and ozone, has to be assessed on a case-by-case basis.

4.6.2.1 CHANGES IN PLANETARY-WAVE DRAG

The global transport of constituents in the stratosphere can be described in terms of advection by the mean meridional circulation together with eddy transport effects; both of these quantities are first-order terms in the zonal mean continuity equation (Andrews et al., 1987; Mahlman et al., 1980). The stratospheric meridional circulation, known as the Brewer-Dobson circulation (BDC), is primarily driven by mechanical forcing arising from stratospheric (and mesospheric) wave drag, plus seasonal variations in radiative heating. Likewise, large-scale eddy transports are linked to dissipating waves, and hence to stratospheric wave drag, although this linkage is difficult to quantify. This forcing originates from upward-propagating, tropospherically generated waves. Unforced natural variability (i.e., excluding solar variations or volcanic eruptions) arises primarily from dynamics through variability in wave drag, although model results suggest it can be affected by chemical-radiative feedbacks that could change in the presence of anthropogenic forcing (e.g., Shindell et al., 1999; Butchart et al., 2000). Wave-drag variability can be internal to the stratosphere, or can arise from variability in the tropospheric wave sources. The amount of wave drag within the stratosphere is related to the vertical component of the Eliassen-Palm (EP) flux in the lower stratosphere, and this quantity (also referred to as the planetary wave driving) is a convenient proxy used to quantify PWD.

Planetary-wave drag (PWD) is largely restricted to winter and spring for well-understood reasons (Andrews et al., 1987), and drives the spring buildup of extratropical column ozone seen in Figure 4-35. The relationship between PWD and ozone buildup is not simple, but a clear positive correlation has been found in the interannual variability of NH extratropical PWD and total ozone buildup in January (Fusco and Salby, 1999; Randel et al., 2002), as illustrated by Figure 4-36. Such dynamically induced ozone changes would be expected to be seen mainly between midwinter and late summer; each year ozone

essentially returns to photochemical control by the fall (e.g., Chipperfield and Jones (1999) for the polar region), and there is a correlation between winter buildup and summer loss (Fusco and Salby, 1999; Randel et al., 2002). From Figure 4-35 it is evident that this statement applies more to the NH than to the SH, where the late breakup of the vortex does not allow sufficient time for ozone to reach photochemical control before the next year's buildup begins. In contrast, NH ozone exhibits less interannual variability in early fall; indeed the spread of values seen in Figure 4-35 in early fall largely represents the trend shown in Figure 4-8. The fact that the effect of PWD on ozone is seasonal and has essentially no interannual memory suggests (at least for the NH) that decadal changes in PWD can be expected to lead to decadal changes in ozone, all else being equal. For such wave-drag-induced variability, changes in the extratropics should be mirrored (with a negative sign) in the tropics, and this compensation is indeed seen in interannual variability of total ozone (Fusco and Salby, 1999; Randel et al., 2002). Although the basic physics of the connection between PWD and total ozone is well understood, its quantification via correlations is at best a crude measure

of this connection, and this limits our ability to attribute observed changes in total ozone to observed changes in PWD.

4.6.2.2 EFFECTS OF TROPOSPHERIC CIRCULATION AND TROPOPAUSE CHANGES

The tropospheric circulation also affects the ozone distribution, with the direct effects confined to the lowermost stratosphere. The relationship between midlatitude tropopause height and total ozone is well documented (e.g., Bojkov et al., 1993), with roughly a 20-DU decrease for every 1-km increase in tropopause height (Hoinka et al., 1996), independent of season. Day-to-day changes in tropopause height at a given location are associated with the passage of synoptic-scale baroclinic disturbances in the upper troposphere and lowermost stratosphere, which affect ozone through the depth of the lowermost stratosphere (e.g., Salby and Callaghan, 1993; Vigliarolo et al., 2001). Longer-term changes are associated with planetary-scale circulation anomalies, such as the NH annular mode (see next section), which elevate the tropopause at certain longitudes and lower it at others. However, the effect of tropospheric circulation on total

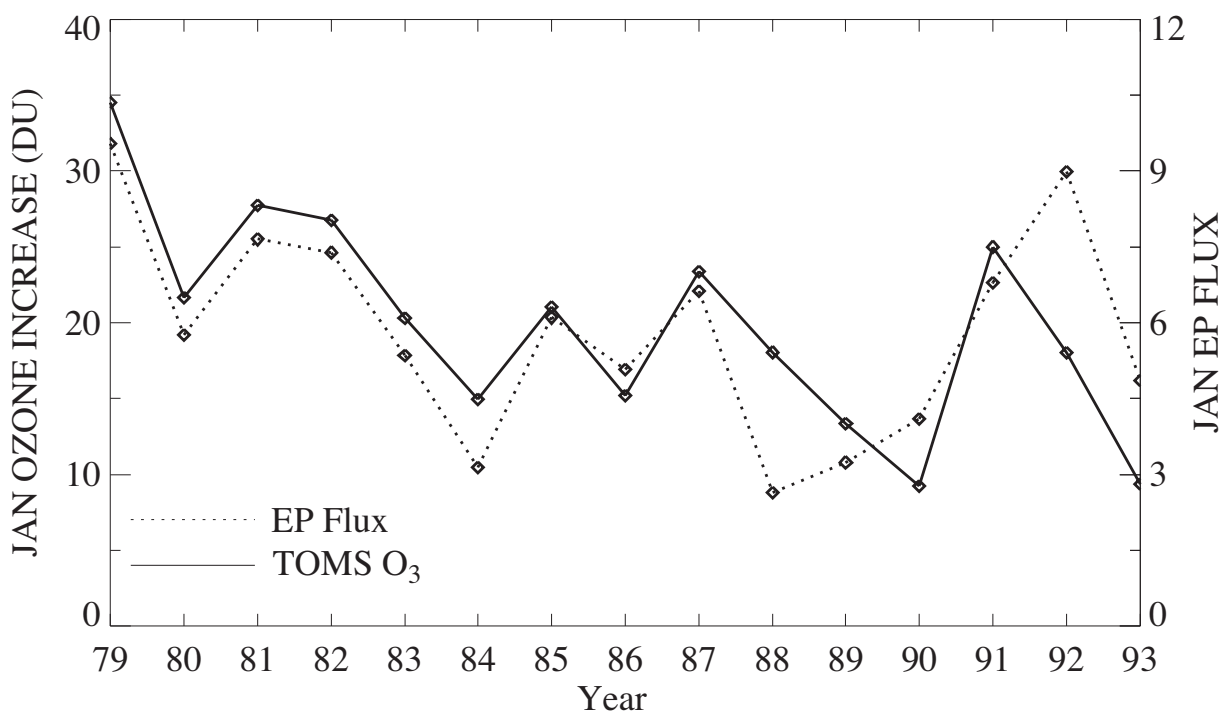


Figure 4-36. Upward Eliassen-Palm (EP) flux at 100 hPa (a measure of the stratospheric planetary wave driving) during January (in normalized units) averaged over 20°-90°N (dashed), compared with the January increase in total ozone over the same latitude range (solid). The regression of TOMS ozone with EP flux has a correlation coefficient of 0.74. Adapted from Fusco and Salby (1999). Randel et al. (2002) showed that the strong positive correlation extends over 1979-2000.

GLOBAL OZONE

ozone, and its relation to tropopause height, is much less well understood than the effect of PWD on total ozone. In particular, the relationship between tropopause height and total ozone mentioned above applies to single stations and is mainly associated with reversible transport; there is no reason to expect it to apply in the zonal mean, or on longer time scales (e.g., seasonal or interannual) over which ozone transport is irreversible.

4.6.2.3 HEMISPHERIC VARIATIONS AND ANNULAR MODES

Both hemispheres exhibit natural variability in PWD, manifested in “strong-vortex” and “weak-vortex” conditions in the stratosphere. The associated modes of variability evident in statistical analyses show out-of-phase behavior between the polar and midlatitude regions, which is primarily zonally symmetric (i.e., annular). These hemispheric patterns are referred to as the NH and SH annular modes (NAM and SAM). The stratospheric NAM and SAM are observed to be coupled to similar tropospheric structures, in both observations (Thompson and Wallace, 1998, 2000) and GCM simulations (Shindell et al., 1999), and there is a strong observed correlation between NAM index and both midlatitude tropopause height and total ozone during the winter-spring period (Brönnimann et al., 2000). The stratosphere-troposphere coupling occurs on sufficiently rapid time scales that the relevant mechanisms must be dynamical, through wave-mean-flow interaction (Baldwin and Dunkerton, 1999), although the specific mechanisms are far from clear (see Section 4.6.5). In the troposphere the NAM is closely associated with the North Atlantic Oscillation (NAO), and some studies have used the NAO as a dynamical proxy for ozone variability (e.g., Appenzeller et al., 2000).

4.6.3 Statistical Analysis of Observations

4.6.3.1 CHANGES IN PLANETARY-WAVE DRIVING

In the NH, there have been long-term changes in various meteorological indicators over the past 30 years or so, which together paint a fairly consistent, albeit incomplete, picture. The Arctic wintertime vortex has been getting colder and stronger (Graf et al., 1995; Pawson and Naujokat, 1999; Thompson et al., 2000), and more persistent (Waugh et al., 1999). Any dynamically induced component of these changes requires a weakened meridional circulation, which at least over the last 10 years (the length of the relevant data record) is consistent with variations in long-lived trace gases in the middle and upper stratosphere (Nedoluha et al., 1998b; Randel et al., 1999). A weakened meridional circulation requires a decrease in

stratospheric wave driving, which has been documented in several studies (Fusco and Salby, 1999; Newman and Nash, 2000; Zhou et al., 2001b; Randel et al., 2002). However, it should be cautioned that these results are quite sensitive to the months and time period considered. For example, Newman and Nash (2000) report significant negative trends in wave driving for January-February (1979-1999), whereas Hu and Tung (2002) do not find the decrease (over 1968-1998) to be statistically significant for November-January. Randel et al. (2002) analyzed data during 1979-2000 for each month separately, and find the wave driving to increase during November and December and to decrease during January and February (with only January near statistical significance) (Figure 4-37). This seasonal variation is consistent with the Arctic early-winter warming and late-winter cooling seen over the same period at 100 hPa (Langematz et al., 2002). A weakened meridional circulation implies a decrease in the NH extratropical winter-spring buildup of ozone, in both polar and midlatitudes, through a decrease in ozone transport.

Because of the seasonality of the winter-spring buildup of ozone, with any interannual memory (in ozone) being largely erased by the return to photochemical control by early fall (Figure 4-35), there is some justification for extending interannual correlations to decadal time scales. This would only be strictly appropriate if the inter-

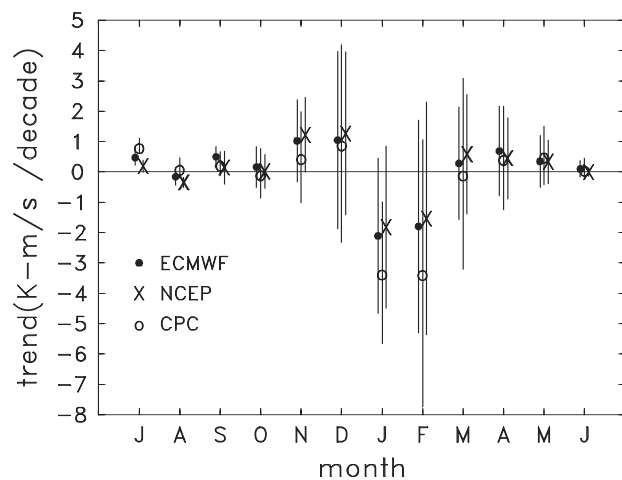


Figure 4-37. Linear trends in monthly averaged NH eddy heat flux ($\overline{v'T'}$) statistics at 100 hPa (proportional to the upward EP flux), calculated for the period 1979-2000. Results for each month were calculated based on meteorological analyses from the European Centre for Medium-Range Weather Forecasts (ECMWF), the NCEP Climate Prediction Center (CPC), and the NCEP/NCAR reanalyses. Error bars denote $\pm 2\sigma$ uncertainty. From Randel et al. (2002).

annual correlations were established in the presence of constant chemical forcing (e.g., Cl_y), which is not the case. With this caveat, the extent of the resulting wave driving contribution to midlatitude ozone trends in winter-spring then depends entirely on the extent of the changes in wave driving for the period in question. Between 1979 and the period 1990-1993, the extent and statistical significance of wave driving changes is particularly sensitive to the last year chosen, because of the especially large variability in wave driving during 1990-1993 (see Figure 4-36), and the estimated impact on ozone is accordingly highly variable (Fusco and Salby, 1999; Randel et al., 2002). Over the longer period 1979-2000, Randel et al. (2002) find that decreases in wave driving (Figure 4-37) may account for ~30% of the observed changes to total ozone in the January-March period.

4.6.3.2 CHANGES IN TROPOSPHERIC CIRCULATION AND TROPOPAUSE HEIGHT

Observations have shown that the NH extratropical tropopause has generally risen in altitude over recent decades. Radiosonde measurements over both Europe and Canada show an increase in altitude of about 300-600 m over the past 30 years, the exact amount depending on location (Forster and Tourpali, 2001; Steinbrecht et al., 2001). Consistent increases are also seen both in the ECMWF reanalysis for 1979-1993 (Hoinka, 1999) and in the NCEP-NCAR reanalysis for 1968-1997 (Thompson et al., 2000); although not all longitudes show an increase, it is present in the zonal mean. An increase in zonal-mean tropopause height is qualitatively consistent with a decrease in stratospheric planetary-wave drag via a weakened meridional circulation (Thuburn and Craig, 2000), but Steinbrecht et al. (1998) found little correlation between changes in monthly mean tropopause height and in lower stratospheric temperatures, arguing against this mechanism. Rather, they found a very strong correlation with mid-tropospheric temperatures, suggesting that the observed tropopause height changes are mainly caused by changes in tropospheric circulation. Moreover, an analysis of ozone profile changes over Payerne, Switzerland (Weiss et al., 2001), found that the tropopause height changes are correlated with significant ozone changes throughout the lowermost stratosphere, but not above, suggesting that they are primarily associated with the observed higher frequency of subtropical intrusions due to synoptic-scale disturbances (Reid et al., 2000; Bojkov and Balis, 2001), rather than with a change in the meridional circulation. However, because of our poor understanding of what controls the zonal-mean midlatitude tropopause height, it is not at all clear that the corre-

lations obtained for month-to-month variability can be extended to decadal time scales. The seasonality characterizing PWD influences does not apply to tropospheric dynamical processes, which affect ozone year-round.

Notwithstanding these concerns, several studies have attempted to estimate the dynamical contribution to total ozone trends by statistical regression against tropopause height or tropospheric circulation indices that are correlated with it. Steinbrecht et al. (1998) analyzed Hohenpeissenberg, Germany, ozonesonde data for 1967-1997 and found that about 25% of the trend in total ozone could be attributed to tropopause height changes. Forster and Tourpali (2001) used 11 ozonesonde stations in Europe and Canada from 1970 to 1997 and found that about one-third of the observed ozone change below 20 km could be associated with the change in tropopause height, which is consistent with the Steinbrecht et al. (1998) result. Both studies concerned annual-mean changes, since the correlation between tropopause height and total ozone exists at all times of the year. Weiss et al. (2001) studied changes in the ozone profile at Payerne for 1967-2000 and showed that the tropospheric dynamical influence on the calculated ozone trend is essentially confined to the lowermost stratosphere (below about 20 km), and its magnitude depends strongly on the period considered (Figure 4-38).

During the winter-spring period, there is a strong correlation between the NAM and various tropospheric circulation indices including tropopause height. Thus, Thompson et al. (2000), Appenzeller et al. (2000), and Steinbrecht et al. (2001) used NAM-like dynamical proxies in statistical trend analyses of total ozone during the winter-spring period and found consistent results to those found using tropopause height, namely, ~1/3 of the observed total ozone trend being statistically associated with the dynamical changes. The relationship between wintertime total ozone, tropopause height, and mid-tropospheric temperature is illustrated by Figure 4-39. Using global dynamical proxies such as the NAM removes the concern about the statistical correlations being dominated by local dynamical effects, and Thompson et al. (2000) showed using hemispheric data that virtually all the spatial structure of tropopause height and total ozone trends during January-March for 1979-1993 is related to the NAM.

Other tropospheric dynamical indicators have also been used: Hood et al. (1999) used 330-K potential vorticity and meridional wind shear from NCEP-NCAR reanalyses for 1979-1998 as dynamical proxies and argued that 40% of the February total ozone trends and 25% of the March trends could be attributed to dynamical changes. So there appears to be a consensus between the

GLOBAL OZONE

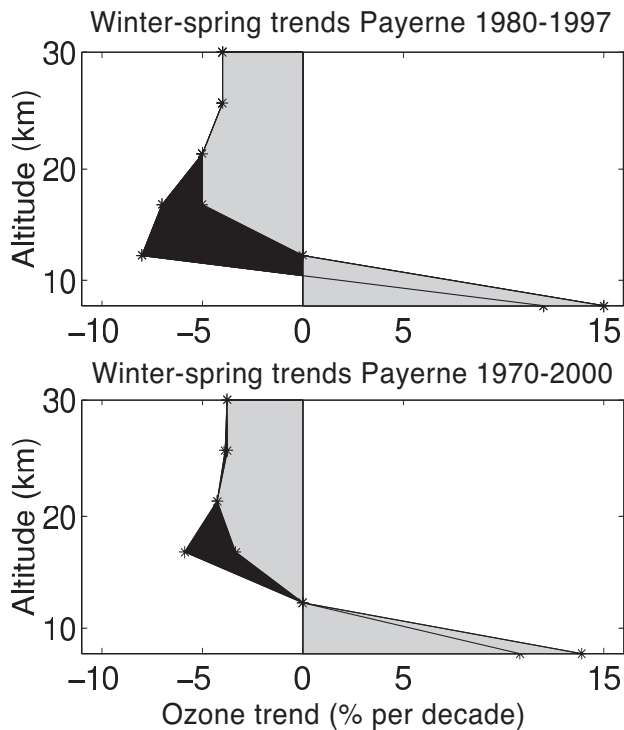


Figure 4-38. Payerne winter-spring ozone sounding trends for 1980-1997 (top) and for 1970-2000 (bottom). On the basis of a statistical analysis, the observed trends can partly be explained by dynamical changes (solid area), while the remaining trend (shaded area) is attributed to anthropogenic (chemical) ozone depletion. From Weiss et al. (2001).

different statistical studies that for decadal time scales, a significant fraction (20-40%) of the observed NH mid-latitude total ozone change is associated with changes in tropospheric circulation. The fact that these different dynamical proxies give reasonably consistent results is not very surprising, however, given the strong correlation between the various meteorological indices.

4.6.3.3 COUPLING ISSUES

An important question to address is whether the recent trends in wave driving and in tropopause height are somehow linked, especially since they lead to similar estimates of the dynamical contribution to total ozone changes. Given the expected association between the NAM and PWD at stratospheric altitudes, the stratosphere-troposphere coupling apparent in the NAM would then imply a connection between wave driving and tropopause height. However, Waugh et al. (1999) found no particular correlation between the NAM index and either the total wave driving or the persistence of the Arctic vortex. Furthermore, the tropopause height trends

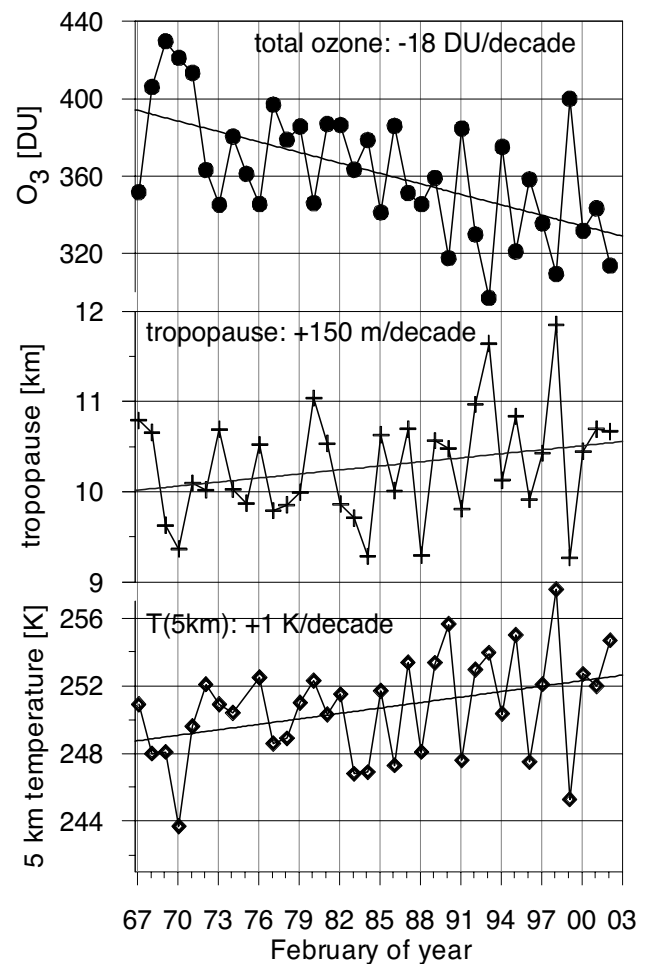


Figure 4-39. February monthly means of total ozone (top), tropopause height (middle), and temperature at 5-km altitude (bottom), at Hohenpeissenberg (47.8°N, 11.0°E). Updated from Steinbrecht et al. (2001) through February 2002.

exist in all seasons, suggesting that although they might lead to PWD changes during winter-spring, the converse cannot be true. So while there is a certain self-consistency between the various dynamical trends, without a clear mechanism connecting the NAM, PWD, and tropopause height, any such connection in the context of long-term trends remains speculative. This question will probably not be answerable until the origin of the changes in the individual dynamical quantities has been identified. Having said that, it would seem unlikely that the statistical effects of wave driving and tropopause height (or NAM) on ozone could simply be added.

4.6.4 Modeling Studies

Another way to estimate the contribution of dynamical changes to ozone changes is by using CTMs driven

by the observed wind and temperature fields. This has recently become possible on a multiannual basis because of the advance in CTM capabilities (Chipperfield, 1999). Hadjinicolaou et al. (1997), using parameterized ozone chemistry, and Chipperfield (1999), using full chemistry, found that the variations in NH midlatitude total ozone in the early 1990s can be largely accounted for by circulation changes alone, including the aftermath of the Mt. Pinatubo volcanic eruption (Figure 4-40). There is, however, a chemical feedback, in that colder winters lead to more polar chemical ozone loss, which is transported to midlatitudes. Hadjinicolaou et al. (1997) identified significant PSC-induced ozone losses both in the polar region and at midlatitudes, especially during the cold winters of 1996 and 1997. Chipperfield (1999) identified a long-term 2-3% reduction at 50°N from polar processing, and

about a 1% reduction from direct midlatitude Cl activation reaching 3% in 1992/1993. Nevertheless a contribution to the very low total O₃ anomaly seen in 1993, relative to the years 1992 and 1994, was attributed to circulation changes (possibly the result of the eruption of Mt. Pinatubo itself), as illustrated in Figure 4-40. From a similar integration covering the 20-year period of 1980-1998, Hadjinicolaou et al. (2002) further argued that at least half of the observed NH midlatitude trend from December through February during this period could be accounted for by dynamical forcing (Figure 4-41), and that the modeled total ozone was strongly correlated with both the NAM and stratospheric wave driving. Hadjinicolaou et al. (2002) furthermore found that the latitudinal and seasonal characteristics of the dynamically induced modeled ozone decrease were consistent with observations,

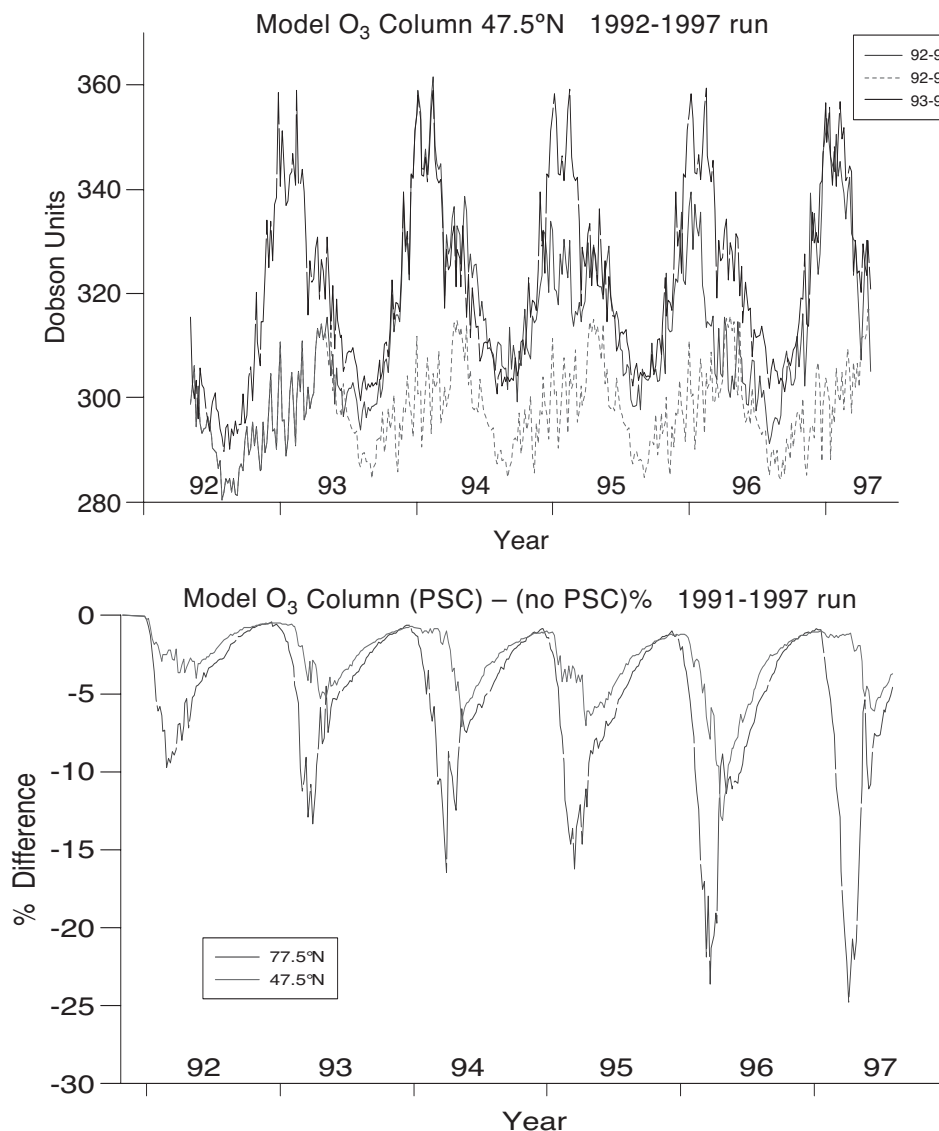


Figure 4-40. Results from a 3-D CTM with parameterized O₃ chemistry. Top panel: Zonal mean column ozone (DU) at 47.5°N for three experiments: annually varying meteorological forcing, repeated 1992/1993 forcing, and repeated 1993/1994 forcing. The interannual variability in ozone is controlled by the meteorological variability. Bottom panel: Difference in zonal mean column O₃ at 47.5°N and 77.5°N between two runs (with annually varying meteorology): one run included the effects of PSCs and the other did not. The colder winters show a larger difference. From Hadjinicolaou et al. (1997).

GLOBAL OZONE

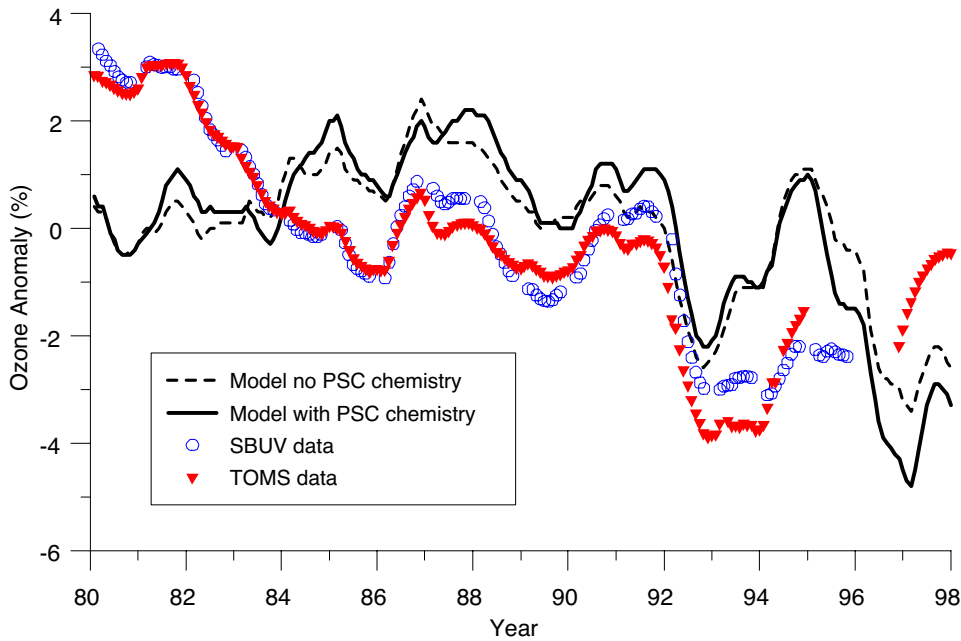


Figure 4-41. Anomaly of column ozone at 30°N-60°N for 1980-1998 from 3-D model simulations with parameterized ozone chemistry compared with satellite data. The chemical forcing is held constant in time, so the modeled trend in ozone is dynamically induced. From Hadjinicolaou et al. (2002).

although the vertical structure was not particularly close. Results from the parameterized ozone runs of Hadjinicolaou et al. (2002) can be compared with the full-chemistry 3-D simulations shown in Figure 4-34, which use constant halogen loading. This shows that dynamical variations do produce much of the short-term variability, but the largest contribution to the modeled trend with time-dependent halogen loading is due to halogen chemistry, rather than dynamics. It should be noted that the CTM results are further from observations in the SH than in the NH, and in particular do not match the decadal-scale variability well. This is perhaps because of the poorer quality of the analyzed winds and temperatures in the SH.

A complementary approach to that of CTMs is using stratosphere-only dynamical-chemical models with explicit representation of planetary waves, driven by observed forcing at the tropopause. This approach was used by Kinnersley and Tung (1998) to study Arctic ozone, and by Fusco and Salby (1999) to study midlatitude ozone. Both studies confirmed the large effect of interannual variations in wave driving on total ozone. Fusco and Salby (1999) found results consistent with those of Hadjinicolaou et al. (1997), including the latitudinal structure of the ozone trends.

4.6.5 Cause of the Dynamical Changes

The question then arises as to why the dynamical changes have occurred. This can ultimately only be answered with GCMs. The first question to resolve is whether chemical ozone depletion might somehow have caused the circulation changes. There has been signifi-

cant attention paid to stratospheric cooling induced by ozone losses (see Section 4.4), but considerably less to associated dynamical feedbacks.

With regard to stratospheric PWD, there is no clear mechanism that would predict ozone loss leading to a decrease in PWD. In contrast to the effect of PWD on ozone, which is clear (if difficult to accurately quantify), the effect of the zonal-wind and temperature structure on PWD is not well understood. Chen and Robinson (1992) and Limpasuvan and Hartmann (2000) have argued that stronger vertical shear of the zonal wind in high latitudes reduces the strength of stratospheric PWD (although they disagree on the details of the mechanism), whereas Hu and Tung (2002) argue for precisely the opposite effect. These studies appeal to different physical mechanisms than does the study of Shindell et al. (1999), which focuses on the zonal wind (not its vertical shear) in subtropical (not high) latitudes. In any case, the seasonality of the relation between NH PWD and ozone means that spring-time ozone depletion cannot be used to explain reduced wintertime PWD. Although Langematz et al. (2002) find a reduction in stratospheric PWD from their imposed ozone changes, this reduction is not statistically significant and only amounts to about one-fourth of the observed PWD changes. Thus although a contribution from the dynamical feedback from ozone changes cannot be excluded, it appears that other factors must contribute to changes in PWD.

With regard to tropospheric circulation changes, it is more difficult to draw conclusions, partly because of our more limited understanding of the tropopause region.

The observed lower stratospheric cooling attributable to ozone decreases would be expected to raise tropopause height on radiative grounds alone. Although this direct effect has not been quantified, Thuburn and Craig (2000) removed all the stratospheric ozone in an idealized GCM experiment and found the extratropical tropopause rose by only 1 km, which suggests that the observed ozone losses of several percent could not account for a rise of 300–600 m. Furthermore, as noted earlier, the observed increase in tropopause height appears to be statistically associated with tropospheric warming, rather than with stratospheric temperature changes (Steinbrecht et al., 1998). Recent GCM studies confirm this: Langematz et al. (2002) found no significant change in mid-tropospheric circulation (including the NAM) arising from imposed ozone changes; Shindell et al. (2001) found an increase in the NAM index, but not of sufficient magnitude to account for the observed change; Santer et al. (2002) found that observed ozone changes had a small positive (but statistically insignificant) effect on tropopause height changes over the past 20 years. Thus, it appears that although the ozone decreases may have led to changes in tropospheric circulation (including tropopause height) that are qualitatively consistent with the observed changes, they are of insufficient magnitude, implying that other factors must contribute. However, it should be noted that most GCMs cannot resolve the observed tropopause height changes, so they must be inferred by interpolation (see Santer et al., 2002), and furthermore the observed ozone changes are not well quantified close to the tropopause.

The subsequent question is whether the circulation changes might be the result of GHG-induced climate change. On the basis of radiative balance, the expected tropospheric warming and stratospheric cooling should lead to an increase in tropopause height at midlatitudes, and to a strengthened meridional temperature gradient in the upper troposphere/lower stratosphere. The GCM study of Santer et al. (2002) showed a mean extratropical tropopause pressure decrease of 3 hPa/decade resulting from changes in WMGGs; this corresponds to an extratropical tropopause height increase of about 120 m/decade, which is roughly consistent with observed changes over recent decades. Perlwitz and Graf (1995) proposed that these changes would act to weaken NH stratospheric PWD, and Shindell et al. (1999, 2001) indeed found such a dynamical feedback in their GCM study of the response of the stratosphere to GHG forcing. However, other GCM studies come to the opposite conclusion; for example, Butchart and Scaife (2001), Schnadt et al. (2002), and Langematz et al. (2002) found that GHG-induced changes lead instead to stronger PWD and a more intense Brewer-Dobson circulation (BDC). Caution is

also warranted because the trend in the NAM index seems to have dropped substantially in the last 5 years or so, and the recent behavior may well be a manifestation of natural variability. As Hartmann et al. (2000) emphasize, the fact that the NAM is a mode of atmospheric variability means that it can be affected by even a relatively small external forcing, and its response may be highly sensitive. It also makes secular changes difficult to separate from natural low-frequency climate variability, because they bear the same fingerprint.

4.6.6 Effects of Mt. Pinatubo Eruption

The volcanic eruption of Mt. Pinatubo in June 1991 produced an increase in stratospheric aerosols that persisted for several years (e.g., Figure 4-18) and that significantly perturbed stratospheric circulation and chemistry. There was a decrease in tropical ozone for several months following the eruption, attributed to a transient increase in tropical upwelling (Schoeberl et al., 1993). Large ozone decreases were observed in NH extratropics for several years following the eruption, primarily during the winter-spring seasons (largest in 1992/1993), as documented in ozonesonde and satellite data (Kerr et al., 1993; Hofmann et al., 1994; Gleason et al., 1993). Smoothed time series of NH midlatitude ozone anomalies suggest the Mt. Pinatubo effect persisted during approximately 1992–1996 (Figure 4-7). However, although the Mt. Pinatubo aerosol was transported into the extratropics of both hemispheres and covered much of the globe by early 1992, column and profile ozone measurements in SH midlatitudes (Figures 4-6 and 4-15) do not show a pronounced ozone decrease comparable to that seen in the NH. This lack of a SH Mt. Pinatubo signal in ozone is curious, in light of the 2-D model simulations that suggest a chemical signal of comparable magnitude between hemispheres (Figure 4-33).

The NH extratropical ozone losses following eruption of Mt. Pinatubo have been characterized as primarily a chemical depletion in several modeling studies (Brasseur and Granier, 1992; Tie et al., 1994; Kinnison et al., 1994; Rosenfield et al., 1997) and in WMO (1995, 1999). The evidence for a chemical mechanism is provided by observations of increases in stratospheric HNO_3 and decreases in NO_2 following the eruption (e.g., Koike et al. (1994); see also Figure 4-21), enhanced ClO in the lower stratosphere (Fahey et al., 1993; Froidevaux et al., 2000), together with the observed vertical profile of ozone changes (decreases in the lower stratosphere over 12–22 km, and increases above 24 km; Hofmann et al. (1994)). The lack of a corresponding Mt. Pinatubo ozone signal in SH midlatitudes is even more puzzling in light of the large perturbations in stratospheric NO_2 that were observed at Lauder, New

GLOBAL OZONE

Zealand (Figure 4-21). These NO_2 anomalies are evidence of anomalous chemistry acting on the Mt. Pinatubo aerosol in SH midlatitudes, which would be expected to lead to increased ClO and associated ozone losses.

The model simulations of Hadjinicolaou et al. (1997) called into question a purely chemical mechanism for NH midlatitude ozone loss, because they simulated a post-Mt. Pinatubo decrease in a CTM based solely on analyzed meteorological fields (Figures 4-40 and 4-41). Results in the 3-D CTM calculations shown in Figure 4-34 suggest a contribution of roughly 50% from chemistry and 50% from dynamics for the NH midlatitude ozone decrease, consistent with the recent coupled chemistry GCM study of Al-Saadi et al. (2001). The dynamical contribution to midlatitude ozone loss arises from reduced transport, and the relation to the volcanic aerosols has been studied in several idealized models. Observations show that the volcanic aerosols act to warm the tropical stratosphere (Figure 4-22), persisting for several years. Robock and Mao (1992), Graf et al. (1994), and Kirchner et al. (1999) argued that the change in the zonal winds implied by thermal wind balance would then reduce the PWD in the NH winter, essentially putting the atmosphere into a high-NAM-index state. This dynamical feedback is expected to operate only in the NH during winter-spring, because of the strength and sensitivity of PWD, and to be much weaker in the SH. The decrease in PWD leads to a weaker BDC during several NH winters following the eruption, causing less midlatitude ozone from transport effects, and also colder temperatures in the lower stratosphere (which can enhance chemical loss preferentially in the NH). The overall effect on ozone would be a combination of dynamical and chemical effects, with an inter-hemispheric asymmetry. Although these model results are suggestive, the causal relationships are difficult to quantify in observations because of natural variability of the winter stratosphere, and quantified understanding of the global response to the eruption of Mt. Pinatubo is an ongoing research topic.

4.6.7 Conclusions

There is now evidence based on both empirical/observational and modeling studies that a sizable fraction of the trends in total column ozone reported over northern midlatitudes during the past 20 or so years has occurred as a result of decadal changes in atmospheric dynamics. It is hard to quantify this fraction accurately, partly because of the large uncertainty (due mainly to interannual climate noise) in both the observed ozone changes and the estimated dynamical changes, reflected in the sensitivity of the trends to the length of the record, and partly because

the effects are not really separable because of nonlinear feedbacks. There is no doubt that this has occurred on a regional basis, with, for example, the reported ozone trends over mainland Europe being significantly enhanced by long-term changes in dynamics. There is now much stronger evidence than at the time of the previous Assessment (WMO, 1999) that the same is true for the Northern Hemisphere as a whole. The available evidence suggests that the dynamical feedbacks from ozone changes (whether chemical or dynamical) probably act in the same sense as the observed changes, but are of insufficient magnitude to account for them. The cause of the dynamical changes is, at the present time, unknown; neither greenhouse-gas forcing nor natural variability can be excluded.

4.7 IMPLICATIONS FOR CLIMATE OF UPDATED STRATOSPHERIC OZONE CHANGES

This section presents a brief update of the understanding of the impact of changes in stratospheric ozone on climate. IPCC (2001) presented a detailed review of recent work on the climate impact of tropospheric ozone changes; this is not a topic of this section.

IPCC (2001) gave a central estimate of $-0.15 \pm 0.1 \text{ W m}^{-2}$ for the radiative forcing due to stratospheric ozone loss over the period 1979-1997 and included an extensive discussion of the forcing/response relationship for stratospheric ozone changes. Forster et al. (2001) computed the ozone radiative forcing using the Randel and Wu (1999) ozone trends and three different radiative transfer schemes. They estimate a forcing of between -0.08 and -0.15 W m^{-2} , which is on the low side of the IPCC estimate. Hansen et al. (2000) and Hansen and Sato (2001) estimate a forcing of $-0.1 \pm 0.1 \text{ W m}^{-2}$; this more recent estimate is less negative than their previous estimate of -0.2 W m^{-2} because the more recent ozone trend estimates they use show more middle-stratospheric ozone loss than they had used in their earlier estimates. Schnadt et al. (2002), using ozone trends derived from their coupled chemistry-climate model, estimate a 1980-1990 forcing of -0.02 W m^{-2} ; this smaller value may be related to that model's underestimation of the Northern Hemisphere midlatitude ozone loss. Bengtsson et al. (1999) performed time-dependent GCM experiments including observed changes in stratospheric ozone for the period 1979-1997. They found that the ozone reductions in that period lead to a clear cooling, not only in the lower stratosphere, but also in the troposphere. In their model the relative cooling effect was larger in the upper than in the lower troposphere. They point out that this reduces the upper tropospheric warming by the well-mixed greenhouse gases,

resulting in an upper tropospheric temperature change in better agreement with observations.

Over the past 20 years, stratospheric ozone changes may have offset about 20% of the forcing due to well-mixed greenhouse gases, consistent with the values reported in WMO (1999); because the ozone change has been concentrated in this period, the offset since the 19th century is much smaller, about 5%.

An area of recent interest is the degree to which radiative forcing is a useful predictor of climate change; earlier work was discussed in Section 10.3 of WMO (1999). A key unresolved issue is whether the surface temperature response to a given ozone radiative forcing is the same as that due to an identical forcing from, for example, changes in carbon dioxide. If we take r to be the ratio of the global-mean surface temperature response for a global-mean ozone (or any other) radiative forcing to the global-mean surface temperature response for the same global-mean radiative forcing but due to carbon dioxide, then, as discussed by Shine (2000), there is little agreement among available GCM results. Hansen et al. (1997) imposed stratospheric and tropospheric ozone changes on their model and found a value of r of about 0.7 to 0.8 (for simulations including cloud feedbacks). Christiansen (1999), using idealized ozone changes, found r to be near unity for lower stratospheric ozone changes but 1.4 for upper stratospheric ozone changes. Forster and Shine (1999), using observed stratospheric ozone changes, found r to be 1.4. More recently, Stuber et al. (2001) obtained a value of r of 1.8 for idealized stratospheric ozone changes, as a result of a strong stratospheric water vapor feedback in their model. Joshi et al. (2002) provide a comparison of three different GCMs (including that of Stuber et al. (2001)) using the Stuber et al. (2001) perturbation. They found that r varies from 1.25 to 1.8, but interestingly for all three models, the lower stratospheric ozone perturbation generated the largest value of r amongst a range of other climate perturbations.

Hence there remains a lack of consensus as to whether the climate is more or less sensitive to a given radiative forcing due to stratospheric ozone changes than it is to the same radiative forcing due to carbon dioxide changes, but there is now some indication that it may be more sensitive. This will act to modestly enhance the relative importance of stratospheric ozone changes on climate, relative to what would be inferred from radiative forcing alone.

4.8 FUTURE CHANGES IN OZONE

Following the controls on halogen-containing source gases due to the Montreal Protocol (and its

Amendments), the stratospheric loading of chlorine and bromine should decrease in the coming decades (see Chapter 1). Accordingly, over the time scale of the next 50 years, the stratospheric ozone layer is expected to “recover” from the effects of halogen-induced depletion. However, because of other atmospheric changes, future ozone levels may differ from those in the past. These other changes include the radiative effects (stratospheric cooling) of increased GHGs, the chemical effects of certain GHGs (e.g., CH₄), dynamical changes, and changes to the aerosol loading. There are many ways of defining the recovery of stratospheric ozone. These include: a decrease (or reversal) of the rate of ozone decline, an increase in column ozone (or ozone at some specific altitude), a return to some past ozone level, or a reestablishment to a new “unperturbed” level. Under certain plausible scenarios, it is possible that stratospheric ozone will not return to 1980 levels and indeed may not stabilize within the next century.

The detection of recovery will require long time series of high-quality observations. Weatherhead et al. (2000) estimated the length of ozone datasets needed to detect a statistically significant increasing trend in ozone. Even assuming no external perturbations (e.g., from volcanoes), Weatherhead et al. (2000) estimate at least 15 years of observations will be required. This estimate also assumes that no interruptions occur in the time series (e.g., due to data gaps and instrument changes). These calculations show that the unequivocal detection of recovery will not be made in the near future and emphasize that long-term observations should be obtained.

The stratospheric 2-D models used to interpret past changes in ozone in Section 4.5 have also been used to predict the future evolution of ozone over the time period 2000-2050. WMO (1999) discussed the issue of future ozone and presented a number of 2-D model calculations. These calculations focused on the sensitivity of the rate of recovery to different halocarbon scenarios. In this Assessment the impact of different halocarbon scenarios on the decrease in the stratospheric halogen loading is discussed in Chapter 1. Here we take the baseline halocarbon scenario (Table 4B-2 in Appendix 4B) and use the chemical models to investigate the expected evolution of stratospheric ozone under expected GHG changes, and the sensitivity of this to changes in CH₄, N₂O, and CO₂ from these scenarios. (Note that the models do not simulate possible future changes to tropospheric ozone; see Section 4.8.4.) Table 4B-1 (Appendix 4B) lists the model experiments performed. The two standard GHG scenarios, runs MA2 and MB2, are taken from IPCC (2001) scenarios A2 and B2, respectively (Table 4B-3 in Appendix 4B). IPCC (2001) described four scenario families that made dif-

GLOBAL OZONE

ferent assumptions about economic and social development. These scenarios are all considered to be “equally likely,” and here we have chosen two to illustrate the different sensitivity of CH_4 and N_2O changes. The 2-D model runs assumed constant aerosol loading based on the actual 1997 values. Six sensitivity runs were performed to investigate $\pm 20\%$ changes in the rate of change of CH_4 , N_2O , and CO_2 from 2000 onward. Finally, the impact of volcanic eruptions was considered by assuming episodic eruptions (i.e., a repeat of the 1979-2000 aerosol loading) and a constant, enhanced loading corresponding to 1993.

4.8.1 Effect of Decreasing Halogens

Figure 4-42 shows the predicted evolution of global and midlatitude ozone from the 2-D models for run MA2. The models generally predict a local minimum in column ozone in about 2000, followed by a steady increase. There is, however, a large spread in the predicted time at which global ozone returns to 1980 levels, ranging from 2025 until after 2050. The figure can be compared with Figure 12-6 from WMO (1999), where the model runs were based on a “maximum allowed production” halocarbon scenario, and none of the models predicted a return to the 1980 global ozone level before the end of the simulations in 2050. Updates to chemical kinetics, especially key NO_x reactions, are probably an important contributor to the overall more rapid increase in the simulations presented here. Note that the two interactive models (NOCAR and GSFC-INT) have the more rapid rates of predicted column ozone increases in Figure 4-42, due primarily to changes in the US discussed below. This more rapid ozone increase due to the effect of increasing CO_2 was also present in the coupled 2-D model studies of Rosenfield et al. (2002).

Figure 4-43 shows the predicted evolution of ozone in the upper stratosphere (38-43 km). The two models that include temperature feedbacks from increasing GHGs (GSFC-INT and NOCAR) show a significantly faster increase in ozone. In contrast, the models that use fixed climatological temperatures show a more gradual increase, and by 2050 the predicted ozone is still less than 1980 values. An additional run was performed with the NOCAR model (NOCAR2) that used fixed CO_2 after 2000, thereby keeping upper stratospheric temperatures effectively constant. The difference in temperature between these two runs in the US was about 6 K by 2050. Figure 4-43 shows that this NOCAR2 run exhibits a much slower rate of increase, in line with the other fixed-temperature 2-D models, highlighting the importance of temperature changes on future US ozone. The cooling

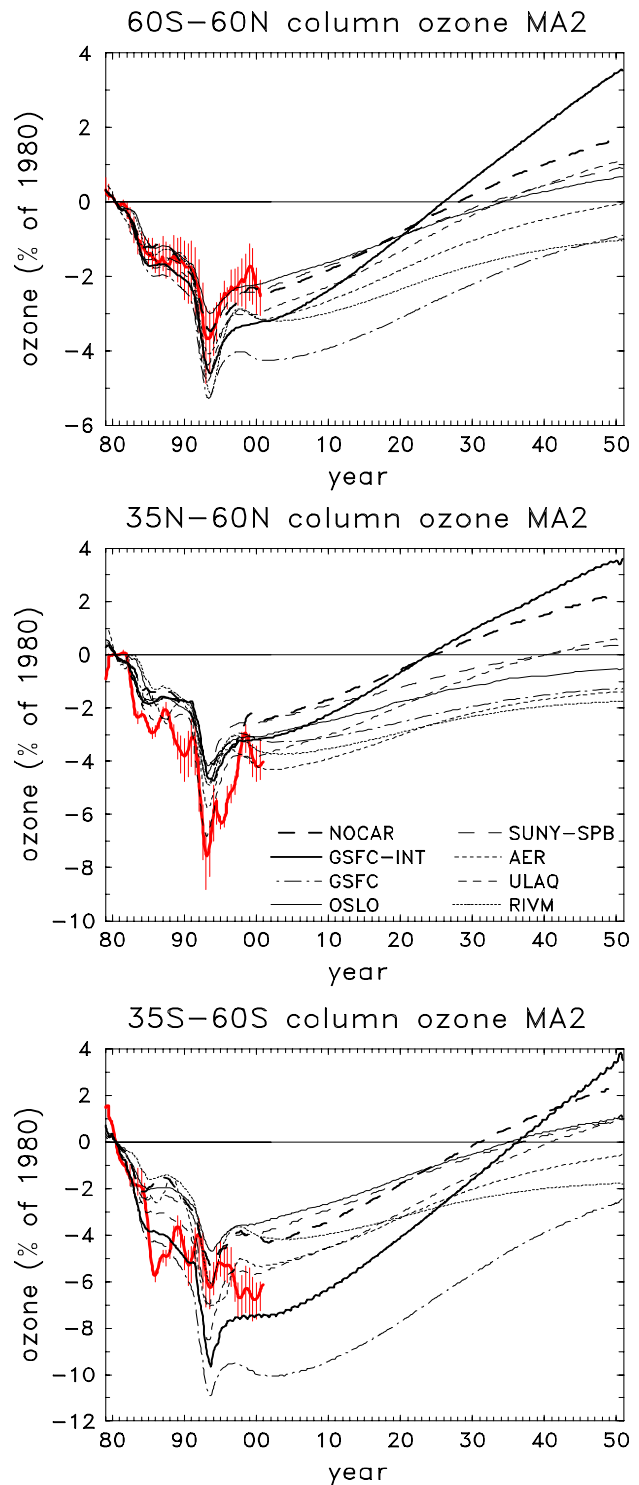


Figure 4-42. Predicted future evolution of column ozone averaged over latitude bands 60°S - 60°N (top), 35°N - 60°N (middle), and 35°S - 60°S (bottom), from a suite of eight 2-D models. Results are shown for GHG scenario MA2. The plots also include the model results and observations of past trends (red lines) prior to 2000 (see Section 4.5.3).

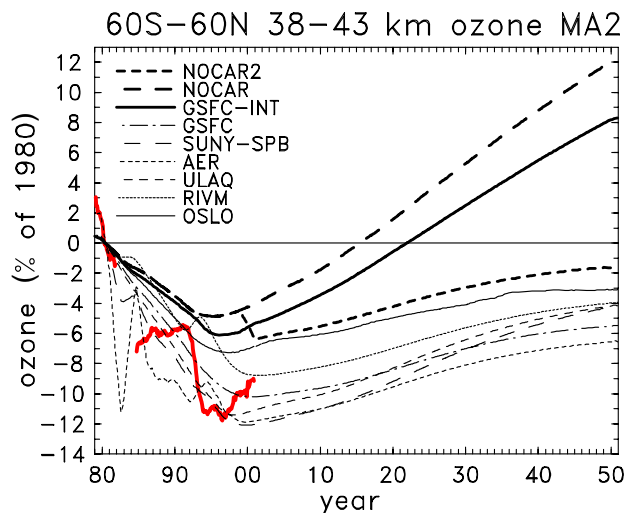


Figure 4-43. Predicted future evolution of US ozone (38-43 km), averaged over latitudes 60°S-60°N from the eight 2-D models shown in Figure 4-42. An additional model run (labeled NOCAR2) used the NOCAR model but with fixed CO₂ after 2000 (with CO₂ set to 1980 values, accounting for the discontinuity near 2000). The models used GHG scenario MA2. The plots also include the model results and observations (SAGE I+II; red lines) of past changes prior to 2000 (see Section 4.5.3).

not only has the direct effect on the rates of chemical reactions, but also can lead to circulation changes that in turn will affect the US abundance of, for example, CH₄ and NO_y. However, the dominant effect is likely to be the decreased rate of ozone-destroying gas-phase chemical reactions due to colder temperatures. This is a well-understood feedback (e.g., Haigh and Pyle, 1979) that is captured by the NOCAR and GSFC-INT models. However, these models underestimate the observed depletion in the late 1990s, and so their predicted increase starts from too high a value. For the models with fixed temperatures, the predicted increase in CH₄ should also tend to increase O₃ near 40 km (by increasing the rate of conversion from ClO to HCl). Therefore, other factors (e.g., the increase in NO_x, from N₂O, or the increase in HO_x) are apparently exerting a dominant influence by 2050.

4.8.2 Influence of Changing Climate Gases

The IPCC scenarios given in Table 4B-3 in Appendix 4B show a range in the predicted evolution of CH₄, N₂O, and CO₂ under different assumptions. The effect of this uncertainty in CH₄ and N₂O on the future evolution of ozone has been investigated using one representative model (which uses fixed temperatures). A

decrease (increase) in the rate of CH₄ growth increases (decreases) the time for O₃ recovery to 1980 levels. However, the effect of a 20% change in CH₄ is to shift the recovery by only about 2 years. This uncertainty in the growth of CH₄ essentially covers the range of all IPCC (2001) scenario families except B1, which predicts a CH₄ growth some 85% less than the A2 scenario. In contrast, a decrease (increase) in the rate of N₂O growth decreases (increases) the time for recovery, but again the effect is small. For N₂O the various IPCC scenarios represent a variation in N₂O growth of +8% to -50% compared with A2. Therefore, for both gases the modeled direct chemical sensitivity of the rate of recovery to the range in the IPCC scenarios is smaller than the inter-model differences (and uncertainties). Uncertainties in CO₂ could lead to a large uncertainty in future O₃ through the important feedback discussed in Section 4.8.1.

A recent 2-D model study by Randeniya et al. (2002) supports and extends the analysis presented here, as well as that of WMO (1999), on the direct chemical effects of future N₂O and CH₄ increases. These authors based model runs from 2000 to 2100 on two IPCC scenarios with different rates of N₂O increase and both an increase and decrease in CH₄. (Note, however, that their model ignored the effect of temperature feedbacks from GHG increases.) Figure 4-44 shows the calculated percent annual change in ozone at 45°N for 2000-2100 from

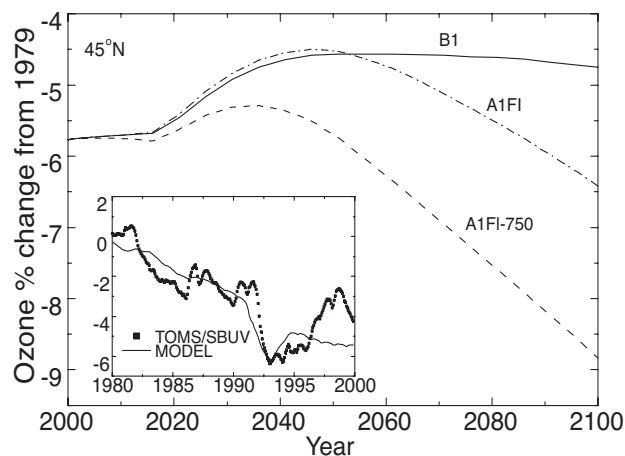


Figure 4-44. Percent change in annual average stratospheric ozone at 45°N from 1979 levels for the period 2000-2100 calculated with a 2-D model and a range of GHG scenarios. The GHG scenarios are based on IPCC (2001) scenarios B1 and A1F1, with a third scenario based on A1F1 but with reduced CH₄ emissions (labeled by A1F1-750). The insert shows modeled and observed ozone changes from 1980 to 2000. From Randeniya et al. (2002, Figure 2).

GLOBAL OZONE

their study. In agreement with the fixed-temperature models shown here, that study found that ozone increases between about 2000 and 2050. However, different behavior could occur at longer time horizons. Increasing levels of N_2O in the 21st century should be expected to increase NO_x , which will lead to enhanced ozone loss in the middle stratosphere. Moreover, as chlorine abundances decline, such increasing NO_x would no longer form $ClONO_2$ in the lower stratosphere and could hence lead to substantial ozone loss. Only when both N_2O is assumed to stop increasing and methane is assumed to decrease in the latter half of the 21st century does their model predict a stabilized ozone layer. This study makes clear that the large perturbations in NO_x , ClO_x , and HO_x that could occur in conjunction with various possible future scenarios for N_2O , CFCs, and CH_4 in the latter half of the 21st century may complicate long-term ozone changes, and could even prevent a return to 1980 levels. However, as Section 4.8.1 shows, the strong influence of CO_2 on cooling the upper stratosphere means that the coupled radiative effects of future CO_2 increases also need to be considered, which will tend to increase ozone over this time period.

Figure 4-45 shows the sensitivity of global ozone to different aerosol scenarios. Assuming an enhanced, but constant, aerosol loading causes lower O_3 values throughout the period 2000-2050. The largest difference occurs early in the 21st century with an additional decrease of 2%. As chlorine in the atmosphere declines, the additional effect of the enhanced aerosol loading decreases, and by 2050 the difference compared with the background aerosol is an additional 1% global loss. The episodic aerosol scenario also shows this behavior; the transient ozone depletion associated with a Mt. Pinatubo-size eruption is largest in the early 21st century (additional 2.5% loss in 2013, compared with additional 1.5% loss in 2034).

4.8.3 Other Stratospheric Influences

4.8.3.1 DYNAMICAL EFFECTS

As discussed in Section 4.6, two dynamical influences appear to have contributed to NH midlatitude ozone decreases over 1980-2000: a decrease in wave driving and an increase in tropopause height. These mechanisms likewise have the potential to influence future ozone. If the past dynamical changes represent natural variability, then one cannot extrapolate past dynamical trends, and ozone recovery could be either hastened or delayed by dynamical variability. If, on the other hand, the past dynamical changes represent the dynamical response to GHG-induced climate change, then one might expect these

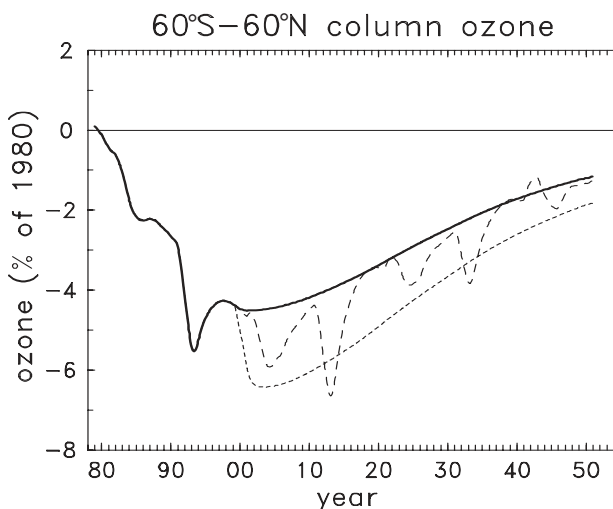


Figure 4-45. Predicted evolution of global column ozone ($60^\circ S-60^\circ N$) for one representative model for the MA2 scenario, which assumes a constant 1997 aerosol loading (solid line) along with results from sensitivity experiments that assume a constant 1993 aerosol loading (dotted line) and an episodic loading that repeats the 1979-2000 values (dashed line).

changes to increase in magnitude in the future. This would decrease future ozone levels and delay ozone recovery.

Unfortunately, our ability to predict future dynamical influences is very poor, for two reasons. First, dynamical processes affecting ozone exhibit significant temporal variability and are highly sensitive to other aspects of the atmospheric circulation. This means that the GHG-induced signal is inherently difficult to isolate or to represent accurately in GCMs, while the climate noise is relatively high (especially in the NH). Second, coupled chemistry GCMs, which are the tools needed to address this question, are still in their infancy (see Chapter 3). As discussed in Section 4.6.5, predictions of GHG-induced dynamical changes by such models do not even agree on the sign of the changes: some models predict weakened PWD, which would decrease midlatitude (and polar) ozone via reduced transport, while others predict strengthened PWD. Note that these dynamical changes would also affect the lifetime of stratospheric pollutants, with stronger PWD leading to a reduced lifetime (Butchart and Scaife, 2001). (This latter effect acts on the several-year time scale associated with the BDC, in contrast to the effect of PWD on ozone transport, which is essentially instantaneous.) Thus, the direct effect of PWD on ozone transport (no matter what its sign) would be reinforced over decadal time scales by altered chemical ozone loss arising from PWD-induced change in stratospheric chlorine loading.

4.8.3.2 FUTURE EFFECTS OF AIRCRAFT

Future subsonic and potential supersonic aviation have been calculated to impact atmospheric ozone. The IPCC Special Report on *Aviation and the Global Atmosphere* (IPCC, 1999) summarized the present understanding regarding future aviation emission levels and their effect on ozone. Model calculations were performed for forecasted (to 2015) and projected (to 2050) increases in NO_x emissions (1.7 Tg in 1992, 4.1 Tg in 2015, 7.2 Tg in 2050) from subsonic aviation. The calculated impacts increase with fleet emissions, rising from +0.4% to +1.2% (total column change at 45°N latitude) between 1992 and 2050. The impact is primarily confined to the troposphere, with approximately 25% of the change occurring in the stratosphere.

The impact on column ozone of a potential fleet of supersonic aircraft was estimated by IPCC (1999) and Kawa et al. (1999). The estimated effect on column ozone (at 45°N latitude) in 2050 of a combined supersonic and subsonic fleet is -0.4% relative to no aircraft and -1.5% relative to a 2050 subsonic-only fleet, with all the supersonic-induced change occurring in the stratosphere. For the presumed emission levels of NO_x, the predicted decrease in ozone is dominated by the influence of aircraft-emitted H₂O on odd-hydrogen abundances.

Aircraft impact studies conducted since the IPCC (1999) report have examined the sensitivity of model predictions to changing model parameterizations and input parameters. Schoeberl and Morris (2000) employed a trajectory model to evaluate the transport of subsonic and supersonic aircraft exhaust into the stratosphere. Their simulations indicate that there is less upward diffusion of supersonic emissions than found in Kawa et al. (1999) and that subsonic emissions do not significantly penetrate the 380-K potential temperature surface (i.e., they are confined to the lowermost stratosphere). The trajectory model results point to possible excessive diffusion in the global models. However, the sensitivity of ozone change to the reduced transport remains to be explored.

The importance of meteorological conditions on the calculated impacts of supersonic aircraft has been examined by Rogers et al. (2000). Three-dimensional model calculations were performed identically to those used in the IPCC Assessment, except that the model was forced with an annually varying meteorological analysis. The varying meteorology results in a calculated O₃ perturbation that exhibits interannual variability that is of similar magnitude (i.e., 50 ppbv) to the dispersion found among the models used in the IPCC (1999) and Kawa et al. (1999) assessments. This finding strengthens arguments presented in IPCC and Kawa et al. regarding the

substantial influence of model transport differences on the ozone impact computations.

The impacts of supersonic aircraft on stratospheric sulfate and PSC abundances have also received further scrutiny. Kärcher et al. (2000) have coupled a detailed analytical formulation for the near-field aerosol plume to a far-field plume model and a 2-D global aerosol model. Predicted changes in sulfate aerosol surface area density due to the operation of a supersonic fleet using the detailed microphysical treatment are similar to the earlier IPCC estimates. The Kärcher et al. analysis indicates that the sulfur-to-sulfate conversion efficiency and emission index of particulate organic matter are the most important parameters affecting large-scale cloud and chemical impacts.

The effects of supersonic NO_x and H₂O emissions on PSC formation have been examined by Considine et al. (2000) using a PSC parameterization formulated for inclusion in a global 3-D chemistry and transport model. The increased levels of polar NO_x and H₂O arising from the aircraft emissions are found to induce an earlier onset of PSC formation, denitrification, and dehydration in the Southern Hemisphere polar vortex. Resulting increases in active chlorine are calculated to produce approximately 1% decreases in lower stratospheric vortex O₃ concentrations.

It should also be noted that increases in the use of other types of aircraft or other routes, not considered in the Assessments discussed above, might lead to significant emissions in the stratosphere. In particular, a large increase in the use of small “executive” jets or introduction of near-supersonic commercial jets could affect stratospheric ozone. Also, increased use of subsonic polar routes could have important implications for the stratosphere. The potential effects of these will need to be assessed in more detail.

4.8.3.3 ROCKET EMISSIONS

Additional modeling and observation results have been reported on rocket combustion emissions and plume wake chemistry since the previous Assessment (WMO, 1999), in which it was concluded that stratospheric accumulation of chlorine and alumina exhaust from current launch activities leads to small (<0.1%) global column ozone decreases. The new data support this conclusion. They also reveal new chemical and physical processes that could influence future estimates of ozone loss associated with rocket launches.

Large (~100%) ozone loss has been observed and characterized in the local wakes of Delta II (Ross et al., 2000) and Atlas IIAS (Ross et al., 1999a) rockets powered by a combination of solid propellant (NH₄ClO₄/Al;

GLOBAL OZONE

ammonium perchlorate/aluminum) and liquid propellant (LOX/kerosene; liquid oxygen/kerosene). The cumulative ozone losses in the Delta II and Atlas IIAS wakes are comparable with those observed in solid-propellant-only Titan IV rockets, even though the total solid rocket motor (SRM) emissions are a factor of 9 and 11 greater for the Titan IV rocket than for the Delta and Atlas rockets, respectively.

This apparent nonlinear scaling of ozone loss with total SRM emissions is not predicted by plume wake models because the LOX/kerosene emissions are not expected to destroy ozone locally. To explain the observations, it has been suggested that exhaust products of the hydrocarbon-fueled engines of the Delta and Atlas rockets, possibly soot, catalyze ozone depletion. This suggestion remains to be tested because suitable gas and particle emission data for LOX/hydrocarbon-fueled rocket engines are not available. In situ particle number density and composition measurements made recently in an enormous aerosol cloud at 20 km altitude were linked to a Soyuz rocket launch 12 days earlier (Newman et al., 2001). These measurements constitute the first stratospheric data on emissions from a hydrocarbon-fueled rocket.

Danilin et al. (2001a) investigated the global implications of large, local ozone loss due to chlorine and alumina emissions from the current Space Shuttle (SRM/LOX-hydrogen) fleet. They modeled the accumulation of ozone losses in two Shuttle wakes (followed by dilution) and found this immediate wake effect not to be globally significant relative to the ozone loss on the longer time scale of plume dispersion and mixing with ambient background air globally. The relative significance of ozone loss accumulated in the plume on intermediate time scales (i.e., greater than 2 days) has not been evaluated.

The impact of alumina particles on ozone depletion is calculated to increase with surface area density (Danilin et al., 2001b). Particle measurements in SRM wakes have revealed a trimodal size distribution, in general agreement with rocket plume wake models (Ross et al., 1999b). However, the fraction of particle mass contained in the smallest (i.e., submicron) size modes differs by more than a factor of 5 between data obtained from large Titan IV and Shuttle SRMs (Ross et al., 1999b) and from a small Athena II SRM (Schmid et al., 2002). The large variance may reflect real differences between the emissions of large and small SRMs or differences in measurement techniques. In either case, because particle surface area density is most influenced by the submicron particle modes, the variance between the results of Ross et al. and Schmid et al. adds significant uncertainty to the predicted global impact of SRM emissions. Assuming the Schmid et al. particle distribution with its larger number

of submicron particles for the larger SRMs would result in the ozone impacts from emitted alumina and chlorine being roughly comparable. Alternatively, assuming the Schmid et al. distribution only for small SRMs would imply that ozone loss relative to total SRM emission varies inversely with SRM size, a feature not included in models.

The effect of plume-wake processing on the reactivity of rocket-emitted alumina particles and the associated ozone loss has yet to be fully explored. The reactivity depends strongly on the composition of the wake particles. Some insight into the composition of rocket particles has been gained from measurements of H₂O vapor and CO₂ in the lower stratospheric wake of an Athena II SRM (Gates et al., 2002). These data show that a fraction of the H₂O emissions condensed onto particles and remained condensed for more than 40 minutes after launch, long beyond when temperatures rose above the estimated frost point. Gates et al. (2002) argue that, for this to occur, the water surface layer of the particles is either coated with HNO₃ or combined with HNO₃ to form nitric acid trihydrate (NAT). In either case, the HNO₃ would serve to inhibit evaporation of the volatile aerosol component. Popp et al. (2002) measured ~30 parts per billion (ppb) HNO₃ in the Athena II wake, likely sufficient to explain the observed persistence of condensed volatiles. It is not clear if HNO₃ is produced during SRM combustion, during intense chemical processing in the plume wake, or by a combination of the two processes. In any case, the Athena II observations indicate that SRM plume wake particles are more complex and likely to be more reactive than previously considered.

Space launch activity has undergone substantial growth over the last decade (60% increase per decade; FAA, 2000). If this growth rate is realized through SRM use and is sustained over the next several decades, the associated ozone depletion from stratospheric chlorine and particle injection might become significant. Under some plausible scenarios, ozone loss due to rockets may become greater than that due to chlorofluorocarbons by the year 2050. However, recent technology developments indicate that growth in hydrocarbon engine emissions may exceed growth in SRM emissions. The change in calculated ozone impact resulting from SRM replacement by hydrocarbon engines cannot be confidently estimated at this time.

4.8.4 Future Tropospheric Ozone

The future evolution of tropospheric ozone was considered in some detail in the recent Third Assessment Report (TAR) of the Intergovernmental Panel on Climate Change (IPCC, 2001), and here we focus primarily on the

results presented therein. Research groups involved in 3-D tropospheric chemistry modeling were invited to participate in the TAR through a model intercomparison activity. Ten different models submitted results for both the year 2000 (Y2000), and for one scenario for the year 2100 (Y2100). The groups were asked to run with a standard set of emissions for NO_x , CO, and volatile organic compounds (VOCs) for 2000 and for abundances of long-lived gases; the standard simulation for 2000 provided the baseline from which changes in greenhouse gases were calculated.

The model simulations for 2000 were tested by comparison with the seasonal cycle of ozone at five locations (20°N-75°N) for 700, 500, and 300 hPa, and the simulation for CO was compared with surface concentrations from five sites (40°S-80°N). The models captured the broad seasonal patterns for CO and ozone, but there was a wide dispersion among the models for both gases. Most models were within 30% of the ozone observations. However, it should be noted that there were large variations in the calculation of the present-day tropospheric ozone budget. In particular, there is disagreement between models on the sign of the net photochemical production, possibly driven by differences in the calculated flux of ozone from the stratosphere.

A large number of scenarios for future emissions were developed for the IPCC Assessment, but only one of these, designated the Special Report on Emissions Scenarios (SRES) A2p, was used for the Y2100 standard calculation; a CH_4 abundance of 4.3 parts per million by volume (ppmv) was specified for Y2100. The TAR notes that the SRES scenarios assume few controls on CO, NO_x , and VOCs, and that A2p has overall the highest emissions. It was chosen so that once the response of ozone and OH to these extreme emissions was understood, other scenarios and intermediate years could be interpolated with some confidence.

The increase in the tropospheric column of ozone from Y2000 to Y2100 calculated by the ten 3-D models was 16.6 to 26.5 DU, and the TAR adopted a best estimate of 22 DU. Although the increases in the tropospheric ozone column given by the various models were rather consistent, the spatial and vertical distributions of the ozone changes varied considerably from model to model. A footnote added in proof to the TAR notes that these “tropospheric” column changes erroneously included the lower stratosphere, and that the troposphere-only changes are 25-33% less, or about 16 DU. The present-day column of tropospheric ozone is about 34 DU, so the calculated increase is a substantial fraction of the current amount in

the troposphere, and it is a few percent of the total column of midlatitude ozone.

The TAR used the standard Y2000 and Y2100 calculations, along with three other cases (Y2000 with a 10% increase in CH_4 , Y2100 with no increase in NO_x emissions, and Y2100 with no increase in NO_x , VOC, and CH_4) to define simple linear relationships for the absolute change in tropospheric ozone and the relative change in OH as a function of the CH_4 abundance, and the emission rates for NO_x , CO, and VOC. These relationships were then used to estimate the evolution of six different emission scenarios from 2000 to 2100. The changes in the tropospheric ozone column for 2000 to 2100 for the six scenarios are from -4 to +22 DU, whereas the changes for 2000 to 2050 are from 4 to 15 DU. Clearly, the scenario selected for the Y2100 model study represents an extreme case.

The calculations that were carried out for the TAR did not allow for changes in stratospheric ozone, nor did they allow for changes in climate. Calculations with the coupled ocean-atmosphere-chemistry model at the Hadley Centre (U.K.) have shown that the increases predicted for tropospheric ozone and CH_4 by 2100 are smaller in simulations that allow for climate change than in those that do not (Johnson et al., 2001). Trace gas emissions were taken from the same scenario, A2, as in the TAR, but CH_4 was calculated based on emissions. In the control run, ozone at 650 hPa increased from 40 ppbv to 65 ppbv at midlatitudes, whereas in the run with changing climate, ozone increased to only 49 ppbv. The increase in CH_4 was from 1.67 ppmv in 1990 to 3.65 ppmv in 2100 in the control run, but to only 3.23 ppmv in the climate change run. Most of the difference for both gases occurred after 2040. The main causes for smaller changes in ozone and CH_4 in the climate change run were (1) an increase in photochemical destruction of ozone caused by higher water vapor, and (2) a decrease in the CH_4 lifetime caused by the higher temperatures increasing the rate coefficient for $\text{OH} + \text{CH}_4$, and by higher OH.

While these results indicate that estimates of future tropospheric ozone may be reduced in a future climate, there are other feedbacks that may result in higher tropospheric ozone levels. For example, increased deep convection in a future climate could lead to increases in NO_x production by lightning (e.g., Toumi et al., 1996). Climate change may also lead to increases in temperature-dependent emissions (e.g., isoprene) or changes in the flux of ozone from the stratosphere, resulting in additional increases in tropospheric ozone. Current uncertainties in our knowledge about such feedbacks hinder our ability to predict future changes.

4.9 SYNTHESIS OF CURRENT UNDERSTANDING OF PAST AND FUTURE CHANGES IN OZONE

Table 4-5 summarizes the important processes that we believe have contributed to the observed past changes in global ozone, our estimated level of scientific understanding of these processes, and their likely importance in causing the observed trend in column ozone. Our level of scientific understanding is given on a scale from low to high. The impact on global ozone is rated from negligible to important. The table also summarizes the processes that will affect the future evolution of the ozone layer, an estimate of the likely importance of that process, and a measure of our confidence in that prediction. The stated confidence ranges from high to low. The importance for column ozone ranges from minor to important.

4.9.1 Discussion of Past Changes

There is very high confidence that gas-phase chlorine chemistry is the main driver of ozone trends in the upper stratosphere. This is based on overall reasonable agreement between observed and modeled ozone trends in the upper stratosphere, in terms of vertical profile (Figure 4-30) and latitudinal structure (e.g., WMO, 1999, Figure 6-20). Although there are substantial inter-model differences in the magnitude of the trends near 40-45 km for the simulations examined here (Figure 4-30), these are strongly related to differences in modeled temperature trends in the upper stratosphere, and also to changes in constituents such as CH₄ (although a quantitative analysis of these effects is beyond the scope of this Assessment). In the upper stratosphere, lower temperatures cause a slow down of the gas-phase chemical loss reactions due to chlorine, while CH₄ controls the ClO/HCl partitioning (as is apparent in observations in Figure 4-29), and therefore larger CH₄ trends lead to smaller ozone trends. Note that long-term global observations of upper stratospheric CH₄ over 1979-2000 are unavailable to compare and constrain the model results. Upper stratospheric CH₄ measurements from HALOE during 1991-2000 show substantial inter-annual variability and changes in “trends” that are not well understood at present (Randel et al., 1999), and these are difficult to extrapolate to the longer 1979-2000 period. Although the processes responsible for upper stratospheric ozone losses are reasonably well understood, the contribution to column ozone trends is relatively small: only 15-30% of the extratropical column ozone losses for 1980-2000 originate at altitudes above 25 km.

In the lower stratosphere, there is fairly high confidence that halogen-related chemistry is responsible for a large fraction of the midlatitude ozone trends. This is

based on the fact that 2-D and 3-D models with imposed halogen trends are able to approximately simulate the latitudinal, vertical, and seasonal characteristics of observed midlatitude ozone trends. There are important caveats to this attribution, because the 2-D models all overestimate observed ozone trends in the tropics and underestimate the magnitude and seasonality of trends in the midlatitude NH, and there is relatively large inter-model variability for trend calculations in the midlatitude SH. The underestimate of NH midlatitude trends during winter-spring may be due to a number of factors: effects of water vapor trends and uncertainties in bromine amount and chemical reaction rates, lack of detailed polar vortex chemistry and mixing to midlatitudes in 2-D models, and the contribution of dynamically induced ozone changes in observations. Also, the precise mechanisms for the decadal-scale ozone changes that occur in the models are not simply isolated, and the relative importance of polar processing (and export to midlatitudes) versus in situ activation awaits clarification. The overestimates of tropical ozone trends may be related to relatively weak dynamical isolation of the tropics in many models (Hall et al., 1999; see also Figure 4-28), and the large inter-model variability in SH extratropics is associated with simulation of the Antarctic ozone hole and transport out of the vortex.

Although the models are able to approximately simulate the 20-year trends in midlatitudes, both 2-D and 3-D simulations are less successful at simulating the actual time series of midlatitude ozone. This is particularly the case in the SH, where models overestimate SH ozone losses after the eruption of Mt. Pinatubo and miss substantial ozone declines observed during the middle 1980s. Variability in the wave-driven Brewer-Dobson circulation contributes to interannual ozone changes in the lower stratosphere during winter and spring, and this factor is relatively more important in the NH where wave driving is stronger and highly variable. Although the contribution of this process to decadal ozone trends is difficult to quantify, it probably accounts for 30% or less of the observed NH trends during 1979-2000.

The lowermost stratosphere is the region where the ozone trends, and their causes, are least certain. Long records of ozonesonde data are limited to relatively few stations over NH midlatitudes. The role of chemistry is difficult to quantify because of low temperatures and occasionally high humidity. This makes the role of heterogeneous chemistry on aerosols and cirrus particles uncertain. Dynamics plays a relatively large role for ozone variability in the lowermost stratosphere. This region is sensitive to the Brewer-Dobson circulation (from above), and empirical studies over NH midlatitudes show strong relationships between ozone and changes in tropo-

Table 4-5. Summary of understanding of past long-term midlatitude stratospheric ozone changes and expected importance in the future.

Influence	Process	Level of Scientific Understanding (LOSU) ^a	Region of Local Change	Contribution to Past Column Changes and Sign of Forcing ^b	Likely Importance for Future Column Change Over Next 50 Years
Chemical					
CFCs, halons, and other Cl/Br source gases	Cl _y /Br _y processing from vortex Cl _y T-dependent gas-phase chemistry in US	Medium Very high	Tropopause-30 km 25-50 km	Important; negative Important; negative	Decreasing over time Decreasing over time
	Cl _y /Br _y gas-phase chemistry in LS/LMS	High	Tropopause-25 km	Important; negative	Decreasing over time
	N ₂ O ₅ + H ₂ O on sulfate aerosol	High	Tropopause-30 km	Important; negative	Decreasing over time
	Cl _y processing on cold liquid aerosol	Medium	Tropopause-20 km	Important; negative	Decreasing over time
CH ₄	CH ₄ chemistry	High	Tropopause-50 km	Minor; positive	Minor
	HO _x chemistry	High	Tropopause-20 km and 30-50 km	Minor; negative	Minor
	Effect on H ₂ O and heterogeneous chemistry	Medium	Tropopause-20 km	Minor; negative	Minor
	NO _y chemistry	Very high	25-45 km	Minor; negative	Increasing over time
N ₂ O	HO _x and heterogeneous chemistry	Medium	Tropopause-50 km	Minor; negative	Unknown
H ₂ O	NO _x , HO _x , aerosols	Medium	Tropopause-20 km	Minor; positive	Minor
Aircraft	Cl _y , alumina, soot	Medium	Tropopause-50 km	Negligible; negative	Minor
Rockets					
Dynamical and radiative					
Stratospheric planetary waves	Transport	Medium	15-30 km	Important; positive, negative	Important
Tropospheric circulation	Stratosphere-troposphere exchange and LMS dynamics ^c	Medium-low	Tropopause-20 km	Important; positive, negative	Important
Radiatively active species (CO ₂ , CH ₄ , N ₂ O, H ₂ O) GHG direct effect ^d	Thermal structure	Medium-high	Tropopause-50 km	Minor; positive (US), negative (L-S/LMS)	Important
Other					
Solar irradiance	Modulation of photolysis rates	Medium	Tropopause-50 km	Negligible; positive, negative	Minor
Volcanoes	Heterogeneous chemistry	Medium	Tropopause-25 km	Important; negative	Transient; possibly large
Tropospheric O ₃ precursors	RO ₂ -NO _x chemistry	Medium	Surface-tropopause	Minor; positive	Important

^a The meaning of LOSU for dynamical influences is different from that used for the chemical influences. The relevant physics and mechanisms of the stratospheric planetary wave forcings are well understood. However, it is hard to quantify their past effect in the real atmosphere. For tropospheric circulation changes, uncertainties come from our lack of clear understanding of the mechanisms controlling tropopause height. For direct GHG changes, uncertainties come from factors influencing how well the changes in H₂O near the tropopause are known. For future changes, the LOSU for all processes is limited by the quality of predictive models.

^b The meaning of "forcing" for the effects of stratospheric planetary waves and tropospheric circulation on ozone is different than for chemical forcings. Here "forcing" is used in the sense that decadal changes in these dynamical properties of the atmosphere have occurred that can cause decadal changes in ozone. The possible causes of these dynamical changes are discussed in Section 4.6.

^c Tropopause height is a proxy for LMS dynamics.

^d GHG direct effect means the radiative impact of changes in GHGs and any consequent changes in the thermal structure of the atmosphere GHG effect. The direct greenhouse effect of GHGs is a forcing in the same way as the chemical forcings are defined, namely, an increase in atmospheric concentrations of certain gases as a result of anthropogenic activity has an effect on the atmosphere that can, in principle, be separated and determined.

GLOBAL OZONE

spheric circulation and tropopause height (forcing from below). The interrelationships between ozone and circulation parameters in the lowermost stratosphere are poorly quantified at present, and estimates of circulation effects on decadal changes in ozone are highly uncertain.

Overall, the balance of evidence still suggests that increases in halogens have been the most important driver for long-term changes in global ozone. However, compared with previous Assessments, the longer observation time series now available have emphasized other factors, such as dynamical variability, which modulate ozone in the lower part of the stratosphere.

4.9.2 Discussion of Future Changes

Over the next 50 years the stratospheric burden of chlorine is expected to return to the same level as that which existed in 1980 (Chapter 1). Accordingly, the reversal of the halogen forcing of the observed past trends in global ozone is expected to lead to an ozone increase. However, a number of other factors may affect the rate and extent of this recovery from the halogen-induced depletion.

In the upper stratosphere, where past trends have been due to chlorine chemistry, ozone is expected to return to 1980 values well before 2050. Coupled 2-D model calculations suggest that a cooling of the stratosphere (due to GHG increases) will significantly increase US ozone through a slowdown of the gas-phase chemical loss reactions (Figure 4-43). Without this cooling, similar models predict that US ozone would not have returned to 1980 levels by 2050, highlighting the important impact of this feedback.

In the lower stratosphere, the decrease in stratospheric chlorine will also lead to a recovery from the observed depletion of the past two decades. Although bromine has also contributed to LS O₃ changes, the reduction in chlorine is expected to dominate future trends. A range of 2-D models indicate that NH and SH midlatitude column ozone (which is dominated by the LS) will return to 1980 levels between 2025 and 2050, although there is a large uncertainty in this timing (Figure 4-42). The models that include the effect of stratospheric cooling on gas-phase chemistry indicate that this will also significantly accelerate the rate of column ozone increase in this period. An important caveat to these predictions is that the 2-D models examined here do not include a detailed treatment of polar processes and mixing to midlatitudes. Heterogeneous processing of chlorine species in the polar vortex may significantly affect midlatitude ozone, and over the next decade or so stratospheric cooling could enhance polar ozone loss (see Chapter 3). Therefore, in

the near future continued midlatitude ozone losses may still be observed.

Midlatitude ozone will be most susceptible to enhanced chemical loss by volcanic eruptions in the next 20 years or so while stratospheric chlorine levels remain high. During this period, a large eruption, similar in magnitude to that of Mt. Pinatubo in 1991, may cause a similar transient decrease in column ozone that lasts a few years. Predicted changes in N₂O and CH₄ will have a relatively small impact on column ozone over the next 50 years.

Any future changes in stratospheric circulation and transport could have the potential to affect global column ozone. At present it is not possible to predict what these changes may be and therefore what effect they may have on column ozone. This is a major limitation on our predictive capability.

Beyond 2050 the stratosphere will return to one in which halogens play less of a role in controlling the distribution of ozone. Ozone trends may then be dominated by trends in other gases that produce chemical species known to catalytically destroy ozone (e.g., H₂O, N₂O, and CH₄). For example, under some possible scenarios, future increases in N₂O may lead to enhanced loss due to enhanced NO_y chemistry. However, it seems that the radiative cooling of future increased GHGs, which will lead to increased US ozone, may dominate. In the future low-halogen atmosphere, the cooling of the stratosphere will also have less leverage to destroy ozone through polar processing. Combined with the fact that model studies predict an increase in tropospheric ozone by 2100, it seems likely that by the end of this century the atmosphere may contain more ozone than in the recent past.

REFERENCES

- Al-Saadi, J.A., R.B. Pierce, T.D. Fairlie, M.M. Kleb, R.S. Eckman, W.L. Grose, M. Natarajan, and J.R. Olson, Response of middle atmosphere chemistry and dynamics to volcanically elevated sulfate aerosol: Three-dimensional coupled model simulations, *J. Geophys. Res.*, 106, 27255-27275, 2001.
- Andrews, D.G., J.R. Holton, and C.B. Leovy, *Middle Atmosphere Dynamics*, Academic Press, 489 pp., Orlando, Fla., 1987.
- Angell, J.K., On the relation between atmospheric ozone and sunspot number, *J. Clim.*, 2, 1404-1416, 1989.
- Appenzeller, C., A.K. Weiss, and J. Staehelin, North Atlantic Oscillation modulates total ozone winter trends, *Geophys. Res. Lett.*, 27, 1131-1134, 2000.
- Austin, J., A three-dimensional coupled chemistry-climate model simulation of past stratospheric

- trends, *J. Atmos. Sci.*, *59*, 218-232, 2002.
- Austin, J., J.R. Knight, and N. Butchart, Three-dimensional chemical model simulations of the ozone layer: 1979-2015, *Quart. J. Roy. Meteorol. Soc.*, *126*, 1533-1556, 2000.
- Baldwin, M.P., and T.J. Dunkerton, Propagation of the Arctic Oscillation from the stratosphere to the troposphere, *J. Geophys. Res.*, *104*, 30937-30946, 1999.
- Barnes, J.E., and D.J. Hofmann, Variability in the stratospheric background aerosol over Mauna Loa Observatory, *Geophys. Res. Lett.*, *28*, 2895-2898, 2001.
- Barnes, R.J., A. Sinha, and H.A. Michelsen, Assessing the contribution of the lowest triplet state to the near-UV absorption spectrum of HOCl, *J. Phys. Chem. A*, *102*, 8855-8859, 1998.
- Bekki, S., The possible role of aircraft-generated soot in the middle latitude ozone depletion, *J. Geophys. Res.*, *102*, 10751-10758, 1997.
- Bengtsson, L., E. Roeckner, and M. Stendel, Why is global warming proceeding much slower than expected?, *J. Geophys. Res.*, *104*, 3865-3876, 1999.
- Bloss, W.J., D.M. Rowley, R.A. Cox, and R.L. Jones, Kinetics and products of the IO self-reaction, *J. Phys. Chem. A*, *105*, 7840-7854, 2001.
- Bluth, G.J.S., S.D. Doiron, C.C. Schnetzler, A.J. Krueger, and L.S. Walter, Global tracking of the SO₂ clouds from the June 1991 Mount Pinatubo eruptions, *Geophys. Res. Lett.*, *19*, 151-154, 1992.
- Bodeker, G.E., J.C. Scott, K. Kreher, and R.L. McKenzie, Global ozone trends in potential vorticity coordinates using TOMS and GOME intercompared against the Dobson network: 1978-1998, *J. Geophys. Res.*, *106*, 23029-23042, 2001.
- Bojkov, R.D., and D.S. Balis, Characteristics of episodes with extremely low ozone values in the northern middle latitudes 1957-1999, *Annales Geophysicae*, *19*, 797-807, 2001.
- Bojkov, R.D., and V.E. Fioletov, Estimating the global ozone characteristics during the last 30 years, *J. Geophys. Res.*, *100*, 16537-16552, 1995.
- Bojkov, R.D., C.S. Zerefos, D.S. Balis, I.C. Ziomas, and A.F. Bais, Record low total ozone during northern winters of 1992 and 1993, *Geophys. Res. Lett.*, *20*, 1351-1354, 1993.
- Bojkov, R.D., V.E. Fioletov, and A.M. Shalamjansky, Total ozone changes over Eurasia since 1973 based on reevaluated filter ozonometer data, *J. Geophys. Res.*, *99*, 22985-22999, 1994.
- Bojkov, R.D., E. Kosmidis, J.J. DeLuisi, I. Petropavlovskikh, V.E. Fioletov, S. Godin, and C. Zerefos, Vertical ozone distribution characteristics deduced from ~44,000 re-evaluated Umkehr profiles (1957-2000), *Meteorol. Atmos. Phys.*, *79*, 127-158, 2002.
- Borrmann, S., S. Solomon, L. Avallone, D. Toohey, and D. Baumgardner, On the occurrence of ClO in cirrus clouds and volcanic aerosol in the tropopause region, *Geophys. Res. Lett.*, *24*, 2011-2014, 1997.
- Braesicke, P., A. Jrrar, P. Hadjinicolaou, and J.A. Pyle, Variability of total ozone due to the NAO as represented in two different model systems, *Meteorol. Z.*, submitted, 2002.
- Brasseur, G., and C. Granier, Mount Pinatubo aerosols, chlorofluorocarbons, and ozone depletion, *Science*, *257*, 1239-1242, 1992.
- Bregman, B., P.-H. Wang, and J. Lelieveld, Chemical ozone loss in the tropopause region on subvisible ice clouds, calculated with a chemistry-transport model, *J. Geophys. Res.*, *107*, 2002.
- Brönnimann, S., J. Luterbacher, C. Schmutz., H. Wanner, and J. Staehelin, Variability of total ozone at Arosa, Switzerland, since 1931 related to atmospheric circulation indices, *Geophys. Res. Lett.*, *27*, 2213-2216, 2000.
- Brown, S.S., R.K. Talukdar, and A.R. Ravishankara, Reconsideration of the rate constant for the reaction of hydroxyl radicals with nitric acid, *J. Phys. Chem. A*, *103*, 3031-3037, 1999.
- Brown, S.S., J.B. Burkholder, R.K. Talukdar, and A.R. Ravishankara, Reaction of hydroxyl radical with nitric acid: Insights into its mechanism, *J. Phys. Chem. A*, *105*, 1605-1614, 2001.
- Burrows, J.P., M. Weber, M. Buchwitz, V. Rozanov, A. Ladstätter-Weißmayer, A. Richter, R. DeBeek, R. Hoogen, K. Bramstedt, K.-U. Eichmann, and M. Eisinger, The Global Ozone Monitoring Experiment (GOME): Mission concept and first scientific results, *J. Atmos. Sci.*, *56*, 151-175, 1999.
- Butchart, N., and A.A. Scaife, Removal of chlorofluorocarbons by increased mass exchange between the stratosphere and the troposphere in a changing climate, *Nature*, *410*, 799-802, 2001.
- Butchart, N., J. Austin, J.R. Knight, A.A. Scaife, and M.L. Gallani, The response of the stratospheric climate to projected changes in the concentrations of well-mixed greenhouse gases from 1992 to 2051, *J. Clim.*, *13*, 2142-2159, 2000.
- Carlsaw, K.S., T. Peter, and S.L. Clegg, Modeling the composition of liquid stratospheric aerosols, *Rev. Geophys.*, *35*, 125-154, 1997.
- Chance, K., W.A. Traub, D.G. Johnson, K.W. Jucks, P. Ciarpallini, R.A. Stacknik, R.J. Salawitch, and

GLOBAL OZONE

- H.A. Michelsen, Simultaneous measurements of stratospheric HO_x, NO_x, and Cl_x: Comparison with a photochemical model, *J. Geophys. Res.*, *101*, 9031-9043, 1996.
- Chandra, S., and R.D. McPeters, The solar cycle variation of ozone in the stratosphere inferred from NIMBUS 7 and NOAA 11 satellites, *J. Geophys. Res.*, *99*, 20665-20671, 1994.
- Chen, P., and W.A. Robinson, Propagation of planetary waves between the troposphere and stratosphere, *J. Atmos. Sci.*, *49*, 2533-2545, 1992.
- Chipperfield, M.P., Multiannual simulations with a three-dimensional chemical transport model, *J. Geophys. Res.*, *104*, 1781-1805, 1999.
- Chipperfield, M.P., and R.L. Jones, Relative influences of atmospheric chemistry and transport on Arctic ozone trends, *Nature*, *400*, 551-554, 1999.
- Choi, W., and M.T. Leu, Nitric acid uptake and decomposition on black carbon (soot) surfaces: Its implications for the upper troposphere and lower stratosphere, *J. Phys. Chem. A*, *102*, 7618-7630, 1998.
- Christiansen, B., Radiative forcing and climate sensitivity: The ozone experience, *Quart. J. Roy. Meteorol. Soc.*, *125*, 3011-3035, 1999.
- Considine, D.B., R.S. Stolarski, S.M. Hollandsworth, C.H. Jackman, and E.L. Fleming, A Monte Carlo uncertainty analysis of ozone trend predictions in a two-dimensional model, *J. Geophys. Res.*, *104*, 1749-1765, 1999.
- Considine, D.B., A.R. Douglass, P.S. Connell, D.E. Kinnison, and D.A. Rotman, A polar stratospheric cloud parameterization for the global modeling initiative three-dimensional model and its response to stratospheric aircraft, *J. Geophys. Res.*, *105*, 3955-3973, 2000.
- Cronkhite, J.M., R.E. Stickel, J.M. Nicovich, and P.H. Wine, Laser flash photolysis studies of radical-radical reaction kinetics: The HO₂ + IO reaction, *J. Phys. Chem. A*, *103*, 3228-3236, 1999.
- Danilin, M., M. Ko, and D. Weisenstein, Global implications of ozone loss in a space shuttle wake, *J. Geophys. Res.*, *106*, 3591-3601, 2001a.
- Danilin, M., R. Shia, M. Ko, D. Weisenstein, N. Sze, J. Lamb, T. Smith, P. Lohn, and M. Prather, Global stratospheric effects of the alumina emissions by solid-fueled rocket motors, *J. Geophys. Res.*, *106*, 12727-12738, 2001b.
- De Mazière, M., M. Van Roozendaal, C. Herman, P.C. Simon, P. Demoulin, G. Roland, and R. Zander, Quantitative evaluation of post-Pinatubo NO₂ reduction and recovery, based on 10 years of FTIR and UV-visible spectroscopic measurements at the Jungfraujoch, *J. Geophys. Res.*, *103*, 10849-10858, 1998.
- DeMore, W.B., S.P. Sander, D.M. Golden, R.F. Hampson, M.J. Kurylo, C.J. Howard, A.R. Ravishankara, C.E. Kolb, and M.J. Molina, *Chemical Kinetics and Photochemical Data for Use in Stratospheric Modeling: Evaluation Number 12, JPL Publication 97-4*, Jet Propulsion Laboratory, Pasadena, Calif., 1997.
- Dessler, A.E., D.B. Considine, J.E. Rosenfield, S.R. Kawa, A.R. Douglass, and J.M. Russell III, Lower stratospheric chlorine partitioning during the decay of the Mt. Pinatubo aerosol cloud, *Geophys. Res. Lett.*, *24*, 1623-1626, 1997.
- Disselkamp, R.S., M.A. Carpenter, J.P. Cowin, C.M. Berkowitz, E.G. Chapman, R.A. Zaveri, and N.S. Laulainen, Ozone loss in soot aerosols, *J. Geophys. Res.*, *105*, 9767-9771, 2000.
- Donahue, N.M., R. Mohrschladt, T.J. Dransfield, J.G. Anderson, and M.K. Dubey, Constraining the mechanism of OH + NO₂ using isotopically labeled reactants: Experimental evidence for HOONO formation, *J. Phys. Chem. A*, *105*, 1515-1520, 2001.
- Drdla, K., R.F. Pueschel, A.W. Strawa, R.C. Cohen, and T.F. Hanisco, Microphysics and chemistry of sulphate aerosols at warm stratospheric temperatures, *J. Geophys. Res.*, *104*, 26737-26751, 1999.
- Dubey, M.K., M.P. McGrath, G.P. Smith, and F.S. Rowland, HCl yield from OH + ClO: Stratospheric model sensitivities and elementary rate theory calculations, *J. Phys. Chem. A*, *102*, 3127-3133, 1998.
- Dvortsov, V.L., and S. Solomon, Response of the stratospheric temperatures and ozone to past and future increases in stratospheric humidity, *J. Geophys. Res.*, *106*, 7505-7514, 2001.
- Dvortsov, V.L., M.A. Geller, S. Solomon, S.M. Schauffler, E.L. Atlas, and D.R. Blake, Rethinking reactive halogen budgets in the midlatitude lower stratosphere, *Geophys. Res. Lett.*, *26*, 1699-1702, 1999.
- Erle, F., A. Grendel, D. Perner, U. Platt, and K. Pfeilsticker, Evidence of heterogeneous bromine chemistry on cold stratospheric sulphate aerosols, *Geophys. Res. Lett.*, *25*, 4329-4332, 1998.
- Evans, S.J., R. Toumi, J.E. Harries, M.P. Chipperfield, and J.M. Russell III, Trends in stratospheric humidity and the sensitivity of ozone to these trends, *J. Geophys. Res.*, *103*, 8715-8725, 1998.
- FAA (Federal Aviation Administration), *2000 Commercial Space Transportation Forecast*, 68 pp., Washington, D.C., 2000.
- Fahey, D.W., S.R. Kawa, E.L. Woodbridge, P. Tin, J.C. Wilson, H.H. Jonsson, J.E. Dye, D. Baumgardner,

- S. Borrmann, D.W. Toohey, L.M. Avallone, M.H. Proffitt, J. Margitan, M. Loewenstein, J.R. Podolske, R.J. Salawitch, S.C. Wofsy, M.K.W. Ko, D.E. Anderson, M.R. Schoeberl, and K.R. Chan, In situ measurements constraining the role of sulfate aerosols in mid-latitude ozone depletion, *Nature*, *363*, 509-514, 1993.
- Fairbrother, D., D. Sullivan, and H. Johnston, Global thermodynamic atmospheric modeling: Search for new atmospheric heterogeneous reactions, *J. Phys. Chem. A*, *101*, 7350-7358, 1997.
- Fioletov, V.E., J.B. Kerr, E.W. Hare, G.J. Labow, and R.D. McPeters, An assessment of the world ground-based total ozone network performance from the comparison with satellite data, *J. Geophys. Res.*, *104*, 1737-1748, 1999.
- Fioletov, V.E., G.E. Bodeker, J.B. Kerr, A.J. Miller, R.D. McPeters, and R. Stolarski, The global ozone and zonal total ozone variations estimated from ground-based and satellite measurements: 1964-2000, *J. Geophys. Res.*, in press, 2002.
- Fish, D.J., and M.R. Burton, The effect of uncertainties in kinetic and photochemical data on model predictions of stratospheric ozone depletion, *J. Geophys. Res.*, *102*, 25537-25542, 1997.
- Fish, D.J., H.K. Roscoe, and P.V. Johnston, Possible causes of stratospheric NO₂ trends observed at Lauder, New Zealand, *Geophys. Res. Lett.*, *27*, 3313-3316, 2000.
- Fitzenberger, R., H. Bösch, C. Camry-Peyret, M.P. Chipperfield, H. Harder, U. Platt, B.-M. Sinnhuber, T. Wagner, and K. Pfeilsticker, First profile measurements of tropospheric BrO, *Geophys. Res. Lett.*, *27*, 2921-2924, 2000.
- Fleming, E.L., S. Chandra, C.H. Jackman, D.B. Considine, and A.R. Douglass, The middle atmospheric response to short and long-term solar UV variations: Analysis of observations and 2D model results, *J. Atmos. Terr. Phys.*, *57*, 333-365, 1995.
- Fleming, E.L., C.H. Jackman, R.S. Stolarski, and D.B. Considine, Simulation of stratospheric tracers using an improved empirically based two-dimensional model transport formulation, *J. Geophys. Res.*, *104*, 23911-23934, 1999.
- Forster, P.M. de F., and K.P. Shine, Stratospheric water vapour changes as a possible contributor to observed stratospheric cooling, *Geophys. Res. Lett.*, *26*, 3309-3312, 1999.
- Forster, P.M. de F., and K.P. Shine, Assessing the climate impact of trends in stratospheric water vapour, *Geophys. Res. Lett.*, *29* (6), 1086, doi: 10.1029/2001GL013909, 2002.
- Forster, P.M. de F., and K. Tourpali, Effect of tropopause height changes on the calculation of ozone trends and their radiative forcing, *J. Geophys. Res.*, *106*, 12241-12251, 2001.
- Forster, P.M. de F., M. Ponater, and W.Y. Zhong, Testing broadband radiation schemes for their ability to calculate the radiative forcing and temperature response to stratospheric water vapour and ozone changes, *Meteorol. Z.*, *10*, 387-393, 2001.
- Froidevaux, L., J.W. Waters, W.G. Read, P.S. Connell, D.E. Kinnison, and J.M. Russell III, Variations in the free chlorine content of the stratosphere (1991-1997): Anthropogenic, volcanic, and methane influences, *J. Geophys. Res.*, *105*, 4471-4481, 2000.
- Fusco, A.C., and M.L. Salby, Interannual variations of total ozone and their relationship to variations of planetary wave activity, *J. Clim.*, *12*, 1619-1629, 1999.
- Garcia, R., and S. Solomon, A numerical model of the zonally averaged dynamical and chemical structure of the middle atmosphere, *J. Geophys. Res.*, *88*, 1379-1400, 1983.
- Gates, A.M., L.M. Avallone, D.W. Toohey, A.P. Rutter, P.D. Whitefield, D. Hagen, M.N. Ross, T.L. Thompson, R.L. Herman, R.R. Friedl, and P.F. Zittel, In situ measurements of carbon dioxide, 0.37-4.0 μm particles, and water vapor in the stratospheric plumes of three rockets, *J. Geophys. Res.*, in press, 2002.
- Gerecke, A., A. Thielmann, L. Gutzwiller, and M.J. Rossi, The chemical kinetics of HONO formation resulting from heterogeneous interaction of NO₂ with flame soot, *Geophys. Res. Lett.*, *13*, 2453-2456, 1998.
- Gierens, K., U. Schumann, M. Helten, H. Smit, and A. Marengo, A distribution law for relative humidity in the upper troposphere and lower stratosphere derived from three years of MOZAIC measurements, *Annales Geophysicae*, *17*, 1218-1226, 1999.
- Gierens, K., U. Schumann, M. Helten, H. Smit, and P.-H. Wang, Ice-supersaturated regions and subvisible cirrus in the northern midlatitude upper troposphere, *J. Geophys. Res.*, *105*, 22743-22753, 2000.
- Gleason, J.F., P.K. Bhartia, J.R. Herman, R.D. McPeters, P.A. Newman, R.S. Stolarski, L. Flynn, G. Labow, D. Larko, C. Seftor, C. Wellemeyer, W.D. Komhyr, A.J. Miller, and W. Planet, Record low global ozone in 1992, *Science*, *260*, 523-526, 1993.
- Godin, S., M. Marchand, and A. Hauchecorne, Influence of the Arctic polar vortex erosion on the lower stratospheric ozone amounts at Haute-Provence

GLOBAL OZONE

- Observatory (44°N, 6°E), *J. Geophys. Res.*, in press, 2002.
- Golden, D.M., and G.P. Smith, Reaction of OH + NO₂ + M: A new view, *J. Phys. Chem. A*, *104*, 3991-3997, 2000.
- Goldfarb, L., P. Keckhut, M.-L. Chanin, and A. Hauchecorne, Cirrus climatology results from lidar measurements at OHP (44°N, 6°E), *Geophys. Res. Lett.*, *28*, 1687-1690, 2001.
- Graf, H.-F., J. Perlwitz, and I. Kirchner, Northern hemisphere midlatitude circulation after violent volcanic eruptions, *Beitr. Phys. Atmos.*, *67*, 3-13, 1994.
- Graf, H.-F., J. Perlwitz, I. Kirchner, and I. Schult, Recent northern hemisphere climate trends, ozone changes, and increased greenhouse gas forcing, *Beitr. Phys. Atmos.*, *68*, 233-248, 1995.
- Grooß, J.-U., C. Brühl, and T. Peter, Impact of aircraft emissions on tropospheric and stratospheric ozone, I, Chemistry and 2-D model results, *Atmos. Environ.*, *32*, 3173-3184, 1998.
- Hadjinicolaou, P., J.A. Pyle, M.P. Chipperfield, and J.A. Kettleborough, Effect of interannual meteorological variability on midlatitude O₃, *Geophys. Res. Lett.*, *24*, 2993-2996, 1997.
- Hadjinicolaou, P., A. Ijarrar, J.A. Pyle, and L. Bishop, The dynamically-driven long-term trend in stratospheric ozone over northern mid-latitudes, *Quart. J. Roy. Meteorol. Soc.*, *128*, 1393-1412, 2002.
- Haigh, J.D., and J.A. Pyle, A two-dimensional calculation including atmospheric carbon dioxide and stratospheric ozone, *Nature*, *279*, 222-224, 1979.
- Hall, T.M., D.W. Waugh, K.A. Boering, and R.A. Plumb, Evaluation of transport in atmospheric models, *J. Geophys. Res.*, *104*, 18815-18839, 1999.
- Hansen, J.E., and M. Sato, Trends of measured climate forcing agents, *Proc. Natl. Acad. Sci.*, *98*, 14778-14783, 2001.
- Hansen, J.E., M. Sato, and R. Ruedy, Radiative forcing and climate response, *J. Geophys. Res.*, *102*, 6831-6864, 1997.
- Hansen, J.E., M. Sato, R. Ruedy, A. Lacis, and V. Oinas, Global warming in the twenty-first century: An alternative scenario, *Proc. Natl. Acad. Sci.*, *97*, 9875-9880, 2000.
- Hanson, D.R., and A.R. Ravishankara, Heterogeneous chemistry of bromine species in sulfuric acid under stratospheric conditions, *Geophys. Res. Lett.*, *22*, 385-388, 1995.
- Harder, H., H. Bösch, C. Camy-Peyret, M. P. Chipperfield, R. Fitzenberger, S. Payan, D. Perner, U. Platt, B.-M. Sinnhuber, and K. Pfeilsticker, Comparison of measured and modeled stratospheric BrO: Implications for the total amount of stratospheric bromine, *Geophys. Res. Lett.*, *27*, 3695-3698, 2000.
- Hartmann, D.L., J.M. Wallace, V. Limpasuvan, D.W.J. Thompson, and J.R. Holton, Can ozone depletion and global warming interact to produce rapid climate change?, *Proc. Natl. Acad. Sci.*, *97*, 1412-1417, 2000.
- Hendricks, J., E. Lippert, H. Petry, and A. Ebel, Heterogeneous reactions on and in sulfate aerosols: Implications for the chemistry of the midlatitude tropopause region, *J. Geophys. Res.*, *104*, 5531-5550, 1999.
- Hendricks, J., E. Lippert, H. Petry, and A. Ebel, Implications of subsonic aircraft NO_x emissions for the chemistry of the lowermost stratosphere: Model studies on the role of bromine, *J. Geophys. Res.*, *105*, 6745-6759, 2000.
- Herndon, S.C., P.W. Villalta, D.D. Nelson, J.T. Jayne, and M.S. Zahniser, Rate constant measurements for the reaction of HO₂ with O₃ from 200 to 300 K using a turbulent flow reactor, *J. Phys. Chem. A*, *105*, 1583-1591, 2001.
- Hervig, M.E., and T. Deshler, Stratospheric aerosol surface area and volume inferred from HALOE, CLAES, and ILAS measurements, *J. Geophys. Res.*, *103*, 25345-25352, 1998.
- Hervig, M.E., and T. Deshler, Evaluation of aerosol measurements from SAGE II, HALOE, and balloonborne optical particle counters, *J. Geophys. Res.*, *107* (D3), 4031, doi: 10.1029/2001JD000703, 2002.
- Hervig, M.E., K.S. Carslaw, T. Peter, T. Deshler, L.L. Gordley, G. Redaelli, U. Biermann, and J.M. Russell III, Polar stratospheric clouds due to vapor enhancement: HALOE observations of the Antarctic vortex in 1993, *J. Geophys. Res.*, *102*, 28185-28194, 1997.
- Hofmann, D.J., Increase in the stratospheric background sulfuric-acid aerosol mass in the past 10 years, *Science*, *248*, 996-1000, 1990.
- Hofmann, D.J., Aircraft sulfur emissions, *Nature*, *349*, 659-659, 1991.
- Hofmann, D.J., S.J. Oltmans, W.D. Komhyr, J.M. Harris, J.A. Lathrop, T. Deshler, B.J. Johnson, A. Torres, and W.A. Matthews, Ozone loss in the lower stratosphere over the United States in 1992-1993: Evidence for heterogeneous chemistry on the Pinatubo aerosol, *Geophys. Res. Lett.*, *21*, 65-68, 1994.
- Hofmann, D., P. Bonasoni, M. De Mazière, F. Evangelisti, G. Giovanelli, A. Goldman, F. Goutail, J. Harder, R. Jakoubek, P.V. Johnston, J. Kerr, W.A.

- Matthews, T. McElroy, R.L. McKenzie, G. Mount, U. Platt, J.-P. Pommereau, A. Sarkissian, P. Simon, and S. Solomon, Intercomparison of UV/visible spectrometers for measurements of stratospheric NO₂ for the Network for the Detection of Stratospheric Change, *J. Geophys. Res.*, *100*, 16765-16791, 1995.
- Hoinka, K.P., Temperature, humidity, and wind at the global tropopause, *Mon. Wea. Rev.*, *127*, 2248-2265, 1999.
- Hoinka, K.P., H. Claude, and U. Köhler, On the correlation between tropopause pressure and ozone above Central Europe, *Geophys. Res. Lett.*, *23*, 1753-1756, 1996.
- Hood, L.L., and D.A. Zaff, Lower stratospheric stationary waves and the longitudinal dependence of ozone trends in winter, *J. Geophys. Res.*, *100*, 25791-25800, 1995.
- Hood, L.L., J.P. McCormack, and K. Labitzke, An investigation of dynamical contributions to midlatitude ozone trends in winter, *J. Geophys. Res.*, *102*, 13079-13093, 1997.
- Hood, L.L., S. Rossi, and M. Beulen, Trends in lower stratospheric zonal winds, Rossby wave breaking behavior, and column ozone at northern midlatitudes, *J. Geophys. Res.*, *104*, 24321-24339, 1999.
- Hu, Y., and K.-K. Tung, Interannual and decadal variations of planetary wave activity, stratospheric cooling, and Northern Hemisphere annular mode, *J. Clim.*, *15*, 1659-1673, 2002.
- Huang, T.Y.W., and G.P. Brasseur, Effect of long-term solar variability in a 2-dimensional interactive model of the middle atmosphere, *J. Geophys. Res.*, *98*, 20413-20427, 1993.
- Hurst, D.F., G.S. Dutton, P.A. Romashkin, P.R. Wamsley, F.L. Moore, J.W. Elkins, E.J. Hints, E.M. Weinstock, R.L. Herman, E.J. Moyer, D.C. Scott, R.D. May, and C.R. Webster, Closure of the total hydrogen budget of the northern extratropical lower stratosphere, *J. Geophys. Res.*, *104*, 8191-8200, 1999.
- IPCC (Intergovernmental Panel on Climate Change), *Aviation and the Global Atmosphere*, edited by J.E. Penner, D.H. Lister, D.J. Griggs, D.J. Dokken, and M. McFarland, 373 pp., Cambridge University Press, Cambridge, U.K., 1999.
- IPCC (Intergovernmental Panel on Climate Change), *Climate Change 2001: The Scientific Basis: Contribution of Working Group I to the Third Assessment Report of the Intergovernmental Panel on Climate Change*, edited by J.T. Houghton, Y. Ding, D.J. Griggs, M. Noguer, P.J. van der Linden, X. Dai, K. Maskell, and C.A. Johnson, 881 pp., Cambridge University Press, Cambridge, U.K., 2001.
- Iraci, L.T., and M.A. Tolbert, Heterogeneous interaction of formaldehyde with cold sulfuric acid: Implications for the upper troposphere and lower stratosphere, *J. Geophys. Res.*, *102*, 16099-16107, 1997.
- Jackman, C.H., E.L. Fleming, S. Chandra, D.B. Conidine, and J.E. Rosenfield, Past, present, and future modeled ozone trends with comparisons to observed trends, *J. Geophys. Res.*, *101*, 28753-28767, 1996.
- Jäger, H., O. Uchino, T. Nagai, T. Fujimoto, V. Freudenthaler, and F. Homburg, Ground-based remote sensing of the decay of the Pinatubo eruption cloud at three northern hemisphere sites, *Geophys. Res. Lett.*, *22*, 607-610, 1995.
- Johnson, C.E., D.S. Stevenson, W.J. Collins, and R.G. Derwent, Role of climate feedback on methane and ozone studied with a coupled ocean-atmosphere-chemistry model, *Geophys. Res. Lett.*, *28*, 1723-1726, 2001.
- Joshi, M.M., K.P. Shine, M. Ponater, N. Stuber, R. Sausen, and L. Li, A comparison of climate response to different radiative forcings in three general circulation models: Towards an improved metric of climate change, *Clim. Dyn.*, submitted, 2002.
- Kalberer, M., M. Ammann, H.W. Gaggeler, and U. Baltensperger, Adsorption of NO₂ on carbon aerosol particles in the low ppb range, *Atmos. Environ.*, *33*, 2815-2822, 1999.
- Kalnay, E., M. Kanamitsu, R. Kistler, W. Collins, D. Deaven, L. Gandin, M. Iredell, S. Saha, G. White, J. Woollen, Y. Zhu, M. Chelliah, W. Ebisuzaki, W. Higgins, J. Janowiak, K.C. Mo, C. Ropelewski, J. Wang, A. Leetmaa, R. Reynolds, R. Jenne, and D. Joseph, The NCEP/NCAR 40-year reanalysis project, *Bull. Amer. Meteorol. Soc.*, *77*, 3303-3325, 1996.
- Kärcher, B., R.P. Turco, F. Yu, M.Y. Danilin, D.K. Weisenstein, R.C. Miake-Lye, and R. Busen, A unified model for ultrafine aircraft particle emissions, *J. Geophys. Res.*, *105*, 29379-29386, 2000.
- Kawa, S.R., J.G. Anderson, S.L. Baughcum, C.A. Brock, W.H. Brune, R.C. Cohen, D.E. Kinnison, P.A. Newman, J.M. Rodriguez, R.S. Stolarski, D. Waugh, and S.C. Wofsy, *Assessment of the Effects of High-Speed Aircraft in the Stratosphere: 1998*, NASA/TP-1999-209237, NASA Goddard Space Flight Center, Greenbelt, Md., 1999.
- Keim, E.R., D.W. Fahey, L.A. Del Negro, E.L.

GLOBAL OZONE

- Woodbridge, R.S. Gao, P.O. Wennberg, R.C. Cohen, R.M. Stimpfle, K.K. Kelly, E.J. Hints, J.C. Wilson, H.H. Jonsson, J.E. Dye, D. Baumgardner, S.R. Kawa, R.J. Salawitch, M.H. Proffitt, M. Loewenstein, J.R. Podolske, and K.R. Chan, Observations of large reductions in the NO/NO_y ratio near the midlatitude tropopause and the role of heterogeneous chemistry, *Geophys. Res. Lett.*, *23*, 3223-3226, 1996.
- Kerr, J.B., D.I. Wardle, and D.W. Tarasick, Record low ozone values over Canada in early 1993, *Geophys. Res. Lett.*, *20*, 1979-1982, 1993.
- Kerr, J.B., C.T. McElroy, and D.W. Wardle, The Brewer instrument calibration center 1984-1996, in *Atmospheric Ozone: Proc. XVIII Ozone Symp.*, 12-21 September 1996, L'Aquila, Italy, edited by R.D. Bojkov and G. Visconti, 915-918, Parco Scientifico e Tecnologico D'Abruzzo, L'Aquila, Italy, 1998.
- Kinnersley, J.S., and K.-K. Tung, Modeling the global interannual variability of ozone due to the equatorial QBO and to extratropical planetary wave variability, *J. Atmos. Sci.*, *55*, 1417-1428, 1998.
- Kinnison, D.E., K.E. Grant, P.S. Connell, D.A. Rotman, and D.J. Wuebbles, The chemical and radiative effects of the Mount Pinatubo eruption, *J. Geophys. Res.*, *99*, 25705-25731, 1994.
- Kirchner, I., G.L. Stenichikov, H.-F. Graf, A. Robock, and J.C. Antuna, Climate model simulation of winter warming and summer cooling following the 1991 Mount Pinatubo volcanic eruption, *J. Geophys. Res.*, *104*, 19039-19055, 1999.
- Kirk-Davidoff, D.B., E.J. Hints, J.G. Anderson, and D.W. Keith, The effect of climate change on ozone depletion through changes in stratospheric water vapour, *Nature*, *402*, 399-401, 1999.
- Knight, G.P., and J.N. Crowley, The reactions of IO with HO₂, NO, and CH₃SCH₃: Flow tube studies of kinetics and product formation, *Phys. Chem. Chem. Phys.*, *3*, 393-410, 2001.
- Knight, G.P., T. Beiderhase, F. Helleis, G.K. Moorgat, and J.N. Crowley, Reaction of HO₂ with ClO: Flow tube studies of kinetics and product formation between 215 and 298 K, *J. Phys. Chem. A*, *104*, 1674-1685, 2000.
- Knudsen, B.M., and J.-U. Groö, Northern midlatitude stratospheric ozone dilution in spring modeled with simulated mixing, *J. Geophys. Res.*, *105*, 6885-6890, 2000.
- Ko, M.K.W., N.D. Sze, C.J. Scott, and D.K. Weisenstein, On the relation between stratospheric chlorine/bromine loading and short-lived tropospheric source gases, *J. Geophys. Res.*, *102*, 25507-25517, 1997.
- Koike, M., N.B. Jones, W.A. Matthews, P.V. Johnston, R.L. McKenzie, D. Kinnison, and J. Rodriguez, Impact of Pinatubo aerosols on the partitioning between NO₂ and HNO₃, *Geophys. Res. Lett.*, *21*, 597-600, 1994.
- Langematz, U., An estimate of the impact of observed ozone losses on stratospheric temperature, *Geophys. Res. Lett.*, *27*, 2077-2080, 2000.
- Langematz, U., K. Krüger, M. Kunze, K. Labitzke, and G. Roff, Thermal and dynamical changes of the stratosphere since 1979 and their link to ozone and CO₂ changes, *J. Geophys. Res.*, submitted, 2002.
- Lanzendorf, E.J., T.F. Hanisco, P.O. Wennberg, R.C. Cohen, R.M. Stimpfle, and J.G. Anderson, Comparing atmospheric [HO₂]/[OH] to modeled [HO₂]/[OH]: Identifying discrepancies with reaction rates, *Geophys. Res. Lett.*, *28*, 967-970, 2001.
- Lary, D.J., and D.E. Shallcross, Potential importance of the reaction CO + HNO₃, *J. Geophys. Res.*, *105*, 11617-11623, 2000.
- Lary, D.J., M.P. Chipperfield, R. Toumi, and T. Lenton, Heterogeneous atmospheric bromine chemistry, *J. Geophys. Res.*, *101*, 1489-1504, 1996.
- Lary, D.J., D.E. Shallcross, and R. Toumi, Carbonaceous aerosols and their potential role in atmospheric chemistry, *J. Geophys. Res.*, *104*, 15929-15940, 1999.
- Lean, J., G. Rotman, H. Kyle, T. Woods, J. Hickey, and L. Puga, Detection and parameterization of variations in solar mid- and near-ultraviolet radiation (200-400 nm), *J. Geophys. Res.*, *102*, 29939-29956, 1997.
- Lee, H., and A.K. Smith, Simulation of the combined effects of solar cycle, QBO, and volcanic forcing on stratospheric ozone changes in recent decades, *J. Geophys. Res.*, in press, 2002.
- Li, Y.M., and J.S. Francisco, High-level ab initio molecular orbital theory study of the structure, vibrational spectrum, stability, and low-lying excited states of HOONO, *J. Chem. Phys.*, *113*, 7976-7981, 2000.
- Liley, J.B., P.V. Johnston, R.L. McKenzie, A.J. Thomas, and I.S. Boyd, Stratospheric NO₂ variations from a long time series at Lauder, New Zealand, *J. Geophys. Res.*, *105*, 11633-11640, 2000.
- Limpasuvan, V., and D.L. Hartmann, Wave-maintained annular modes of climate variability, *J. Clim.*, *13*, 4414-4429, 2000.
- Lipson, J.B., T.W. Beiderhase, L.T. Molina, M.J. Molina, and M. Olzmann, Production of HCl in the OH plus ClO reaction: Laboratory measurements and statistical rate theory calculations, *J. Phys. Chem. A*,

- 103, 6540-6551, 1999.
- Logan, J.A., I.A. Megretskaya, A.J. Miller, G.C. Tiao, D. Choi, L. Zhang, R.S. Stolarski, G.J. Labow, S.M. Hollandsworth, G.E. Bodeker, H. Claude, D. DeMuer, J.B. Kerr, D.W. Tarasick, S.J. Oltmans, B. Johnson, F. Schmidlin, J. Staehelin, P. Viatte, and O. Uchino, Trends in the vertical distribution of ozone: A comparison of two analyses of ozonesonde data, *J. Geophys. Res.*, 104, 26373-26399, 1999.
- Longfellow, C., T. Imamura, A. Ravishankara, and D. Hanson, HONO solubility and heterogeneous reactivity on sulfuric acid surfaces, *J. Phys. Chem. A*, 102, 3323-3332, 1998.
- Mahieu, E., R. Zander, P. Demoulin, M. De Mazière, F. Mélen, C. Servais, G. Roland, L. Delbouille, J. Poels, and R. Blomme, Fifteen years-trend characteristics of key stratospheric constituents monitored by FTIR above the Jungfraujoch, in *Stratospheric Ozone 1999, Proc. 5th European Symp.*, 27 September-1 October 1999, St. Jean de Luz, France, edited by N.R.P. Harris, M. Guirlet, and G.T. Amanatidis, *Air Pollution Research Rep. 73, EUR 19340*, 99-102, European Commission, Luxembourg, 2000.
- Mahlman, J.D., H. Levy II, and W.J. Moxim, Three-dimensional tracer structure and behavior as simulated in two ozone precursor experiments, *J. Atmos. Sci.*, 37, 655-685, 1980.
- Manney, G.L., R. Swinbank, S.T. Massie, M.E. Gelman, A.J. Miller, R. Nagatani, A. O'Neill, and R.W. Zurek, Comparison of U.K. Meteorological Office and U.S. National Meteorological Center stratospheric analyses during northern and southern winter, *J. Geophys. Res.*, 101, 10311-10334, 1996.
- Marchand, M., S. Godin, A. Hauchecorne, F. Lefèvre, S. Bekki, and M. Chipperfield, Influence of polar ozone loss on northern midlatitude regions estimated by a high-resolution chemistry transport model during winter 1999-2000, *J. Geophys. Res.*, in press, 2002.
- Mateer, C.L., and J.J. DeLuisi, A new Umkehr inversion algorithm, *J. Atmos. Terr. Phys.*, 54, 537-556, 1992.
- McCormick, M.P., J.M. Zawodny, R.E. Viegas, J.C. Larsen, and P.-H. Wang, An overview of SAGE I and II ozone measurements, *Planet. Space Sci.*, 37, 1567-1586, 1989.
- McLinden, C.A., S.C. Olsen, M.J. Prather, and J.B. Liley, Understanding trends in stratospheric NO_y and NO₂, *J. Geophys. Res.*, 106, 27787-27793, 2001.
- McPeters, R.D., and G.J. Labow, An assessment of the accuracy of 14.5 years of Nimbus-7 TOMS version 7 ozone data by comparison with the Dobson network, *Geophys. Res. Lett.*, 23, 3695-3698, 1996.
- McPeters, R.D., P.K. Bhartia, A.J. Krueger, and J.R. Herman, *Earth Probe Total Ozone Mapping Spectrometer (TOMS) Data Products User's Guide, NASA Technical Publication 1998-206985*, 64 pp., NASA Goddard Space Flight Center, Greenbelt, Md., 1998.
- Michelsen, H.A., C.M. Spivakovsky, and S.C. Wofsy, Aerosol-mediated partitioning of stratospheric Cl_y and NO_y at temperatures above 200 K, *Geophys. Res. Lett.*, 26, 299-302, 1999.
- Mickley, L.J., J.P. Abbatt, J.E. Frederick, and J.M. Russell III, Response of summertime odd nitrogen and ozone at 17 mbar to Mount Pinatubo aerosol over the southern midlatitudes: Observations from the Halogen Occultation Experiment, *J. Geophys. Res.*, 102, 23573-23582, 1997.
- Millard, G.A., A.M. Lee, and J.A. Pyle, A model study of the connection between polar and midlatitude ozone loss in the Northern Hemisphere lower stratosphere, *J. Geophys. Res.*, in press, 2002.
- Miller, A.J., S.M. Hollandsworth, L.E. Flynn, G.C. Tiao, G.C. Reinsel, L. Bishop, R.D. McPeters, W.G. Planet, J.J. DeLuisi, C.L. Mateer, D. Wuebbles, J. Kerr, and R.M. Nagatani, Comparisons of observed ozone trends and solar effects in the stratosphere through examination of ground-based Umkehr and combined solar backscattered ultraviolet (SBUV) and SBUV 2 satellite data, *J. Geophys. Res.*, 101, 9017-9022, 1996.
- Miller, A.J., R.M. Nagatani, L.E. Flynn, S. Kondragunta, E. Beach, R. Stolarski, R. McPeters, P.K. Bhartia, and M. DeLand, A cohesive total ozone data from the SBUV(2) satellite system, *J. Geophys. Res.*, in press, 2002.
- Nagashima, T., M. Takahashi, M. Takigawa, and H. Akiyoshi, Future development of the ozone layer calculated by a general circulation model with fully interactive chemistry, *Geophys. Res. Lett.*, 29 (8), 1162, doi: 10.1029/2001GL014026, 2002.
- Nedoluha, G.E., R.M. Bevilacqua, R.M. Gomez, D.E. Siskind, B.C. Hicks, J.M. Russell III, and B.J. Connor, Increases in middle atmosphere water vapor as observed by the Halogen Occultation Experiment and the ground-based water vapor millimeter-wave spectrometer from 1991 to 1997, *J. Geophys. Res.*, 103, 3531-3543, 1998a.
- Nedoluha, G.E., D.E. Siskind, J.T. Bacmeister, R.M. Bevilacqua, and J.M. Russell III, Changes in upper stratospheric CH₄ and NO₂ as measured by HALOE and implications for changes in transport,

GLOBAL OZONE

- Geophys. Res. Lett.*, 25, 987-25,990, 1998b.
- Newman, P.A., and E.R. Nash, Quantifying the wave driving of the stratosphere, *J. Geophys. Res.*, 105, 12485-12497, 2000.
- Newman, P.A., J.C. Wilson, M.N. Ross, C.A. Brock, P.J. Sheridan, M.R. Schoeberl, L.R. Lait, T.P. Bui, M. Loewenstein, and J.R. Podolske, Chance encounter with a stratospheric kerosene rocket plume from Russia over California, *Geophys. Res. Lett.*, 28, 959-962, 2001.
- Nickolaisen, S.L., C.M. Roehl, L.K. Blakeley, R.R. Friedl, J.S. Francisco, R. Liu, and S.P. Sander, Temperature dependence of the HO₂ + ClO reaction, 1, Reaction kinetics by pulsed photolysis-ultraviolet absorption and ab initio studies of the potential surface, *J. Phys. Chem. A*, 104, 308-319, 2000.
- Nizkorodov, S.A., W.W. Harper, B.W. Blackmon, and D.J. Nesbitt, Temperature dependent kinetics of the OH/HO₂/O₃ chain reaction by time-resolved IR laser absorption spectroscopy, *J. Phys. Chem. A*, 104, 3964-3973, 2000.
- Oinas, V., A.A. Lacis, D. Rind, D.T. Shindell, and J.E. Hansen, Radiative cooling by stratospheric water vapor: Big differences in GCM results, *Geophys. Res. Lett.*, 28, 2791-2794, 2001.
- Oltmans, S.J., A.S. Lefohn, H.E. Scheel, J.M. Harris, H. Levy, I.E. Galbally, E.G. Brunke, C.P. Meyer, J.A. Lathrop, B.J. Johnson, D.S. Shadwick, E. Cuevas, F.J. Schmidlin, D.W. Tarasick, H. Claude, J.B. Kerr, O. Uchino, and V. Mohnen, Trends of ozone in the troposphere, *Geophys. Res. Lett.*, 25, 139-142, 1998.
- Oltmans, S.J., H. Vömel, D.J. Hofmann, K.H. Rosenlof, and D. Kley, The increase in stratospheric water vapor from balloonborne frostpoint hygrometer measurements at Washington, D.C., and Boulder, Colorado, *Geophys. Res. Lett.*, 27, 3453-3456, 2000.
- Park, J.H., M.W.K. Ko, C.H. Jackman, R.A. Plumb, J.A. Kaye, and K.H. Sage, *Models and Measurements Intercomparison II, NASA/TM-1999-209554*, 502 pp., NASA Langley Research Center, Hampton, Va., 1999.
- Pawson, S., and B. Naujokat, The cold winters of the middle 1990s in the northern lower stratosphere, *J. Geophys. Res.*, 104, 14209-14222, 1999.
- Perlwitz, J., and H.-F. Graf, The statistical connection between tropospheric and stratospheric circulation of the Northern Hemisphere in winter, *J. Clim.*, 8, 2281-2295, 1995.
- Petrovavlovskikh, I., D. Theisen, J. DeLuisi, R.D. Bojkov, and E. Kosmidis, On shifts in the long-term Umkehr radiance records and their influence on retrieved ozone profiles, *Geophys. Res. Lett.*, 28, 255-258, 2001.
- Pfeilsticker, K., W.T. Sturges, H. Bösch, C. Camy-Peyret, M.P. Chipperfield, A. Engel, R. Fitzenberger, M. Müller, S. Payan, and B.-M. Sinnhuber, Lower stratospheric organic and inorganic bromine budget for the Arctic winter 1998/99, *Geophys. Res. Lett.*, 27, 3305-3308, 2000.
- Piani, C., W.A. Norton, A.M. Iwi, E.A. Ray, and J.W. Elkins, Transport of ozone-depleted air on the breakup of the stratospheric polar vortex in spring/summer 2000, *J. Geophys. Res.*, in press, 2002.
- Pitari, G., and V. Rizi, An estimate of the chemical and radiative perturbation of stratospheric ozone following the eruption of Mt. Pinatubo, *J. Atmos. Sci.*, 50, 3260-3276, 1993.
- Pommereau, J.-P., A. Garnier, B.M. Knudsen, G. Letrenne, M. Durand, M. Nunes-Pinharanda, L. Denis, F. Vial, A. Hertzog, and F. Cairo, Accuracy of analyzed stratospheric temperature in the winter Arctic vortex from infrared Montgolfier long-duration balloon flights, I, Measurements, *J. Geophys. Res.*, in press, 2002.
- Popp, P., B.A. Ridley, J.A. Neuman, L.M. Avallone, D.W. Toohey, P.F. Zittel, O. Schmid, R.L. Herman, R.S. Gao, M.J. Northway, J.C. Holecek, D.W. Fahey, T.L. Thompson, K.K. Kelly, J.G. Walega, F.E. Grahek, J.C. Wilson, M.N. Ross, and M.Y. Danilin, The emission and chemistry of reactive nitrogen species in the plume of an Athena II solid-fuel rocket motor, *Geophys. Res. Lett.*, in press, 2002.
- Portmann, R.W., S.S. Brown, T. Gierczak, R.K. Talukdar, J.B. Burkholder, and A.R. Ravishankara, Role of nitrogen oxides in the stratosphere: A reevaluation based on laboratory data, *Geophys. Res. Lett.*, 26, 2387-2390, 1999.
- Ramaswamy, V., and M.D. Schwarzkopf, Effects of ozone and well-mixed gases on annual-mean stratospheric temperature trends, *Geophys. Res. Lett.*, in press, 2002.
- Ramaswamy, V., M.L. Chanin, J. Angell, J. Barnett, D. Gaffen, M. Gelman, P. Keckhut, Y. Koshelkov, K. Labitzke, J.J.R. Lin, A. O'Neill, J. Nash, W. Randel, R. Rood, K. Shine, M. Shiotani, and R. Swinbank, Stratospheric temperature trends: Observations and model simulations, *Rev. Geophys.*, 39, 71-122, 2001.
- Randel, W.J., and F. Wu, A stratospheric ozone trends data set for global modeling studies, *Geophys. Res. Lett.*, 26, 3089-3092, 1999.

- Randel, W.J., F. Wu, J.M. Russell III, and J. Waters, Space-time patterns of trends in stratospheric constituents derived from UARS measurements, *J. Geophys. Res.*, *104*, 3711-3727, 1999.
- Randel, W.J., F. Wu, and D.J. Gaffen, Interannual variability of the tropical tropopause derived from radiosonde data and NCEP reanalyses, *J. Geophys. Res.*, *105*, 15509-15523, 2000.
- Randel, W.J., F. Wu, and R. Stolarski, Changes in column ozone correlated with the stratospheric EP flux, *J. Meteorol. Soc. Japan*, *80*, 849-862, 2002.
- Randeniya, L.K., P.F. Vohralik, and I.C. Plumb, Stratospheric ozone depletion at northern midlatitudes in the 21st century: The importance of future concentrations of greenhouse gases nitrous oxide and methane, *Geophys. Res. Lett.*, *29* (4), 1051, doi: 10.1029/2001GL014295, 2002.
- Reid, S.J., A.F. Tuck, and G. Kiladis, On the changing abundance of ozone minima at northern midlatitudes, *J. Geophys. Res.*, *105*, 12169-12180, 2000.
- Robock, A., and J.P. Mao, Winter warming from large volcanic eruptions, *Geophys. Res. Lett.*, *19*, 2405-2408, 1992.
- Roehl, C.M., H. Zhang, G.A. Blake, and P.O. Wennberg, Photodissociation of HNO₄ in the near IR, *J. Phys. Chem. A.*, in press, 2002.
- Rogers, H.L., M.P. Chipperfield, S. Bekki, and J.A. Pyle, The effects of supersonic aircraft on stratospheric chemistry modeled with varying meteorology, *J. Geophys. Res.*, *105*, 29359-29367, 2000.
- Roscoe, H.K., P.V. Johnston, M. Van Roozendaal, A. Richter, A. Sarkissian, J. Roscoe, K.E. Preston, J.-C. Lambert, C. Hermans, W. Decuyper, S. Dzienus, T. Winterrath, J. Burrows, F. Goutail, J.-P. Pommereau, E. D'Almeida, J. Hottier, C. Coureul, R. Didier, I. Pundt, L.M. Bartlett, C.T. McElroy, J.E. Kerr, A. Elokhov, G. Giovanelli, F. Ravegnani, M. Premuda, I. Kostadinov, F. Erle, T. Wagner, K. Pfeilsticker, M. Kenntner, L.C. Marquard, M. Gil, O. Puentedura, M. Yela, D.W. Arlander, B.A. Kastad Hoiskar, C.W. Tellefsen, K. Karlsen Tornkvist, B. Heese, R.L. Jones, S.R. Aliwell, and R.A. Freshwater, Slant column measurements of O₃ and NO₂ during the NDSC intercomparison of zenith-sky UV-visible spectrometers in June 1996, *J. Atmos. Chem.*, *32*, 281-314, 1999.
- Rosenfield, J.E., D.B. Considine, P.E. Meade, J.T. Bacmeister, C.H. Jackman, and M.R. Schoeberl, Stratospheric effects of Mount Pinatubo aerosol studied with a coupled two-dimensional model, *J. Geophys. Res.*, *102*, 3649-3670, 1997.
- Rosenfield, J.E., A.R. Douglass, and D.B. Considine, The impact of increasing carbon dioxide on ozone recovery, *J. Geophys. Res.*, *107* (D6), 4049, doi: 10.1029/2001JD000824, 2002.
- Rosenlof, K.H., S.J. Oltmans, D. Kley, J.M. Russell III, E.-W. Chiou, W.P. Chu, D.G. Johnson, K.K. Kelly, H.A. Michelsen, G.E. Nedoluha, E.E. Remsburg, G.C. Toon, and M.P. McCormick, Stratospheric water vapor increases over the past half-century, *Geophys. Res. Lett.*, *28*, 1195-1198, 2001.
- Rosier, S.M., and K.P. Shine, The effect of two decades of ozone change on stratospheric temperature as indicated by a general circulation model, *Geophys. Res. Lett.*, *27*, 2617-2620, 2000.
- Ross, M.N., R.F. Friedl, D.E. Anderson, G. Ash, M.R. Berman, B. Gandrud, W.T. Rawlins, E.C. Richard, and A.F. Tuck, Study blazing new trails into effects of aviation and rocket exhaust in the atmosphere, *Eos Trans. Amer. Geophys. Union*, *80*, pp. 437, 442-443, 1999a.
- Ross, M.N., P.D. Whitefield, D.E. Hagan, and A.R. Hopkins, In situ measurement of the aerosol size distribution in stratospheric solid rocket motor exhaust plumes, *Geophys. Res. Lett.*, *26*, 819-822, 1999b.
- Ross, M.N., D.W. Tooney, W.T. Rawlins, E.C. Richard, K.K. Kelly, A.F. Tuck, M.H. Proffitt, D.E. Hagen, A.R. Hopkins, P.D. Whitefield, J.R. Benbrook, and W.R. Sheldon, Observation of stratospheric ozone depletion associated with Delta II rocket emissions, *Geophys. Res. Lett.*, *27*, 2209-2212, 2000.
- Rowley, D.M., W.J. Bloss, R.A. Cox, and R.L. Jones, Kinetics and products of the IO plus BrO reaction, *J. Phys. Chem. A*, *105*, 7855-7864, 2001.
- Rummukainen, M., I.S.A. Isaksen, B. Rognerud, and F. Stordal, A global model tool for three-dimensional multiyear stratospheric chemistry simulations: Model description and first results, *J. Geophys. Res.*, *104*, 26437-26456, 1999.
- Russell, J.M., L.L. Gordley, J.H. Park, S.R. Drayson, W.D. Hesketh, R.J. Cicerone, A.F. Tuck, J.E. Frederick, J.E. Harries, and P.J. Crutzen, The Halogen Occultation Experiment, *J. Geophys. Res.*, *98*, 10777-10797, 1993.
- Salby, M.L., and P.F. Callaghan, Fluctuations of total ozone and their relationship to stratospheric air motions, *J. Geophys. Res.*, *98*, 2715-2727, 1993.
- Sander, S.P., R.R. Friedl, D.M. DeMore, D.M. Golden, M.J. Kurylo, R.F. Hampson, R.E. Huie, G.K. Moortgat, A.R. Ravishankara, C.E. Kolb, and M.J. Molina, *Chemical Kinetics and Photochemical Data for Use in Stratospheric Modeling (Supplement to Evaluation 12: Update of Key Reactions)*:

GLOBAL OZONE

- Evaluation Number 13, JPL Publication 00-3*, Jet Propulsion Laboratory, Pasadena, Calif., 2000.
- Santer, B.D., R. Sausen, T. Wigley, J.S. Boyle, K. Achutaroa, C. Doutriaux, J.E. Hansen, G. Meehl, E. Roeckner, R. Ruedy, G. Schmidt, and K.E. Taylor, Behavior of tropopause height and atmospheric temperature in models, reanalyses, and observations, I, Decadal changes, *J. Geophys. Res.*, in press, 2002.
- Schauffler, S.M., E.L. Atlas, D.R. Blake, F. Flocke, R.A. Lueb, J.M. Lee-Taylor, V. Stroud, and W. Travnicek, Distributions of brominated organic compounds in the troposphere and lower stratosphere, *J. Geophys. Res.*, *104*, 21513-21535, 1999.
- Schmid, O., J.M. Reeves, C. Wiedinmyer, C.A. Brock, D.W. Toohey, L.M. Avallone, A.M. Gates, and M.N. Ross, Size-resolved measurements of particle emission indices in the stratospheric plume of an Athena II Rocket, *J. Geophys. Res.*, in press, 2002.
- Schnadt, C., M. Dameris, M. Ponater, R. Hein, V. Grewe, and B. Steil, Interaction of atmospheric chemistry and climate and its impact on stratospheric ozone, *Clim. Dyn.*, *18*, 501-517, 2002.
- Schoeberl, M.R., and G.A. Morris, A Lagrangian simulation of supersonic and subsonic aircraft exhaust emissions, *J. Geophys. Res.*, *105*, 11833-11839, 2000.
- Schoeberl, M.R., P.K. Bhartia, and J.R. Herman, Tropical ozone loss following the eruption of Mt. Pinatubo, *Geophys. Res. Lett.*, *20*, 29-32, 1993.
- Seidel, D.J., R.J. Ross, J.K. Angell, and G.C. Reid, Climatological characteristics of the tropical tropopause as revealed by radiosondes, *J. Geophys. Res.*, *106*, 7857-7878, 2001.
- Sexton, D.M.H., H. Grubb, K.P. Shine, and C.K. Folland, Design and analysis of climate model experiments for the efficient estimation of anthropogenic signals, *J. Clim.*, in press, 2002.
- Shindell, D.T., Climate and ozone response to increased stratospheric water vapor, *Geophys. Res. Lett.*, *28*, 1551-1554, 2001.
- Shindell, D.T., R.L. Miller, G.A. Schmidt, and L. Pandolfo, Simulation of recent northern winter climate trends by greenhouse-gas forcing, *Nature*, *399*, 452-455, 1999.
- Shindell, D.T., G.A. Schmidt, R.L. Miller, and D. Rind, Northern Hemisphere winter climate response to greenhouse gas, ozone, solar, and volcanic forcing, *J. Geophys. Res.*, *106*, 7193-7210, 2001.
- Shine, K.P., Radiative forcing of climate change, *Space Sci. Rev.*, *94*, 363-373, 2000.
- Shine, K.P., M.S. Bourqui, P.M. de F. Forster, S.H.E. Hare, U. Langematz, P. Braesicke, V. Grewe, M. Ponater, C. Schnadt, C.A. Smith, J.D. Haigh, J. Austin, N. Butchart, D.T. Shindell, W.J. Randel, T. Nagashima, R.W. Portmann, S. Solomon, D.J. Seidel, J. Lanzante, S. Klein, V. Ramaswamy, and M.D. Schwarzkopf, A comparison of model-simulated trends in stratospheric temperatures, *Quart. J. Roy. Meteorol. Soc.*, in press, 2002.
- Simmons, A.J., A. Untch, C. Jacob, P. Kallberg, and P. Uden, Stratospheric water vapor and tropical tropopause temperatures in ECMWF analyses and multi-year simulations, *Quart. J. Roy. Meteorol. Soc.*, *125*, 353-386, 1999.
- Smith, C.A., Radiative effects of observed trends in stratospheric water vapour, Ph.D. thesis, Imperial College, London, 2001.
- Smith, C.A., R. Toumi, and J.D. Haigh, Seasonal trends in stratospheric water vapour, *Geophys. Res. Lett.*, *27*, 1687-1690, 2000.
- Smith, C.A., J.D. Haigh, and R. Toumi, Radiative forcing due to trends in stratospheric water vapour, *Geophys. Res. Lett.*, *28*, 179-182, 2001.
- Smith, J.B., E.J. Hints, N.T. Allen, R.M. Stimpfle, and J.G. Anderson, Mechanisms for midlatitude ozone loss: Heterogeneous chemistry in the lowermost stratosphere?, *J. Geophys. Res.*, *106*, 1297-1309, 2001.
- Smyshlyaev, S.P., and M.A. Geller, Analysis of SAGE II observations using data assimilation by the SUNY-SPB two-dimensional model and comparison to TOMS data, *J. Geophys. Res.*, *106*, 32327-32335, 2001.
- Smyshlyaev, S.P., V.L. Dvortsov, M.A. Geller, and V. Yudin, A two-dimensional model with input parameters from a general circulation model: Ozone sensitivity to different formulations for the longitudinal temperature variation, *J. Geophys. Res.*, *103*, 28373-28387, 1998.
- Solomon, S., Stratospheric ozone depletion: A review of concepts and history, *Rev. Geophys.*, *37*, 275-316, 1999.
- Solomon, S., R.R. Garcia, and A.R. Ravishankara, On the role of iodine in ozone depletion, *J. Geophys. Res.*, *99*, 20491-20499, 1994.
- Solomon, S., R.W. Portmann, R.R. Garcia, L.W. Thomason, L.R. Poole, and M.P. McCormick, The role of aerosol variations in anthropogenic ozone depletion at northern midlatitudes, *J. Geophys. Res.*, *101*, 6713-6727, 1996.
- Solomon, S., S. Borrmann, R.R. Garcia, R.W. Portmann, L.W. Thomason, L.R. Poole, D. Winker, and M.P. McCormick, Heterogeneous chlorine chemistry in

- the tropopause region, *J. Geophys. Res.*, *102*, 21411-21429, 1997.
- Solomon, S., R.W. Portmann, R.R. Garcia, W. Randel, F. Wu, R. Nagatani, J. Gleason, L. Thomason, L.R. Poole, and M.P. McCormick, Ozone depletion at mid-latitudes: Coupling of volcanic aerosols and temperature variability to anthropogenic chlorine, *Geophys. Res. Lett.*, *25*, 1871-1874, 1998.
- SPARC (Stratospheric Processes and Their Role in Climate), *SPARC/IOC/GAW Assessment of Trends in the Vertical Distribution of Ozone*, edited by N. Harris, R. Hudson, and C. Phillips, *SPARC Report No. 1, Global Ozone Research and Monitoring Project—Report No. 43*, 289 pp., World Meteorological Organization, Geneva, 1998.
- SPARC (Stratospheric Processes and Their Role in Climate), *Assessment of Upper Tropospheric and Stratospheric Water Vapour*, edited by D. Kley, J.M. Russell III, and C. Phillips, *SPARC Report No. 2, WCRP 113*, 312 pp., World Meteorological Organization, Geneva, 2000.
- Steinbrecht, W., H. Claude, U. Köhler, and K.P. Hoinka, Correlations between tropopause height and total ozone: Implications for long-term changes, *J. Geophys. Res.*, *103*, 19183-19192, 1998.
- Steinbrecht, W., H. Claude, U. Köhler, and P. Winkler, Interannual changes of total ozone and Northern Hemisphere circulation patterns, *Geophys. Res. Lett.*, *28*, 1191-1194, 2001.
- Stordal, F., I.S.A. Isaksen, and K. Horntveit, A diabatic circulation two-dimensional model with photochemistry: Simulations of ozone and long-lived tracers with surface sources, *J. Geophys. Res.*, *90*, 5757-5776, 1985.
- Strawa, A.W., K. Drdla, G.V. Ferry, S. Verma, R.F. Pueschel, M. Yasuda, R.J. Salawitch, R.S. Gao, S.D. Howard, P.T. Bui, M. Loewenstein, J.W. Elkins, K.K. Perkins, and R. Cohen, Carbonaceous aerosol (soot) measured in the lower stratosphere during POLARIS and its role in stratospheric chemistry, *J. Geophys. Res.*, *104*, 26753-26766, 1999.
- Stuber, N., M. Ponater, and R. Sausen, Is the climate sensitivity to ozone perturbations enhanced by stratospheric water vapor feedback?, *Geophys. Res. Lett.*, *28*, 2887-2890, 2001.
- Sturges, W.T., D.E. Oram, L.J. Carpenter, S.A. Penkett, and A. Engel, Bromoform as a source of stratospheric bromine, *Geophys. Res. Lett.*, *27*, 2081-2084, 2000.
- Tarasick, D.W., D.I. Wardle, J.B. Kerr, J.J. Bellefleur, and J. Davies, Tropospheric ozone trends over Canada: 1980-1993, *Geophys. Res. Lett.*, *22*, 409-412, 1995.
- Tarasick, D.W., J.B. Kerr, D. Wardle, J. Davis, and V.E. Fioletov, Trends in the vertical distribution of ozone over Canada from ozonesondes: 1980-1999, in *Atmospheric Ozone, Proc. Quadrennial Ozone Symp.*, Sapporo, Japan, 3-8 July 2000, edited by R.D. Bojkov and K. Shibasaki, 85-86, NASDA/EORC, Tokyo, 2000.
- Thomason, L.W., L.R. Poole, and T. Deshler, A global climatology of stratospheric aerosol surface area density deduced from Stratospheric Aerosol and Gas Experiment II measurements: 1984-1994, *J. Geophys. Res.*, *102*, 8967-8976, 1997.
- Thompson, D.W.J., and J.M. Wallace, The Arctic Oscillation signature in the wintertime geopotential height and temperature fields, *Geophys. Res. Lett.*, *25*, 1297-1300, 1998.
- Thompson, D.W.J., and J.M. Wallace, Annual modes in the extratropical circulation, I, Month-to-month variability, *J. Clim.*, *13*, 1000-1016, 2000.
- Thompson, D.W.J., J.M. Wallace, and G.C. Hegerl, Annual modes in the extratropical circulation, II, Trends, *J. Clim.*, *13*, 1018-1038, 2000.
- Thuburn, J., and G.C. Craig, Stratospheric influences on tropopause height: The radiative constraint, *J. Atmos. Sci.*, *57*, 17-28, 2000.
- Tie, X.X., G.P. Brasseur, B. Briegleb, and C. Granier, Two-dimensional model simulation of Pinatubo aerosol and its effect on stratospheric ozone, *J. Geophys. Res.*, *99*, 20545-20562, 1994.
- Tie, X.X., C. Granier, W. Randel, and G.P. Brasseur, Effects of interannual variation in temperature on heterogeneous reactions and stratospheric ozone, *J. Geophys. Res.*, *102*, 23519-23527, 1997.
- Toumi, R., J.D. Haigh, and K.S. Law, A tropospheric ozone-lightning climate feedback, *Geophys. Res. Lett.*, *23*, 1037-1040, 1996.
- Tyndall, G.S., C.S. Kegley-Owen, J.J. Orlando, and A. Fried, Tunable diode laser study of the reaction $\text{OH} + \text{ClO} \rightarrow \text{HCl} + \text{O}_2$, *J. Phys. Chem. A.*, *106*, 1567-1575, 2002.
- van den Broek, M.M.P., A. Bregman, and J. Lelieveld, Model study of stratospheric chlorine activation and ozone loss during the 1996/7 winter, *J. Geophys. Res.*, *105*, 28961-28977, 2000.
- Van Roozendaal, M., M. De Mazière, C. Hermans, P.C. Simon, J.-P. Pommereau, F. Goutail, X.X. Tie, G. Brasseur, and C. Granier, Ground-based observations of stratospheric NO_2 at high and midlatitudes in Europe after the Mt. Pinatubo eruption, *J. Geophys. Res.*, *102*, 19171-19176, 1997.
- Velders, G.J.M., *Scenario Study of the Effects of CFC*,

GLOBAL OZONE

- HCFC, and HFC Emissions on Stratospheric Ozone, RIVM Report 722201006*, National Institute of Public Health and the Environment, Bilthoven, The Netherlands, 1995.
- Vigliarolo, P.K., C.S. Vera, and S.B. Diaz, Southern Hemisphere winter ozone fluctuations, *Quart. J. Roy. Meteorol. Soc.*, *127*, 559-578, 2001.
- Wang, H.J., D.M. Cunnold, and X. Bao, A critical assessment of Stratospheric Aerosol and Gas Experiment ozone trends, *J. Geophys. Res.*, *101*, 12495-12514, 1996.
- Wang, H.J., D.M. Cunnold, L.W. Thomason, J.M. Zawodny, and G.E. Bodeker, Assessment of SAGE version 6.1 ozone data quality, *J. Geophys. Res.*, in press, 2002.
- Wang, J.J., and L.F. Keyser, HCl yield from the OH + ClO reaction at temperatures between 218 and 298 K, *J. Phys. Chem.*, *105*, 6479-6489, 2001.
- Wang, P.-H., P. Minnis, M. McCormick, and G. Kent, A 6-year climatology of cloud occurrence frequency from Stratospheric Aerosol and Gas Experiment II observations (1985-1990), *J. Geophys. Res.*, *101*, 29407-29429, 1996.
- Waugh, D.W., W.J. Randel, S. Pawson, P.A. Newman, and E.R. Nash, Persistence of the lower stratospheric polar vortices, *J. Geophys. Res.*, *104*, 27191-27201, 1999.
- Weatherhead, E.C., G.C. Reinsel, G.C. Tiao, C.H. Jackman, L. Bishop, S.M.H. Frith, J. DeLuise, T. Keller, S.J. Oltmans, E.L. Fleming, D.J. Wuebbles, J.B. Kerr, A.J. Miller, J. Herman, R. McPeters, R.M. Nagatani, and J.E. Frederick, Detecting the recovery of total column ozone, *J. Geophys. Res.*, *105*, 22201-22210, 2000.
- Webster, C.R., H.A. Michelsen, M.R. Gunson, J.J. Margitan, J.M. Russell III, G.C. Toon, and W.A. Traub, Response of lower stratospheric HCl/Cl_y to volcanic aerosol: Observations from aircraft, balloon, space shuttle, and satellite instruments, *J. Geophys. Res.*, *105*, 11711-11719, 2000.
- Weisenstein, D.K., M.K.W. Ko, I.G. Dyominov, G. Pitari, L. Ricciardulli, G. Visconti, and S. Bekki, The effects of sulfur emissions from HSCT aircraft: A 2-D model intercomparison, *J. Geophys. Res.*, *103*, 1527-1547, 1998.
- Weiss, A.K., J. Staehelin, C. Appenzeller, and N.R.P. Harris, Chemical and dynamical contributions to ozone profile trends of the Payerne (Switzerland) balloon soundings, *J. Geophys. Res.*, *106*, 22685-22694, 2001.
- WMO (World Meteorological Organization), *Report of the International Ozone Trends Panel: 1988, Global Ozone Research and Monitoring Project—Report No. 18*, Geneva, 1990.
- WMO (World Meteorological Organization), *Scientific Assessment of Ozone Depletion: 1994, Global Ozone Research and Monitoring Project—Report No. 37*, Geneva, 1995.
- WMO (World Meteorological Organization), *Scientific Assessment of Ozone Depletion: 1998, Global Ozone Research and Monitoring Project—Report No. 44*, Geneva, 1999.
- Zerefos, C.S., K. Tourpali, B.R. Bojkov, D.S. Balis, B. Rognerund, and I.S.A. Isaksen, Solar activity-total ozone relationships: Observations and model studies with heterogeneous chemistry, *J. Geophys. Res.*, *102*, 1561-1569, 1997.
- Zhou, S., M.A. Geller, and M. Zhang, Cooling trend of the tropical cold point tropopause temperatures and its implications, *J. Geophys. Res.*, *106*, 1511-1522, 2001a.
- Zhou, S., A.J. Miller, J. Wang, and J.K. Angell, Trends of NAO and AO and their associations with stratospheric processes, *Geophys. Res. Lett.*, *28*, 4107-4110, 2001b.

Appendix 4A

DESCRIPTION OF OZONE DATASETS

A brief description of the various observational ozone datasets used in this Assessment is included here. More detailed discussions can be found in the *Report of the International Ozone Trends Panel: 1988* (WMO, 1990) and previous Assessments.

4A.1 Ground-Based Total Ozone Measurements

Three types of ground-based instruments are used for long-term monitoring of total ozone content. Their characteristics and performance have been discussed in numerous WMO Assessments (e.g., WMO, 1995, 1999), and therefore only a brief description is provided here. The longest records of continuous reliable measurements are available from stations equipped with Dobson spectrophotometers. The first regular Dobson measurements started in the 1920s, and a worldwide network of Dobson instruments was established in the 1950s and early 1960s. Recent intercomparisons show that at present Dobson instruments at main sites agree with the World Standard Dobson 83 within 0.5% (WMO, 1995, 1999).

The Brewer spectrophotometer, developed in the early 1980s, can measure total ozone with approximately the same uncertainty as the Dobson spectrophotometer. All Brewer instruments are calibrated against the traveling standard Brewer instrument, and the traveling standard is calibrated against the Brewer triad at Toronto (Kerr et al., 1997). The Dobson and Brewer calibrations are independent, and the fact that there is no systematic difference between the two types of instruments adds to confidence in the data quality.

Filter ozonometers are widely used in the former Soviet Union countries, and long-term reliable records are available from 1972. This instrument is less accurate than the Dobson and Brewer instruments, and the calibration is traceable to the Dobson reference. Filter ozonometer observations are important for estimations of long-term ozone variations over vast regions where no Dobson and Brewer data are available and where observations from several stations can be averaged to reduce the random errors (Bojkov et al., 1994).

Total ozone data available from the World Ozone and Ultraviolet Radiation Data Center (WOUDC) were used here, including stations with reliable data and without any major calibration problems in their records. Fioletov et al. (1999) presented a recent review of the ground-based network performance. Data are available from 45 stations with continuous records starting before 1983 (WMO, 1999), and a larger set (up to 109 stations) was used to estimate zonal and global ozone averages for the period 1979-2001, following the methodology described in Bojkov and Fioletov (1995).

4A.2 Satellite Total Ozone Measurements and Merged Datasets

TOTAL OZONE MAPPING SPECTROMETER (TOMS)

In a TOMS measurement, ozone is derived using the “backscattered albedo,” the ratio of the radiance backscattered from the Earth-atmosphere system to the extraterrestrial solar irradiance. The solar irradiance is measured using an onboard diffuser plate. Instrument change should cancel when using this ratio, except for change in the diffuser plate itself, something that proved to be a problem for Nimbus-7 (N7). This was solved by using a triple diffuser for the Meteor-3 (M3) and Earth Probe (EP) instruments. All the TOMS datasets used for this report have been processed using the version 7 (v7) algorithm. Each TOMS instrument has had unique hardware problems, but in-orbit calibration techniques have been used to maintain the relative calibration of each instrument to approximately 1%/decade accuracy. For long-term trend determination there is the additional uncertainty of the relative calibration of EP TOMS, M3 TOMS, and N7 TOMS.

GLOBAL OZONE

NIMBUS-7 TOMS: NOVEMBER 1978 TO APRIL 1993

The absolute accuracy of the Nimbus-7 (N7) TOMS instrument depends on the radiometric calibration that was performed pre-launch, using standard lamps and laboratory diffuser plates. The time-dependent (in-orbit) calibration is maintained by a technique in which the ratio of two long-wavelength channels (non-ozone sensitive) is stabilized. Although instrument changes in N7 TOMS were becoming significant by the end of its life, the calibration was maintained to within ~1%/decade. This is supported by a comparison with a network of 39 Dobson stations that have nearly complete coverage over the entire N7, M3, EP period (McPeters and Labow, 1996). This comparison showed that the drift of N7 TOMS relative to this Dobson network was less than 0.5%/decade, with an average offset of 0.83%.

It is strongly suspected that there is an error in the N7 TOMS data due to “togglng.” In approximately 1983, N7 TOMS began to exhibit small errors in the synchronization of the chopper wheel and the electronics. The instrument appeared to “toggle” between two possible states, and when the calibration was set, one of the two states had to be chosen as the “correct” state. It now appears that the incorrect choice was made, resulting in an error of somewhat less than 1% between 1982 and 1988. This error has little effect on the overall trends for this instrument, but because of the accident of its timing it is likely that it increases the apparent amplitude of any solar cycle term in a regression model. This error will be corrected when these data are reprocessed with a v8 algorithm.

METEOR-3 TOMS: AUGUST 1991 TO DECEMBER 1994

The absolute calibration of the Meteor-3 (M3) TOMS instrument was explicitly set to be the same as that of the N7 TOMS instrument. During the period of overlap when both instruments were operating (8/91-4/93) a normalization factor was derived for the M3 instrument based on a subset of the data for which strict match-up criteria in space and time were met. This makes the M3 dataset a consistent extension of the N7 dataset rather than a totally independent dataset.

The time dependence of M3 TOMS was independently maintained. This was the first instrument to have a triple diffuser assembly: a cover diffuser, a working diffuser that was used weekly, and a reference diffuser that was exposed only a few times a year. This approach was very successful; the well-protected reference diffuser showed no detectable signs of degradation after years of operation. (The same is true of the Earth Probe diffuser after more than 5 years in space.) Precession of the orbit of the Meteor-3 spacecraft led to periods of lower quality data when the orbit was near the terminator, but the effect of these missing data on long-term changes should be minimal since these periods are distributed evenly through the data record.

EARTH PROBE TOMS: JULY 1996 TO DECEMBER 2000

The pre-launch radiometric calibration procedure used for the Earth Probe (EP) TOMS instrument was described in detail by McPeters et al. (1998). Comparison of EP TOMS ozone with that from the 39 Dobson stations through April 2000 shows an average difference of 1.5%. However, a wavelength calibration performed on the QuikTOMS instrument infers that there were small wavelength errors in the EP instrument, which will reduce the EP TOMS ozone values by about 0.5% when a planned reprocessing is done. This will bring the difference with the Dobson measurement down to about 1%, and make the EP data consistent with N7 to within about 0.2%, well within the expected calibration errors of the two instruments.

As with the M3 instrument, EP maintains its time-dependent calibration using a triple diffuser plate. The calibration appears to have been very stable through 1999, but in 2000 artifacts began to appear in the TOMS data related to the look angle. By the summer of 2000, ozone when measured to the left of the orbital track was on average 6 DU lower than when measured to the right of the orbital track. Analysis showed that this cross-track bias was caused by real changes in the optical properties of the scan mirror. The principle that instrument errors should cancel in the radiance-to-irradiance ratio works to some extent, but the angle of the scan mirror when it is viewing the diffuser plate is quite different from when it is looking at the Earth, leading to residual error. It is expected that this scan angle-dependent error will be corrected when the data are next reprocessed. The EP TOMS data should be fully usable for analysis of long-term change through the end of 1999, and an empirical scan bias correction has been derived that should make the EP data usable through the end of the year 2000. However, by 2001 the changes in the optical properties of the scan mirror have become so large that the EP data should not be used for trend determination at this time.

SOLAR BACKSCATTER ULTRAVIOLET (SBUV, SBUV/2)

The long-term collection of total ozone measurements from the Solar Backscatter Ultraviolet (SBUV) spectrometer began with its launch on the NASA Nimbus-7 (N7) spacecraft in 1978. With the demonstrated success of this instrument, the National Oceanic and Atmospheric Administration (NOAA) adopted it (with some modifications) for launch on the NOAA afternoon operational satellite series beginning in 1985, and designated it SBUV/2. Thus far, the NOAA series has included NOAA-9, -11 and -14; NOAA-16 was launched in late 2000. The SBUV retrieval algorithm provides both total ozone and the vertical distribution of ozone in ~5-km-thick layers, and the data here use the version 6 backscatter ultraviolet (BUV) retrieval discussed in Chapter 1 of the SPARC/IOC report (SPARC, 1998). The differences in total ozone between instruments are approximately 1 to 2%. The temporal overlap of instruments can be used to account for calibration biases between instruments, and Miller et al. (2002) have derived a continuous, intercalibrated dataset incorporating measurements from Nimbus-7 (11/78 to 2/85), NOAA-9 (3/85 to 12/88 and 1/94 to 12/95), NOAA-11 (1/89 to 12/93 and 7/98 to 12/00), and NOAA-14 (1/96 to 6/98). The separate time periods for NOAA-9 and -11 data result from the precession of the satellite orbits, and the corresponding loss of BUV measurements as the orbit drifts from local day to night.

There can be substantial biases in the SBUV/2 retrieved ozone for measurements made at very high solar zenith angle (SZA), and the gridded analyses used here only included data for SZA up to 80°. For the “normal” afternoon orbit of SBUV/2, this results in a loss of data at high southern latitudes during local winter (data are unavailable poleward of ~55°S). However, the combination of this SZA cutoff and the orbital drifts of NOAA-9 and -11 results in increased data loss at high southern latitudes for some years, namely, 1988, 1992, 1993, and 1998, when winter data are unavailable poleward of ~45°S. This undersampling by the SBUV+SBUV/2 data is one potential source of difference with the other datasets over SH midlatitudes.

MERGED TOMS+SBUV/2

The Goddard merged ozone dataset was derived using measurements from six satellite instruments: the Nimbus-7 TOMS and SBUV; the NOAA-9, -11, -14, and -16 SBUV/2; and the Earth Probe TOMS. The D-pair (306 nm-311 nm) measurements from SBUV and SBUV/2 instruments were used to stabilize their calibrations as a function of time. The overlaps of these instruments with N7 and EP TOMS were used to establish the relative calibration of each instrument. These were then all adjusted to the first 2 years of EP TOMS as a reference. During this process it was discovered that the N7 TOMS exhibited time-dependent calibration shifts, in part due to a 1.5-DU error in 1984 when the instrument went into the “toggling” mode. The N7 TOMS calibration has been adjusted for these calibration shifts, leading to a deduced trend over its lifetime that is smaller than that shown in previous studies. The data, and information about how they were constructed, can be found at http://code916.gsfc.nasa.gov/Data_services/merged.

NIWA ASSIMILATED DATASET

The National Institute of Water and Atmospheric Research (NIWA) assimilated total ozone dataset is derived from combining measurements obtained by TOMS instruments flown on the Nimbus-7, Meteor-3, Earth Probe, and ADEOS (Advanced Earth Observing Satellite) satellites, together with the Global Ozone Monitoring Experiment (GOME) instrument flown on the European Remote Sensing (ERS)-2 satellite (Burrows et al., 1999). A description of these datasets and their homogenization is provided in Bodeker et al. (2001). Briefly, comparisons between TOMS data and measurements from the ground-based Dobson spectrophotometer network were used to remove offsets and drifts in the Nimbus-7 and Earth Probe satellite data. Statistical model fits to the Nimbus-7 and Meteor-3 differences were used to adjust the Meteor-3 TOMS data. Adjusted Earth Probe TOMS data were similarly used to correct ADEOS TOMS data and GOME data.

COMPARISON OF COLUMN OZONE DATASETS

Some systematic differences between the separate total ozone datasets described above were found. Figure 4A-1 shows the 1979-1987 annual mean percentage differences between the zonal averages estimated from four satellite datasets and the ground-based data as a function of latitude. All datasets agree to within 1% of the ground-based data at 40°-50°N. However, larger differences of 2-4% are seen in the tropics and the Southern Hemisphere for the TOMS, SBUV-SBUV/2, and merged satellite datasets (the NIWA dataset uses adjustments to fit the ground-based data, and hence

GLOBAL OZONE

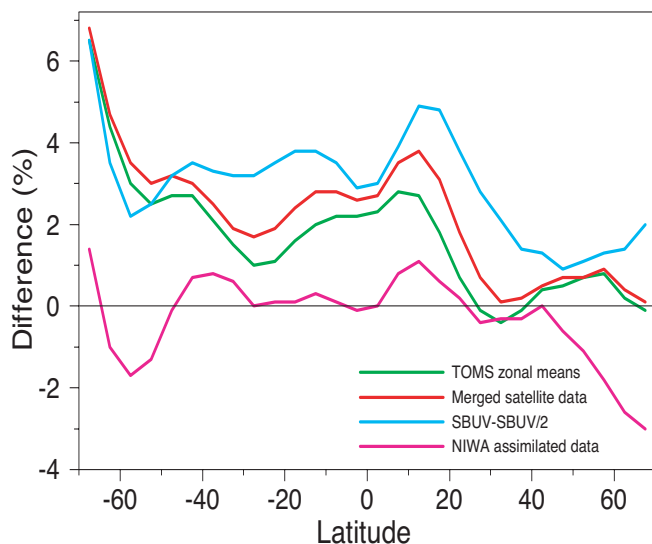


Figure 4A-1. The difference between total ozone zonal means estimated from four datasets and ground-based data, as a function of latitude for the period 1979-1987. Monthly means calculated from the ground-based data have been subtracted from the monthly means of each of the other four datasets, and annual averages calculated; results expressed in percent of the ground-based means. From Fioletov et al. (2002).

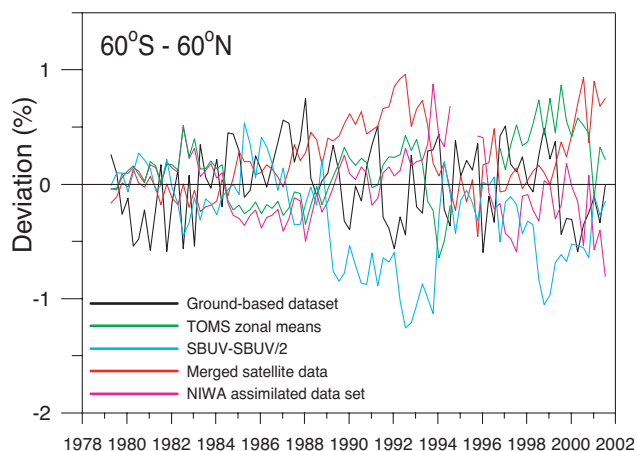


Figure 4A-2. Differences between the five estimates of deseasonalized ozone anomalies over 60°N-60°S (shown in Figure 4-2) and their average. The average of all five estimates was calculated for each season, and then subtracted from all five datasets. Updated from Fioletov et al. (2002).

the mean differences are small). Satellite data are 5-6% higher than ground-based measurements over the Antarctic. For the entire 60°S-60°N zone the area-weighted differences between the other datasets and ground-based zonal averages are the following: 1.5% higher for the TOMS, 2.1% higher for the merged satellite dataset, 0% for the NIWA assimilated dataset, and 3% higher for the SBUV-SBUV/2 dataset.

Deseasonalization removes systematic differences between the datasets, and the deseasonalized total ozone deviations agree to within a root mean square (rms) difference of 0.6-0.8 % (depending on the dataset) over the 1979-2001 period. However, the differences vary in time, as shown in Figure 4A-2, where the individual data records are compared with the average of all five datasets. The range of differences is typically ~1%, but can be as high as 2% at certain times (notably 1991-1993). The SBUV-SBUV/2 dataset is on the low end of the ensemble for much of the period after 1989.

4A.3 Ozone Profile Measurements

Long-term ozone profile datasets include satellite, ground-based Umkehr, and ozonesonde (balloon) measurements. The satellite data are near-global, whereas the Umkehr and ozonesonde measurements are taken at only a few stations, mostly located in northern midlatitudes. The primary satellite data source is derived from the Stratospheric Aerosol and Gas Experiment (SAGE I and SAGE II) measurements, which cover the altitude region ~15-50 km. Although ozone profile information is also available from SBUV-SBUV/2 satellite measurements, there are important uncertainties in the long-term calibration and changes associated with orbital precession of the NOAA-9 and -11 spacecraft, and therefore a homogeneous long-term profile dataset useful for trend analyses is not available at present. Detailed descriptions and intercomparisons of the SAGE, Umkehr, and ozonesonde measurement techniques and instruments can be found in SPARC (1998), and only brief summaries are provided here.

SAGE I

The SAGE measurement technique (McCormick et al., 1989) is based on solar occultation, with ozone profile measurements obtained at sunrise and sunset on each of 14 orbits per day. This technique provides high vertical resolution (~1 km) and very small long-term drifts resulting from instrument calibration. However, spatial sampling is limited, and it takes approximately one month to sample the latitude range 60°N to 60°S. SAGE I ozone profile data cover the time period February 1979 to November 1981. A difficulty in combining the SAGE I and SAGE II data for trend studies arises from an apparent error in the reference altitude for SAGE I. An empirical altitude correction has been applied to the SAGE I data in an attempt to remove this bias (H.J. Wang et al., 1996).

SAGE II

SAGE II ozone profile data commenced in November 1984 and continue to the present (December 2002). The analysis here used SAGE II version 6.1 (v6.1), which was released in March 2002. It includes a new algorithm for altitude registration, which results in a large reduction in the scatter in the transmission profile. There is evidence that the vertical resolution has been significantly improved over previous versions and is now approximately 0.75 km; v6.1 is placed on a 0.5-km altitude grid. The species separation and inversion in v6.1 is similar to that used in v5.96 (the basis for the SAGE II ozone data in WMO (1999)), but v6.1 incorporates an aerosol model that improves the ozone retrievals in the presence of enhanced aerosol (H.J. Wang et al., 2002). The primary change to v6.1 was the method of estimating the species errors, which now include terms for the Rayleigh scattering and aerosol model uncertainties. In general, the ozone results are of good quality down to the tropopause. The data analyzed here exclude time periods of enhanced aerosol extinction following the eruption of Mt. Pinatubo in June 1991.

UMKEHR OZONE PROFILE MEASUREMENTS

Ground-based measurements use the Umkehr technique for measuring the profile of ozone concentration. It consists of observing a series of ultraviolet wavelengths of solar radiation, some of which are strongly absorbed by atmospheric ozone. A sequence of radiance measurements is made as the Sun rises or sets, and information about the ozone profile is obtained from an inversion algorithm applied to the measurements (e.g., Mateer and Deluisi, 1992). A new Umkehr retrieval algorithm (ALG-99) has been developed by Petropavlovskikh et al. (2001), with results discussed extensively in Bojkov et al. (2002). ALG-99 utilizes latitudinally and seasonally dependent first-guess ozone profiles. Unlike previous versions, the new first-guess profiles do not depend on total ozone, and therefore the influence of the total ozone trend on the retrieval has been largely reduced.

Relatively long records of Umkehr measurements (exceeding 15-20 years) are available from 13 stations. However, time series from many stations have significant discontinuities resulting from occasional changes in instrumentation. Careful analysis of the individual time series in addition to station histories suggests that the long-term data are of sufficient quality at only a relatively few stations. The results here are based on data from Arosa, Switzerland (47°N); Belsk, Poland (52°N); Boulder, Colorado, U.S. (40°N); and Haute-Provence, France (44°N).

OZONESONDES

A network of stations provides ozone profile information from balloonborne sondes, which measure ozone from the ground to about 30 km, with a vertical resolution of ~150 m. Details of ozonesonde measurements and data processing are discussed in SPARC (1998). One important detail is that each sonde profile is normalized to coincident total ozone measurements, and the amount of data available for trend analyses depends on the chosen limits of this normalization factor (SPARC, 1998; Logan et al., 1999). Data are available to the end of 2000 for all the stations used in the SPARC (1998) analysis, which include 14 locations spanning the latitude range 32°N-75°N. The Uccle dataset has been reprocessed since the SPARC study. The ozonesondes at Uccle switched from Brewer Mast to electrochemical concentration cell (ECC) sondes in March 1997, with a transition period during which both sondes were used, to allow adjustment for any discontinuity in the dataset.

Appendix 4B

2-D MODEL SCENARIOS

Table 4B-1. Definition of the 2-D model scenarios. All model runs used the halocarbon scenario described in Table 4B-2 below. IPCC refers to IPCC (2001).

Scenario	Period	Motivation	CH ₄	N ₂ O	CO ₂	Aerosol
MC2	1979-2000	Best past trend	IPCC	IPCC	IPCC	D. Considine
MA2	2000-2050	Control A2	IPCC A2	IPCC A2	IPCC A2	Background
MB2	2000-2050	Control B2	IPCC B2	IPCC B2	IPCC B2	Background
MLCH4	2000-2050	Low CH ₄	0.8 × A2 increase post- 2000	IPCC A2	IPCC A2	Background
MHCH4	2000-2050	High CH ₄	1.2 × A2	IPCC A2	IPCC A2	Background
MLN2O	2000-2050	Low N ₂ O	IPCC A2	0.8 × A2	IPCC A2	Background
MHN2O	2000-2050	High N ₂ O	IPCC B2	1.2 × A2	IPCC B2	Background
MLCO2	2000-2050	Low CO ₂	IPCC A2	IPCC A2	0.8 × A2	Background
MHCO2	2000-2050	High CO ₂	IPCC A2	IPCC A2	1.2 × A2	Background
MEPI	2000-2050	Episodic aerosol	IPCC A2	IPCC A2	IPCC A2	Episodic
MENH	2000-2050	Enhanced back-ground aerosol	IPCC A2	IPCC A2	IPCC A2	Enhanced

Table 4B-2. Halocarbon scenario used in the 2-D model calculations. This scenario is essentially the same (except for a few small deviations) as the baseline scenario Ab described in Tables 1-13 and 1-16 of Chapter 1.

Time	CFC-11	CFC-12	CFC-113	CFC-114	CFC-115	CCl ₄	CH ₃ CCl ₃	HCFC-22	HCFC-141b	HCFC-142b	Halon-1211	Halon-1202	Halon-1301	Halon-2402	CH ₃ Br	CH ₃ Cl
1950	0.39	5.81	0.19	1.13	0.00	34.54	0.00	0.00	0.00	0.00	0.00	0.00	0.00	0.00	7.02	483.42
1955	2.96	14.59	0.53	2.39	0.00	41.16	0.05	0.25	0.00	0.00	0.00	0.00	0.00	0.00	7.09	492.78
1960	9.16	29.81	1.18	3.63	0.00	51.13	1.44	1.28	0.00	0.00	0.00	0.00	0.00	0.00	7.26	510.97
1965	23.26	59.14	2.44	4.90	0.00	63.63	4.59	3.82	0.00	0.10	0.00	0.00	0.00	0.00	7.44	528.77
1970	52.62	114.74	4.93	6.37	0.12	75.36	15.96	10.11	0.00	0.21	0.02	0.00	0.00	0.01	7.66	540.55
1975	105.99	203.64	9.84	8.14	0.50	85.04	39.20	21.17	0.00	0.30	0.12	0.00	0.04	0.04	7.93	546.48
1980	162.26	295.85	19.52	10.28	1.33	93.03	78.53	36.72	0.00	0.36	0.42	0.01	0.24	0.11	8.20	549.05
1985	205.27	382.18	36.72	12.64	2.91	99.62	105.68	56.32	0.00	0.51	1.04	0.02	0.74	0.20	8.55	550.10
1990	256.34	474.07	67.97	15.36	5.06	105.67	124.91	81.33	0.00	1.24	2.27	0.03	1.66	0.31	8.95	550.51
1995	270.62	524.80	83.23	16.18	7.49	103.66	108.63	111.78	2.09	5.27	3.25	0.04	2.33	0.42	9.40	550.68
2000	262.64	540.48	81.70	16.38	8.97	97.94	49.81	140.15	10.81	10.61	3.97	0.05	2.82	0.41	9.31	550.72
2005	250.66	541.09	78.01	16.41	9.15	92.25	21.85	172.56	23.71	18.91	4.14	0.02	3.17	0.37	8.81	550.72
2010	236.07	522.50	73.87	16.27	9.15	80.13	10.79	180.55	34.65	24.28	3.76	0.01	3.40	0.31	8.44	550.72
2015	218.15	497.02	69.68	16.07	9.13	66.11	5.67	168.54	39.14	26.12	3.19	0.00	3.52	0.26	8.44	550.72
2020	198.88	472.78	65.70	15.84	9.10	54.55	2.75	141.32	36.78	24.67	2.59	0.00	3.56	0.21	8.17	550.72
2025	179.90	449.72	61.95	15.59	9.07	45.01	1.22	110.25	30.68	21.49	2.05	0.00	3.52	0.17	8.17	550.72
2030	162.01	427.79	58.41	15.34	9.04	37.13	0.51	84.70	24.33	18.19	1.59	0.00	3.44	0.13	8.17	550.72
2035	145.52	406.92	55.07	15.09	9.01	30.64	0.21	65.05	18.85	15.20	1.22	0.00	3.33	0.10	8.17	550.72
2040	130.51	387.08	51.93	14.84	8.98	25.28	0.08	50.08	14.38	12.56	0.93	0.00	3.19	0.08	8.17	550.72
2045	116.94	368.20	48.96	14.60	8.95	20.85	0.03	38.03	10.80	10.26	0.70	0.00	3.04	0.06	8.17	550.72
2050	104.72	350.24	46.16	14.36	8.92	17.21	0.01	26.56	7.55	8.06	0.52	0.00	2.88	0.05	8.17	550.72

Table 4B-3. GHG scenarios (from IPCC, 2001). Scenarios A2 and B2 were used in the model runs. CO₂ is from the Integrated Science Assessment Model (ISAM) reference CO₂ scenario (p. 807 of IPCC, 2001).

Time	CH ₄ (ppbv)				N ₂ O (ppbv)				CO ₂ (ppmv)			
	IS92a	A2	B1	B2	IS92a	A2	B1	B2	IS92a	A2	B1	B2
1970	1420	1420	1420	1420	295	295	295	295	326	325	325	325
1980	1570	1570	1570	1570	301	301	301	301	338	337	337	337
1990	1700	1700	1700	1700	308	308	308	308	354	353	353	353
2000	1810	1760	1760	1760	319	316	316	316	372	369	369	369
2010	1964	1861	1827	1839	328	325	324	323	393	390	388	388
2020	2145	1997	1891	1936	339	335	333	328	418	417	412	408
2030	2343	2163	1927	2058	350	347	341	333	446	451	437	429
2040	2561	2357	1919	2201	361	360	349	338	476	490	463	453
2050	2793	2562	1881	2362	371	373	357	342	509	532	488	478